UNIVERSITY OF SOUTHAMPTON

FACULTY OF ENGINEERING, SCIENCE AND MATHEMATICS

School of Civil Engineering and the Environment

Structural and geotechnical interpretation of strain gauge data from laterally loaded reinforced concrete piles

by

Nicola Bicocchi

Thesis for the degree of Doctor of Philosophy

May 2011

Abstract

Four instrumented sites, with a total of 14 instrumented piles, have been analysed to understand the structural behaviour of the piles and the geotechnical behaviour of the stabilised slopes. Vibrating wire strain gauges are used for the calculation of the bending moment applied to the piles, while inclinometers are used to measure the displacements. A review of the instrumentation has been carried out and a methodology for processing and analysing strain gauges data has been developed.

Concrete is a material with a complex behaviour. Shrinkage, creep, cracking, temperature variations, strength and modulus of elasticity of concrete are critically analysed to understand their influence on the concrete pile behaviour and on the function of the strain gauges. The results show that creep and shrinkage effects can be neglected in underground reinforced concrete structures in saturated clay, while cracking effects and temperature variations have to be analysed case by case. A correction method has been developed to consider the difference between the coefficient of thermal expansion of the strain gauges and that of the concrete. Two types of pile have been analysed, standard reinforced concrete piles and circular concrete-filled steel tubular piles. A review of their behaviour in bending that considers the development of cracking is presented.

Two methods for the calculation of bending moment in the piles have been developed taking into account realistic stress/strain curves and the effects of concrete cracking. The bending moment results are compared with the inclinometer profiles using an improved version of an existing curve fitting method. The comparison shows good agreement between the two instrument results.

A critical analysis of the pile/soil behaviour has been carried out comparing the results from the instrumented sites with theoretical mechanisms for landslide stabilising piles presented elsewhere. The results show a good match with the theoretical mechanisms as well as showing that the slopes have been successfully stabilised.

Other observations have been made during analysis of the monitoring data. These include the seasonal effects of climate and vegetation on stabilised slopes and the structural effect of the external grout ring in laterally loaded circular concrete-filled steel tubular piles.

Contents

Contents i

List of Figures vii

List of Tables xv

List of Symbols xvi

Form of declaration xix

Acknowledgments xxi

1 Introduction 1

1.1 Background . . . 1
1.2 Aims and objectives of the research . . . 3
1.3 Summary of the chapter contents . . . 4
1.4 Main conventions and definitions . . . 5

2 Background 7

2.1 Instrumentation . . . 7
2.1.1 Vibrating wire strain gauges . . . 7
2.1.2 Inclinometers . . . 12
2.1.3 Thermistors . . . 13
2.1.4 Data-logger . . . 13
2.2 Concrete material . . . 13
2.2.1 Portland cement . . . 14
2.2.2 Hydration of cement . . . 14
2.3 Properties of concrete . . . 16
2.3.1 Strength of concrete . . . 16
2.3.2 Young's modulus of concrete E_c and stress/strain curves . . . 16
2.3.2.1 Stress/strain curves for standard reinforced concrete piles 17
2.3.2.2 Stress/strain curves for circular concrete-filled steel tubular piles . . . 19
2.4 Creep and shrinkage . . . 20
2.4.1 Shrinkage . . . 20

2.4.1.1 Plastic shrinkage . . . 21
2.4.1.2 Autogenous shrinkage . . . 21
2.4.1.3 Drying shrinkage . . . 22
2.4.1.4 Carbonation shrinkage . . . 23
2.4.2 Creep . . . 23
2.4.3 Influences of particular concrete mixes on shrinkage and creep . 24
2.4.3.1 Ground Granulated Blast-furnace Slag (GGBS) . . . 25
2.4.3.2 Fly ash . . . 25
2.4.4 Previous work . . . 25
2.4.4.1 Gawin et al. (2006) . . . 25
2.4.4.2 Goel et al. (2007) . . . 26
2.4.4.3 Barr et al. (2003) . . . 26
2.4.4.4 Fellenius et al. (2009) . . . 26
2.4.4.5 Neville (1995) . . . 27
2.4.5 Creep and shrinkage in underground structures conclusions . . . 29
2.5 Cracking . . . 30
2.5.1 Standard reinforced concrete pile . . . 30
2.5.1.1 How strain gauges respond to cracks in standard reinforced concrete . . . 31
2.5.2 Circular concrete-filled steel tubular piles . . . 32
2.6 Temperature . . . 33
2.7 Conclusions . . . 34

3 Instrumented sites 37
3.1 Grange Hill . . . 37
3.1.1 The piles . . . 38
3.1.2 The instruments . . . 40
3.2 Leatherhead . . . 40
3.2.1 The piles . . . 41
3.2.2 The instruments . . . 42
3.3 Mill Hill . . . 42
3.3.1 The piles . . . 44
3.3.2 The instruments . . . 45
3.4 Ironbridge . . . 45
3.4.1 The geology . . . 49
3.4.2 The pile type . . . 49
3.4.3 Phase I . . . 50
3.4.4 Phase II . . . 52
3.4.5 Lloyd's Head . . . 53
3.5 Concrete sampling: properties of the materials and respective assumptions 54
3.6 Conclusions . . . 55

4 Interpretation of strain gauge data **59**
4.1 Vibrating wire strain gauge: from reading to absolute strain 59
4.2 Datum setting 60
4.2.1 Effects of concrete setting on strain gauges 60
4.2.2 Method for the choice of a datum in long term analysis 61
4.2.3 Datum setting conclusions 64
4.2.4 Example 64
4.3 Removal of interference 67
4.4 Temperature corrections 71
4.4.1 Strain/temperature graphs and correlations 73
4.4.2 Effects of temperature changes on strain gauges readings 74
4.4.2.1 Behaviour of a vibrating wire strain gauge in relation with thermal variations 74
4.4.2.2 Coefficient of thermal expansion of concrete 74
4.4.2.3 Temperature correction formula 76
4.4.3 Temperature correction method 76
4.4.4 Case history 77
4.4.4.1 Grange Hill 77
4.4.4.2 Mill Hill 81
4.4.4.3 Leatherhead 82
4.4.5 Temperature correction conclusions 82
4.5 Broken connections: the case of UP22 84
4.6 Detecting concrete cracking with strain gauges 86
4.7 Conclusions 88

5 Calculation of bending moment using strain gauge data **89**
5.1 Background and problems 90
5.1.1 Basic method: application and limitations 90
5.1.2 The position of the neutral axis 91
5.1.3 Cracking in reinforced concrete 92
5.1.4 Axial strain effects 93
5.2 Bending moment calculation method 94
5.2.1 Automatic cracking model (ACM) 95
5.2.2 Manual correction model (MCM) 99
5.2.2.1 Manual correction of cracking effects 100
5.3 Application of bending moment calculation methods to case histories . . 102
5.3.1 Discussion of the application of the manual correction model (MCM) 102
5.3.2 Application of ACM and MCM 104
5.3.2.1 The effects of the tensile strain limit of concrete (ε_{t0c}) on ACM 112
5.3.3 Axial strain 114
5.4 Bending moment calculation conclusions 118

6 Inclinometer results and curve fitting analysis **121**
6.1 Inclinometer results . . . 121
6.1.1 Grange Hill . . . 122
6.1.2 Mill Hill . . . 123
6.1.3 Leatherhead . . . 124
6.1.4 Ironbridge . . . 125
6.2 Curve fitting method . . . 126
6.2.1 Discussion about the stiffness used in the curve fitting method . 128
6.2.2 Setting of the curve fitting datums . . . 129
6.3 Comparison between bending moment and displacements results . . . 130
6.3.1 Grange Hill Pile1 . . . 130
6.3.2 Mill Hill Pile1 . . . 132
6.3.3 Leatherhead Pile2 . . . 133
6.3.4 Ironbridge L2P30 . . . 134
6.4 Comparison between bending moment and displacements results: conclusions . . . 135

7 Geotechnical interpretation **137**
7.1 Grange Hill . . . 140
7.2 Mill Hill . . . 143
7.3 Leatherhead . . . 147
7.4 Ironbridge . . . 150
7.4.1 Phase I . . . 150
7.4.2 Phase II . . . 153
7.4.3 Lloyd's Head . . . 156
7.5 Comparison between bending moment calculation methods . . . 157
7.6 Conclusions about the geotechnical interpretation of instrumented sites . 159

8 Conclusions **161**
8.1 Conclusions . . . 161
8.2 Further work . . . 163

References **165**

References **165**

A Appendix **169**
A.1 Grange Hill . . . 170
A.1.1 Pile1 . . . 170
A.1.2 Pile2 . . . 171
A.1.3 Pile3 . . . 173
A.2 Leatherhead . . . 174
A.2.1 Pile1 . . . 174
A.2.2 Pile2 . . . 176

A.3 Mill Hill . . . 178
A.3.1 Pile1 . . . 178
A.3.2 Pile2 . . . 179
A.4 Ironbridge . . . 181
A.4.1 Phase I . . . 181
A.4.1.1 L1P30 . . . 181
A.4.1.2 L2P30 . . . 183
A.4.1.3 UP22 . . . 184
A.4.2 Phase II . . . 186
A.4.2.1 UT81 . . . 186
A.4.2.2 LT56 . . . 187
A.4.3 Lloyd's Head . . . 189
A.4.3.1 P58Row1 . . . 189
A.4.3.2 P58Row2 . . . 190

List of Figures

1.1 Ironbridge stabilisation works, during the installation of the piles (left) and after the completion (right). 1

2.1 Schematic drawings for the different types of strain gauges 9
2.2 Embedded strain gauges 10
2.3 Sister Bar 10
2.4 Welded strain gauges 11
2.5 Stress/strain curve for concrete [BS EN 1992 (2004)] 18
2.6 Idealised stress/strain curve for steel [BS EN 1992 (2004)] 18
2.7 Stress/strain curve for the concrete core of a hollow steel pipe pile [Liang and Fragomeni (2010)] 19
2.8 Stress/strain curve for the steel of a hollow steel pipe pile [Liang and Fragomeni (2010)] 20
2.9 Pickett's paradox (Acker and Ulm (2001)) 23
2.10 Theoretical strain vs. time curve for a concrete sample under load . . . 24
2.11 Conceptual crack formation, spacing and effective concrete area in tension based on Borosnyoi and Balazs (2005) 31

3.1 Grange Hill Site, main instrumented section 38
3.2 Grange Hill piles 39
3.3 Leatherhead, main instrumented section 41
3.4 Leatherhead piles 42
3.5 Mill Hill section 43
3.6 Mill Hill instrumented section plan 43
3.7 Mill Hill piles 45
3.8 Plan of Ironbridge site 47
3.9 Profile of Phase I and Phase II 48
3.10 Profile of Lloyd's Head 48
3.11 Simplified geology section of Phase I 49
3.12 Phase I, section and plan 51
3.13 Phase I, instrumented piles 52
3.14 Phase II, instrumented piles 53
3.15 Lloyd's Head, instrumented piles 54

4.1 Grange Hill Pile 1, temperatures 62
4.2 Grange Hill Pile 1, temperatures after concrete setting 63
4.3 Grange Hill Pile 1, early stage strain development for section 4-14 63
4.4 Ironbridge UP22, early stage strain development for section 11-26 64
4.5 Grange Hill Pile 1, first month of recorded temperatures after pouring of concrete 65
4.6 Grange Hill Pile 1, *digit* profiles before the setting of the datum 66
4.7 Grange Hill Pile 1, strain profiles after datum setting. 66
4.8 Grange Hill Pile 1, general interferences before correction 68
4.9 Grange Hill Pile 1, general interference after correction. 68
4.10 Mill Hill Pile 1, harmonic errors before correction 69
4.11 Mill Hill Pile 1, after harmonic errors correction 69
4.12 Grange Hill Pile 1 SG5, complex interferences before correction 70
4.13 Grange Hill Pile 1 SG5, complex interference after correction. 70
4.14 Grange Hill Pile 1, seasonal strain variation in the instrumented section at the top of the pile 71
4.15 Mill Hill Pile 1, seasonal strain variation in the instrumented section at the top of the pile 72
4.16 Leatherhead Pile 2, seasonal strain variation in the instrumented section at the top of the pile 72
4.17 Grange Hill Pile1, strain/temperature graph 73
4.18 Grange Hill Pile 1, temperature corrections 77
4.19 Grange Hill Pile2, strain/temperature graph 78
4.20 Grange Hill Pile1, uncorrected strain profiles 79
4.21 Grange Hill Pile1, corrected strain profiles 79
4.22 Grange Hill Pile1, strain profiles comparison 80
4.23 Grange Hill Pile1, axial strain profiles comparison 80
4.24 Mill Hill Pile1, strain/temperature graph 81
4.25 Mill Hill Pile2, strain/temperature graph 82
4.26 Leatherhead Pile1, strain/temperature graph 83
4.27 Leatherhead Pile2, strain/temperature graph 83
4.28 Ironbridge UP22 temperature profiles 85
4.29 Strains and bending moment profiles for SG 4-14 Pile1 86
4.30 Strains and bending moment profiles for SG 4-14 Pile2 87
4.31 Measured strains in section 4-14P2 before and after cracking 87
4.32 Measured strains in section 4-14P1 before and after cracking 88

5.1 The effect of different values of the Young's modulus in the calculation of the bending moment 91
5.2 Grange Hill Pile1 section 4-14, time profile of the position of the global neutral axis (X) 92
5.3 Development of tensile axial strain during cracking of concrete in bending 93
5.4 Strain distribution for the calculation of *Grad* 96

5.5 Strain distribution due to bending and axial loads 98
5.6 Examples of concrete and steel sections used for the calculation of bending moment 98
5.7 Particulars of the pile sections used for the calculation of the bending moment 99
5.8 Diagrams for the manual correction of a cracked section 101
5.9 Grange Hill Pile1, comparison between ACM, MCM uncorrected and MCM corrected bending moment profiles 103
5.10 Grange Hill Pile1, comparison between ACM, MCM uncorrected and MCM corrected axial strains profiles 103
5.11 Ironbridge L2P30, bending moment vs. depth profiles 104
5.12 Ironbridge instrumented pile. 105
5.13 Grange Hill Pile1, bending moment vs. depth profiles 109
5.14 Mill Hill Pile1, bending moment vs. depth profiles 110
5.15 Leatherhead Pile2, bending moment vs. depth profiles 111
5.16 Sensitivity comparison for the bending moment profiles 112
5.17 Grange Hill Pile1 SG4-14, comparison between bending moment profiles calculated with MCM, ACM (ε_{t0c}= 72$\mu\varepsilon$) and ACM (ε_{t0c}= 200$\mu\varepsilon$). . . 113
5.18 Grange Hill Pile1 SG4-14, comparison between bending moment profiles calculated with MCM, ACM (ε_{t0c}= 72$\mu\varepsilon$), ACM (ε_{t0c}= 72$\mu\varepsilon$) corrected, ACM (ε_{t0c}= 200$\mu\varepsilon$) and ACM (ε_{t0c}= 200$\mu\varepsilon$) corrected. 114
5.19 Leatherhead Pile2,comparison between bending moment and axial strains profiles 115
5.20 Mill Hill Pile1,comparison between bending moment and axial strains profiles 116
5.21 Grange Hill Pile1,comparison between bending moment and axial strains profiles 117
5.22 Ironbridge L2P30,comparison between bending moment and axial strains profiles 118

6.1 Inclinometer displacement profiles for the instrumented piles at Grange Hill. 122
6.2 Displacement versus time profiles for the instrumented piles at Grange Hill 122
6.3 Inclinometer displacement profiles for the instrumented piles at Mill Hill. 123
6.4 Displacement versus time profiles for the instrumented piles at Mill Hill 123
6.5 Inclinometer displacement profiles for the instrumented piles at Leatherhead. 124
6.6 Displacement versus time profiles for the instrumented piles at Leatherhead 125
6.7 Inclinometer displacement profiles for the instrumented piles at Ironbridge Phase I. 125
6.8 Displacement versus time profiles for the instrumented piles at Ironbridge Phase I 126
6.9 Mathematical operations in the curve fitting model 128

6.10 Grange Hill Pile1, bending moment and displacement comparison using the curve fitting method. 130
6.11 Grange Hill Pile1, bending moment and displacement comparison using the curve fitting method and a 10% reduction of the stiffness of the pile in the MCM. 131
6.12 Grange Hill Pile1, shear force and soil pressure profiles calculated using the curve fitting method and a 10% reduction of the stiffness of the pile in the MCM. 131
6.13 Mill Hill Pile1, bending moment and displacement comparison using the curve fitting method. 132
6.14 Leatherhead Pile2, bending moment and displacement comparison using the curve fitting method 132
6.15 Leatherhead Pile2, bending moment and displacement comparison using the curve fitting method 133
6.16 Leatherhead Pile2, bending moment and displacement comparison using the curve fitting method 133
6.17 Ironbridge L2P30, bending moment and displacement comparison using the curve fitting method 134
6.18 Ironbridge L2P30, bending moment and displacement comparison using the curve fitting method and a 15% reduction of the stiffness of the pile. 134
6.19 Ironbridge L2P30, shear force and soil pressure profiles calculated using the curve fitting method and a 15% reduction of the stiffness of the pile. 135

7.1 Pile behaviour modes for different depths of soil increment from Poulos (1999) 139
7.2 Grange Hill Pile1, displacements and bending moments (calculated with MCM) for the whole monitoring period 140
7.3 Grange Hill Pile1, shear force and soil pressure profiles calculated using the curve fitting method for the 23 July 2010 results and a 10% reduction of the stiffness of the pile. 140
7.4 Grange Hill, plan of the inclinometers 142
7.5 Grange Hill, comparison between pile displacements and soil displacements in between the piles. 142
7.6 Mill Hill Pile1, displacements and bending moments (calculated with MCM) for the full monitoring period 143
7.7 Leatherhead Pile2, bending moment and displacement comparison using the curve fitting method 143
7.8 Mill Hill Pile1, measured strains for the instruments in the top half of the pile. 144
7.9 Mill Hill Pile1, bending moment (MCM) versus time. 145
7.10 Axial strain for the top four sections of Mill Hill Pile1. 145
7.11 Mill Hill, plan of the inclinometers. 146

7.12 Mill Hill, displacements measured in Pile3, Slope1 and Slope2 on the 8 July 2010. 147
7.13 Leatherhead Pile2, displacements and bending moments (calculated with MCM) along the full monitoring period 148
7.14 Leatherhead Pile2, bending moment and displacement comparison using the curve fitting method 148
7.15 Leatherhead, plan of the piles instrumented with inclinometers 149
7.16 Leatherhead, displacements profiles for all the instrumented piles, 10 June 2010. 149
7.17 Ironbridge L2P30, displacements and bending moments (calculated with ACM) for the full monitoring period 150
7.18 Ironbridge L2P30, shear force and soil pressure profiles calculated using the curve fitting method and a 15% reduction of the stiffness of the pile. 150
7.19 Ironbridge L2P30, bending moment (ACM) versus time 152
7.20 Ironbridge UT81, displacements and bending moments (calculated with ACM) for the full monitoring period 153
7.21 Ironbridge UT81, bending moment and displacement comparison using the curve fitting method. 154
7.22 Ironbridge UT81, shear force and soil pressure profiles calculated using the curve fitting method. 154
7.23 Ironbridge UT81, bending moment (ACM) versus time 155
7.24 Ironbridge Lloyd's Head, bending moment profiles (calculated with ACM) for P58Row1 and P58Row2. 156
7.25 Comparison between the bending moment profiles coming from different models for Grange Hill Pile 1 and Leatherhead Pile 2. 157
7.26 Comparison between the bending moment profiles coming from different models for Mill Hill Pile 1 and Ironbridge L2P30. 158

A.1 Grange Hill Pile1, strain profiles for all the instruments in the pile. . . 170
A.2 Grange Hill Pile1, bending moment profiles for all the instrumented sections in the pile. 170
A.3 Grange Hill Pile1, displacements and bending moments (calculated with MCM) for the whole monitoring period 171
A.4 Grange Hill Pile2, strain profiles for all the instruments in the pile. . . 171
A.5 Grange Hill Pile2, bending moment profiles for all the instrumented sections in the pile. 172
A.6 Grange Hill Pile2, displacements and bending moments (calculated with MCM) for the whole monitoring period 172
A.7 Grange Hill Pile3, strain profiles for all the instruments in the pile. . . 173
A.8 Grange Hill Pile3, bending moment profiles for all the instrumented sections in the pile. 173
A.9 Grange Hill Pile3, displacements and bending moments (calculated with MCM) for the whole monitoring period 174

A.10 Leatherhead Pile1, strain profiles for all the instruments in the pile. . . 174
A.11 Leatherhead Pile1, bending moment profiles for all the instrumented sections in the pile. 175
A.12 Leatherhead Pile1, displacements and bending moments (calculated with MCM) along the full monitoring period 175
A.13 Leatherhead Pile2, strain profiles for all the instruments in the pile. . . 176
A.14 Leatherhead Pile2, bending moment profiles for all the instrumented sections in the pile. 176
A.15 Leatherhead Pile2, displacements and bending moments (calculated with MCM) along the full monitoring period 177
A.16 Mill Hill Pile1, strain profiles for all the instruments in the pile. 178
A.17 Mill Hill Pile1, bending moment profiles for all the instrumented sections in the pile. 178
A.18 Mill Hill Pile1, displacements and bending moments (calculated with MCM) for the full monitoring period 179
A.19 Mill Hill Pile2, strain profiles for all the instruments in the pile. 179
A.20 Mill Hill Pile2, bending moment profiles for all the instrumented sections in the pile. 180
A.21 Mill Hill Pile2, displacements and bending moments (calculated with MCM) for the full monitoring period 180
A.22 Ironbridge L1P30, strain profiles for all the instruments in the pile. . . 181
A.23 Ironbridge L1P30, bending moment profiles for all the instrumented sections in the pile. 182
A.24 Ironbridge L1P30, displacements and bending moments (calculated with ACM) for the full monitoring period 182
A.25 Ironbridge L2P30, strain profiles for all the instruments in the pile. . . 183
A.26 Ironbridge L2P30, bending moment profiles for all the instrumented sections in the pile. 183
A.27 Ironbridge L2P30, displacements and bending moments (calculated with ACM) for the full monitoring period 184
A.28 Ironbridge UP22, strain profiles for all the instruments in the pile. . . . 184
A.29 Ironbridge UP22, bending moment profiles for all the instrumented sections in the pile. 185
A.30 Ironbridge UP22, displacements and bending moments (calculated with ACM) for the full monitoring period 185
A.31 Ironbridge UT81, strain profiles for all the instruments in the pile. . . . 186
A.32 Ironbridge UT81, bending moment profiles for all the instrumented sections in the pile. 186
A.33 Ironbridge UT81, displacements and bending moments (calculated with ACM) for the full monitoring period 187
A.34 Ironbridge LT56, strain profiles for all the instruments in the pile. 187

A.35 Ironbridge LT56, bending moment profiles for all the instrumented sections in the pile. 188
A.36 IronbridgeLT56, displacements and bending moments (calculated with ACM) for the full monitoring period 188
A.37 Ironbridge P58Row1, strain profiles for all the instruments in the pile. . 189
A.38 Ironbridge P58Row1, bending moment profiles for all the instrumented sections in the pile. 189
A.39 Ironbridge P58Row1, bending moment profiles (calculated with ACM) for the full monitoring period. 190
A.40 Ironbridge P58Row2, strain profiles for all the instruments in the pile. . 190
A.41 Ironbridge P58Row2, bending moment profiles for all the instrumented sections in the pile. 191
A.42 Ironbridge P58Row2, bending moment profiles (calculated with ACM) for the full monitoring period. 191

List of Tables

2.1 Conventions used by cement chemists 14
2.2 OPC main compounds 14
2.3 Long term (90 days) concrete strength values (f_{cu}) on 100mm cube samples for the different sites 17
2.4 Summary of the results found in literature about shrinkage and creep . . 28

3.1 Grange Hill soil parameters 37
3.2 Mill Hill soil parameters 44
3.3 Concrete samples average results 55
3.4 Long term concrete strength (f_{cu}) values 55
3.5 Summary of the instrumented piles 57

4.1 Influence of cement/sand ratio on coefficients of thermal expansion . . . 75
4.2 Coefficients of thermal expansion for 1:6 concretes 75
4.3 Coefficients of thermal expansion for mass concretes 75

5.1 Parameters used in the ACM and MCM models for each site. 108

List of Symbols

A	Matrix of the strains measured by the up-slope strain gauges
ACM	Automatic Cracking Model
α	General coefficient of thermal expansion
α_c	Coefficient of thermal expansion of concrete
α_e	Effective coefficient of thermal expansion of a pile
α_{sg}	Coefficient of thermal expansion of a strain gauge
E_c	Modulus of elasticity of concrete
E_{cm}	Secant modulus of elasticity of concrete
E_g	Modulus of elasticity of grout
E_s	Modulus of elasticity of steel
ε_a	Absolute strain in strain gauge data analysis
ε_c	Concrete strain
ε_{c1}	Compressive strain in the concrete at peak stress
ε_{sg}	Strain measured by a strain gauge
ε_{t0c}	Strain limit of concrete in tension
ε_{tu}	Ultimate tensile strain of concrete in CFST piles
f	Frequency
f_{ck}	Characteristic compressive strength of concrete
$f_{ck,cube}$	Characteristic compressive cube strength of concrete at 28 days
f_{cm}	Mean value of concrete cylinder compressive strength
$f_{ctk,0,05}$	Characteristic axial tensile strength of concrete 0.05 fractile
f_{ctm}	Mean value of the axial tensile strength of concrete

f_{cu}	Ultimate compressive strength in a laboratory test
f_{yk}	Characteristic yield strength of reinforcement
I	Second moment of area
I_c	Second moment of area of a concrete slice
I_g	Second moment of area of a grout slice
I_s	Second moment of area of a steel slice
L	Length of the pile
MCM	Manual Correction Model
$\mu\varepsilon$	microstrain
ψ	Curvature
R	Strain gauge reading
σ_c	Concrete stress
T_0	Temperature datum
T_1	Temperature reading
X	Matrix of the global positions of the neutral axis
z_s	Depth of the slip surface

Form of declaration

I, Nicola Bicocchi, declare that the thesis entitled *Structural and geotechnical interpretation of strain gauge data from laterally loaded reinforced concrete piles,* and the work presented in the thesis are both my own, and have been generated by me as the result of my own original research.

I confirm that:

- This work was done wholly while in candidature for a research degree at this University.
- Where any part of this thesis has previously been submitted for a degree or any other qualification at this university or any other institution, this has been clearly stated.
- Where I have consulted the published work of others, this is always clearly attributed.
- Where I have quoted from the work of others, the source is always given. With the exception of such quotations, this thesis is entirely my own work.
- I have acknowledged all main sources of help.
- Where the thesis is based on work done by myself jointly with others, I have made clear exactly what was done by others and what I have contributed myself.

Signed:.....

Date:.....

Acknowledgments

I would like to thank the following people or organizations who have, in one form or another, provided precious help, support and advice over the last three and a half years of research.

First of all I would like to express my sincere thanks and gratitude to my supervisors Prof. William Powrie and Dr. Joel Smethurst for their guidance, help encouragement and patience which made possible to carry out this research.

Alex Zacharopoulos for his help, advice and long discussions about the structural analysis of piles.

Dr. Alan Bloodworth for his comments and advice on my 9 months report and Transfer report.

The Engineering and Physical Sciences Research Council that provided the studentship for carrying out this research.

Gemma for all her love, patience, support and wonderful time together outside the research project.

My family for their endless support and motivation throughout my entire life.

My housemates Marco, Lorenzo and Francesca for the wonderful time together, for the huge dinners and the constructive discussions.

All the friends that I have luckily met during my years in Britain who made it an invaluable life experience.

Chapter 1

Introduction

1.1 Background

Most of the earthworks for highways and railways were built decades ago, often over 100 years in the case of the railways. The design and construction methods used, in some cases, were not to modern standards. In some other cases, gradual deterioration and weathering of the structures has diminished their performance over the years. Today slope failure or excessive displacements are common problems affecting highway and railway slopes (both embankments and cuttings) in clay soils [O'Brien (2007)]. The problem is extremely delicate for railway embankments where even small displacements can modify the position of the tracks. To maintain high safety standards for modern fast trains, this can not be allowed. Highways, and other roads, can tolerate small movements, but the increasing volume of traffic, and thus load, can make movements too large and potentially dangerous for traffic vehicles. The road system is also subjected to an increasing volume of traffic, which in some cases requires a widening of the major roads and their supporting infrastructures. To limit the occupation of land (and thus to limit the costs) there is the tendency to build steeper slopes and retaining structures.

Figure 1.1: *Ironbridge stabilisation works, during the installation of the piles (left) and after the completion (right).*

Discrete piles are used increasingly to stabilise slope failures or as a preventative

method to increase the factor of safety of the slope. The method consists of one or more rows of piles in which the piles are spaced apart from each other and not connected in any way. The piles extend through the unstable soil into a stable layer (a bedrock where possible), acting as a restraint. The advantages of discrete piles over a retaining wall are reduced cost due to material saving and low environmental impact since the piles are completely buried in the slope (fig. 1.1). The method is still in development to understand which distance between the piles is most appropriate in relation to the soil characteristics, the loads applied to the pile and the expected behaviour of the structure. In particular the number of case studies about discrete piles is much smaller than for axially loaded piles and for active laterally loaded piles (where the load is applied at the top of the pile).

There are some uncertainties in understanding the measurements of the long term behaviour of discrete piles. These uncertainties are connected with the calculation of the effective bending moment profile and the relative displacement of the pile and of the soil; the calculation of the pattern of soil pressures acting on the pile resulting from slope movements; and the specific long term behaviour of a discrete concrete pile. Effective determination of bending moment profile is dependant on the different instruments used to measure the bending strains, concrete parameters and theories used to calculate bending moment. For example, there can be quite large differences between assuming concrete is uncracked or fully cracked [Ng et al. (1992)]. This generates a range in the results from the same instruments which only increases the uncertainties. Creep, shrinkage and temperature effects can also influence the data output of some instruments leading to a further error in the bending moment results. Fellenius et al. (2009) analysed some of the effects of temperature and shrinkage in piles, but the research about the effects of creep on concrete piles is still poor. Some other difficulties lie in the calculation of the soil pressure distribution from measured bending strains and displacements, and different authors have approached the problem in different ways [Nip and Ng (2005), de Sousa Coutinho (2006)], leaving the choice of the best method unclear. All this makes the analysis of the long term structural behaviour of a concrete discrete pile difficult.

It is necessary to monitor discrete piles in different conditions (type of slope, material, dimensions and parameters) to fully understand their behaviour. Of particular interest is the behaviour over long periods of time since the pile can follow different mechanisms to resist the movement of the unstable slope. Idealised failure modes for rigid piles stabilising sliding ground have been introduced by Broms (1964) and further analysed by Viggiani (1981) and Poulos (1999). The pile can be fixed in the stable layer and the unstable soil flows around it; the pile can rigidly rotate around a point close to its base; or it can be dragged by the unstable layer, ploughing through the stable one. The ultimate mechanism is typically determined during the design phase, but the pile can have a different intermediate behaviour during service depending on many factors (soil parameters, spacing, depth of the slip surface, design of the pile, concrete parameters). The analysis of case histories can widen the understanding of the influence of

the different parameters. A long term analysis can reveal the complex behaviour of the pile/slope interaction and the impact of seasonal variations on the pile displacements. This is important in clay slopes where the seasonal variation of water content can play a central role in instability and shrinkage and swelling in clay materials. Increasing pore water pressure in the slope can lead to slope movements that increase the load on the piles and, potentially, cause displacements of the entire structure. The magnitude of the seasonal variations are connected with the type of vegetation covering the slope, increasing the complexity of the problem. Only a few studies have been carried out on the effects of vegetation on the pile behaviour in volume sensitive clays (e.g.Crilly and Driscoll (2000)).

During monitoring, the type of instruments used plays a major role. There is usually the possibility to check between different instruments, to verify the results obtained. The analysis of the instrumental data have to take into account all the actions affecting the structure and the concrete properties. It is likely that an appropriate method must be used for each instrument and adapted to the specific structure to obtain reliable information. As introduced earlier, the interpretation of the results must also take into account specific concrete processes and parameters which can modify the behaviour of each instrument. For example, the presence of cracking modifies the stiffness of the pile; the evaluation of the Young's modulus of concrete affects the magnitude of the bending moment calculated [Ng et al. (1992)]; the magnitude of shrinkage can modify the strains in the pile [Fellenius et al. (2009)], and the development of creep which can also affect the bending strain.

To monitor piles, it is common to use inclinometers, which measure the displacements along the pile. Strain gauges (usually the vibrating wire type) are also increasingly used to measure the strains in specific locations of the pile. The influence of some of the above on both instruments are not fully established and developed, but there is the potential to generate a method to fully analyse the behaviour of piles that takes into account all the influences and parameters.

1.2 Aims and objectives of the research

The aim of this research is to understand the structural and geotechnical behaviour of an instrumented reinforced concrete pile using measured strains and displacement data. Instrumented piles from four sites are considered. The following objectives have to be met in order to reach the aim of the research:

1. Understanding and quantification of the concrete processes (shrinkage, creep, cracking and temperature) and parameters (stress/strain curves and strength of concrete) on the piles and their effects on the instrumentation;

2. Development of a method to interpret the data coming from the instruments (vibrating wire strain gauges and inclinometers) which takes into account the concrete processes and parameters;

3. Development of a more accurate method for the calculation of the bending moment affecting the piles (both standard reinforced concrete and circular concrete-filled steel tubular piles) that takes into account the non-linearity of the stress/strain curves and the effects of cracking;

4. Improving the method for the comparison of bending moment and displacement profiles to check the consistency of strain gauge and inclinometer results and to develop shear force and soil pressure profiles;

5. Study of the geotechnical behaviour of the piles, analysing:

   - pile/slope interactions,
   - soil pressure distribution,
   - relative movements between the pile and the soil.

1.3 Summary of the chapter contents

Chapter 2: Background

All the technical details and theoretical principles of the instrumentation used (vibrating wire strain gauges, inclinometers, thermistors and data-loggers) are considered. The relevant literature about concrete materials and properties (strength of concrete and stress/strain curves for different types of pile) is presented. Particular attention is placed on the analysis of shrinkage, creep and cracking effects (concrete processes) and on the way they affect the instrumentation readings.

Chapter 3: Instrumented sites and raw data

This chapter shows the layout of each instrumented site, with technical plans, views and sections of each instrumented pile. The position and the identification for each instrument are shown.

Chapter 4: Interpretation of strain gauge data

The analysis of strain gauge data is explained in detail and considers how to obtain absolute strains from the data-logger reading; how to correctly set the datum; and how to remove interferences. The temperature correction approaches used are demonstrated using three case histories. A method for detecting concrete cracking with strain gauges is considered and applied to two particular cases.

Chapter 5: Calculation of bending moment using strain gauge data

Two new methods are developed for the calculation of the bending moment in the piles using strain gauge data. One automatically considers the opening of cracks (Automatic Cracking Method, ACM), while the other considers the concrete uncracked until the strain gauges show the presence of a crack, then the results are manually corrected

for each cracking event (Manual Correction Model, MCM). The models are tested by application to four different piles from four different sites and the results are used to understand which model is giving the best results in the particular situations.

Chapter 6: Inclinometer results and curve fitting analysis

The typical displacement profiles calculated from the inclinometer readings for each site are presented. The curve fitting method used for the comparison between strain gauges and inclinometer results is discussed. This method is used to develop approximated shear force and soil pressure profiles. The application of the method to a typical pile from each site and the respective results (bending moment, displacement, shear force and soil pressure profiles) are presented.

Chapter 7: Geotechnical interpretation

The structural behaviour of the piles and the pile/soil interactions for each site are analysed and discussed using the measurements and results developed in the previous chapters. The geotechnical behaviour of the piles is compared with the theoretical results developed by Poulos (1999).

Chapter 8: Conclusions

Summary of all the conclusions reached during the analysis of the instrumented piles.

Appendix

The measured data (strains, temperatures and displacements) and the calculated results (bending moments and axial strains) are shown for every instrumented pile used in this thesis.

1.4 Main conventions and definitions

The main conventions and definitions used in thesis are listed below for clarity:

- **Strains.** Positive strains show tension, negative strains show compression. Strains are measured in $\mu\varepsilon$(microstrains).
- **Bending moment.** Positive bending moment shows that the pile is bending up-slope, while negative bending moment is given by the pile bending down-slope. Bending moments are given in kNm.
- **Displacements.** Positive displacements show that the pile is moving down-slope, while negative show that it is moving up-slope. Displacements are measured in mm.
- **Axial strain.** The average of two strain gauge readings in the same instrumented section. Axial strains are measured in $\mu\varepsilon$(microstrains).

Chapter 2

Background

The study of instrumented reinforced concrete piles requires a wide understanding of concrete properties, concrete behaviour, and the interactions with the instrumentation. Concrete has a complicated behaviour and most of its properties vary with time and with the level of stress applied to the member. The main instrumentation used (vibrating wire strain gauges and inclinometers) records strains and displacements. This means that the analysis of the structural behaviour has to be carried out starting from the strains to obtain the bending moments affecting the pile. This approach is completely opposite to that used during design. The analysis is also complicated by the on site conditions, which means that the piles are subjected to all effects (loading, cracking, shrinkage and creep, temperature, instrumental errors) at the same time and many of these effects are out of direct control. Also for this reason, it is necessary to have a clear understanding of the behaviour of concrete and its effect on the instrumentation which give strain or displacement readings for all effects at once. During the analysis , it is necessary to identify, quantify and separate the different effects.

This chapter analyses the instrumentation and its functioning; the different properties and effects of concrete; and the interaction between the concrete and the instrumentation.

2.1 Instrumentation

This section describes the instruments used in the research. They can be divided into two groups:

Principal instruments : Vibrating Wire Strain Gauges and Inclinometers used to measure primary effects (strains and displacements).

Secondary instruments : Thermistors and Data-loggers used to measure temperatures and to record data.

2.1.1 Vibrating wire strain gauges

A vibrating wire strain gauge works on the principle that the fundamental natural frequency of a wire is related to the tension within it [Nield et al. (2003)]. Thus the

instrument measures the frequency of a wire tensioned between two plates fixed to the structure. Using physical relations is then possible to obtain the strain variation of the wire (par. 4.1). An accuracy of a few με can be achieved using the manufacturer calibration. This is possible because for this type of strain gauge, the measured strain depends only on the frequency of vibration and the original gauge length. Once a datum is set, the instrument measures the variation of strain of the structure to which it is connected. It is important to highlight that strain gauges do relative measurements only.

There are several types of vibrating wire strain gauges which are suited to different purposes; in this research Embedded Strain Gauges, Sister Bars and Welded Strain Gauges are used. The first two types are used to measure the strains in the concrete, while the last gives the strains on the steel reinforcement to which it is welded. All these instruments are based on the same principle of operation, but they use different methods to transfer strain from the concrete or the steel to the vibrating wire:

Embedded Strain Gauges (figures 2.1 and 2.2) have two small end plates attached to the principal rods and between which the vibrating wire is connected. The body of the strain gauge is then fixed with two small diameter rods and ties to the reinforcement bars to keep the instrument in position during the cage installation. The overall length is usually between 0.10 and 0.15m. They are delicate instruments and it is necessary to install the cage into the concrete with great care.

Sister Bars use a reinforcement bar (usually about 1.40m long) to which the vibrating wire is connected over a short central section. The bar is positioned close to the other reinforcement bars of the cage and fixed with ties to keep it in position during the cage installation (figures 2.1 and 2.3). The overall instrument length is usually between 1.00 to 1.40m. Sister Bars are less delicate then Embedded Strain Gauges because the instrument itself is slightly more protected by the rest of the reinforcement bars.

Welded Strain Gauges have the same body as the Embedded type, but the connections consist of two steel brackets (figures 2.1 and 2.4). The brackets are first welded to the reinforcement and the strain gauge body is then connected later when the temperature has returned to normal. This is to avoid damage to the vibrating wire gauge coming from the high temperatures during welding.

Strain gauges are usually installed in pairs in the same cross section of the pile in the direction of the maximum bending strain.

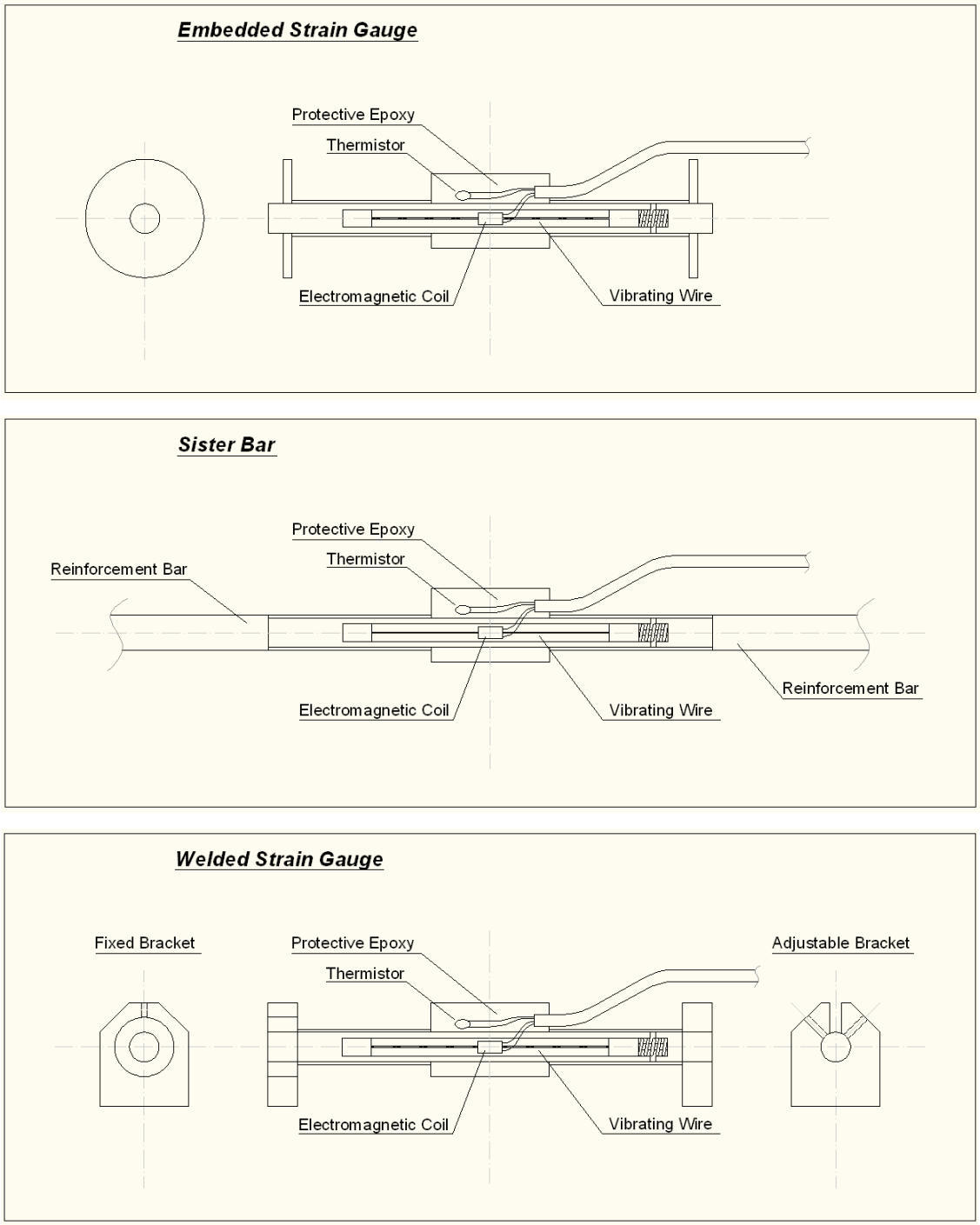

Figure 2.1: *Schematic drawings for the different types of strain gauges*

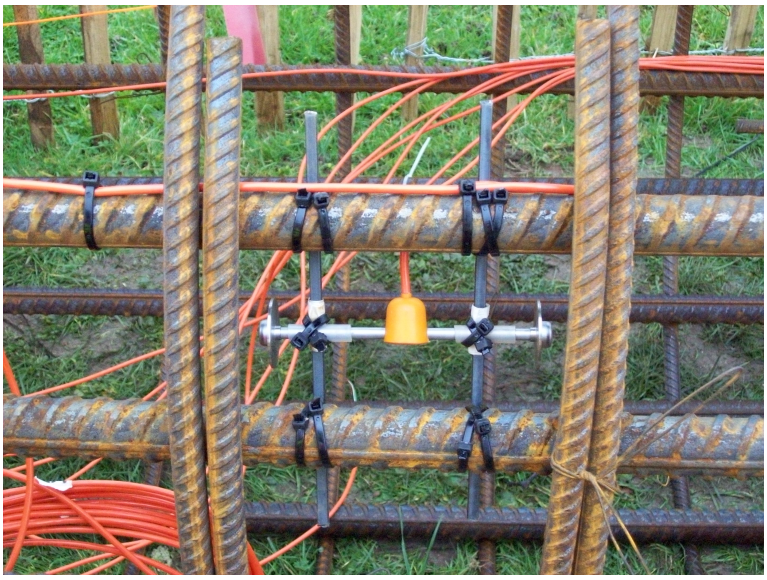

Figure 2.2: *Embedded strain gauges*

Figure 2.3: *Sister Bar*

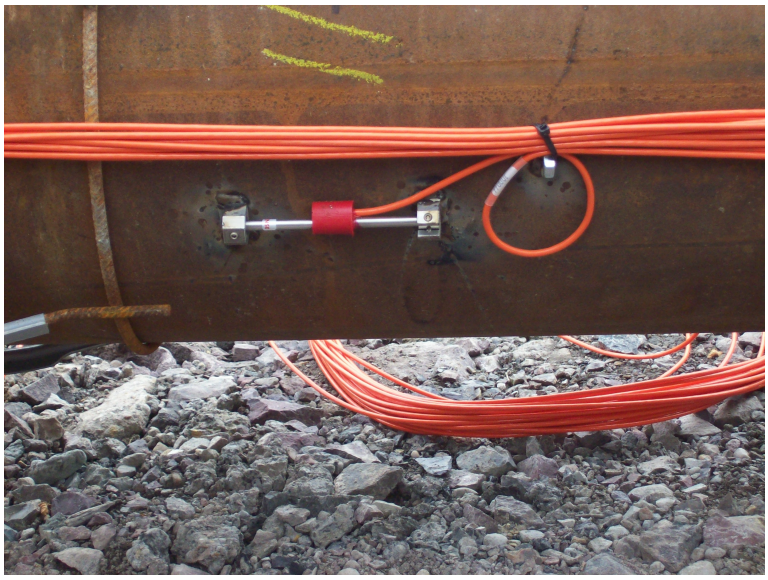

Figure 2.4: *Welded strain gauges*

Strain gauges are designed to operate continuously; this means they are connected to a data-logger that reads the instruments at a fixed time interval (e.g. every hour). In this way it is possible to record an accurate strain history of the structure that can also show daily cycles.

Due to their principle of operation and their suitability for long term recording, strain gauges have some obvious advantages but also some disadvantages. These have to be known in order to analyse and interpret the data in the correct manner:

Thermal effects are one of the most important potential problems because the frequency readings of the vibrating wire are so accurate that the slightest variation in environmental temperature will modify them. To avoid this, every strain gauge is equipped with a thermistor that measures the temperature and makes it possible to correct the readings if necessary. This will be discussed further in par. 4.4.

Curing effects include an increase in temperature due to exothermic chemical reactions during the hardening of the concrete. The peak temperature is usually reached about 2 days after pouring, and can be over 60^{o}C (in the analysed data it reached around 40°C). Dissipation of the heat usually takes 10-30 days depending on the thickness of the structure and the environmental conditions [Muir Wood (2004)]. During the curing process the strain gauges respond mostly to thermal effects rather than strain effects. Corrections for this are discussed in par. 4.2.1 and par. 4.2.2). It must not be forgotten that in this same period shrinkage effects (plastic and autogenous shrinkage) also take place in the concrete (par. 2.4.1). Thus it is extremely important to set a reliable strain datum (par. 4.2.2) and to adjust the data to this to ensure an accurate long term analysis.

Interference and breakage, may also affect the readings. Since strain gauges are very

delicate instruments they have to be installed with great care. The most vulnerable point is the installation of the cages and the pouring of concrete; at this stage the strain gauge can be seriously damaged and this can compromise the entire instrumentation effort. Thus it is necessary to install the cages and pour the concrete with great care, using devices such as spacers for the cages and in some cases additional steel plates that protect the gauges from falling concrete. The instruments can show interference in the readings, and some short periods of inactivity/incorrect reading. These can be explained by ground water getting into the instrument core or into the cables. Consequently it is necessary to install the strain gauges and cables taking care not to let the latter gets in tension during the installation of the cages and the pouring of concrete. In this way they should remain watertight and without unnecessary stresses which can cause them to rupture. Another cause of interference is the sensitivity of the strain gauge to electromagnetic fields. In the presence of a strong electromagnetic field (such as from welding equipment), the strain gauge-cable acts as an antenna. Interference can also be produced by strong sources of vibrations such as pneumatic drills or the installation of driven piles. Interference can also be caused by problems in the data-logger (par. 2.1.4). Examples of interferences and cleaning methods are shown in par. 4.3.

2.1.2 Inclinometers

An inclinometer is an instrument used to measure the lateral displacements and rotations of a structure or of a slope, in a vertical plane. It comprises a pipe (usually made of PVC or aluminium) installed into the structure or into the slope. Inside the pipe there are two pairs of perpendicular tracking grooves in which a probe can run. The probe is the real measuring instrument; it contains a gravity-sensing transducer to measure the inclination of the pipe casing where it deviates from the vertical. The inclination is usually recorded every 50 cm, starting from the bottom. The instrument then automatically calculates the displacements of the structure from the vertical, referring to the bottom of the pipe which is assumed not to move. To evaluate the incremental displacements it is necessary to compare two or more readings separated in time [Dunnicliff (1993)]. As the variation of strain for strain gauges, inclinometers give a displacement relative to the chosen datum.

The type of inclinometer used in this research is a discontinuous instrument which always needs an operator to read it. This means that while for the strain gauges data are produced every hour, an inclinometer reading is usually produced only every three or four months. On the other hand the inclinometer is not influenced by interference or thermal effects and this make it a reliable instrument. Also continuous reading, or in place inclinometers exist on the market; they are formed of a string of probes permanently positioned inside the case. The probes are then connected to a data-logger for continuous reading.

2.1.3 Thermistors

The word "Thermistor" is the union of the two words "Thermometer" and "Transistor" and the instrument is used to measure the temperature. Essentially a thermistor is composed of semi-conductive material which, changes its resistance very markedly with temperature, connected to a measuring instrument. Any device used to "read" the semiconductor must apply only a very small current, otherwise the temperature of the thermistor will be changed significantly. This kind of instrument is usually used for monitoring the temperature of another instrument (in this case a strain gauge) so that a temperature correction can be applied [Dunnicliff (1993)].

2.1.4 Data-logger

Usually considered of marginal importance, the data-logger is at the heart of the data collection system. It is very important to protect and upkeep it, because any kind of misreading of the instruments or breakage can lose important information. Common problems with data-loggers are :

Breakdown of the power supply and consequent loss of all the functions. The usual cause of low voltage is the battery breakage or theft/vandalism of the solar panel used to recharge it or of the modem used for the remote control. It is very important to check frequently the functionality of the machine (usually just by downloading the data) to avoid long periods of inactivity. A heavy duty cabinet with strong locks and welded connections for the solar panel and antenna are advised.

Overheating caused by sun exposure can modify the readings and the recording of the data. If possible, it is best to install the data-logger in a protected place (e.g. inside a building or next to a structure).

External damage has to be avoided as much as possible. It is very important to cover and protect all the cable connections from the attack by rodents or other animals.

Water ,and humidity in general, have to be avoided inside the data-logger box due to the presence of electronic circuits.

2.2 Concrete material

Concrete is generally composed of cement (in the majority of cases Portland cement) and aggregates (different kinds of sand and gravel). Other cementitious materials (fly ash and Ground Granulated Blast-furnace Slag) can be used, but generally in small proportions in combination with Portland cement. It is thus important to understand the chemistry and reactions that take place within the Portland cement as concrete behaviour and the concrete processes analysed later are intimately connected to it.

2.2.1 Portland cement

The definition of Ordinary Portland Cement (OPC) is generally given as:

a cement obtained by intimately mixing together calcareous and argillaceous (or other silica-, alumina-) and iron oxide-bearing materials, burning them together at a clinkering temperature, and grinding the resulting clinker. Gypsum, or nowadays other materials, may also be added or blended after burning. [Neville (1995)].

The raw materials for the production of OPC are primarily calcareous materials, such as limestone or chalk, and alumina and silica, found as clay or shale. These materials are found all over the world making OPC the most common type of cement. Using different methods, depending on the type of production process (wet, dry or semi-dry), the raw materials are crushed, blended and mixed and then introduced in the kiln. Here the admixture is burned at 1450^{o}C and the clinker is produced. Gypsum or other materials are then added and the admixture is ground and prepared to be used for the production of concrete or mortar. In this final stage the OPC is composed of four main compounds as shown in Table 2.2. Other minor compounds are also present in the cement. The most important of these are the alkalis (oxide of sodium Na_2O and potassium K_2O), which can have a large influence on the cement hardened properties following hydration.

Formula	*Convention*
CaO	C
SiO_2	S
Al_2O_3	A
Fe_2O_3	F
H_2O	H

Table 2.1: *Conventions used by cement chemists [Neville (1995)]*

Name of compound	*Oxide composition*	*Abbreviation*
Tricalcium silicate	$3CaO.SiO_2$	C_3S
Dicalcium silicate	$2CaO.SiO_2$	C_2S
Tricalcium aluminate	$3CaO.Al_2O_3$	C_3A
Tetracalcium aluminoferrite	$4CaO.Al_2O_3.Fe_2O_3$	C_4AF

Table 2.2: *OPC main compounds [Neville (1995)]*

2.2.2 Hydration of cement

The hydration of cement is the set of complex chemical reactions which occurs when the cement comes into contact with water. These reactions are necessary to transform the cement powder into a bonding agent. In the presence of water the compounds of cement (silicates and aluminates) form products of hydration which in time produce a firm and hard mass. The two calcium silicates (C_3S and C_2S) are the main cementitious compounds in cement, and the physical behaviour of cement during hydration is similar

to that of the two compounds alone [Neville (1995)].

The exact reactions of the hydration of C_3S and C_2S are not certain. Usually it is assumed that the main product of the hydration of both compounds is $C_3S_2H_3$ as shown in the non-stoichiometric equations:

$$2C_3S + 6H \rightarrow C_3S_2H_3 + 3Ca(OH)_2 \tag{2.1}$$

$$2C_2S + 4H \rightarrow C_3S_2H_3 + Ca(OH)_2 \tag{2.2}$$

Both reactions are exothermic and are responsible for the increase in temperature during the hardening of cement and concrete. It is important to note that the rate of hydration decreases continuously, so that even after years there remains an appreciable amount of unhydrated cement. Considerable strength is possessed long before the reactions of hydration are complete. Thus it seems that a small amount of the hydrate binds together the unhydrated remainder. Further hydration results in little increase in strength [Neville (1995)]. It is possible to divide the hydration process into two parts, the first from the initial contact between cement and water to the end of appreciable production of heat by the hydration reactions; the second taking into account all the hydration reactions that occur after this time.

The products of hydration of C_3A and C_4AF have a negative influence on the cement because the former has a violent reaction with water that leads to immediate stiffening of the paste (flash set); while the latter reacts with the gypsum forming a calcium sulfoaluminate that accelerates the reactions of the silicates. The reason for their presence in the cement is that they are necessary for the cheap and rapid production of OPC. To reduce their negative influence (especially that of C_3A) gypsum is added during the grinding of the clinker.

Many of the mechanical properties of hardened cement depend not so much on the chemical composition of the hydrated cement as on the physical structure of the hydration products. At any stage of hydration, the hardened paste consists of very poorly crystallised hydrates of the various compounds, generally called gel, of crystals of $Ca(OH)_2$, some minor components, unhydrated cement, and the residue of the water-filled spaces in the fresh paste. These voids are called capillary pores, to distinguish them from the gel pores (which are two orders of magnitude smaller, at about 3nm). The actual source of strength of the gel is not fully understood but probably arises from two kinds of cohesive bonds [Neville (1995)]:

- I) the physical attraction between solid surfaces (van der Waals' forces).
- II) chemical bonds. Because cement gel particles cannot be dispersed by addition of water, it seems that the gel particles are cross-linked by chemical forces.

2.3 Properties of concrete

2.3.1 Strength of concrete

As Neville (1995) points out, strength is commonly considered the most valuable property of concrete. Two are the principal strengths usually considered: compressive and tensile. Compressive strength is by far the most important for design purposes while the tensile strength is usually neglected or approximated as a function of the compressive strength. This relation is not of direct proportionality and it is usually expressed with empirical formulae [Neville (1995)]. Tensile strength is also difficult to measure and different tests (flexure, direct tension and splitting) are used. These usually give different results for similar concrete samples making it complicated to express in a numerical relation. It is always necessary to state the tests employed when expressing the ratio of tensile and compressive strengths [Neville (1995)]. The relation that best fits the experimental results (using splitting tensile strength and compressive strength on standard cylinders) in Neville (1995) is also used in BS EN 1992 (2004):

$$f_{ctm} = 0.30 \times f_{ck}^{(2/3)} \tag{2.3}$$

Where f_{ctm} is the mean value of the axial tensile strength of concrete and f_{ck} is the characteristic compressive cylinder strength of concrete at 28 days [BS EN 1992 (2004)].

Both strengths of concrete depend on many factors: water/cement ratio, gel/space ratio, porosity, properties of the aggregates, aggregate/cement ratio, changes in moisture/humidity, changes in temperature and age of concrete [Neville (1995)]. The last three factors are important when considering the properties of a sample of an assigned material at different times, for example in the long term analysis of a concrete structure. Assuming constant moisture/humidity and temperature of the sample, the compressive strength of a concrete produced in 1923 is roughly proportional to the logarithm of the age up to about 50 years, with an increase of about 2.4 times the 28 day strength . The same experiment on concrete samples produced in 1937 shows a logarithm increase in strength for 10 years and then the strength remaining constant or decreasing [Neville (1995)]. Modern concretes show earlier peaks in strength, but still later than 28 days [Neville (1995)]. No more accurate empirical relations are given because of the high number of variables involved. For accurate analysis it is necessary to collect an adequate number of concrete samples and test them in the laboratory at different times to draw the strength/time curve.

2.3.2 Young's modulus of concrete E_c and stress/strain curves

It is well known that concrete does not have a linear elastic behaviour under load (for both compression and tension) [Neville (1995)]. For simplified analysis and practical purposes, it can be assumed that concrete behaves linearly in the first part of loading. The slope of the stress/strain curve is usually approximated by the *secant modulus* [Neville (1995)]. Different codes have different specifications for the determination of the secant modulus and the test specimen and apparatus. To consider the first part

of the concrete stress/strain curve to be linear is one of the main assumptions used in design. For the back-analysis of concrete behaviour using strain data, it is more appropriated to use the full stress/strain relationship. The best approach would be to obtain the stress/strain curves from laboratory tests on concrete samples taken from the analysed piles. In the majority of the cases, this is not possible, mainly for statistical reasons; the number of samples tested, of each kind of concrete, is not high enough to be representative. Different solutions have been used in this research to overcome this problem and stress/strain relationship from BS EN 1992 (2004) and specific laboratory test analysis [Liang and Fragomeni (2010)] have been used. The following paragraphs describe the stress/strain curves used for standard reinforced concrete piles and that used for circular concrete-filled steel tubular piles.

2.3.2.1 Stress/strain curves for standard reinforced concrete piles

In the analysis of standard reinforced piles, the curves described by BS EN 1992 (2004) have been used. Specifically, the concrete is modelled using equation 2.4 (equation 3.14 on page 33 of BS EN 1992 (2004)):

$$\frac{\sigma_c}{f_{cm}} = \frac{k\eta - \eta^2}{1 + (k-2)\eta} \tag{2.4}$$

where:

- σ_c =concrete stress;
- $\eta = {}^{\varepsilon_c}/_{\varepsilon_{c1}}$;
- ε_c = concrete strain;
- k = 1.05 $E_{cm} \times \mid \varepsilon_{c1} \mid / f_{cm}$
- E_{cm} = secant modulus of elasticity of concrete;
- ε_{c1} = compressive strain in the concrete at peak stress;
- f_{cm} = mean value of concrete cylinder compressive strength;
- f_{cm}, ε_{c1} and E_{cm} are taken from table 3.1 of BS EN 1992 (2004) using different values of $f_{ck,cube}$ (characteristic compressive cube strength of concrete at 28 days) depending on the sites (table 2.3). $f_{ck,cube}$is evaluated from laboratory tests (f_{cu}) and compared between different instrumented piles.

Leatherhead *(concrete)*	Grange Hill *(concrete)*	Mill Hill *(concrete)*	Ironbridge *(concrete)*	Ironbridge *(grout)*
f_{cu}= 55 MPa	f_{cu}= 50 MPa	f_{cu}= 50 MPa	f_{cu}= 57 MPa	f_{cu}= 33 MPa

Table 2.3: *Long term (90 days) concrete strength values (f_{cu}) on 100mm cube samples for the different sites*

The stress/strain curve from Equation 2.4 (fig. 2.5) represents the non-linear behaviour of concrete. The concrete in tension is assumed to have the same behaviour as the concrete in compression until the limit $\varepsilon_{t0c} = f_{ctk,0,05}/E_c$. Where $f_{ctk,0,05}$ is the characteristic axial tensile strength of concrete 5% fractile from BS EN 1992 (2004) table 3.1; and E_c is the Young modulus of concrete. The mean characteristic axial tensile strength of concrete is more appropriate for back analysis, but since no recommended values were present, $f_{ctk,0,05}$ (which is generally used in design) was used. The tensile curve and its limit are only an approximation to the behaviour of concrete in tension since no laboratory tests were possible on the concrete used for the piles.

The behaviour of steel was also modelled using BS EN 1992 (2004) with the idealised stress/strain curve shown in fig. 2.6. In practice the program uses only the first segment of this curve as the measured strains are small compared to the curve limits (the value of f_{yk}/E_s is usually greater than $2000\mu\varepsilon$ while the measured strains are never higher than $500\mu\varepsilon$).

The model can easily be modified to follow different stress/strain relations from different codes or laboratory tests.

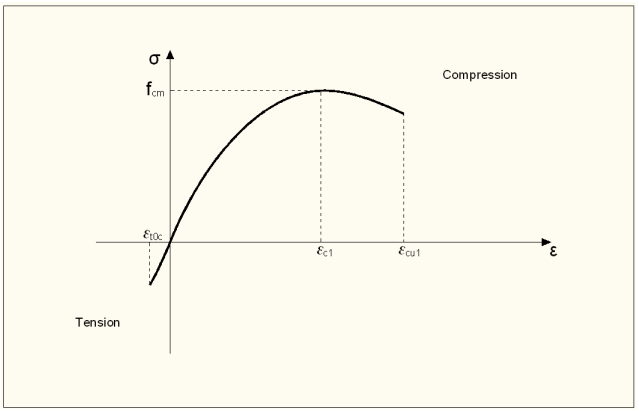

Figure 2.5: *Stress/strain curve for concrete used in the bending moment calculation of standard reinforced concrete piles [BS EN 1992 (2004)]*

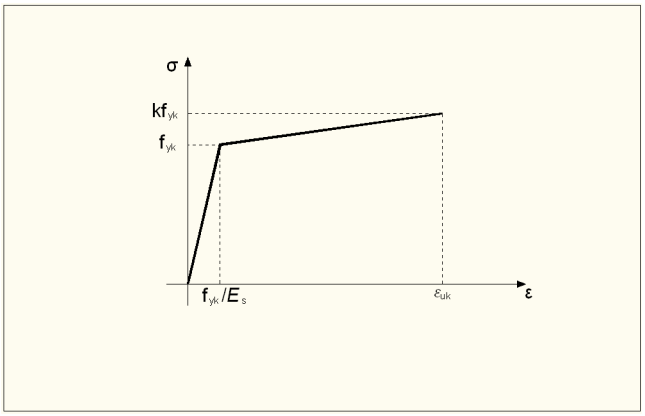

Figure 2.6: *Idealised stress/strain curve for steel (for tension and compression) used in the bending moment calculation of standard reinforced concrete piles [BS EN 1992 (2004)]*

2.3.2.2 Stress/strain curves for circular concrete-filled steel tubular piles

Some of the piles analysed in this research are cast in place circular concrete-filled steel tubular piles; i.e. the pile is formed by a circular hollow steel pipe filled with concrete. To protect the steel tube, a ring of grout or sometime concrete is poured between the shaft and the steel pipe.

The stress/strain curves used for concrete and steel (fig. 2.7 and fig. 2.8) come from the extensive work done by Liang and Fragomeni for both eccentric [Liang and Fragomeni (2010)] and axial loading [Liang and Fragomeni (2009)]. A more in depth analysis of concrete filled steel tubular beam-columns behaviour and the respective numerical analysis has been carried out by Liang (2011a) and Liang (2011b).

The behaviour of the concrete core is very different from that of a standard reinforced concrete pile. The steel pipe restrains the concrete core, increasing its strength and ductility. Confinement gives the concrete core increased strength in tension and a bulk softening behaviour instead of an abrupt breakage when the limit stress (fig. 2.7) is reached [Liang and Fragomeni (2010)]. The explanation of the softening behaviour is discussed in par. 2.5.2.

The external ring (made of grout or concrete) is considered to have the same stress/strain behaviour as the concrete in standard reinforced concrete (par. 2.3.2.1).

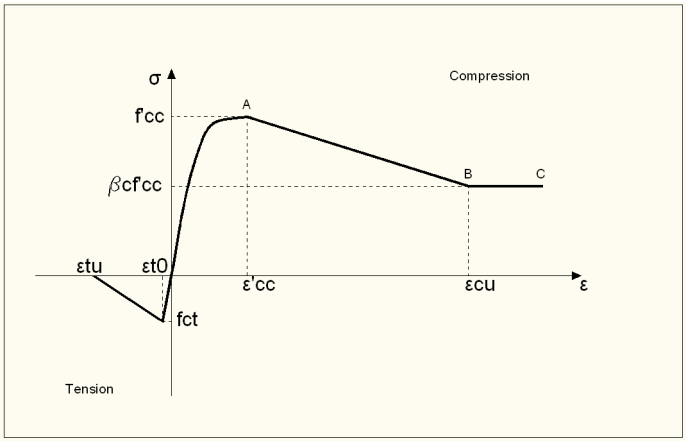

Figure 2.7: *Stress/strain curve for the concrete core of a hollow steel pipe pile [Liang and Fragomeni (2010)] used in the bending moment calculation*

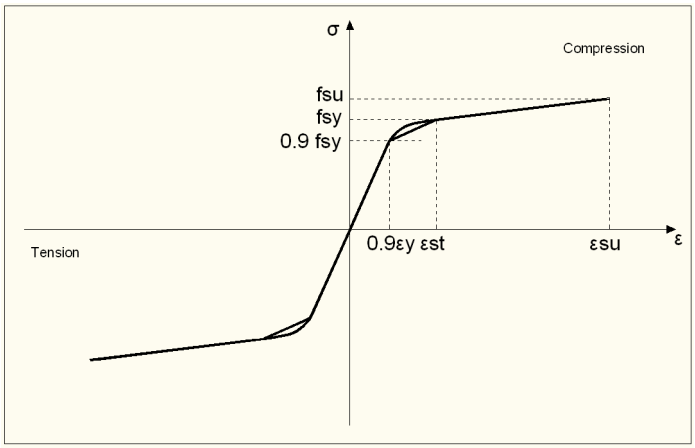

Figure 2.8: *Stress/strain curve for the steel of a hollow steel pipe pile [Liang and Fragomeni (2010)] used in the bending moment calculation*

2.4 Creep and shrinkage

Theoretically every concrete sample and structure is affected by shrinkage and creep effects. Shrinkage is a reduction of strain due to hydration of concrete (at various stages, including after setting), while creep is a variation of the strain of the sample at constant stress and temperature. Shrinkage and creep are both connected to the chemical-physical processes of hydration of concrete, but shrinkage is independent of the stress applied to the sample while creep is highly dependent on it.

The strain gauge readings and the related analysis (for understanding the behaviour of the structure) are affected by the variation of strain due to shrinkage and creep. The instrument can record variation in strain which is not related to the changing of the forces applied to the structure. It is thus important to understand and quantify shrinkage and creep effects in order to take them into account during the structural analysis.

Shrinkage and creep have both macroscopic and microscopic behavioural aspects. This research is concerned with the macroscopic effects only, understanding that the microscopic behaviour is the direct cause. The following paragraphs analyse the two processes in more detail showing that one of the major factors affecting the processes is the humidity/moisture of the concrete and the environment and the respective humidity/moisture gradient. Using information in the literature about shrinkage and creep under different conditions, the difference between the effects of shrinkage and creep on exposed concrete and underground concrete is analysed.

2.4.1 Shrinkage

Concrete shrinkage is the decrease with time of concrete volume due to changes in moisture content and physical-chemical changes [ACI Committee 209 (1992)]. Shrinkage is not connected to the stress in the structural member (i.e. shrinkage is always present in a concrete member). The general process of shrinkage is divided into four mechanisms

depending on the physical-chemical processes taking place within the concrete during its life. It is important to understand each of these mechanisms to appreciate the general process.

2.4.1.1 Plastic shrinkage

Plastic shrinkage takes place while the concrete is still in the plastic state (i.e. just after pouring). It is a volume reduction caused by water being lost during the first part of the hydration process. It is also caused by evaporation, seepage from form-work or, for piles, sorption by dryer soil [Neville (1995)]. Plastic shrinkage starts immediately after pouring and continues until the concrete has gained its initial strength (i.e. when the first part of the hydration process finishes, par.2.2.2). The order of magnitude of the contraction is one per cent of the absolute volume of cement paste [Neville (1995)]. Plastic shrinkage is affected by the amount of water loss. Cracking can develop as a result of shrinkage (plastic shrinkage cracking), but it can be eliminated with a complete prevention of evaporation immediately after casting [Neville (1995)].

For piles and other underground structures, plastic shrinkage is affected by the position of the water table, the soil porosity and the pore water pressures.

Plastic shrinkage affects the strain gauge readings only if the data-logger starts to record immediately after pouring. If the readings start after the concrete has hardened there is no influences on the data.

2.4.1.2 Autogenous shrinkage

Autogenous shrinkage is uniform and it is considered to be an intrinsic characteristic of the material. This phenomenon starts when the concrete gains its initial strength, and is connected to the second part of the hydration process. Hydration of the cement continues long after setting and consumes part of the mixing water. This leads to drying within the material (called self-dessication to distinguish it from the "drying" that occurs by loss of water to the outside) because the reduction of volume by water consumption is only partly offset by the increase of solid matter. The volumetric balance shows a deficit of the order of 10%. The reduction of volume leads to a strain of the mineral matrix [Acker and Ulm (2001)].

For concrete with a normal moisture content (water/cement ratio greater than 0.45) the rate of autogenous shrinkage with time closely matches the evolution of mechanical strength . The rate of shrinkage is also uniform inside the structure [Acker and Ulm (2001)].

Autogenous shrinkage remains less than 10^{-4} (100 $\mu\varepsilon$) in concretes where the water/cement ratio is greater than 0.45, but it increases quickly when the ratio falls below 0.40 and it can reach $3\text{x}10^{-4}$ (300 $\mu\varepsilon$). The total autogenous shrinkage remains moderate but in some cases its effect is not negligible when it is added to the other shrinkages in a long term analysis [Acker and Ulm (2001)].

Autogenous shrinkage is an intrinsic phenomenon that can be considered uniform in the volume of a structural element. This means that in a structural element not restrained by its bearings or its form-work, shrinkage has almost no mechanical effects. On the contrary in an element under conditions of total restraint there will always be damage to the structure (shrinkage cracking), considering that the stresses due to restrained autogenous shrinkage can easily reach the tensile strength of the concrete [Acker and Ulm (2001)].

Since autogenous shrinkage is uniform along the volume of the structure, it also has a uniform compressive effect on the strain gauges.

2.4.1.3 Drying shrinkage

Drying shrinkage is a further volume reduction caused by the removal of water from the unrestrained hydrated cement paste (gel) [Neville (1995)]. The movement of water is affected by environmental conditions (where air humidity or soil moisture content are the most important) and the micro-structure of the concrete (since the water movement is happening in the capillary pores).

In contrast with autogenous shrinkage (self-dessication shrinkage), the kinetics of drying shrinkage do not reflect those of the micro-mechanism that causes it within the material (water-vapour phase change with capillary tension), but rather the spread within the structure of the phenomenon that generates it. The degree of drying varies across the thickness of the concrete section between its maximum value (at the surface) and its minimum value (at the core) [Acker and Ulm (2001)]. The measured drying shrinkage is then a volume average of the effect including the respective skin cracking and micro-cracking. The drying shrinkage, so measured, varies between 2 and 6×10^{-4} [Acker and Ulm (2001)].

Drying shrinkage depends on the size of the structural element and its environment, and therefore it is not an intrinsic characteristic of the material. The process is extremely slow and for a specimen 16 cm in diameter it takes 10 years; beyond a thickness of 50 cm the duration of drying shrinkage is counted in centuries [Acker and Ulm (2001)]. However for normal structures in the open air it is considered that the larger part of drying shrinkage occurs in the first year after pouring. After this, it is usually considered that shrinkage effects are negligible compared with creep effects.

In normal applications it is considered that drying shrinkage starts after form-work removal, as form-work normally prevents water loss from the concrete. In piles and other underground structures, drying shrinkage is affected by the position of water table and the porosity and water content of the soil.

Two kinds of cracking can occur during drying:

-the first occurs during the first few hours and is governed by the water content of the concrete. Shallow cracks appear on the surface of the concrete.

-the second is the result of long term drying. These cracks appear much later and follow a more regular pattern (the cracks are straighter and wider).

Drying shrinkage is also the only partly reversible shrinkage mechanism. Most of the water can be absorbed back into the structure making it swell. This last mechanism is influenced by the water pressure; this means that structures subjected to different water pressures have different degrees of swelling [Neville (1995)].

2.4.1.4 Carbonation shrinkage

Some of the hydration products can carbonate with the carbon dioxide present in the air. This will cause the concrete to contract and gain weight. This surface shrinkage also restricts the other shrinkage mechanisms (drying and to a minor extent autogenous), by reducing moisture movement from the surface of the structure [Gardner and Zhao (1993)]. Carbonation cannot take place when the humidity is less than 25% or when it is 100%. For piles and underground structures the lack of air and possible soil saturation limit the carbonation process.

2.4.2 Creep

As stated earlier, creep is the increase of strain at constant stress and temperature. It is not linear, and follows a different strain-time curve for every kind of material. Creep of concrete is a very complex process and various factors affect it.

It is important to introduce the paradoxical behaviour of concrete, known as the *Pickett effect* [Pickett (1942)]:

1. *At constant humidity (i.e. any exchange of water with the ambient medium is prevented, and the hygrometric equilibrium is reached before loading) and under a constant compression, the less evaporable water concrete contains the less it creeps. The strain obtained by this test is called basic creep.*

2. *At decreasing humidity (the sample then loses water during the creep test), concrete creeps more than if it had remained at the initial humidity. The strain obtained by this test is called drying creep*

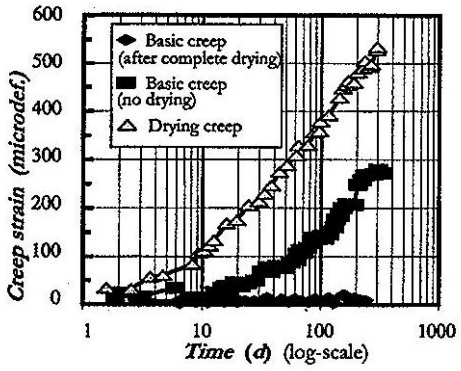

Figure 2.9: *Pickett's paradox (Acker and Ulm (2001))*

This behaviour immediately shows the importance of the ambient humidity and the moisture content of the sample and their respective gradients in the development of

creep (fig. 2.9). A full physical-chemical model, at microscopic level, for the explanation of creep has been developed over several years [Bazant et al. (1997), Bazant (2001) and Bazant et al. (2004)]. The model successfully explains the Pickett effect and ageing (the decrease of creep of concrete with time) which could not be properly reproduced with previous models. Instead of the detailed explanation of creep at microscopic level (which is not a purpose of this research), it is possible just to point out that the development of creep is mainly related to the interaction between the cement gel, the capillary water, the hindered adsorbed water (adsorbed water in the gel micro-pores) and the relative humidity of the water vapour in the capillary pores.

The load plays a role in changing the equilibrium between the different elements. Also in this case the importance of humidity/moisture on the sample is highlighted as one of the principal factors in the process. Section 2.4.4 gives some experimental examples of concrete creep under different environmental conditions.

Other factors play a role in the behaviour of creep for reinforced concrete. Type of concrete, aggregates, type of steel and dimensions of the element are affecting the creep results, but cannot be changed in a sample; while stress, temperature and moisture can affect a specific analysed sample. The rate of creep increases with increased stress and temperature. Creep also increases with the application of cyclic stress. It has to be noted that the increase in creep is never linear during the life of a structural member, but follows a specific curve (fig. 2.10) [Neville (1970), Neville (1995)].

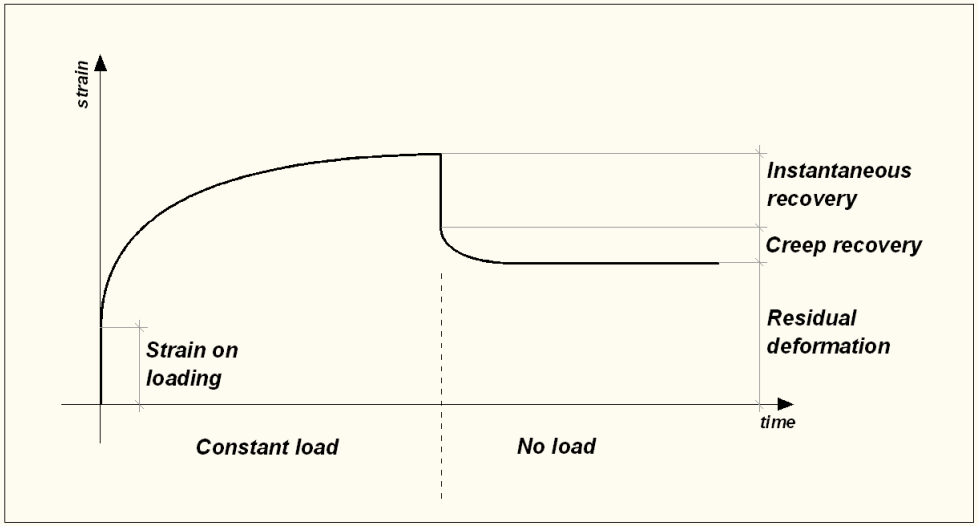

Figure 2.10: *Theoretical strain vs. time curve for a concrete sample under load*

2.4.3 Influences of particular concrete mixes on shrinkage and creep

It is well known that substances in addition to ordinary Portland cement are used in concrete mixes. The presence in the admixtures of other substances can radically change the behaviour of concrete. The piles used in two of the analysed sites were built out of concrete containing Ground Granulated Blast-furnace Slag (in Leatherhead, par. 3.2.1) and Fly Ash (in Grange Hill, par. 3.1.1). The following sections illustrate some of the effects of these substances.

2.4.3.1 Ground Granulated Blast-furnace Slag (GGBS)

To improve the sustainability of concrete structures and the performance of concrete, GGBS can be substituted to part of the Ordinary Portland Cement (OPC). GGBS increases the strength and the durability of concrete, but also has an adverse effect on the autogenous shrinkage behaviour. Experiments show that the presence of GGBS in the concrete admixture generates greater autogenous shrinkage than a common OPC (at the same water/cement ratio). The greater the amount of GGBS, the greater is the autogenous shrinkage. In admixtures with the same content of GGBS, a lower water/cement ratio results in a smaller autogenous shrinkage [Lee et al. (2006)].

2.4.3.2 Fly ash

Fly ash is usually used with the same aim as GGBS, but has a completely different effect on concrete. If the percentage of fly ash used to replace OPC in the cement is between 12% and 30% it has a positive effect on creep characteristics (the samples show less creep); if the percentage of fly ash is greater than 50% there are no effects on creep [Zhao et al. (2006)].

2.4.4 Previous work

This section introduces some experimental and numerical results found in the literature to better understand and quantify the influence of humidity/moisture on shrinkage and creep effects.

2.4.4.1 Gawin et al. (2006)

Hygro-thermo-chemo-mechanical modelling of concrete at early ages and beyond. Part II: shrinkage and creep of concrete

The authors analyse the evolution of shrinkage and creep on a sample and on a structure using an advanced numerical model for concrete. This is quite complex and takes into account all the relevant processes (except cracking) and influences from the beginning of hydration into the long term. The model is validated against several experiments taking into account the different parameters analysed. It is important to notice that the Pickett effect is modelled correctly.

Analysing the assumptions made by the authors shows the importance of the connection between the humidity of the sample and the development of shrinkage and creep. Both the model and the experiments show that at a relative humidity of the air surrounding the sample higher than 80%, the shrinkage strain of a concrete sample is smaller than $100\mu\varepsilon$. Other model results/experiments show the difference in the development of shrinkage in an unloaded slab between a sealed specimen (which represents the autogenous shrinkage, final total strains after 1000 days $<20\mu\varepsilon$) and a drying specimen (which represents the total shrinkage, final total strains after 1000 days $\simeq 700\mu\varepsilon$).

The coupling between shrinkage and creep phenomena is another assumption that the model demonstrates to be very important. The authors introduced shrinkage into

the creep calculation since the effect of the former is to compress the solid skeleton due to an increase of capillary tension, thus adding a virtual additional load to the sample. This assumption allows creep effects even without any applied load, which in the classical approach is considered as a long term shrinkage.

With another experiment and a related numerical model the authors show the development of creep with time, depending on the age at which the sample is loaded. In general the sealed specimens show creep strains (basic creep) between 400 and 600$\mu\varepsilon$, and the drying sample (total creep) between 600 and 1800$\mu\varepsilon$. It has to be pointed out that in a sealed specimen there are no exchanges between the concrete and the environment, so over time water will be going to be consumed due to the self-dessication process of the concrete.

2.4.4.2 Goel et al. (2007)

Comparative study of various creep and shrinkage prediction models for concrete

This paper compares different prediction models and an experimental set of results concerning the development of shrinkage and creep in concrete samples. The main result shown, affecting the present research, is that all the models and experimental data show a shrinkage strain of at least about 400$\mu\varepsilon$. This result refers to samples cast and stored at 23^oC and 5% relative humidity. The creep data and predictions are shown in terms of specific creep for each MPa of axial load.

2.4.4.3 Barr et al. (2003)

Shrinkage of concrete stored in natural environments

Barr et al. (2003) analyse the development of shrinkage in different samples (different concrete mixes, presence of silica fumes or fibre reinforcements) within different environmental conditions (different relative humidities and different temperatures). Data collection was carried out for about a year on several samples of each concrete admixture stored in different environments: a control room with constant temperature (23$\pm$2^oC) and relative humidity (60$\pm$5%); a green area (university park) and the roof of the building. The latter two showed a natural variation of the parameters over time, but the green area had a higher relative humidity while the roof had higher temperature. The study shows quite different shrinkage results between the three different environments, but every sample always shows strains higher than 400$\mu\varepsilon$. The samples were allowed to dry in the specific environment and no water was added.

2.4.4.4 Fellenius et al. (2009)

Long-term monitoring of strain in instrumented piles

This research analyses the behaviour of two instrumented piles and two instrumented laboratory short pile pieces. The laboratory experiment is of major interest for understanding the shrinkage behaviour of piles. The two samples are 500 mm in diameter

and 2.00m long. One simulates a normal bored reinforced pile and the other a PHC pile (closed-toe cylindrical concrete pile, locally called pretensioned spun high strength concrete pile; this is formed by an external prestressed concrete ring driven into the soil which is then filled with concrete grout and occasionally an additional reinforcement cage), with the strain gauges attached to the internal reinforcement cage. These were cast in the laboratory yard, put inside a 800 mm diameter plastic pipe to smooth the temperature variations, instrumented with four vibrating wire strain gauges and monitored for five months. During this period the instruments recorded the different behaviours of the two types of concrete piles after the thermal peak caused by the setting of concrete and the consequent hydration processes. No direct shrinkage effects were measured because the instruments were affected by the temperature effects and the particular behaviour of the structure (in the PHC the prestressed ring restrains the grout core during first phases of hydration). After five months both samples were submerged in water, filling the 800 mm pipe, and monitoring was continued for another year. Immediately after submerging, the specimens began to swell (as shown by the strain gauges measurements). The swelling continued for about three months to a total increment of about $150\mu\varepsilon$. After this the samples show a combination of swelling and temperature effects.

2.4.4.5 Neville (1995)

Shrinkage and creep experiment results

On the swelling of concrete, Neville (1995) points out that concrete cured continuously under water exhibits an increase of volume instead of the usual shrinkage. The swelling is due to the absorption of water by the cement gel. The water molecules act against the cohesive forces and tend to force the gel particles apart, with a resultant swelling pressure. In addition, the ingress of water decreases the surface tension of the gel and a further small expansion takes place. Moreover, swelling is larger at high pressure, such as experienced by deep sea structures.

The development of shrinkage for concretes of fixed proportions, but different aggregates, stored at fixed temperature (21^oC) and relative humidity (50%) is investigated in the experiments. After one year all the samples show shrinkage strains greater than $400\mu\varepsilon$. Neville (1995) also shows another result: the shrinkage of different concrete samples stored at different relative humidities after a 28 days wet curing. The samples stored at 100% relative humidity display a swelling of about $50\mu\varepsilon$ after one year. It is also introduced that if concrete which has been allowed to dry in air of a given relative humidity is subsequently placed in water (or at a higher humidity) it will swell. This is indicative of a partial recovery (between 30% and 60%) of the drying shrinkage.

For creep of concrete, the results of concrete samples of fixed proportions, but different aggregates, stored at fixed temperature (21^oC) and relative humidity (50%) and loaded at the age of 28 days are shown. After one year the samples developed creep strains between $400\mu\varepsilon$ and $1200\mu\varepsilon$. Concrete samples cured in fog for 28 days, then loaded and stored at 100% relative humidity showed creep strains of about $250\mu\varepsilon$.

Author	Relative Humidity	Temperature	Time	Load	Specimen	Measured Effect	Strain
Gawin et al. (2006)	80%	-	-	-	-	Shrinkage	$100\mu\varepsilon$
Gawin et al. (2006)	-	-	1000 days	-	Sealed	Autogenous Shrinkage	$<20\mu\varepsilon$
Gawin et al. (2006)	-	-	1000 days	-	Drying	Total Shrinkage	$\simeq 700\mu\varepsilon$
Gawin et al. (2006)	-	-	-	Yes	Sealed	Basic Creep	400-600$\mu\varepsilon$
Gawin et al. (2006)	-	-	-	Yes	Drying	Total Creep	600-1800$\mu\varepsilon$
Goel et al. (2007)	5%	23^oC	-	-	-	Shrinkage	$>400\mu\varepsilon$
Barr et al. (2003)	60±5%	23 ± 2^oC	-	-	Not sealed	Shrinkage	$>400\mu\varepsilon$
Barr et al. (2003)	Green Area	Green Area	-	-	Not sealed	Shrinkage	$>400\mu\varepsilon$
Barr et al. (2003)	Roof	Roof	-	-	Not sealed	Shrinkage	$>400\mu\varepsilon$
Fellenius et al. (2009)	Submerged	-	3 months	-	Submerged	Swelling	$150\mu\varepsilon$
Neville (1995)	50%	21^oC	1 year	-	-	Shrinkage	$>400\mu\varepsilon$
Neville (1995)	100%	-	1 year	-	28 days wet curing	Swelling	$50\mu\varepsilon$
Neville (1995)	50%	21^oC	1 year	at 28 days	-	Creep	400-1200$\mu\varepsilon$
Neville (1995)	100%	21^oC	1 year	at 28 days	Cured in fog	Creep	$\simeq 250\mu\varepsilon$

Table 2.4: *Summary of the results found in literature about shrinkage and creep*

2.4.5 Creep and shrinkage in underground structures conclusions

This part of the research focuses on the study of concrete bored piles in saturated clay (as described in chapter 3). All of the piles have the majority of their length below the water table. These conditions are quite different from a usual concrete structure in the open air. First of all the hygral conditions (humidity/moisture) are completely different (the relative humidity is extremely high compared with the normal air conditions) and thus the shrinkage and creep processes will develop in a different manner.

During the installation of the pile, the soil does not lose much water, since the pouring of the concrete immediately follows the end of the boring phase. Then, after pouring, the saturated clay maintains the concrete at high moisture conditions for the entire curing phase, limiting (or removing completely) the effects of drying shrinkage. It could also be possible that the concrete experiences some minor swelling (as pointed out in par. 2.4.4.4 and par. 2.4.4.5). Major swelling of the concrete is unlikely since the water pressures in the clay pores are not very high compared with deep sea pressures. From this it can be assumed that drying shrinkage has a negligible effect on concrete piles in saturated clay, and occasionally such piles may experience a certain degree of swelling.

Considering autogenous shrinkage (which is a property of the material and thus always happens), following the results obtained in the experiments and numerical model on the sealed unloaded sample in par. 2.4.4.1 and table 2.4 (autogenous shrinkage of about $20\mu\varepsilon$); considering the effects of water/cement ratio in par. 2.4.1.2 and the particular conditions (the saturated clay prevents water losses and can supply a small quantity of water if necessary, avoiding the drying of concrete), autogenous shrinkage of $<50\mu\varepsilon$ may be assumed (even if the water/cement ratio, for some of the piles, is slightly below 0.40).

For the analysis of creep it is necessary to consider the main factor affecting the piles that is different form structures in the open air: the constant high level of moisture. Applying the first statement of the Pickett effect (par. 2.4.2), it can be hypothesised that the piles in saturated clay experience basic creep only. This already limits the expected range of creep strains at about $250\mu\varepsilon$ (par. 2.4.4.5). The creep experimental and model results, described in par. 2.4.4.1, are not applicable since that sample was sealed while a pile in saturated clay can absorb water.

This discussion leads to expected strains in a pile in saturated clay as follows: no drying shrinkage or possible swelling, less than $50\mu\varepsilon$ of autogenous shrinkage (depending on the water/cement ratio), no drying creep and about $250\mu\varepsilon$ of basic creep (depending on the effective load and the age at load). This means a rough forecast of about $300\mu\varepsilon$ between shrinkage and creep. The strain data from the instrumented piles shows that none of them experience strains of this magnitude, considering that they are also subjected to bending moment. The final assumption about the effects of shrinkage and creep on piles in saturated clay is that they are negligible compared with the bending or axial strains. The hypothesis is that probably the swelling of concrete is more important than stated before (more like the results shown in par. 2.4.4.4) and the creep effects

probably smaller (due to the application of load at a later age), resulting in almost a balance between the two effects.

Piles in saturated clay do not show the same creep and shrinkage strains as structures in the open air (par. 2.4.4.2 and par. 2.4.4.3), but much more limited effects.

2.5 Cracking

This section analyses the behaviour of concrete cracking in tension for the two different types of pile used in this research: a standard reinforced concrete pile and a circular concrete-filled steel tubular pile (described in more depth in chapter 3). Concrete has a limited tensile strength which is not used in design (for safety reasons), but has to be considered in back-analysis. Its real value is related to the concrete characteristics and has to be determined experimentally for an accurate analysis. Unfortunately this was not possible for the instrumented piles analysed. The values from BS EN 1992 (2004) are therefore used, introducing a degree of approximation.

2.5.1 Standard reinforced concrete pile

Concrete cracking does not develop uniformly in a standard reinforced concrete pile. Cracks open when the tensile deformation from applied loads reaches the tensile deformation capacity of concrete [Borosnyoi and Balazs (2005)]. The cracking process can be considered in two parts: crack formation and stabilised cracking (fig. 2.11). During the first phase cracks form at random locations according to the location of areas of weakness. After a crack forms, the tensile forces are carried by the reinforcement in the section and concrete stresses fall to zero (compatibility of strains between concrete and reinforcements is no longer maintained) [Borosnyoi and Balazs (2005)]. With increasing distance (along the pile) from the crack, the tensile stresses in the concrete increase as load is transferred by bond stresses between the concrete and reinforcements. At a certain distance (termed the transfer length), compatibility of strains is recovered again. In the crack formation phase, the zones in which strain compatibility applies are independent of each other. With increasing load new cracks may be formed and the average crack spacing is decreased [Borosnyoi and Balazs (2005)]. The stabilised cracking phase is reached when practically no more new cracks can be formed; the cracks are so close to each other that there is insufficient distance between them for the concrete stress to reach the value corresponding to cracking space. In this phase the average crack spacing remains constant and an increase in load causes an increase of crack width only [Borosnyoi and Balazs (2005)]. This means that all the tensile stresses are effectively carried by the reinforcement. Similar explanations of the cracking process have been given by Bianchini et al. (1968) and Watstain and Bresler (1974).

In design, the tensile loads are considered to be carried only by the reinforcements. In reality, before the stabilised cracking phase is reached, both concrete and steel resist the tensile stresses. The contribution of concrete is considered as an increment to the tensile stiffness of the reinforcements. This effect is known as tension stiffening

[Borosnyoi and Balazs (2005)].

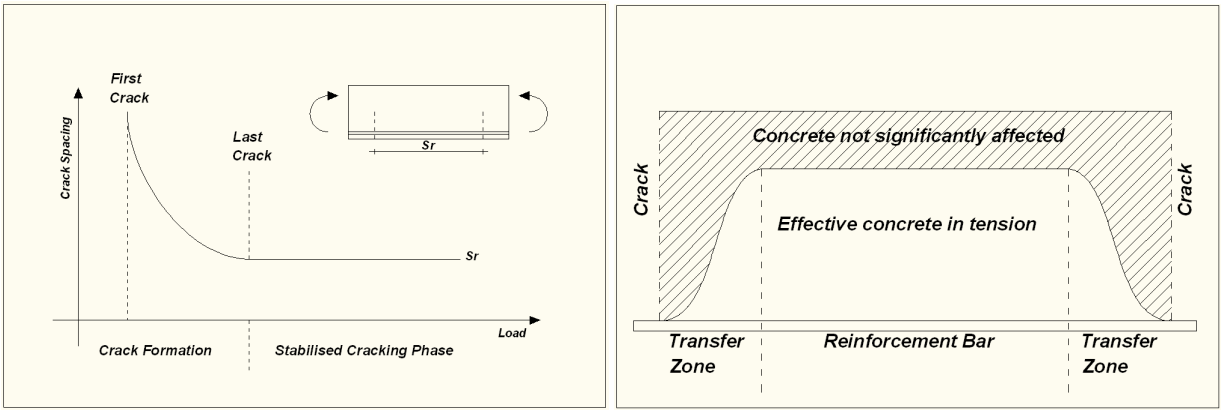

Figure 2.11: *Conceptual crack formation, spacing and effective concrete area in tension based on Borosnyoi and Balazs (2005)*

2.5.1.1 How strain gauges respond to cracks in standard reinforced concrete

As pointed out by Roesler and Barenberg (2000), strain gauge readings in concrete under tension can be misleading because they depend on the position of the instrument relative to the position of cracks. The aim of this section is to understand how strain gauges (at this point the embedded type only) respond in relation to the crack positions and then to identify such behaviour in the recorded strain profiles to detect the cracked zone.

Comparing the explanation of concrete behaviour during cracking given by Borosnyoi and Balazs (2005) (par. 2.5.1) with the results obtained by Roesler and Barenberg (2000) from tests on cracked concrete using strain gauges embedded in the concrete, the following instrument behaviour is apparent:

- if a gauge bridges a crack, the opening of a crack results in a sudden jump in the reading;
- if a gauge is positioned between two cracks, but outside the transfer lengths, it continues to record an increase in tension as further load is applied;
- If a gauge does not bridge a crack, but lies inside the transfer length, it will not accurately give the bending strains representative of either a cracked or an uncracked section.

It can be concluded that strain gauges embedded in concrete work differently depending on their position relative to the cracks [Roesler and Barenberg (2000)]. This can lead to an inaccurate estimation of bending strains. An example of cracking measured by embedded strain gauges is analysed in section 4.6.

In this research, two types of strain gauges have been used to measure the strains in the concrete (embedded strain gauges and sister bars, par. 2.1.1). Different behaviour, with respect to crack opening, is expected from the two instruments. The difference is represented by the length of the gauges and the mechanism of transmission of the

strains. The embedded strain gauges transmit the strains from the concrete to the vibrating wire using two end-plates (par. 2.1.1) and the overall instrument length is between 0.10 and 0.15m. The instruments measure the local strains of the concrete between and around the end-plates. Sister bars transmit the strains using two lengths of steel reinforcement bar and the whole instrument length is usually between 1.00 and 1.40m, thus the instrument measures the concrete strains of a much larger volume of concrete. This means that a crack opening between the two plates of an embedded strain gauge is detected as a jump in the readings. Conversely a crack opening along the length of a sister bar does not show any jump. The reinforcement bars used for the transmission of strains redistribute the stresses along their length (with the same mechanism of a normal reinforcement bar) and the instrument does not record any sudden obvious jump on cracking. Analysis of the data coming from two different sites is shown in section 4.6 and section 5.3.

Other important factors influencing the development of cracks are the number of reinforcements and their positions (both longitudinal bars and shear links) [Hassoun and Al-Manaseer (2005) and Watstain and Bresler (1974)]. With the same area of steel, a concrete member with a few large diameter bars will crack more easily than a member with more smaller diameter bars. Specific design details are also described in BS 8007 (1987). Usually, cracks develop first near the shear links (since the depth of concrete is thinner) and then in the intermediate positions [de Sanctis (2006)]. This could give an apparently random effect in piles where the shear is taken by a continuous spiral reinforcement, whose position may not be known with respect with the strain gauges.

2.5.2 Circular concrete-filled steel tubular piles

This type of pile is formed by a steel pipe filled with concrete. A grout ring is cast between the steel pile and the soil to fill the void between the structure and the ground and to protect the steel (par. 3.4.2). In the following analysis, when referring to circular concrete-filled steel tubular piles, the term "grout" will be used to indicate the material that forms the external ring, while the term "concrete" will refer to the material inside the steel pipe. The grout is a type of weak concrete, generally formed from cement and sand. The restrained concrete inside the pipe behaves differently from a standard reinforced concrete member even though the material characteristics and properties are the same. The strain gauges are welded to the outside of the steel pipe and thus they read the strains in the steel.

Cracking also develops in a different way. Cracks form first in the grout, when the tensile strain threshold is exceeded, in a similar manner to a standard reinforced concrete pile. As the strains increase, the number of cracks increases (and the space between them decreases) until the tensioned grout is fully cracked. Since the grout has low strength characteristics, it easily cracks fully in tension, but it can resist higher strains in compression (the compressive strength of a concrete material is about ten times its tensile strength [Neville (1995)]). No tension stiffening is possible since no reinforcement is present in the external ring. Thus, the grout resists a small tension

but a much bigger compression. This means that the structurally effective component of the grout is the compressed part of the ring until it is crushed. Since the grout is the outermost material (the furthest from the neutral axis), it can resist a relatively large proportion of the bending moment applied to the pile.

Cracking behaviour is different in the restrained concrete. Liang and Fragomeni (2010) model the bulk tensile behaviour of restrained concrete showing that it behaves linearly in tension until the tensile strength of concrete is reached (fig. 2.7). Then the concrete cracks and its bulk tensile strength softens linearly to zero. The ultimate tensile strain of concrete is assumed to be 10 times the strain at cracking [Liang and Fragomeni (2010)]. The restrained concrete stress/strain behaviour developed by Liang and Fragomeni (2010) is based on extensive experimental result analysis and the subsequent non-linear fibre element analysis. Softening of the concrete arises from a volumetric average of the behaviours of the different restrained concrete elements. Dividing the concrete in infinitesimal elements, the cracked concrete elements cannot work in tension while the adjacent uncracked elements can. The opening of a crack also increases the volume of the whole concrete increasing the hoop stresses in the restraining steel pipe, hence fully confining the concrete. Confined concrete has improved mechanical characteristics, as described by Knowles and Park (1969). The volumetric average approach used by Liang and Fragomeni (2010) in their nonlinear approach can also be used in this analysis since the strains are coming from a discrete number of instruments, each describing a discrete section of the pile. This means that the volume averaged restrained concrete contribution in tension is much bigger than that of normal reinforced concrete (and of the grout ring). In fact after the opening of a crack, the volume average restrained concrete behaviour shows to continue to work in tension, while unrestrained concrete or grout does not. The effect is that a crack in the restrained concrete influences the position of the neutral axis in a much smaller way than a crack opening in the grout. It can also be argued that the transfer length in the restrained concrete is smaller than for standard reinforced concrete since the steel pipe surface is bigger and the hoop stresses increase the skin friction between the two materials.

The main resisting element of the pile is the steel pipe which is stressed biaxially due to the confinement effect [Knowles and Park (1969), Liang and Fragomeni (2010)]. Buckling is prevented by the infilling concrete, and failure of the pile would occur due to tension failure of the steel [Patsch et al. (2002)]. The position of the steel pipe (outside the concrete core) makes it possible for it to resist the majority of the applied bending moment since most of it is far from the neutral axis.

Strain gauges connected to the steel pipe seem to not record any jump associated with the developing of cracking in the grout. It is assumed that their readings relate only to the behaviour of the steel pipe.

2.6 Temperature

Reinforced concrete expands linearly when the temperature changes between 0° and 60°C. Like every other concrete parameter, the coefficient of thermal expansion (α_c)

varies with cement/sand ratio, type of aggregates used, humidity, presence of GGBS or fly ash, etc... . An average range for α_c is between $9\times10^{-6}\ ^oC^{-1}$ and $13\times10^{-6}\ ^oC^{-1}$ [Neville (1995)]. A more detailed discussion about the coefficient of thermal expansion and related matters is carried out in section 4.4.2.2.

The only exception to linear behaviour occurs during hardening of the concrete, when the hydration reactions are exothermic and the concrete can be heated by up to 40°C. When the first part of the hydration process ends, and little further heat is produced (par. 2.2.2), the concrete returns to ambient temperature and the above linear relationship applies. The peak in temperature during cement hydration can cause problems in thick structures owing to the differential strains that develop between the core and the skin of the members. For underground structures, the reduction in temperature will generally be slower than for structures in the open air owing to the insulating effect of the soil. The elevated temperature reached during the peak also affects the loss of water by evaporation; this effect is attenuated in underground structures.

2.7 Conclusions

A wide range of topics have been introduced in this chapter to analyse the basic problems and to prepare the discussions carried out in the following chapters. The full range of instruments (vibrating wire strain gauges, inclinometers, thermistors and data-loggers) used are analysed in detail to understand their characteristics (par. 2.1).

The strength of concrete and its development with time are analysed to show that long term analysis of concrete structures have to take into account appropriate long term parameters since the standard 28 days results are not always correct (par. 2.3.1).

Two types of piles are analysed in this research: standard reinforced concrete piles and circular concrete-filled steel tubular piles. Specific stress-strain curves are introduced (par. 2.3.2) to take into account the differences between the two structures and to account that this research focuses on the back-analysis of measured data and not on the design of new structures. This means that factors of safety and simplified curves are not appropriate for an accurate analysis.

Since concrete has a complicated behaviour and since the main instruments used (strain gauges) measure strains, it is important to understand the effects of shrinkage and creep on bored concrete piles in saturated clays (the main type of structures analysed). These effects could show a change in the measured strains not related to a change on the forces applied to the structure. Due to the the high humidity/moisture of the saturated clay, concrete behave differently than on an open-air structure. Thus, in this analysis it is assumed that the effects of shrinkage and creep on piles in saturated clay are negligible compared with the bending or axial strains (par. 2.4.5).

Cracking is also affecting concrete. Its effects are analysed for standard reinforced piles (par. 2.5.1) and circular concrete-filled steel tubular piles (par. 2.5.2). The latter behave very differently from the former due to the restrain of the steel tube on the concrete core. The effect is that a crack in the restrained concrete influences the

position of the neutral axis in a much smaller way than a crack opening in standard reinforced concrete.

Strain gauges are also affected by the opening of a crack. Depending on the relative position of the two (the strain gauge and the crack) and on the type of strain gauge, the reading can be different (par. 2.5.1.1).

Chapter 3

Instrumented sites

In this chapter, the different sites analysed in this research are described and detailed information about the structures and the slopes is given. For some of the sites (Grange Hill, Mill Hill and Ironbridge Phase I) the instrumented piles were installed before the start of this study. For other sites (Leatherhead, Ironbridge Phase II and Ironbridge Lloyd's Head) it was possible to follow all the stages of construction (including the installation of the instruments, building of the piles, installation of the data-logger, actual data collection and upkeep of the instrumentation).

3.1 Grange Hill

This site, situated in Essex (OS grid reference TQ448926), is an 11m high slope in London Clay stabilised with discrete piles (soil parameters in table 3.1). The slope is a cutting and the railway lines are positioned at its toe (Fig. 3.1). The top layer called "Made Ground Granular" is a non-uniform composition of sandy clay, silty sand, broken bricks of approximately gravel size, burnt clay with occasional ash, flints, bricks and steel reinforcement bars [Norwest Holst Soil Engineering Limited report for Infraco BCV Limited (2002)], which make it a heterogeneous layer difficult to analyse.

Material	γ[kN/m^3]	c'[kN/m^2]	φ'[°]
Made Ground Granular	18	0	30
Weathered London Clay	19	2	21
Intact London Clay	19	2	21

Table 3.1: *Grange Hill soil parameters*

Before the installation of the piles the slope was found, on analysis with worst case pore water pressures, to have an insufficient factor of safety with a critical slip surface positioned at the bottom of the "Weathered London Clay" layer [Brown and Root Consulting report for Infraco BCV Limited (2002)]. The instrumented piles were installed at the end of February 2006, and up to the present more than four years of data have been collected. There are two instrumented sections: the major one contains two instrumented piles, inclinometers, and piezometers; the other contains a single

instrumented pile, an inclinometer and piezometers. The recent loading history of this site (after pile installation) commenced with the removal of the piling platform and a slight regrading of the slope. This happened on 30 March 2006 and seems to have had little influence on the measured axial strains and bending moments. The mature dense vegetation that covered the entire slope was removed two months before the beginning of the piling works.

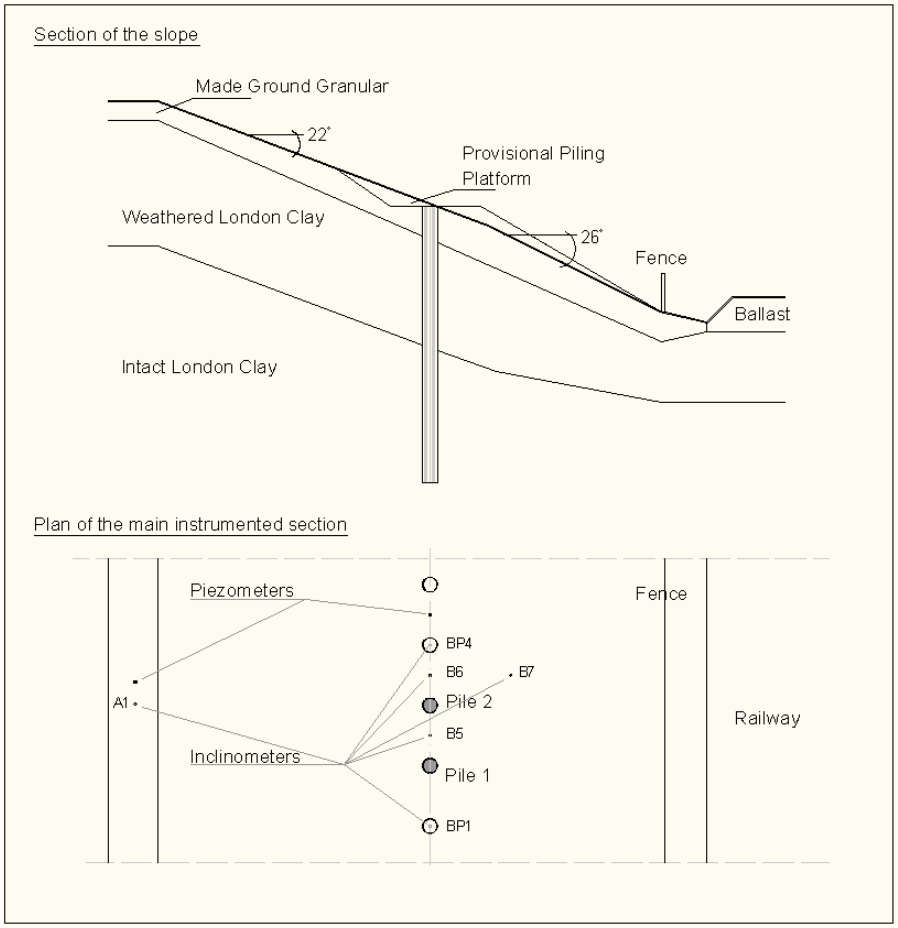

Figure 3.1: *Grange Hill Site, main instrumented section*

3.1.1 The piles

The principal instrumented section contains two identical instrumented piles (Pile 1 and Pile 2). They are 0.6m diameter cast in-situ piles, 11m long, and spaced 1.8m (or three diameters) apart between centres. The piles are reinforced with 7/T40 over the top 4m, with 7/T50 in the central 4m and with 7/T40 over the bottom 3m (fig. 3.2). Reducers were used to connect between different reinforcement diameters instead of the usual bar overlap. This method was used to maintain the geometry of the reinforcements and to simplify the installation of the cages since overlapping of the large diameter bars would not have made it possible to maintain the design cover depth. The secondary instrumented section contains one pile (Pile 3), 0.6m diameter, 10m long, spaced 1.8m (or three diameters) from the centres of the adjacent piles. The pile is reinforced with

6/T25 over the top 2.5m, with 10/T25 in the central 4.5m and 6/T25 over the bottom 3m. The connections between the different sections of cage, in this case, are made by overlapping bars. T12 spiral shear reinforcements and a design cover depth of the reinforcements of 75mm are used for all the piles.

The concrete mix used for the instrumented piles are:

- 35 N/mm^2 concrete
- Water/cement ratio = 0.34
- Portland cement (OPC) = 486kg/m^3
- Pulverised fuel ash (PFA) = 171 kg/m^3
- Sharp marine sand = 1277 kg/m^3
- Admixture = 5.3 kg/m^3

This specific mix with only fine aggregates was chosen to limit damage to the strain gauges during pouring of the concrete. In all other piles the concrete mix had a more standard range of aggregate sizes rather then only sharp marine sand.

The specific concrete mix could be the cause of the cracking and temperature related effects analysed in the following chapters. No results has been found in literature concerning the flexural strength and coefficient of thermal expansion for this particular kind of concrete mix.

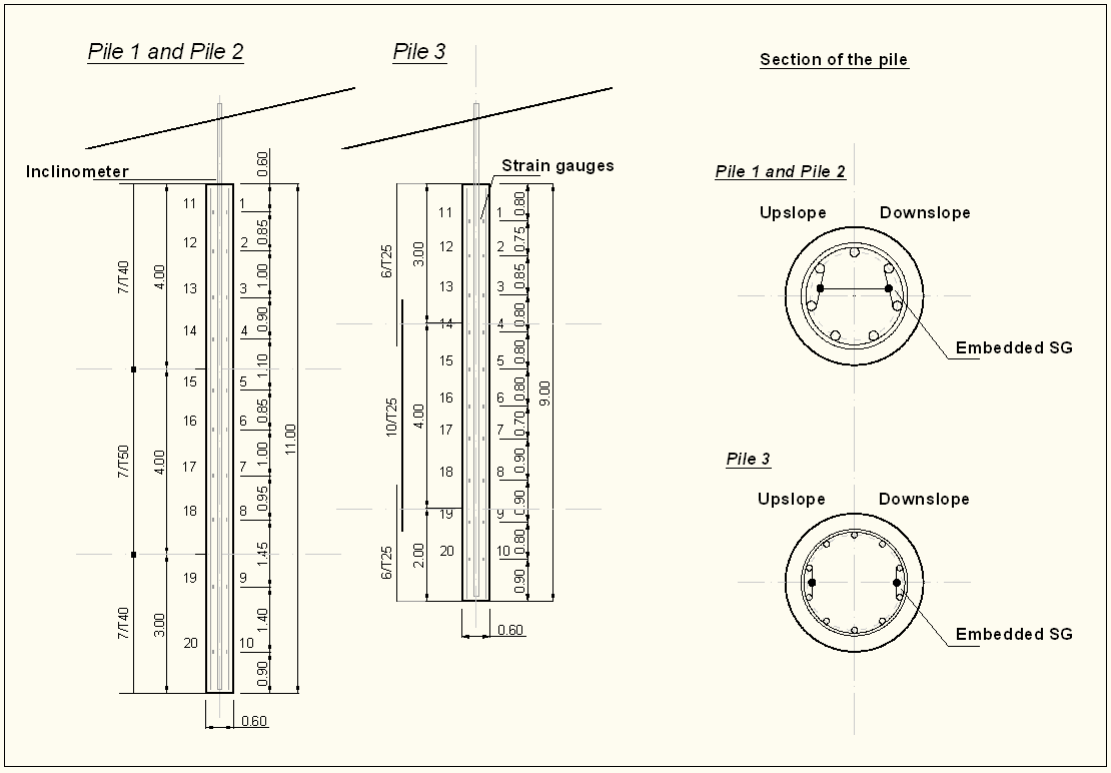

Figure 3.2: *Grange Hill piles*

3.1.2 The instruments

Each pile is instrumented with 20 vibrating wire strain gauges. These instruments are the embedded type shown in fig. 2.2. Those in Pile 1 and Pile 2 have in built thermistors, while those in Pile 3 do not. Fig. 3.2 shows the locations of the pairs of strain gauges. Inclinometers are also present in the centre of each pile, between pairs of piles, and at the top and at the bottom of the slope (fig. 3.1). The piezometers within the slope are used to measure the pore water pressure at different depths (2m, 4m, 6m, 8m and 10m below ground level). A weather station has been installed at the site.

3.2 Leatherhead

This site is situated in Leatherhead, Surrey (OS grid reference TQ145583), and is a 10m high motorway (M25) embankment. The slope consists entirely of London Clay of estimated soil parameters: c'=1.5 kN/m^2, φ'=21°. A row of piles (of 800mm diameter, 2.4m spacing and 12m long) was installed at the crest of the embankment in connection with the widening of the motorway carriageway in 1995. Failure of the embankment was first reported at the beginning of 2002 and a ground investigation was carried out in May 2005 [M25 Sphere, for the Highways Agency (2007)]. This showed that the embankment failure was a shallow rotational non-circular slip affecting the full height of the embankment. The top of the slip was just in front of the original row of piles, which largely protected the carriageway from damage. The toe of the slope is still subjected to occasional flooding from the nearby river. The remedial works (December 2007) consisted of a row of discrete bored piles positioned about 10m from the edge of the carriageway, and the regrading of the entire profile of the slope (Fig. 3.3).

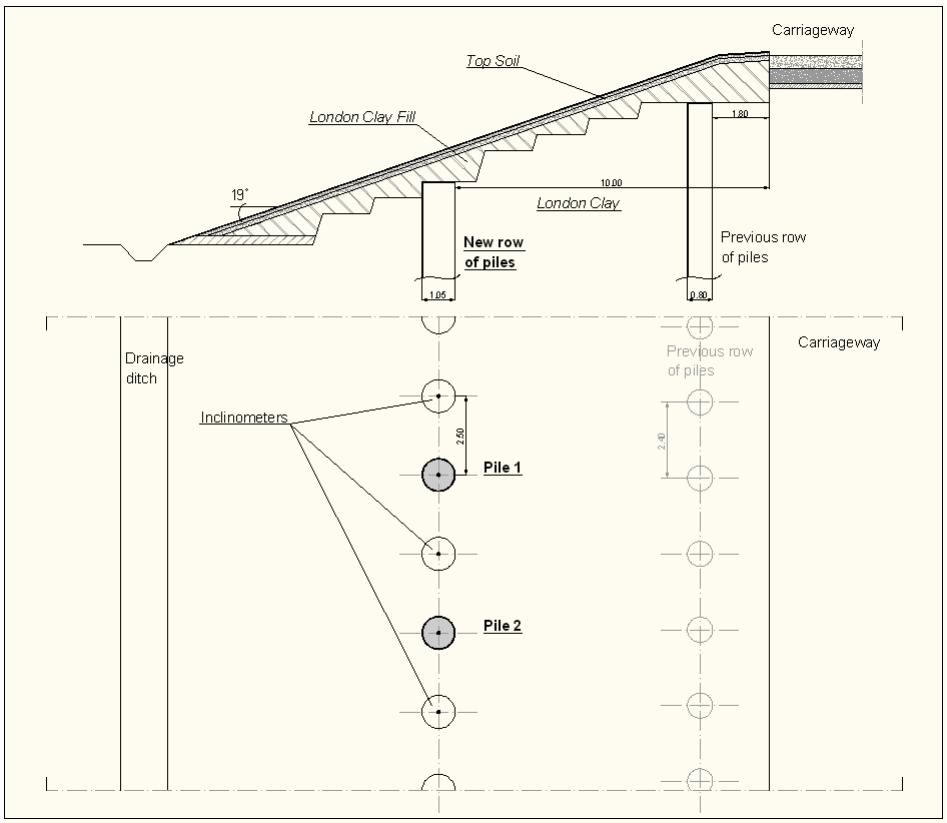

Figure 3.3: *Leatherhead, main instrumented section*

3.2.1 The piles

These piles are continuous flight auger (CFA) piles 1.05m in diameter and 13m in length installed 2.5m apart (about 2.4 diameters). They are reinforced with 20/T32 throughout their length; the shear links are T20 every 250 mm along the whole length of the pile. The instrumented piles are identical to the other piles within the retaining structure.

The concrete mix used was:

- 35 N/mm^2 concrete
- Water/cement ratio = 0.38
- Minimum cement content = 252kg/m^3
- Ground Granulated Blast-furnace Slag (GGBS) = 168kg/m^3
- Gravel = 1006kg/m^3
- Sand = 751kg/m^3
- Free water = 162 l/m^3
- Alkali = 2.00kg/m^3

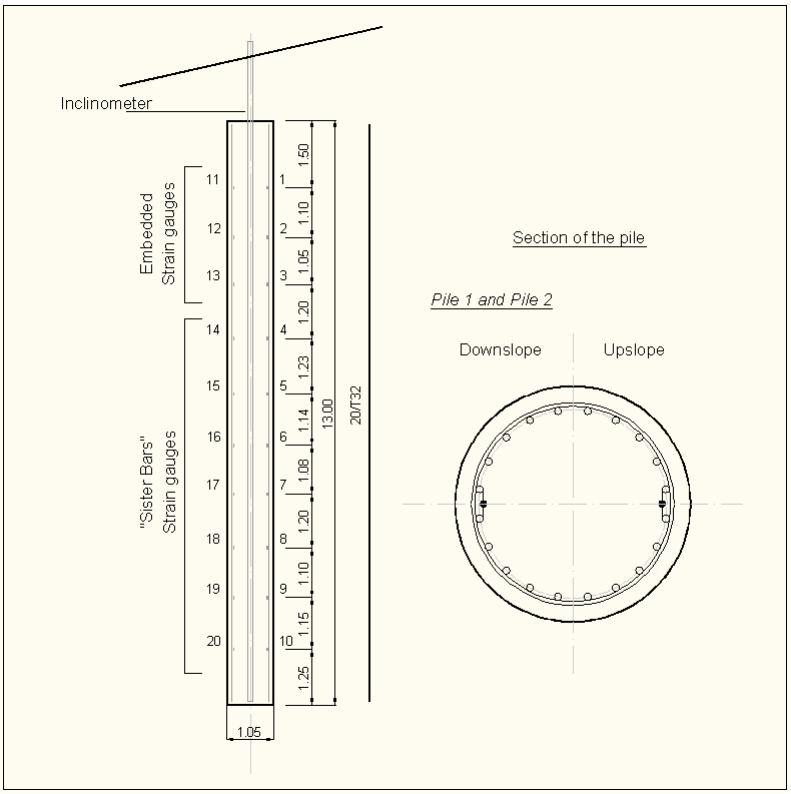

Figure 3.4: *Leatherhead piles*

3.2.2 The instruments

The main instrumented section is formed of five piles, three containing only inclinometers and two with inclinometers and 10 pairs of strain gauges (Fig. 3.4). The strain gauges are of two different kinds: embedded and sister bars. This was not planned but caused by the difficulty of finding 40 sister bar gauges at short notice. The strain gauges were placed in Pile 1 and Pile 2 as shown in fig. 3.4. The embedded strain gauges were placed at the top of the piles so that they had the shortest distance to travel through the concrete as the cage was inserted.

The secondary instrumented section is formed of a single pile containing an inclinometer positioned some distance from the principal instrumented section. This pile will be used to check if the displacements of the embankment are uniform along its length.

3.3 Mill Hill

The site is situated in the London Borough of Barnet (OS grid reference TQ245912) between the Underground stations of Mill Hill East and Finchley Central. It is a 12m high railway embankment made of Anglian Till Clay Fill with a layer of Ash at the top below the ballast (Tab. 3.2 and fig. 3.5) [Mott MacDonald report for Tube Lines (2004)]. The Clay Fill can be in general described as a sandy silty clay with occasional fine to medium gravel. The formation below the Clay Fill is London Clay. The entire embankment is covered by a dense vegetation including many mature trees.

After noting lateral and rotational movements of trees, line-side services and garden fence posts (in 1998) it was decided to assess the factor of safety of the slope. This led to stabilisation of the north side of the embankment with mid-slope discrete piles and a toe berm. The remedial works were completed in December 2004. During the stabilisation works as many mature trees as possible were maintained to ensure that the pore water pressures within the embankment did not increase.

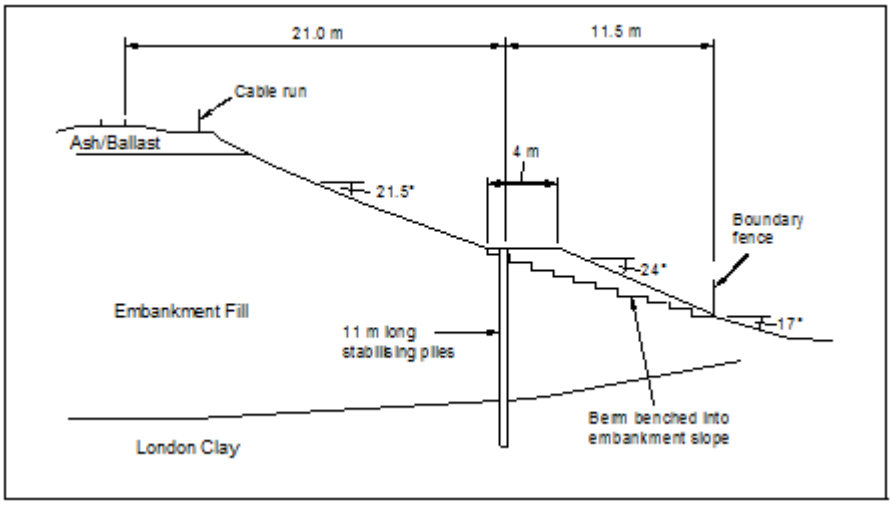

Figure 3.5: *Mill Hill section*

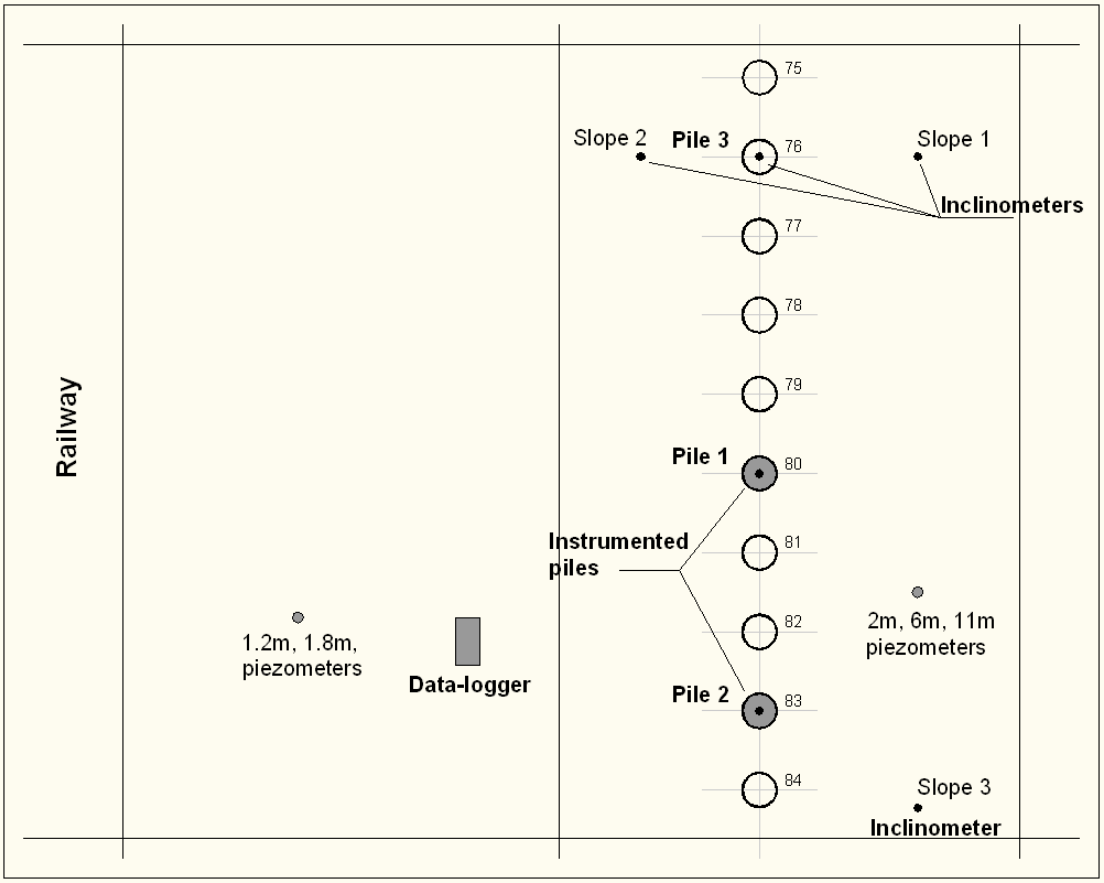

Figure 3.6: *Mill Hill instrumented section plan*

Material	γ[kN/m^3]	c'[kN/m^2]	φ'[^{o}]
Ash	11	0	40
Embankment Fill	19	1	25
Embankment Fill (Presheared)	19	1	18

Table 3.2: *Mill Hill soil parameters*

3.3.1 The piles

The discrete piles at this site are 0.45m diameter cast in-situ reinforced concrete piles. They are 11m long and spaced 0.7m (about 1.5 diameters) apart between centres.The positions of the instrumented piles are shown in fig. 3.6.

The instrumented piles are exactly the same as the other discrete piles in the structure. Each pile is reinforced with 8/T25 along the full length of the pile, with the reinforcement cages in two section of equal length. The connections between the cages are realised by the usual overlapping, and the shear links are T10 every 200mm (in this particular case they are spot welded to the main reinforcements). The design cover depth of the reinforcement is 75mm.

The concrete mix was:

- 35/40 N/mm^2 concrete
- Water/cement ratio = 0.49
- Cement content = 320 kg/m^3
- 4/20mm Graded Shingle = 1157 kg/m^3
- Free water = 157 l/m^3
- Pozzilith Standard WRA = 0.96 l/m^3
- Target Slump (mm) = S2 (40-110)

Since no concrete samples were taken, the concrete parameters were assumed to be the same as those obtained from the tests on concrete samples from the Leatherhead site.

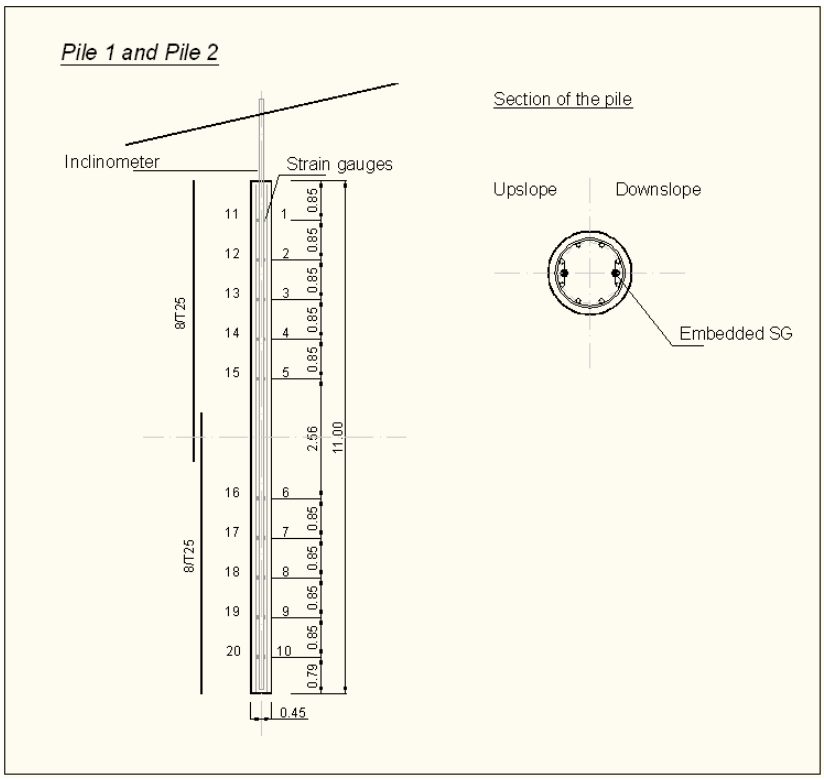

Figure 3.7: *Mill Hill piles*

3.3.2 The instruments

The main instrumented section is shown in fig. 3.6. It contains two instrumented piles (strain gauges and inclinometers), six inclinometers (in piles and in the slope) and seven piezometers in three different boreholes. This instrumented section is meant to give an overall view of the movements of the slope and of the piles. In particular the aim of the instrumented piles 1 and 2 is to understand the behaviour of the retaining structure, while the inclinometers in line with pile 3 are used to check the differential movements between pile and slope.

The instrumented piles contain 10 pairs of strain gauges each, positioned as shown in fig. 3.7. The strain gauges used are all of the embedded type (fig. 2.2). The large gap in the instrumentation at centre of the piles is due the overlapping of the two cage sections. Each pile was formed of two cages instrumented separately and assembled together in the hole before pouring the concrete.

3.4 Ironbridge

The site is located in the Ironbridge Gorge, Telford, Shropshire (OS grid reference SJ685032). The area is part of a UNESCO World Heritage Site (which covers the Ironbridge Gorge area) and it is situated down-stream from the famous "Iron Bridge". The entire area of the gorge is affected by shallow and deep movements of the ground due to the complex geology and its history of mine tunnels and loading from spoil tips. The area is considered to be the birthplace of the industrial revolution and in the 18^{th}

century it was a place of various coal mining and iron industries. This resulted in different areas of instability on the sides of the Gorge due to mining, excessive loading of the slopes with spoil and erosion by the river Severn.

The site of the stabilisation works covers of both sides of the river, the north side for a length of about 200m and the south for about 100m. The north side of the river includes "Phase I" (stabilised during winter 2006/07) and "Phase II" (stabilised during summer 2008); while the south side of the river consists of the "Lloyd's Head" site (stabilised during summer 2008). The complete stabilisation works consist of 5 rows of piles for the north bank of the river, 2 rows of piles for Lloyd's Head, a general profile regrading of both slopes, works to rebuild the damaged roads and improved river protections (fig. 3.8). Phase I includes row 1, row 2, row 3 and the road works to rebuild "The Lloyds" road; Phase II includes row 4, row 5, the regrading works on the lower part of the slope and the river protections; Lloyd's Head includes row 6, row 7, the road works to rebuild "The Lloyd's Head" road, the regrading works and the new river protection.

Both sides experienced large movements that severely damaged the roads crossing the sites. The largest instability movements were located on the north side and consisted of a translational movement of the slope with an initially deep slip surface at the top of the slope which becomes shallower adjacent to the river (fig. 3.9). The installation of the Phase I piles probably stopped the translational movements of the upper part of the slope, but triggered some superficial rotational movements in the lower part. The entire landslide has to be considered as a complex movement, possibly with different slip surfaces in different sections of the slope causing movement at different times. At Lloyd's Head the mechanism of the failure can be represented as the movement of a wedge, since the slope is quite steep and not very wide (fig. 3.10).

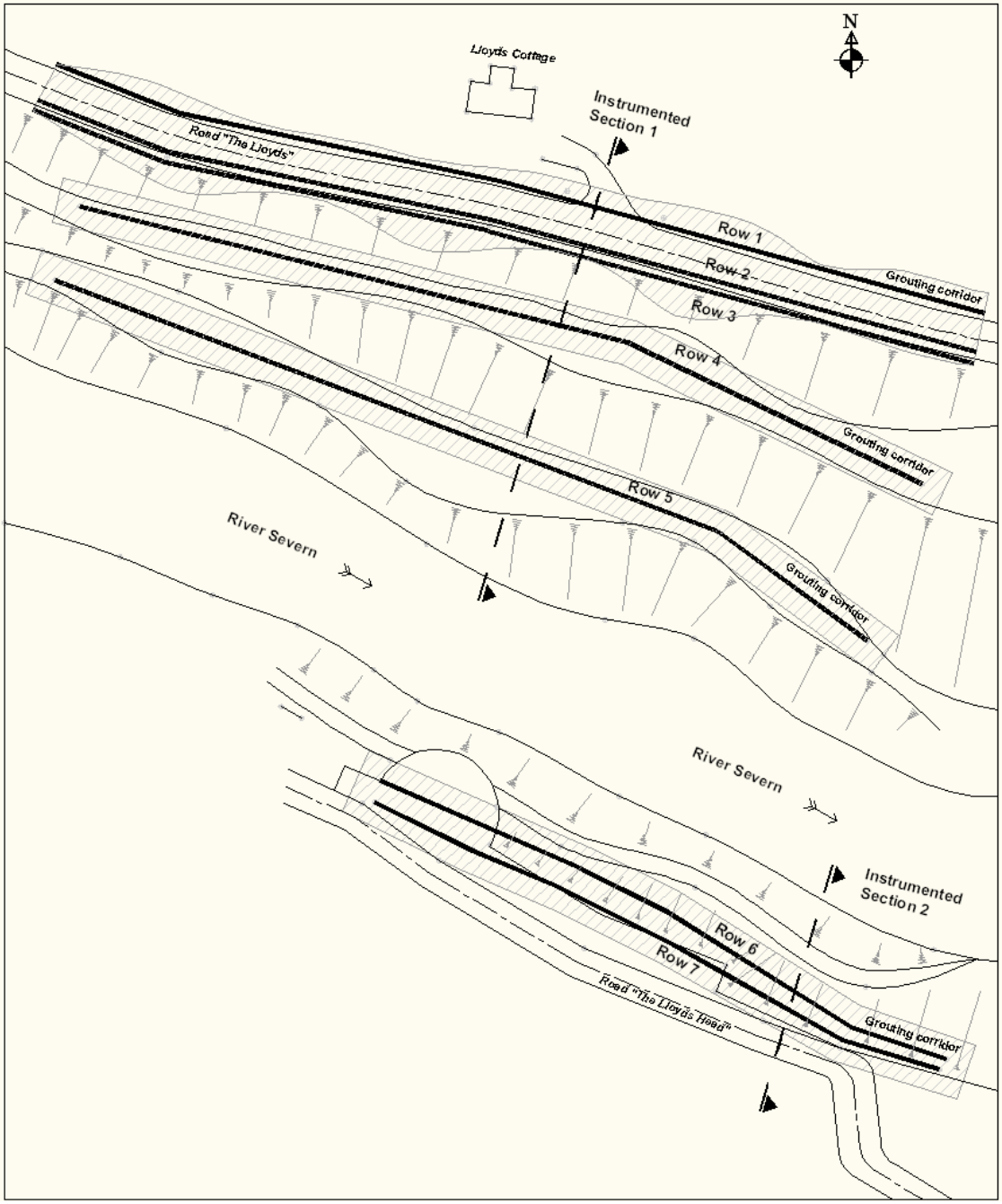

Figure 3.8: *Plan of Ironbridge site*

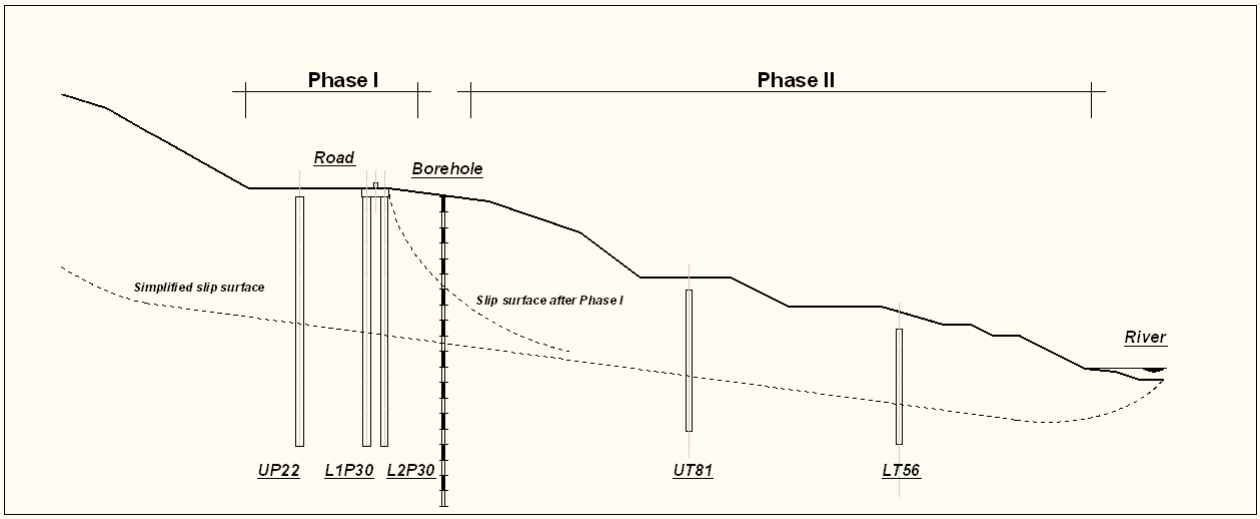

Figure 3.9: *Profile of Phase I and Phase II*

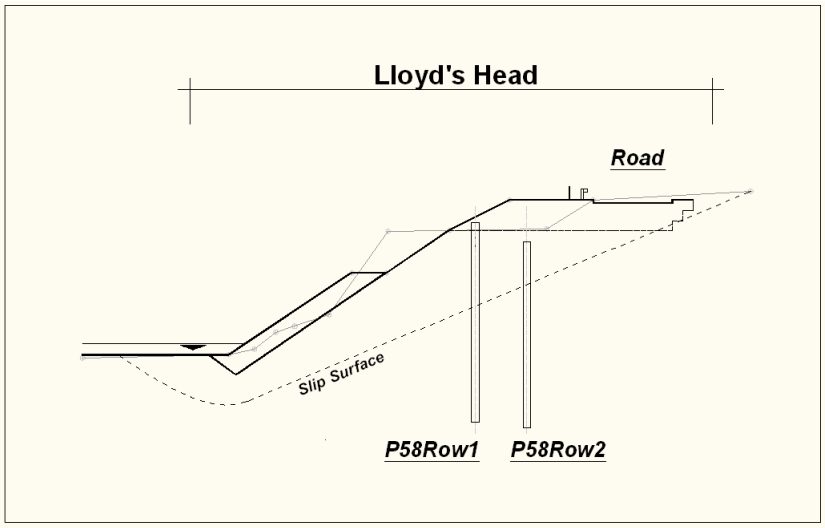

Figure 3.10: *Profile of Lloyd's Head*

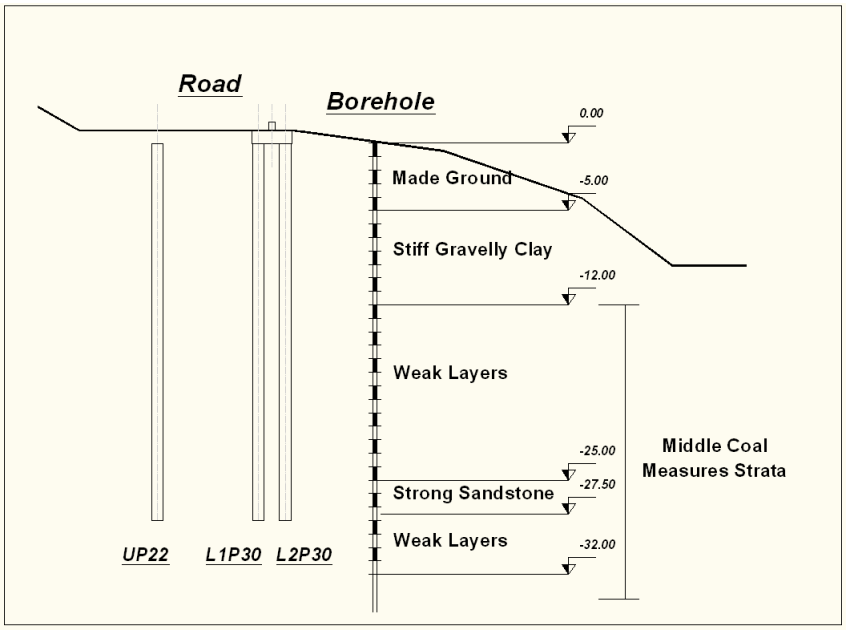

Figure 3.11: *Simplified geology section of Phase I*

3.4.1 The geology

The geology of both sides of the river is quite complex. For the Phase I and Phase II instrumented sections, the nearest borehole is just down-slope of the Phase I instruments. From the geological report it is possible to identify a first superficial layer (about 5m deep) of made ground containing many different materials (clay, sand, slag, bricks, concrete, ash and coal). Below there is another thick layer (about 7m deep) of firm and stiff gravelly clay. This shows that the top layer is probably a fill resulting from mining excavations and other recent industrial activity. The ground investigation report describes several probable shear surfaces (polished surfaces) present in the gravelly clay. It is not possible to verify if they are due to old or current instabilities. Below these two upper layers, there are several thin (from 10cm to 150cm) layers of weak rock (sandstone, mudstone and siltstone), coal, gravel and stiff clay (fig. 3.11), part of the Middle Coal Measures Strata, logged for a further 20m depth. The goemechanical strength and stiffness of the latter are probably greater than the top layers. The reports point out another probable slip surface between 17 and 18m depth below ground level. It has to be noted that at an average depth of about 25m from the ground level (the exact depth is different for each pile) a layer of strong sandstone is present. All the piles are supposed to be anchored into this layer, which is assumed to be stable.

3.4.2 The pile type

One type of pile was used in the stabilisation construction, but the diameters and steel thickness varied from row to row and the lengths varied from pile to pile depending on the depth to the firm sandstone layer. The piles used were cast in-situ bored circular concrete filled steel tubular piles. The piles installed in Phase I, and all the instrumented piles in both Phase I and II have concrete inside the steel pipe and grout in the external

ring between the reinforcement and the soil. The rest of the piles in Phase II have concrete inside and outside the steel pipe. From now on, the word *grout* will be used to indicate the weak concrete material used for the external ring of these piles.

The choice of a circular hollow steel pipe as reinforcement gives significant structural advantages as described in section 2.5.2. This type of pile is considered slender (due to its length), but is able to resist large bending moments due to the steel tube reinforcement. The main disadvantage is the cost, since a large amount of steel is required.

Installation of the piles was preceded by jet-grouting along the proposed pile rows (grouting corridors are shown in fig. 3.8) to fill gaps in the bedrock, resulting particularly from abandoned mine shafts and tunnels. The pile shaft was then excavated using an auger rig with the bore supported by a casing. For the instrumented piles, the reinforcement pipe was then lowered in the shaft and the concrete poured into it through a tremie pipe. Grout was then pumped into the gap between the reinforcement and the casing through a temporary pipe fixed to the outside of the reinforcement. The casing was then pulled out and the rest of the hole filled with grout.

3.4.3 Phase I

There are three instrumented piles in Phase I: UP22, L1P30 and L2P30.

UP22 is part of the first row of piles, built to stop the movements of the slope temporarily while rows 2 and 3 were installed and then to work with them in retaining the upper slope. The pile is 28m long and 860mm in diameter (the internal diameter of the steel pipe is 640mm, the thickness of the steel pipe 10mm, and the thickness of the grout ring of about 100mm). Each pile in this row is spaced 4.5m apart between the centres (fig. 3.12). The instrumented pile was installed on 10 January 2007.

L1P30 is part of the second row of piles and L2P30 is part of the third. These two rows were built simultaneously and were supposed to work together to retain the upper part of the slope and road. Both piles are 28m long and 866mm in diameter (internal diameter of the steel pipe 616mm, thickness of the steel pipe 25mm, thickness of the grout ring about 100mm). Each pile in these rows is spaced 3m apart between centres and the rows are staggered by 1.5m (fig. 3.12). L1P30 was installed the 4 of May 2007 while L2P30 was built the 8 of May 2007.

All the piles in row 2 and 3 were connected together with a 1m high concrete cap (fig. 3.12). The upper parts of the reinforcing steel pipes were not embedded in the cap. Instead the pile-cap connection was formed from reinforcing bars. This connection can be considered as an imperfect hinge rather than a moment connection, which means that the tops of the piles are likely to rotate once the concrete starts to take load.

Each of the three instrumented piles contains 15 pairs of welded strain gauges (par. 2.1.1) and an inclinometer tube (fig. 3.13). During the installation works, most of the cables from UP22 were damaged. This caused some serious problems in the monitoring of this pile, which will be discussed in section 4.5.

After the construction of the pile cap, a new road was built between row 1 and row 2

with the pavement lying on part of the pile cap. About a month after the construction, a deep crack in the soil appeared in front of row 3, indicating that the soil down-slope was still unstable. The works in Phase II followed to stabilise the lower part of the slope.

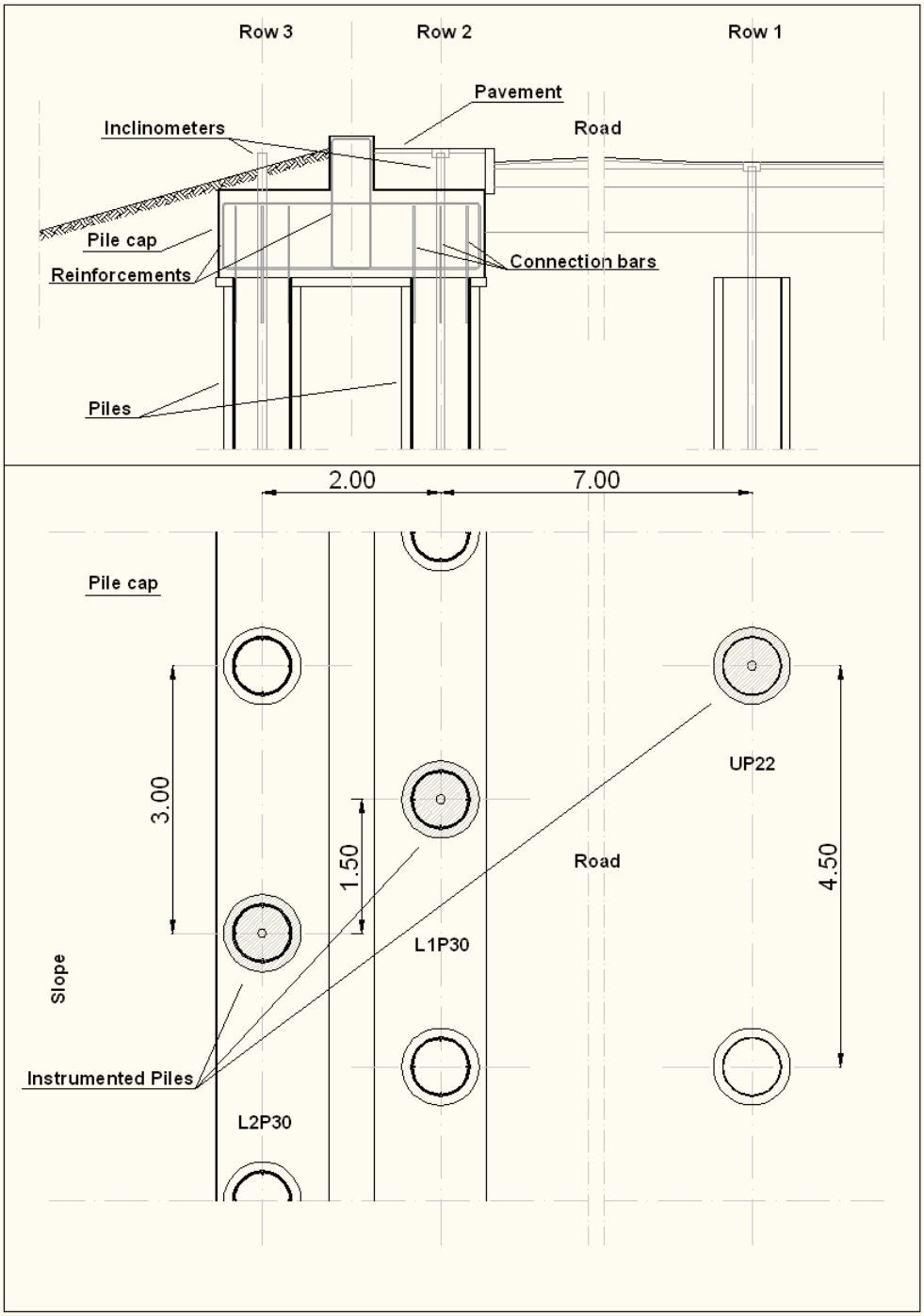

Figure 3.12: *Phase I, section and plan*

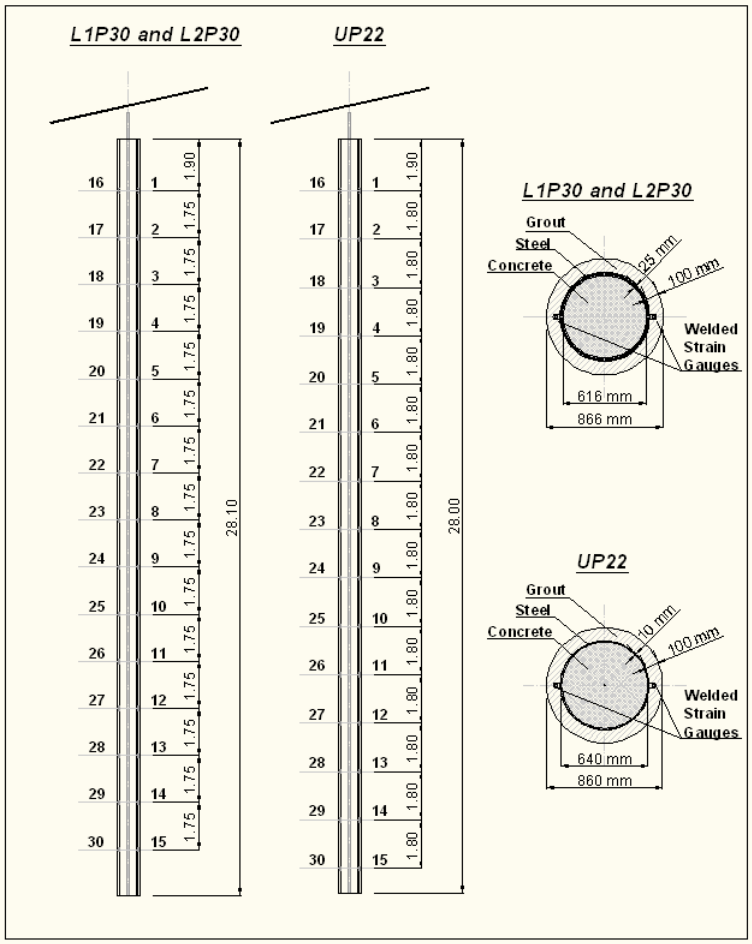

Figure 3.13: *Phase I, instrumented piles*

3.4.4 Phase II

The stabilisation works in Phase II included two rows of piles, an extensive regrading of the lower part of the slope and a new configuration for the river bank. Two piles were instrumented:

- UT81, part of row 4, is 16m long and 670mm in diameter (internal diameter of the steel 470mm, thickness of the steel pipe 10mm, thickness of the grout ring about 100mm). The piles in this row are 1.2m apart between centres (about two diameters). The instrumentation consists of 30 welded strain gauges (positioned in 15 pairs) and an inclinometer tube (fig. 3.14). The pile was installed the 21 August 2008.

- LT56, part of row 5, is 13m long and 670mm in diameter (internal diameter of the steel 470mm, thickness of the steel pipe 10mm, thickness of the grout ring about 100mm). The piles in this row are 1.8m apart between centres (about three diameters). The instrumentation consists of 24 welded strain gauges (positioned in 12 pairs) and an inclinometer tube (fig. 3.14). The pile was installed on 4 August 2008.

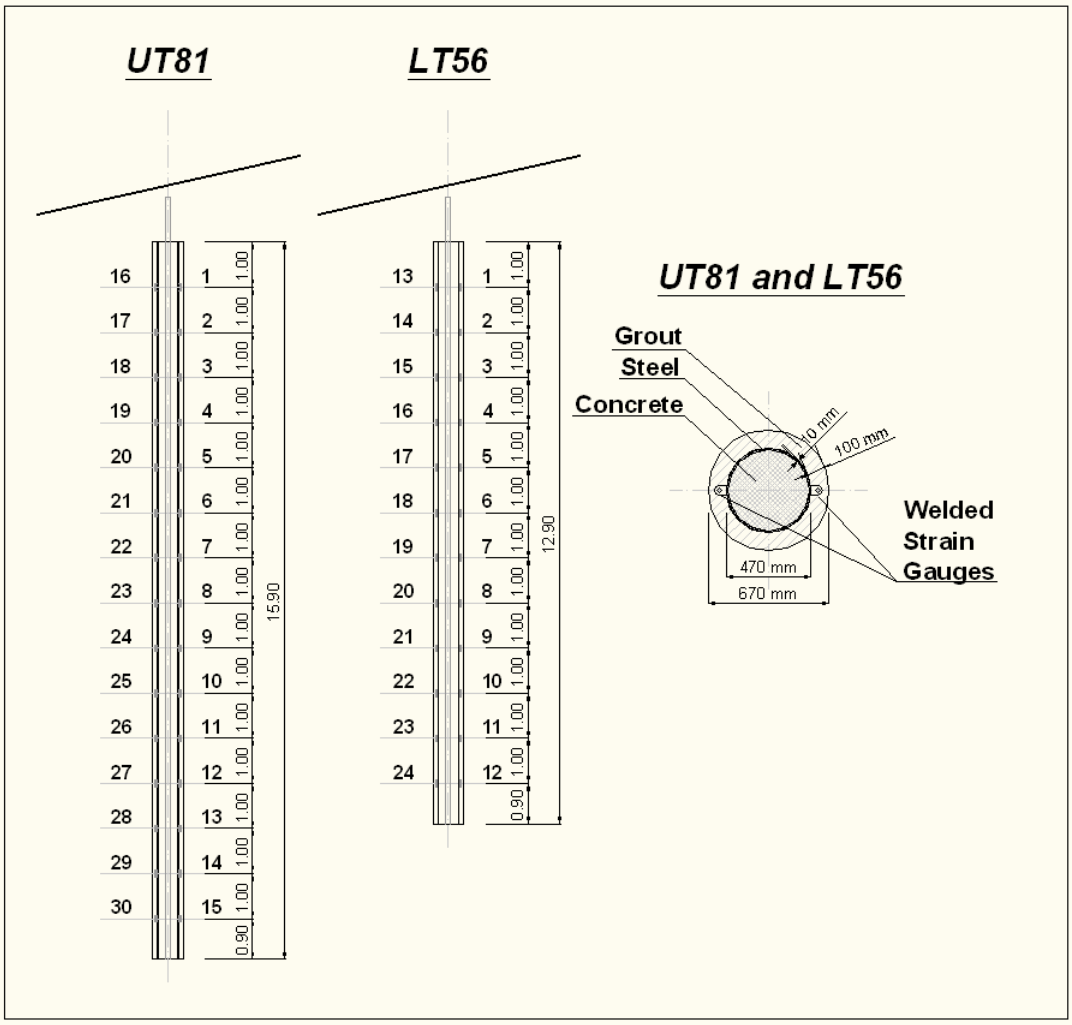

Figure 3.14: *Phase II, instrumented piles*

3.4.5 Lloyd's Head

The Lloyd's Head stabilisation scheme comprises two rows of piles, regrading of the slope and a new configuration for the river bank. When the stabilisation works were finished a new road, parking spaces and a terrace were built on top of the slope (fig. 3.10).

The two rows of piles in the instrumented section are 4.50m apart and the positions of the piles in the two rows are staggered. The two instrumented piles are:

- P58Row1, part of row 6 on fig. 3.8, is 17.40m long and 675mm in diameter (internal diameter of the steel 475mm, thickness of the steel pipe 10mm, thickness of the grout ring about 100mm). The piles in this row are 1.5m apart between centres. The instrumentation consists of 32 welded strain gauges (positioned in 16 pairs, fig. 3.15). The pile was installed the 10 September 2008.

- P58Row2, part of row 7 on fig. 3.8, is 16.20m long and the pile section is equal to P58Row1. The piles in this row are 1.5m apart between centres. The instrumentation consists of 30 welded strain gauges (positioned in 15 pairs, fig. 3.15).

The pile was installed on 9 September 2008.

These two instrumented piles do not contain any inclinometer tubes.

During the installation works, problems in augering the pile bore resulted in the positions of the tops of the piles differing from the original design: P58Row1 was positioned about 1m higher while P58Row2 about 1m lower (fig. 3.15).

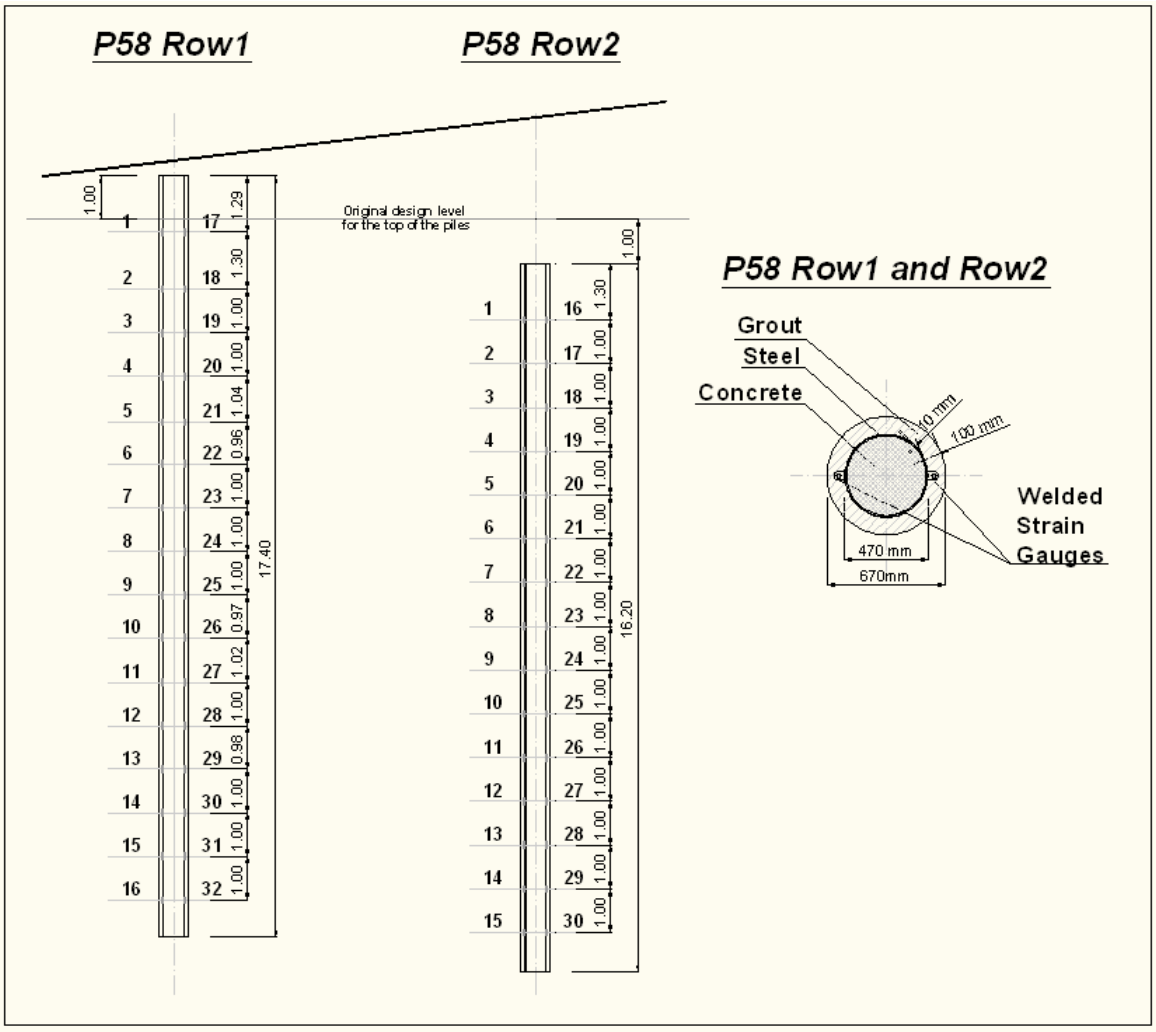

Figure 3.15: *Lloyd's Head, instrumented piles*

3.5 Concrete sampling: properties of the materials and respective assumptions

The concrete strength given in the concrete mix specifications for the different piles is the design strength. This is the minimum strength that the concrete (or grout) should develop 28 days after pouring. This research assesses the long term pile behaviour. As stated in par. 2.3.1, the strength of concrete increases with time following an exponential curve (formula 2.3). To have more accurate strength parameters, concrete samples were collected for the piles installed after November 2007 (the beginning of this research project). This means that concrete samples were collected from the Leatherhead piles

(six samples), and the Ironbridge Phase II piles for both concrete (six samples) and grout (six samples). All the sampling followed the BS EN 12390-2 (2000). Testing followed BS EN 12390-3 (2002) for the samples tested at 28 days (three for each pile). The other samples were cured for 28 days in water then wrapped in wet cloths, sealed in plastic bags (to simulate soil conditions) and kept at laboratory temperature. 90 days after pouring, the samples were tested to BS EN 12390-3 (2002). The average concrete strength results (f_{cu}) are shown in tab. 3.3, which shows an increase in strength with time for all the samples. Most importantly, the f_{cu} values are very different from the assumed design values shown in the previous sections (35MPa for Leatherhead, 32/40MPa for Ironbridge concrete and 8/10MPa for Ironbridge grout).

Leatherhead *(concrete)*		**Ironbridge** *(grout)*		**Ironbridge** *(concrete)*	
28 days	90 days	28 days	90 days	28 days	90 days
f_{cu}= 47 MPa	f_{cu}= 55 MPa	f_{cu}= 30 MPa	f_{cu}= 33 MPa	f_{cu}= 50 MPa	f_{cu}= 57 MPa

Table 3.3: *Concrete samples average results*

The actual strength of the concrete samples is much greater than the design strength. This shows that for the back analysis of the data it is not appropriate to use the design strength parameters, but it is better to test the instrumented pile concrete. Assumptions were made for the other instrumented piles since concrete sampling had not been possible. For the Grange Hill and Mill Hill piles, the assumed strength is 50 MPa, slightly smaller than the Leatherhead piles considering the absence of large aggregates at Grange Hill and the high water/cement ratio at Mill Hill. For Ironbridge Phase I, it was assumed that the piles had similar characteristic to Ironbridge Phase II, so the assumed strengths of both concrete and grout are the same as the tested samples: 57 MPa and 33MPa respectively.

Leatherhead *(concrete)*	**Grange Hill** *(concrete)*	**Mill Hill** *(concrete)*	**Ironbridge** *(concrete)*	**Ironbridge** *(grout)*
f_{cu}= 55 MPa	f_{cu}= 50 MPa	f_{cu}= 50 MPa	f_{cu}= 57 MPa	f_{cu}= 33 MPa

Table 3.4: *Long term concrete strength (f_{cu}) values*

3.6 Conclusions

This chapter summarises the layout of each site, the geology, the design of each pile, the instruments used and the concrete strength. The research is based on four sites with a total of 14 instrumented piles. Three sites (Grange Hill, Leatherhead and Mill Hill) have slopes stabilised with a single row of discrete piles; while one site (Ironbridge) have two slopes, one stabilised with 5 rows of discrete piles and the other with two rows of discrete piles. Grange Hill is a railway cutting in London Clay, three instrumented piles are analysed from this site. Leatherhead is a motorway embankment in London Clay, two instrumented piles are analysed. Mill Hill is a railway embankment in Clay

Fill, two instrumented piles are analysed. Ironbridge is a complex landslide in Made Ground and Middle Coal Measures, seven instrumented piles are analysed. Table 3.5 summarises some of the characteristics of the instrumented piles.

Site	Pile	Type	Diameter [mm]	Length [m]	Distance between centres [m]	Strain Gauges	Inclinometers
Grange Hill	Pile 1	Standard reinforced concrete	600	11.00	1.80 (3 diameters)	20 Embedded	1
	Pile 2	Standard reinforced concrete	600	11.00		20 Embedded	1
	Pile 3	Standard reinforced concrete	600	9.00		20 Embedded	1
Leatherhead	Pile 1	Standard reinforced concrete	1050	13.00	2.50 (2.4 diameters)	6 Embedded 14 Sister bars	1
	Pile 2	Standard reinforced concrete	1050	13.00		6 Embedded 14 Sister bars	1
Mill Hill	Pile 1	Standard reinforced concrete	450	11.00	0.70 (1.5 diameters)	20 Embedded	1
	Pile 2	Standard reinforced concrete	450	11.00		20 Embedded	1
Ironbridge	UP22	Concrete-Filled Steel Tubular Piles	860	28.10	4.50 (5.2 diameters)	30 Welded	1
	L1P30	Concrete-Filled Steel Tubular Piles	866	28.10	2 rows staggered	30 Welded	1
	L2P30	Concrete-Filled Steel Tubular Piles	866	28.00		30 Welded	1
	UT81	Concrete-Filled Steel Tubular Piles	670	15.90	1.20 (1.8 diameters)	30 Welded	1
	LT56	Concrete-Filled Steel Tubular Piles	670	12.90	1.80 (2.7 diameters)	24 Welded	1
	P58 R1	Concrete-Filled Steel Tubular Piles	670	17.40	2 rows staggered	32 Welded	-
	P58 R2	Concrete-Filled Steel Tubular Piles	670	16.20		30 Welded	-

Table 3.5: *Summary of the instrumented piles*

Chapter 4

Interpretation of strain gauge data

This chapter analyses the method used to interpret the strain gauges data. This means how to pass from the signal the instrument transmits to the clean profile of the strains for the analysis of the instrumented structure. Datum setting, data-cleaning and temperature corrections are analysed and examples are given to show the necessity of the correction. The strain profiles for each pile are shown at the end of this chapter as results of the interpretation of strain gauge data. Errors at this stage will compromise the understanding of the pile behaviour in the following chapters.

4.1 Vibrating wire strain gauge: from reading to absolute strain

As introduced in par. 2.1.1, a vibrating wire strain gauge measures the frequency of a vibrating wire. In reality the reading (R) the strain gauge carries out is a period (measured in period$\times 10^7$) that the data-logger transforms into a frequency (f):

$$f = \frac{1}{R/10^7} \tag{4.1}$$

f is measured in Hz.

The period depends on the harmonics the data-logger is set to read. This is explained in more detail in par. 4.3.

Depending on the model and setting, the data-logger can also generate the so called *digit*, instead of the frequency:

$$digit = \frac{f^2}{1000} \tag{4.2}$$

digit is measured in Hz^2.

It is now possible to calculate the absolute strain (ε_a) as:

$$\varepsilon_a = digit \times gaugefactor \tag{4.3}$$

Where *gaugefactor* is a constant given by the producer of the instrument. It is based on the laboratory calibration done when the strain gauge is assembled.In this context,

ε_a is referred as an absolute strain to distinguish it from the relative strain obtained after datum setting (par. 4.2).

The complete formula for the absolute strain (ε_a) is:

$$\varepsilon_{\mathbf{a}} = gaugefactor \times \left[\frac{(10^7/R)^2}{1000}\right] \tag{4.4}$$

ε_a is measured in $\mu\varepsilon$ (microstrains).

In this research, in-place data-loggers produce a digit that permits the use of Equation 4.3 to calculate ε_a; while temporary mini-loggers give out a reading (R) which needs the use of Equation 4.4.

4.2 Datum setting

The previous section explained how to get a strain reading (in $\mu\varepsilon$) from the strain gauges. These readings refer to the length of the tensioned wire. To measure the structural strain changes during time, it is necessary to fix a datum and to subtract its absolute strain to all the other readings. The definition of the datum (i.e. its position on the time line) is very important as it affects all the subsequent calculations, analysis and results. This research focuses on the behaviour of the whole pile so there has to be single datum time for all the strain gauges in the pile. This means that the strain profiles will all show zero at the same time (fig. 4.7).

For practical reasons of optimisation of the program used in the calculation, the datum is set during the calculation of the strains as:

$$\varepsilon_a = (digit - digit_{Datum}) \times gaugefactor \tag{4.5}$$

The datum has to be related to the objectives pursued. If the analysis is focused on the concrete early stages behaviour, the datum should be set just after pouring or even before it. If the research is analysing a particular load occurrence, the datum should be set just before the load is applied. This research is focusing on the long term behaviour of piles under load, and we are not interested in the short term effects of concrete setting. This means that the datum for the strain gauges can be set some time after pouring, when any remaining setting effects are minimal compared with the anticipated load effects. In this way the early age effects are minimised.

4.2.1 Effects of concrete setting on strain gauges

To find the appropriate time datum, it is necessary to analyse the concrete setting processes and their effects on the strain gauge readings.

After pouring, the concrete is affected by different processes: plastic shrinkage develops in the first hours while autogenous shrinkage affects the concrete at later times; the temperature increases (in this research some thermistors recorded up to $40°C$) due to the exothermic hydration reactions in the first hours after pouring (par. 2.2.2) and then takes a long time to dissipate (fig. 4.2). These three processes have a direct effect

on the strain gauge readings. Plastic and autogenous shrinkage, which are intrinsic to the concrete (par. 2.4.1), give a uniform increase in compression to all the strain gauges connected to the concrete (embedded and sister bars) in the same section. The effect of the temperature increase on the instruments (which is also assumed to be uniform on the section) is more complicated (par. 4.4.2), but in this particular case it is to expand the instrument which records a corresponding increase in tension. The two effects are superimposed and their magnitude is related to all the concrete and instrumental parameters. Concrete setting effects do not generate any bending moment since they are uniform along the same section.

In par. 2.4.5 it was assumed that long term shrinkage and creep effects are a negligible portion of the overall pile strains. In view of this, plastic shrinkage was not considered since the measurements on the samples started after concrete setting.

4.2.2 Method for the choice of a datum in long term analysis

Since all the concrete setting effects are superimposed and their development is related to both the concrete parameters and to the environment, their understanding, quantification and correction is complicated. For example, figure 4.1 and figure 4.2 show that the full dissipation of the heat of hydration takes more than three months. After this period the environmental seasonal temperature cycles are predominant. The curves for nearly all the temperatures (the instruments at the top of the piles are more influenced by the air temperature variation) can be divided in two parts: in the first part (before the change in the heat dissipation rate in fig. 4.2) the temperature decreases rapidly, and in the second part (after the change in the heat dissipation rate in fig. 4.2) the dissipation rate is lower. As pointed out before, the focus of this research is the long term behaviour of the piles. To avoid some of the problems related to the early stage effects and processes (par. 4.2.1) it was chosen to set the datum approximately when most of the heat of hydration had been dissipated (fig. 4.2). This gives minimal effects due to temperature changes and plastic shrinkage and avoids most of the effects of autogenous shrinkage. The complete development of the latter cannot be measured without a related monitored concrete sample (unloaded but in the same environmental conditions). The early stage effects are usually seen as a steep increase in strain in the first period of the readings (fig. 4.3). The datum time has to be one for all the instruments on a pile, thus an average time along the pile has to be chosen. The heat of hydration dissipates at different rates along the pile, therefore the thermistors record different curves at different locations.

This approach only minimises the setting effects and it is accepted that some errors in the strain readings remains. The latter are connected to the part of the autogenous shrinkage that develops after the datum and to the temperature dissipation rates that are not the same along the depth of the pile. The errors could be avoided setting the datum when the hydration heat is completely dissipated, but during this time the pile could have been already loaded by the slope and there would be an error in the bending strain measurements and in the following bending moment calculations. It is necessary

that the datum is set before the pile starts to be loaded. The beginning of the bending moment development has to be determined for individual piles and compared with the time when the heat of hydration is mostly dissipated. When the loading on the pile starts before the heat of hydration is dissipated, the datum has to be set before the beginning of the loading. The problem is complicated by the fact that at this stage of the analysis the bending moment has not been calculated yet. The strain gauge readings can give information about the beginning of the loading process on the pile. The two instruments in an instrumented section give similar readings (fig. 4.3) when the section is subjected to uniform effects (shrinkage, temperature, axial loading), while they show different patterns when the section is in bending (fig. 4.4), i.e. the pile is loaded by the slope. When the datum is set very close to the pouring time, the total values of the measured strains and in the axial strain of the sections are affected by errors due to concrete setting effects (par. 4.2.1).

In some cases the data from the early stages after pouring cannot be recorded for technical problems. A piling site is usually very busy and sometimes it is not safe to install the data-logger immediately after pouring. It can happen that the data-logger is installed at the end of the site works, missing not only all the early stage data, but also the first part of the loading and related bending moments. In these cases the datum can be set as the first data recorded.

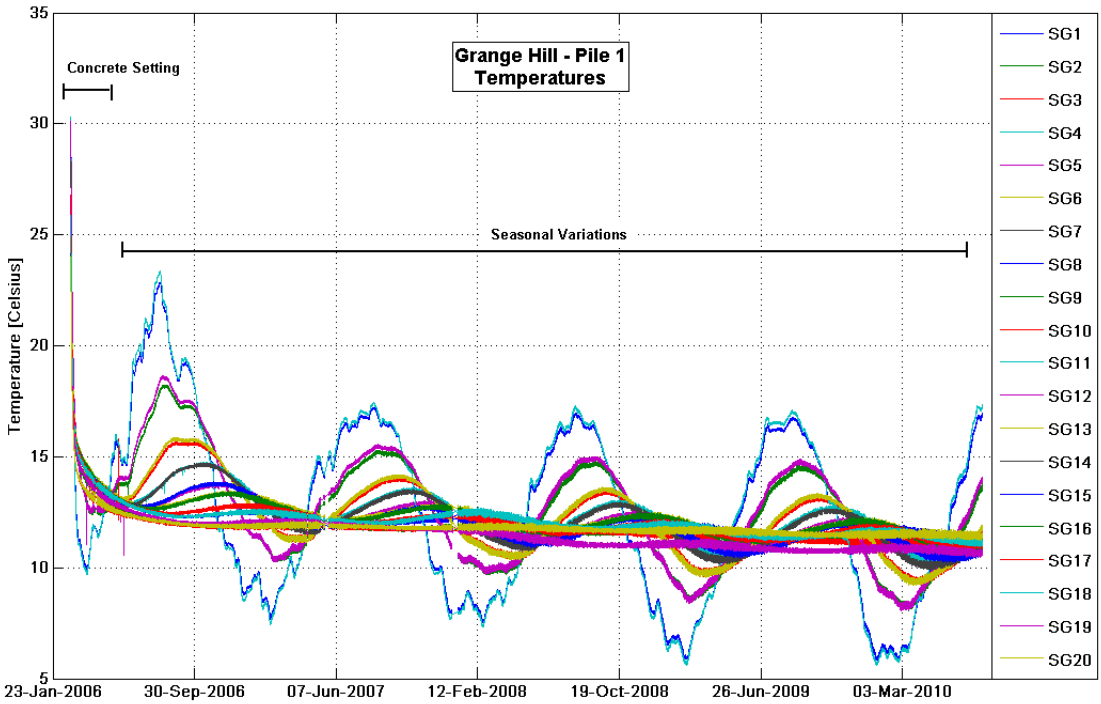

Figure 4.1: *Grange Hill Pile 1, temperatures*

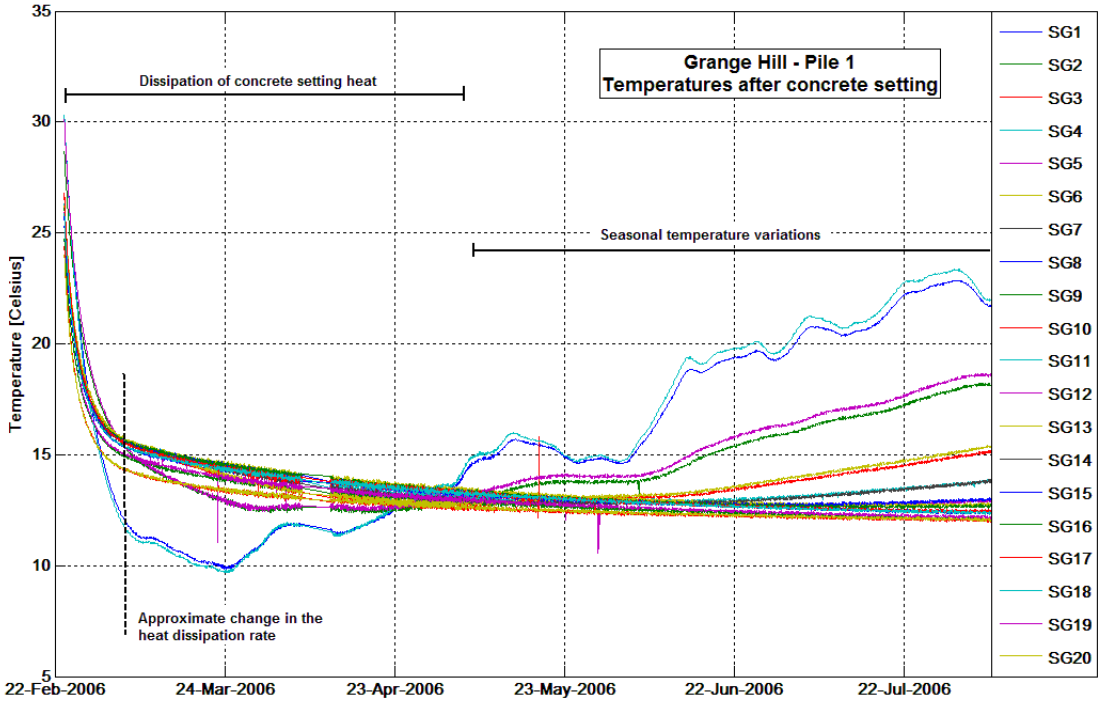

Figure 4.2: *Grange Hill Pile 1, temperatures after concrete setting*

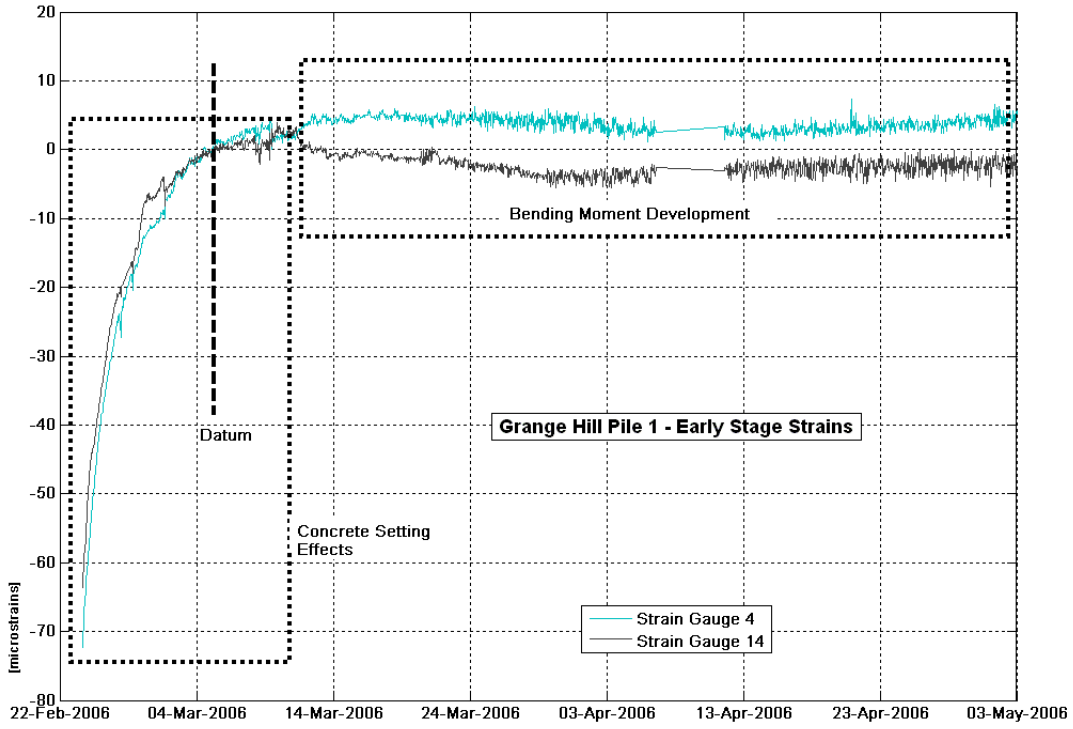

Figure 4.3: *Grange Hill Pile 1, early stage strain development for section 4-14*

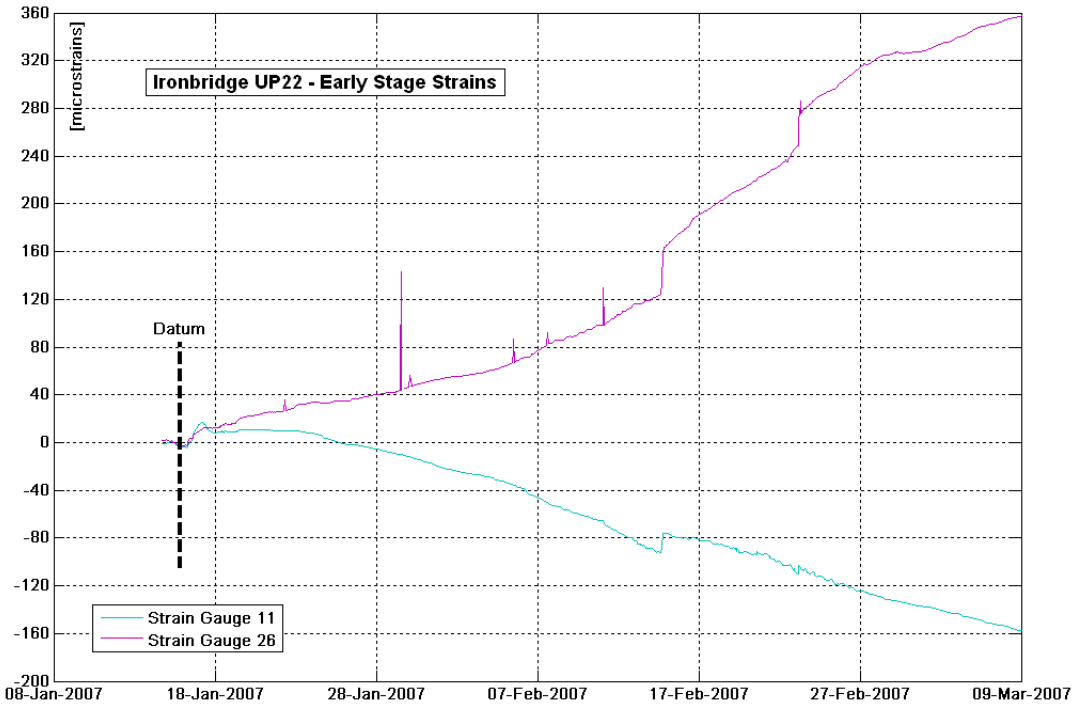

Figure 4.4: *Ironbridge UP22, early stage strain development for section 11-26. No concrete setting effects are present, the instruments only show the development of bending strains.*

4.2.3 Datum setting conclusions

It can be concluded that the datum for long term analysis:

1. Has to be set before the beginning of the loading.
2. Has to minimise the inclusion of concrete setting effects.

Thus it is necessary to identify when the loading begins and when most of the heat of hydration is dissipated, and to compare the two. If the beginning of the loading is the first in time, then the datum has to be set just before it; while if the loading starts later than the change in temperature dissipation rates, the datum has to be set approximately when the temperature dissipation rates changes.

When the first part of the data is missing, the datum can be set as the first reading.

In this analysis the datums for the piles in Grange Hill, Mill Hill and Ironbridge (all the piles except UP22) were set when most of the heat of hydration was dissipated; the datum of UP22 in Ironbridge was set when the loading began; and the datums of the piles in Leatherhead were set when the first reading recorded.

4.2.4 Example

Grange Hill Pile 1 datum setting is now analysed in detail as an example of the application of the method explained above. In this case the data-logger began to record

just after pouring. The instrument temperatures (fig. 4.1 and fig. 4.2) clearly show the dissipation of the heat generated by the hydration reactions. Analysis of the first month of recorded temperatures (fig. 4.5) shows the dissipation curves. It was decided to set the datum on the 5 March 2006, eleven days after pouring (ten days after the installation of the data-logger), when most of the heat of hydration had been dissipated. The temperatures recorded by the pair of instruments in the top section of the pile are influenced by environmental temperature changes, thus is better to not consider them in the datum setting. The choice of this datum generates the changes in strain profiles shown in figure 4.6 and 4.7. Since the datum is used during the calculation of the strains for each instrument, the two graphs (fig. 4.6 and fig. 4.7) have different units on the y axis, *digit* for fig. 4.6 and *microstrain* for fig. 4.7. The shape of the profiles is the same, but the values are scaled by the *gaugefactor* (par. 4.2). The profiles are still affected by the interferences which will be removed using the procedures illustrated in section 4.3.

At this point the development of bending strains was checked. In each instrumented section, the two strain profiles were compared (as in fig. 4.3) to see when the pile began to be affected by the lateral load. The profiles showed that the pile started to bend after the datum, as illustrated by figure 4.3; thus it was decided that the chosen datum was appropriate.

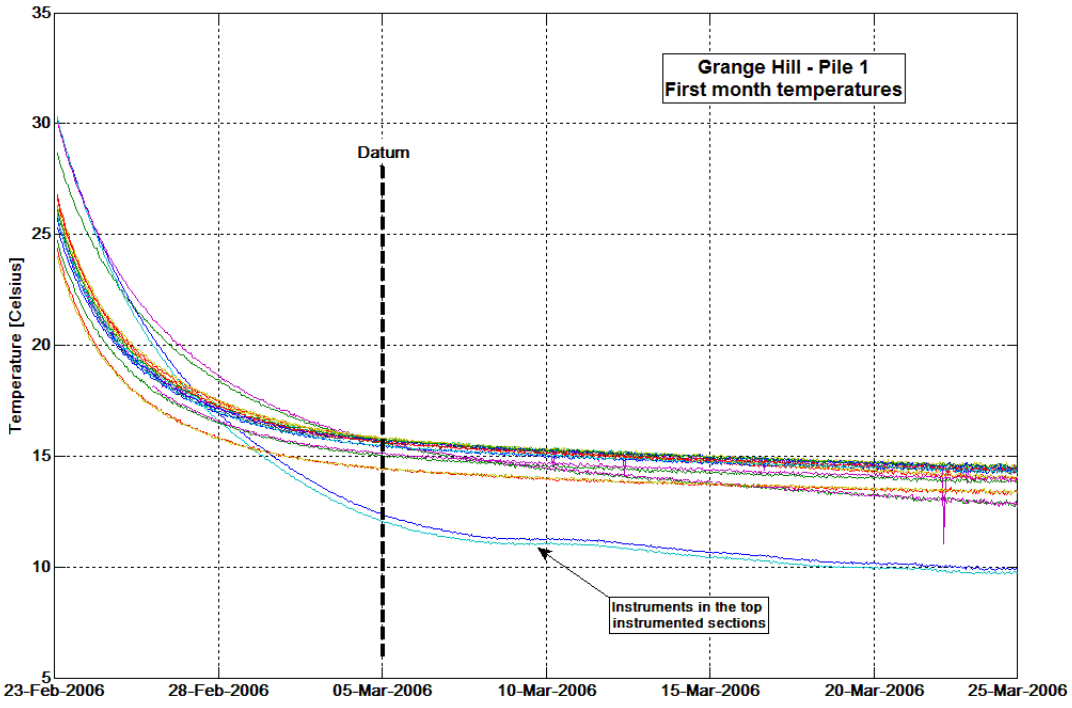

Figure 4.5: *Grange Hill Pile 1, first month of recorded temperatures after pouring of concrete*

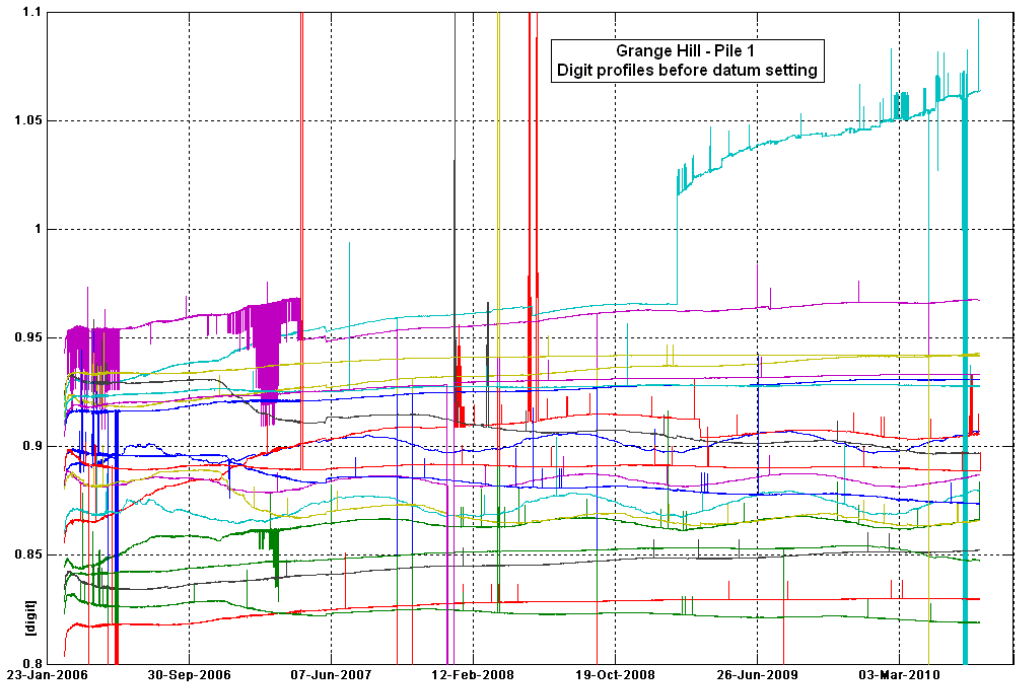

Figure 4.6: *Grange Hill Pile 1,* digit *profiles before the setting of the datum*

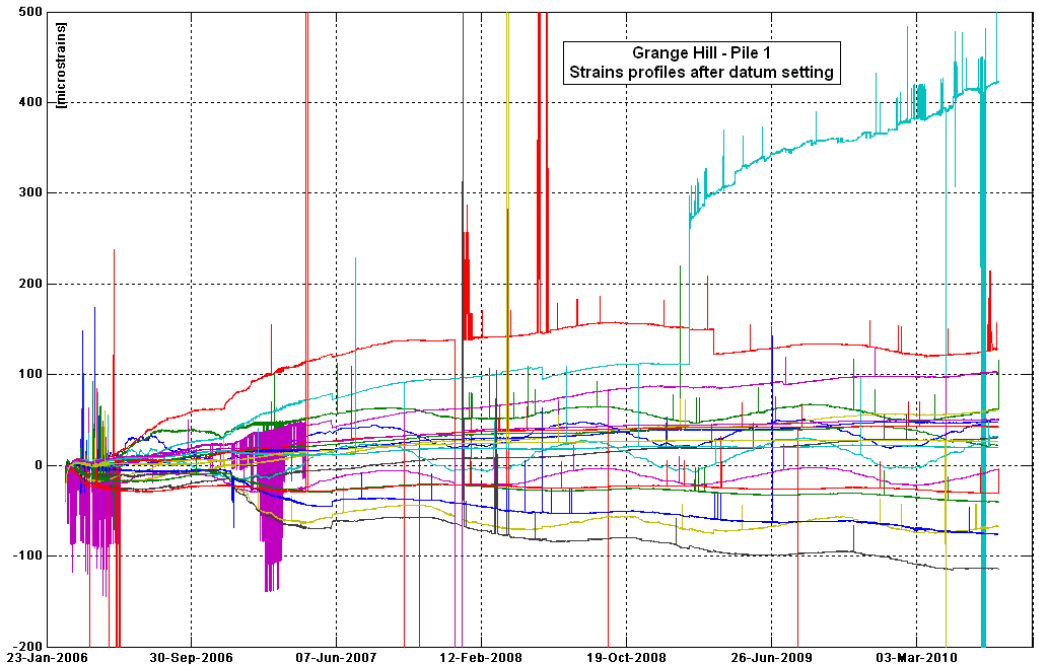

Figure 4.7: *Grange Hill Pile 1, strain profiles after datum setting. All the interferences are still present and will be eliminated with procedures shown in par. 4.3. The cleaned profiles are shown in fig. 4.9.*

4.3 Removal of interference

After the datum is set, it is usually necessary to clean the data from interference and reading errors. The large amount of data recorded for each instrument (a reading every hour in this research) allows the trend of each instrument and any potential interference or error to be identified easily(fig. 4.8). The types of interferences/errors found in this analysis are:

1. **General interference**, caused by humidity in the instruments, loose connections or electromagnetic fields. They are represented by single or multiple jumps in the readings usually surrounded by clear data. In this case, the errors are identified and eliminated manually or using different types of code depending on the program used for the data analysis. The correction leaves gaps in the readings, but a much clearer overall graph (fig. 4.9).

2. **Harmonics errors**, caused by an incorrect setting of the data-logger or partial breakage of of the data-logger multiplexors. The strain gauge reads the period of vibration of the wire, but the data-logger needs to know which harmonic has to be to used in the count of the frequency. A jump, the complete shift and a rescaling of the part of clear data affected appear when the value referring to the harmonics changes (fig. 4.10). The scaling of the data is due to the wrong frequency being calculated by the data-logger (par. 4.1). It can happen that the data-logger had been set wrongly when starting the data recording. In this case the correct data are produced after resetting the harmonics. To correct the harmonics error it is first necessary to identify it (it can be difficult if the wrong setting is made when the recording starts), reset the data-logger with the correct harmonic, adjust the data (rescaling) and shift the graph back to the correct position (fig. 4.11). Also the datum has to be reset if the correction affects it. The harmonic correction is usually done when the data are in the "digit" form (par. 4.1).

3. **Complex interference/error**. Sometimes the two types of error overlap and it is possible to see the trend/pattern of the readings, but some of them are shifted by a constant distances and overlapped (fig. 4.12). This can be caused by a damaged data-logger with loose connections and sometimes from damaged strain gauges. For correcting the data, it is necessary to identify the correct harmonic, reset and fix the data-logger and connections, shift back the data to the correct position and eliminate the interference. A large part of the affected data is usually lost during the correction. The combination of the two errors results in interferences shifted by constant distances (depending on the harmonics). The shape of the graph is maintained, but it is multiplied and shifted. Generally, it is not possible to correct every single reading, so the correct harmonic readings are identified and the others eliminated. Even if little data remain after the correction, the trend of the reading is recovered.

The interferences/error of the first type can occur to strain gauge and thermistor readings while the second and third type are only related to strain gauges.

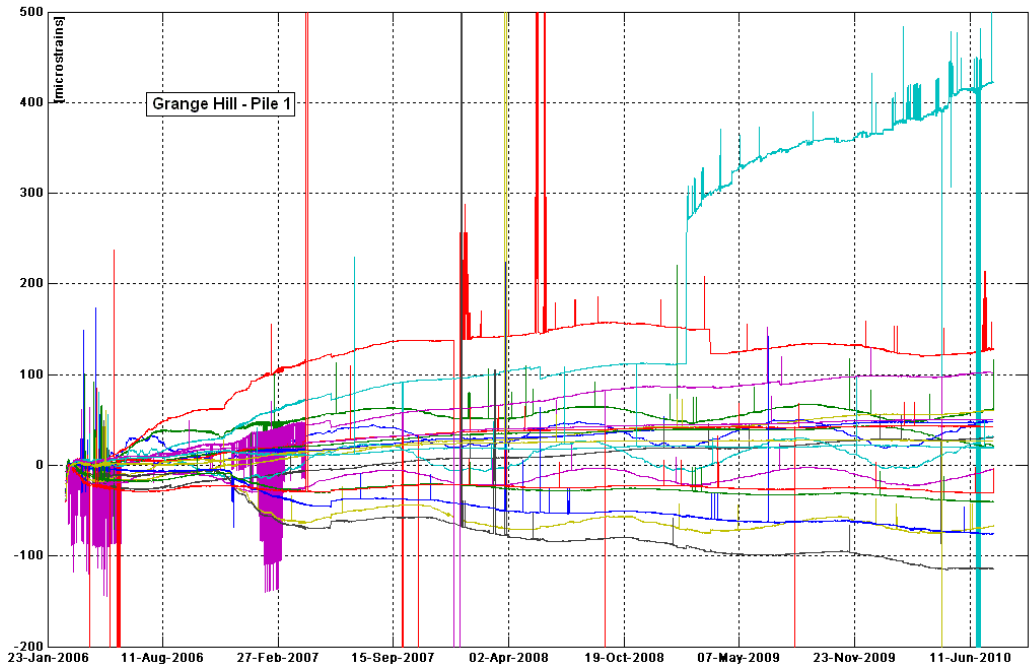

Figure 4.8: *Grange Hill Pile 1, general interference before correction.*

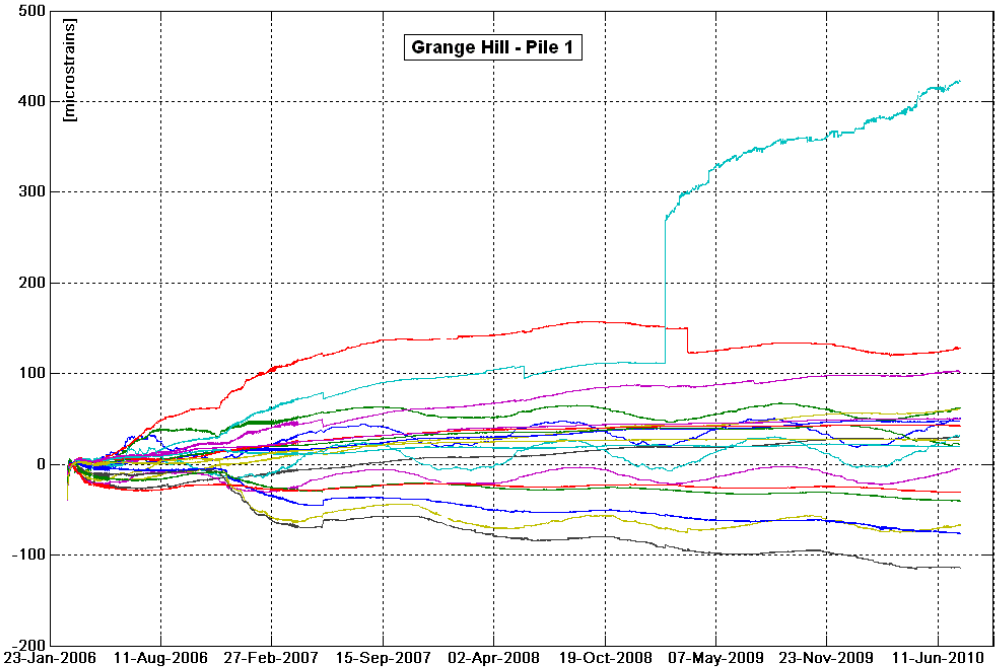

Figure 4.9: *Grange Hill Pile 1, general interference after correction.*

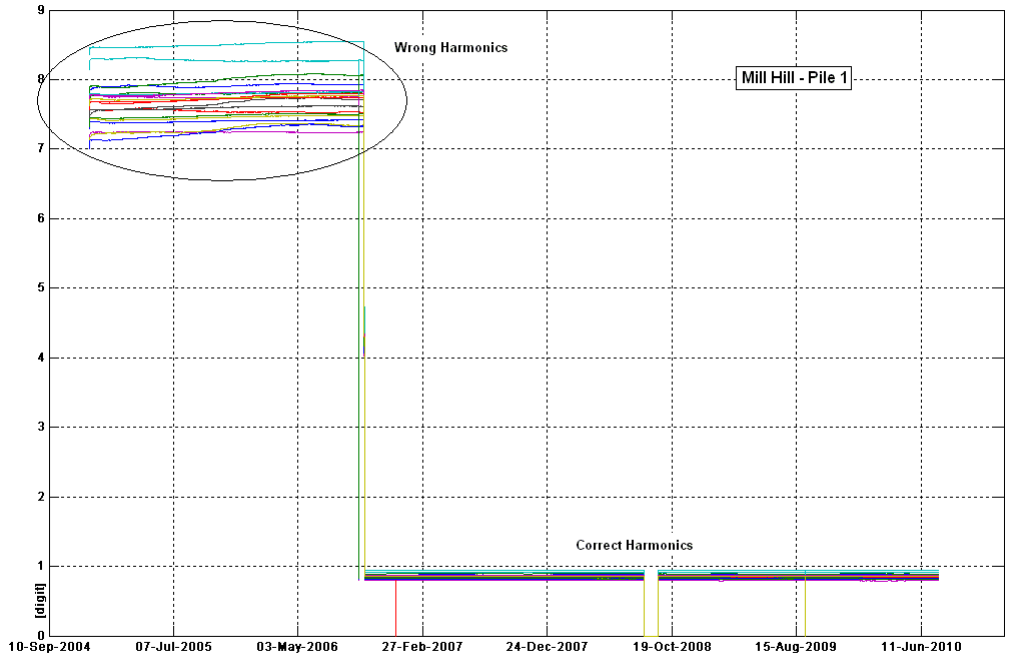

Figure 4.10: *Mill Hill Pile 1, harmonic errors before correction. The first setting of the data-logger was wrong and it was subsequently changed. The readings in the two parts of the graph have different scales due to the different harmonics used by the data-logger in the frequency calculation.*

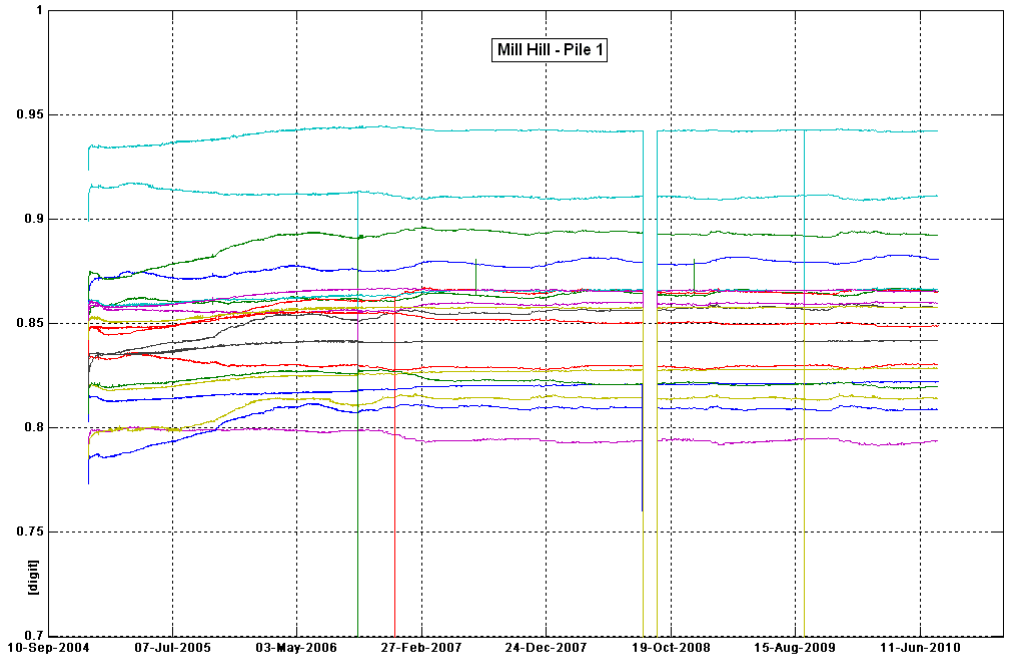

Figure 4.11: *Mill Hill Pile 1, data profiles after correction of the harmonic errors. The datum is not fixed yet.*

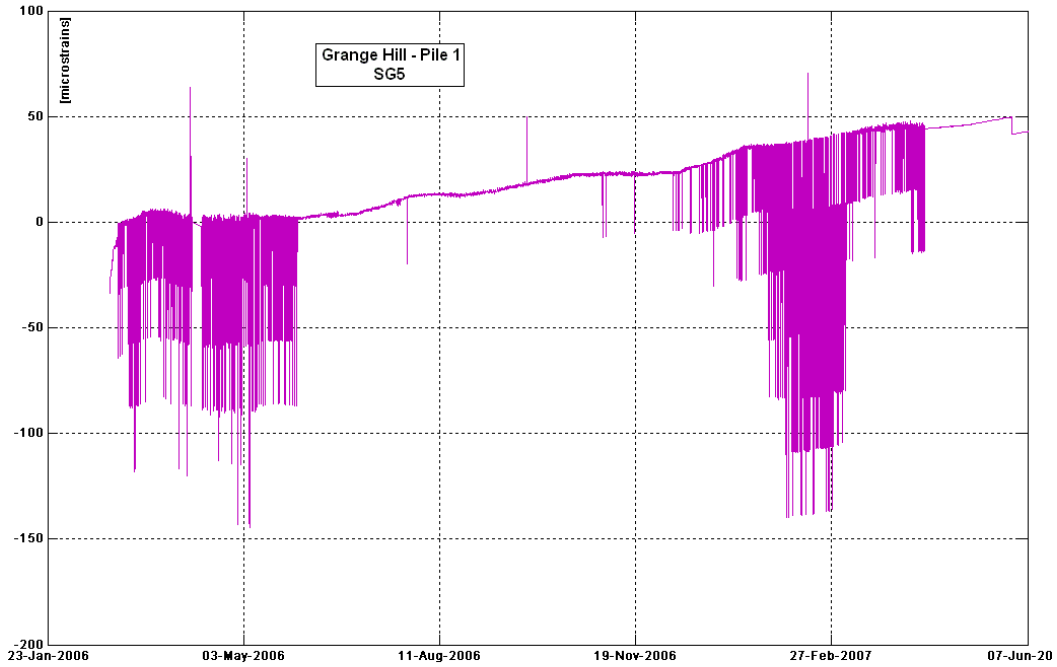

Figure 4.12: *Grange Hill Pile 1 SG5, complex interference before correction. In this case the harmonic errors are already corrected, only the interferences remains. The graph shows how the interferences maintain the shape of the graph, but the points are translated by set amounts.*

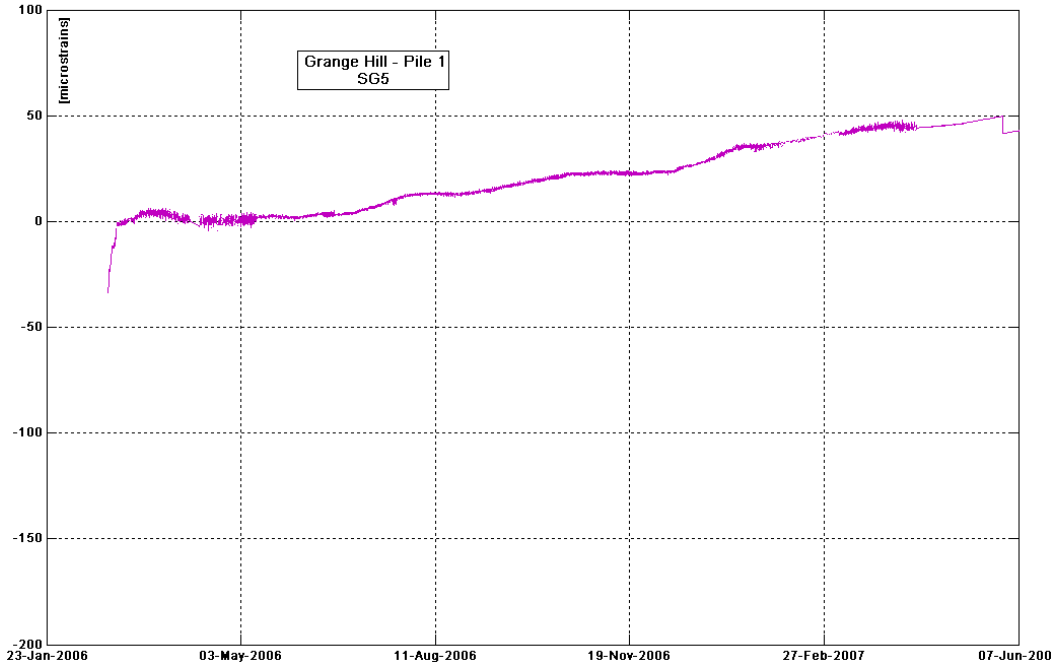

Figure 4.13: *Grange Hill Pile 1 SG5, complex interference after correction.*

4.4 Temperature corrections

During the analysis of strain data from the Grange Hill, Mill Hill and Leatherhead piles, a persistent seasonal strain variation within the upper half of the instrumented piles was noticed (figs. 4.14, 4.15 and 4.16). The peaks and troughs of the graphs are not consistent between the sites and sometimes they are not consistent along the depth of the same pile. Different hypothesis have been analysed during this research to explain this seasonal variation.

The Ironbridge piles are not considered in this section because the strain gauges do not show such similar seasonal variations.

The effects of differential thermal expansion of the concrete/soil system (the coefficient of thermal expansion of concrete is different than the one of saturated clay) were investigated without success. This approach could not fully explain the results recorded and thus was discarded. Instead it was postulated that the differential thermal expansion of the strain-gauge/concrete system was involved in the effect. This section analyses the method used and the results obtained applying the latter. The first part of the analysis uses strain/temperature graphs to identify the existence of a main strain/temperature correlation. If this is present, an appropriate temperature correction is applied to clean the data. Otherwise the recorded data are not heavily influenced by the temperature changes and no corrections are applied.

This approach shows that different piles (built with different concretes and installed in different soils) need different corrections which take into account the effective strain/temperature correlations.

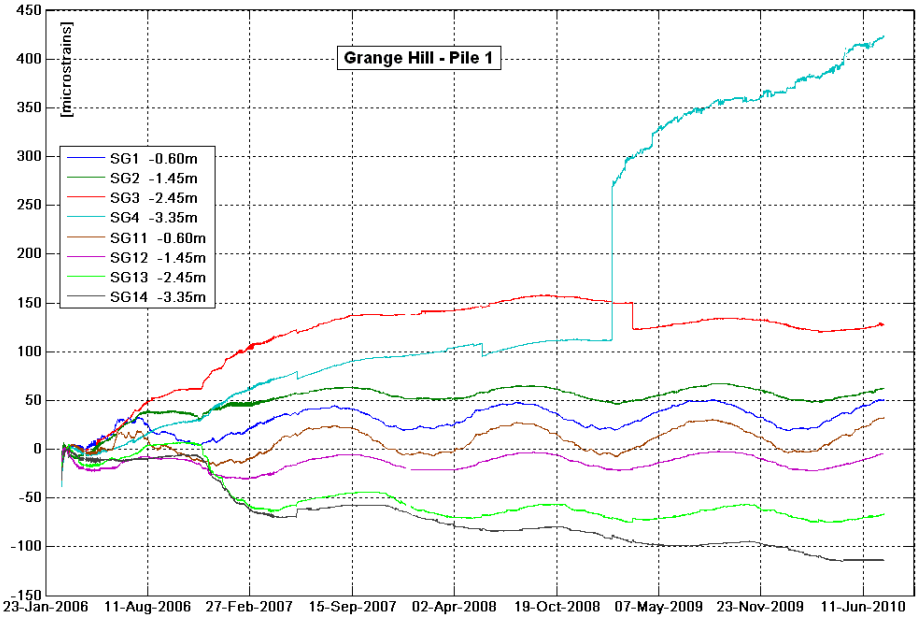

Figure 4.14: *Grange Hill Pile 1, seasonal strain variation in the instrumented section at the top of the pile*

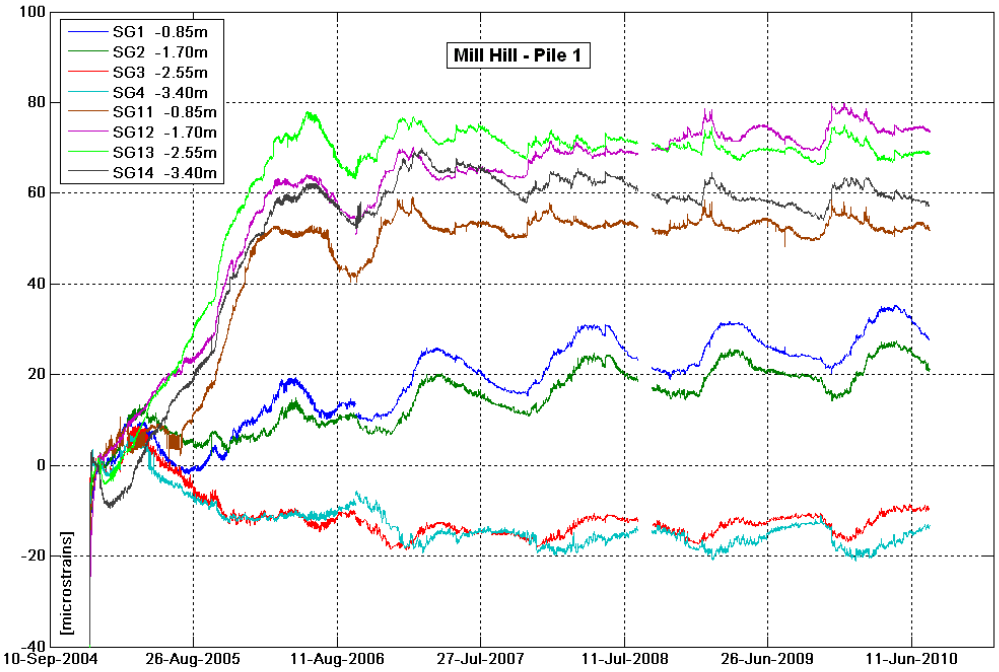

Figure 4.15: *Mill Hill Pile 1, seasonal strain variation in the instrumented section at the top of the pile*

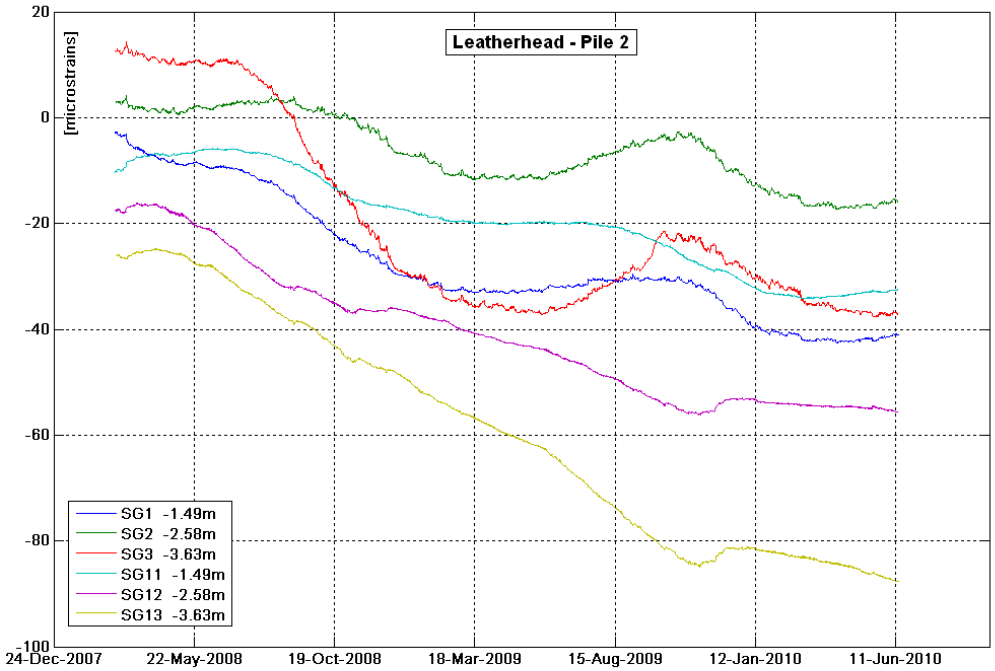

Figure 4.16: *Leatherhead Pile 2, seasonal strain variation in the instrumented section at the top of the pile*

4.4.1 Strain/temperature graphs and correlations

The first part of the analysis is based on the strain/temperature graphs. These are produced using uncorrected strain data (but cleaned from interference) from the strain gauges and the temperatures measured by thermistors at the same level. The plot is usually quite confused, but if a linear strain/temperature correlation is present, seasonal changes in strains are represented by narrow loops with almost the same slope (fig. 4.17 and fig. 4.19). If the loops can be approximated by a line, the slope of this line represents the "effective" coefficient of thermal expansion of the pile (α_e). "Effective" means that the coefficient includes the interactions between the strain gauges and the pile material (concrete), and the effect of the restraints. In the case of piles, these are the pile/soil interactions (mainly skin friction, in the analysed cases). In a theoretical case where no restraints are present, the effective coefficient coincides with the coefficient that shows the interaction between the strain gauges and pile material (par. 4.4.2.3). In the case where the line approximating the seasonal loops is vertical, the temperature is not correlated to the strain variation, since when the temperature changes, the strains remain constant. The analysed plots include all the other actions, effects and processes present in the piles; this makes them very confused in the case where the strain/temperature correlation is not the main seasonal effect.

In this analysis only linear strain/temperature correlations are considered.

The strain/temperature graphs also show the concrete setting phase behaviour, when the concrete is cooling after the first hydration processes and gaining strength (fig. 4.17 for example).

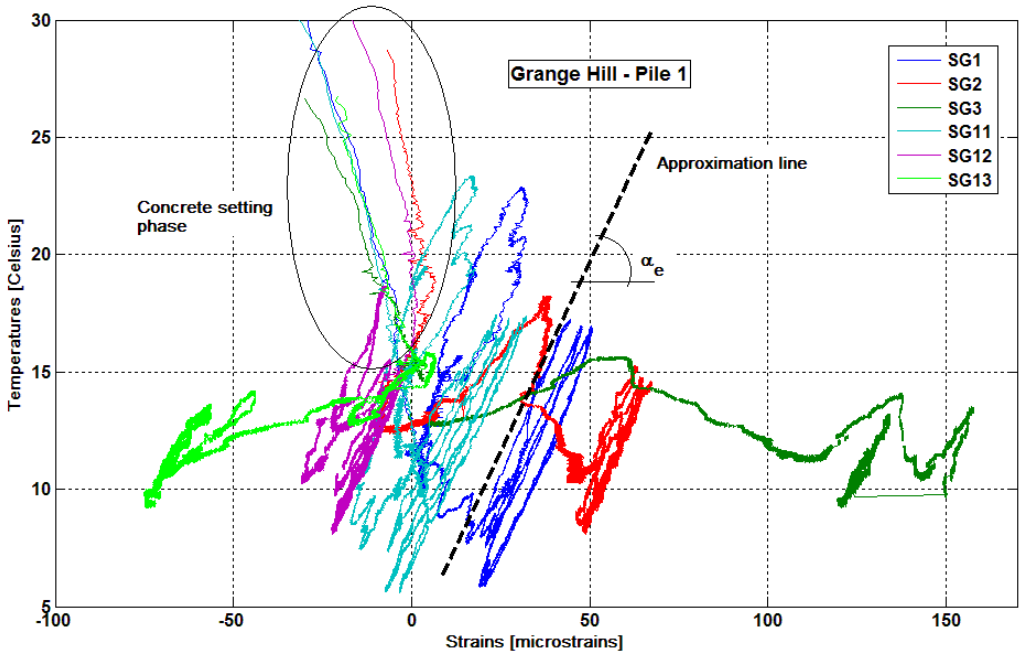

Figure 4.17: *Grange Hill Pile1, strain/temperature plots for the top three instrumented sections.*

4.4.2 Effects of temperature changes on strain gauges readings

This section analyses the effects of temperature changes on strain gauges readings, the formula to correct the readings and the evaluation of the coefficient of thermal expansion of concrete.

In the following strain plots, tension is positive while compression is negative.

4.4.2.1 Behaviour of a vibrating wire strain gauge in relation with thermal variations

A vibrating wire strain gauge measures the frequency of vibration of the wire and compares it with a datum to calculate the increase or decrease of strain of the wire (and thus of the structure to which it is connected). Theoretically, if the wire and the structure have the same coefficient of thermal expansion (α), a change in temperature doesn't cause any change in the readings. In reality, structure and strain gauge are likely to have different values of α. In the analysed cases, the coefficient of thermal expansion of the strain gauge (α_{sg}) was $12\times10^{-6}\,{}^{o}C^{-1}$ (given by the producer), while the coefficient of thermal expansion of the concrete (α_c) could vary between 6 and $13\times10^{-6}\,{}^{o}C^{-1}$ (par. 4.4.2.2). Since no measurements were carried out on the instrumented piles to evaluate α_c, the value suggested by the Eurocode 2 [BS EN 1992 (2004)] was used (α_c=$10\times10^{-6}\,{}^{o}C^{-1}$). The difference between α_c and α_{sg} (when $\alpha_c < \alpha_{sg}$) means that the strain gauge would expand more than the concrete for a given increase in temperature, but since the instrument is restrained by the structure and its expansion is not permitted, the strain gauge reads this as an "artificial" increase in compression when the temperature increases. Vice versa, an "artificial" increase in tension is measured when the temperature decreases. The opposite happens when $\alpha_c > \alpha_{sg}$, an increase in temperature generates an increase in tension in the readings while a decrease in temperature produces a rise in compression. This effect is completely generated by the instrument and is not based on any real physical effect in the structure. It is then necessary to proceed to a correction of the strain gauge readings (par. 4.4.2.3).

The evaluation of the coefficient of thermal expansion of concrete (α_c) greatly affects the temperature corrections and the following analysis of the behaviour of the piles.

4.4.2.2 Coefficient of thermal expansion of concrete

The coefficient of thermal expansion of concrete (α_c) depends both on the composition of the mix and from its hygral state at the time of the temperature change [Neville (1995)]. The constituents of the mix, hydrated cement paste and aggregates, have different coefficients, and the global coefficient of concrete is a resultant of these. Since concrete is a porous material containing water (under different conditions: water held by the hydrated cement paste and adsorbed water), the changes in temperature modify both the true kinetic coefficient and the capillary tensions in the pores [Neville (1995)]. In Table 4.1 the influence of different cement sand ratios is shown, while in Table 4.2 the effects of different aggregates and curing methods are illustrated. Tatro (2006)

back-calculates the coefficients of thermal expansion of mass concrete used in dam construction (Table 4.3). The three tables give an example of the complexity of the problem and of the necessity for laboratory tests on concrete samples for an accurate estimate of the coefficient of thermal expansion. Reproducing the environmental conditions in which the concrete is cured can increase the difficulty of the laboratory test. In this case, in fact, the humidity/moisture conditions are very different than for structures in the open air (as explained in par. 2.4.5).

Cement/sand ratio	Linear coefficient of thermal expansion at age of 2 years
Neat cement	18.5
1:1	13.5
1:3	11.2
1:6	10.1

Table 4.1: *Influence of the cement/sand ratio on the coefficients of thermal expansion of concrete in $10^{-6}\,{}^{o}C^{-1}$ [Neville (1995)]*

Type of aggregate	Air-cured concrete	Water-cured concrete	Air-cured and wetted concrete
Gravel	13.1	12.2	11.7
Granite	9.5	8.6	7.7
Quartzite	12.8	12.2	11.7
Dolerite	9.5	8.5	7.9
Sandstone	11.7	10.1	8.6
Limestone	7.4	6.1	5.9
Portland stone	7.4	6.1	6.5
Blast-furnace slag	10.6	9.2	8.8
Expanded slag	12.1	9.2	8.5

Table 4.2: *Coefficients of thermal expansion for 1:6 concretes in $10^{-6}\,{}^{o}C^{-1}$ [Neville (1995)]*

Dam Name	Aggregate Type	Coefficient of Thermal Expansion
Hoover (USA)	limestone and granite	9.5
Hungry Horse (USA)	sandstone	11.2
Grand Culee (USA)	basalt	7.9
Table Rock (USA)	limestone and chert	7.6
Greers Ferry (USA)	quartz	12.1
Dworshak (USA)	granite-gneiss	9.9
Libby (USA)	quartzite ans argillite	11.0
Jupia (Brazil)	quartzite	13.6

Table 4.3: *Thermal expansion coefficients for mass concrete in $10^{-6}\,{}^{o}C^{-1}$ [Tatro (2006)]*

4.4.2.3 Temperature correction formula

The temperature correction formula used is based on the theory mentioned above (par. 4.4.2.1) and on Batten et al. (1999):

$$\varepsilon = \varepsilon_{sg} - (\alpha_{sg} - \alpha_c)(T_0 - T_1) \tag{4.6}$$

where:

ε is the adjusted structural strain;

ε_{sg} is the measured strain;

T_0 is the temperature datum;

T_1 is the general temperature reading.

In the theoretical case discussed in par. 4.4.1, where a pile with no restraints is subjected to temperature changes:

$$\alpha_e = \alpha_{sg} - \alpha_c \tag{4.7}$$

then

$$\varepsilon = \varepsilon_{sg} - \alpha_e(T_0 - T_1) \tag{4.8}$$

where α_e is the "effective" coefficient of thermal expansion introduced in par. 4.4.1.

In the analysis of pile readings, the temperature datum was set at the same time as the strain datum to maintain the consistency between strains and temperatures. A variation of the datum generates variations in the temperature corrections.

4.4.3 Temperature correction method

The first step is the evaluation of the stress/temperature graphs. If it is possible to approximate the seasonal loops by parallel lines, then a temperature correction can be used to separate temperature effects. The next step is to calculate the slope of the approximating line (α_e) and to use it in equation 4.8. The calculated strains are now corrected from all the temperature effects (both instrumental and effective), and represent only effects that are not associated with temperature. The temperature derived strains (fig. 4.18) then include all the strains associated with the temperature changes, namely the difference between the coefficients of thermal expansion of the gauge and the concrete, the pile/soil interaction due to the different coefficients of thermal expansion and the temperature related strains generated by any other kinds of restraint on the pile. Knowing the coefficient of thermal expansion of concrete (α_c), it is possible to separate the strains generated by the instrument errors from the global measured strains.

If the approximating lines are vertical (or nearly vertical), the change in temperature generates no changes (or very small changes) in strain. In this case the temperature changes are not affecting the readings (or are affecting them only slightly) and no corrections are needed. It is also possible that the correlation between strains and

temperature is not linear; more research is necessary to investigate this.

The last case is represented by an unclear strain/temperature correlation, meaning that the line approximating the seasonal temperature increases is different from that for the temperature decreases. The temperature correction for instrument errors is the only one to be applied in this case.

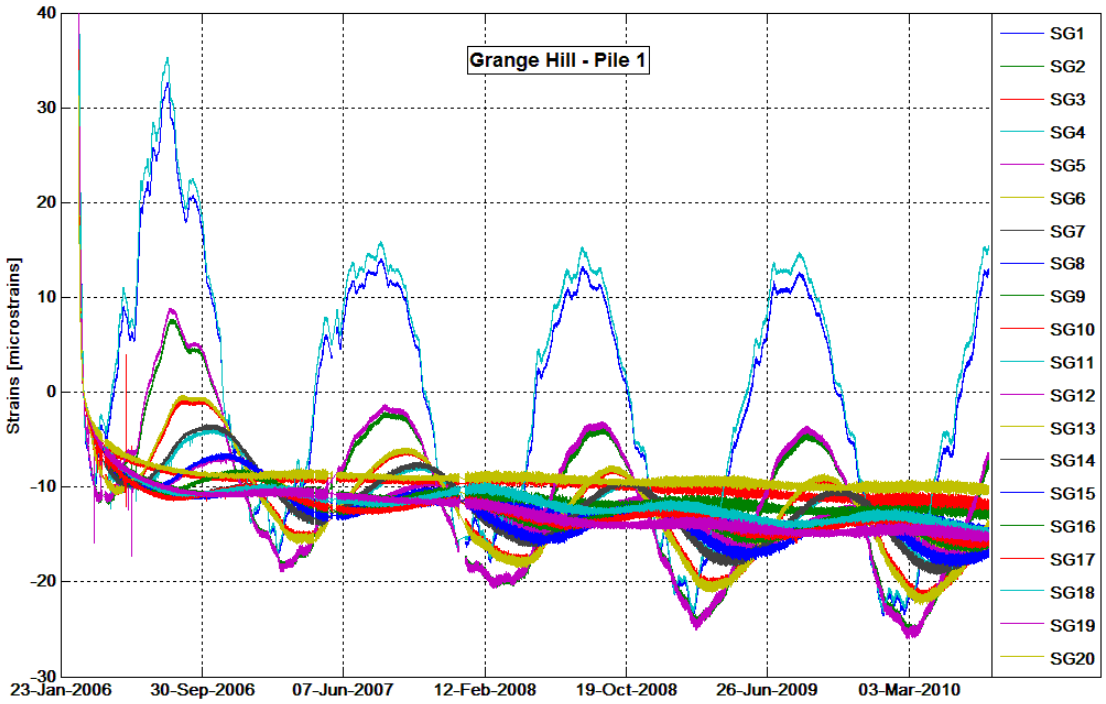

Figure 4.18: *Grange Hill Pile 1, temperature corrections*

4.4.4 Case history

This section analyses the piles from the three instrumented sites at Grange Hill, Mill Hill and Leatherhead to test the theory and method explained above.

4.4.4.1 Grange Hill

Three instrumented piles are monitored at Grange Hill (par. 3.1), but unfortunately the temperatures are recorded correctly in only one (Pile1). It is possible to use Pile1 temperatures in Pile2 with only a minor error as the two piles are close. The use of Pile1 temperatures in Pile3 could generate bigger errors as the two piles are far apart; thus these corrections are not applied to Pile3. The concrete used for building the piles has a modified mix; the only aggregate used was sharp marine sand, 26% of the cement used was pulverised fuel ash, the cement/sand ratio was 0.5 and the water/cement ratio was 0.34. This particular cement mix is possibly responsible of some of the unusual behaviours recorded in this set of piles.

The analysis of the strain/temperature graphs for Pile1 (fig. 4.17) and Pile2 (fig. 4.19) shows that both have the same behaviour. In general, the seasonal changes in strains are represented by narrow loops. The loops have almost the same slope for

increasing and decreasing temperatures, and can be approximated by a straight line. The slope of this line (α_e) is approximately -3×10^{-6} $^oC^{-1}$ for both piles. As explained above, this coefficient includes any instrument errors and the restraints on the pile.

Correcting the strain data of Pile1 (Pile2 has many strain gauges broken and it is not very representative) using the equation 4.8 with α_e= -3×10^{-6} $^oC^{-1}$ completely eliminates the seasonal changes from strain readings (fig. 4.20, 4.21 and fig. 4.22) and axial strains (fig. 4.23). The bending moment was not affected, the temperature correction does not make any difference to the results.

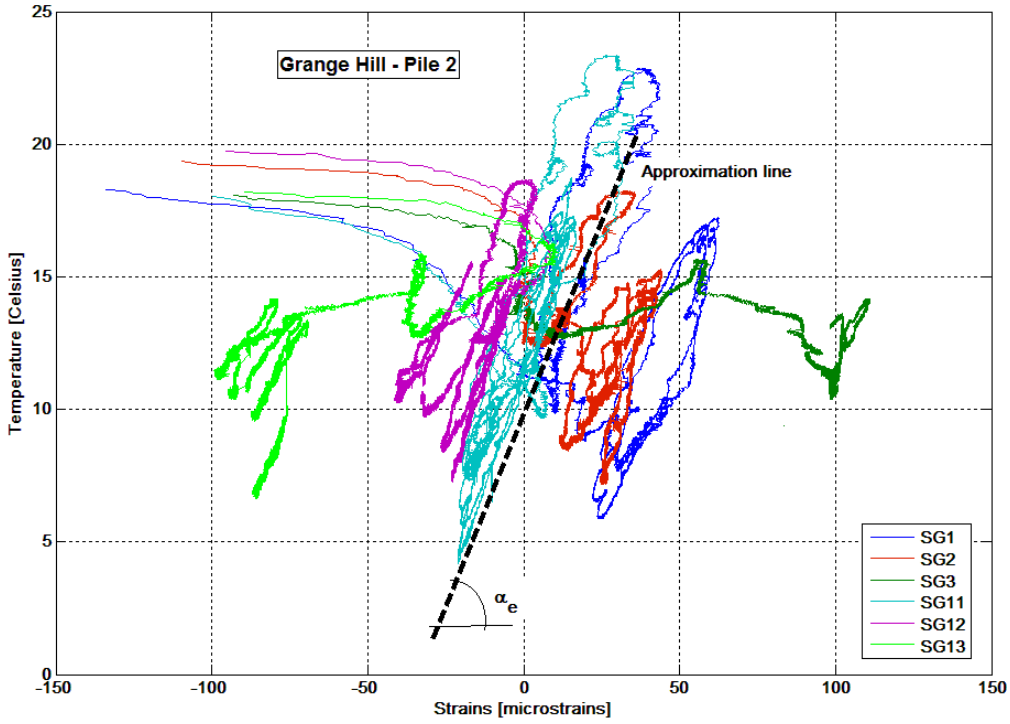

Figure 4.19: *Grange Hill Pile2, strain/temperature graph of the top three instrumented sections.*

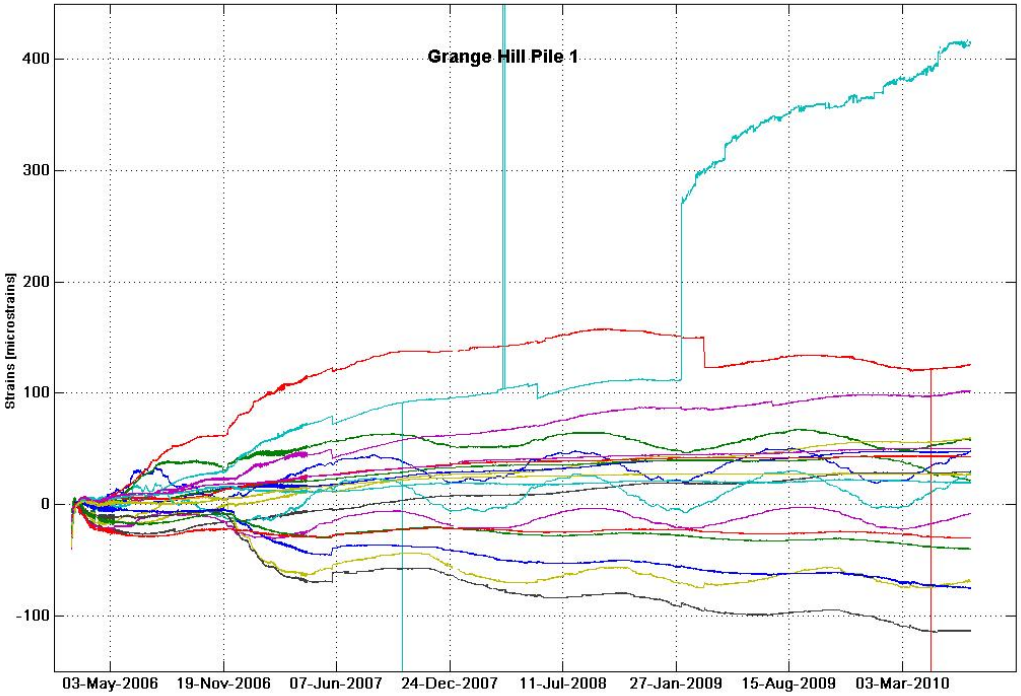

Figure 4.20: *Grange Hill Pile1, uncorrected strain profiles*

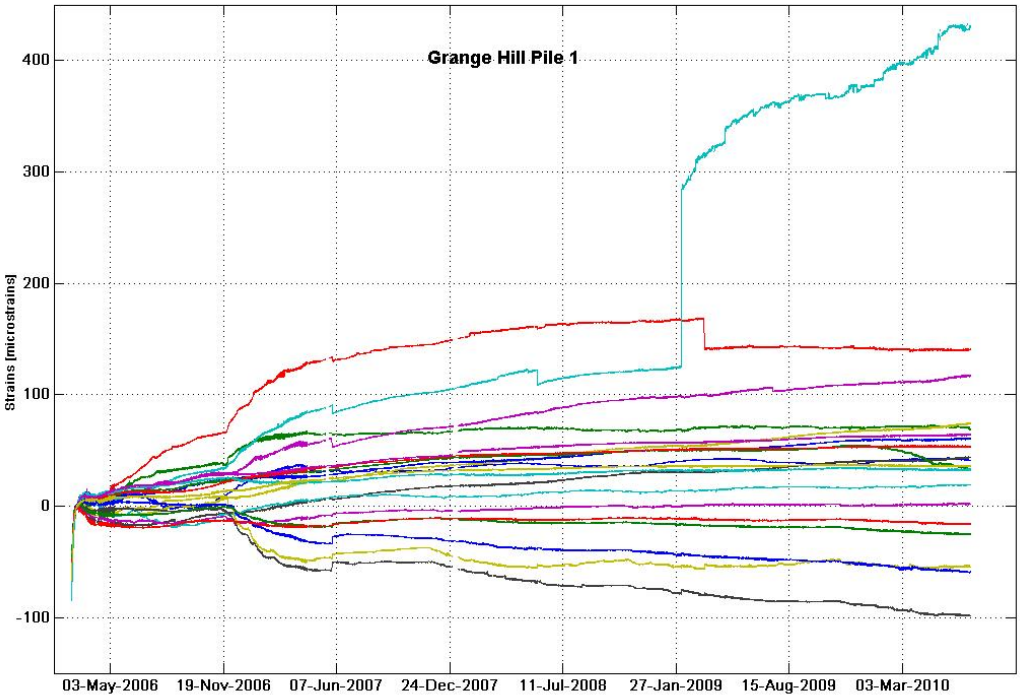

Figure 4.21: *Grange Hill Pile1, corrected strain profiles*

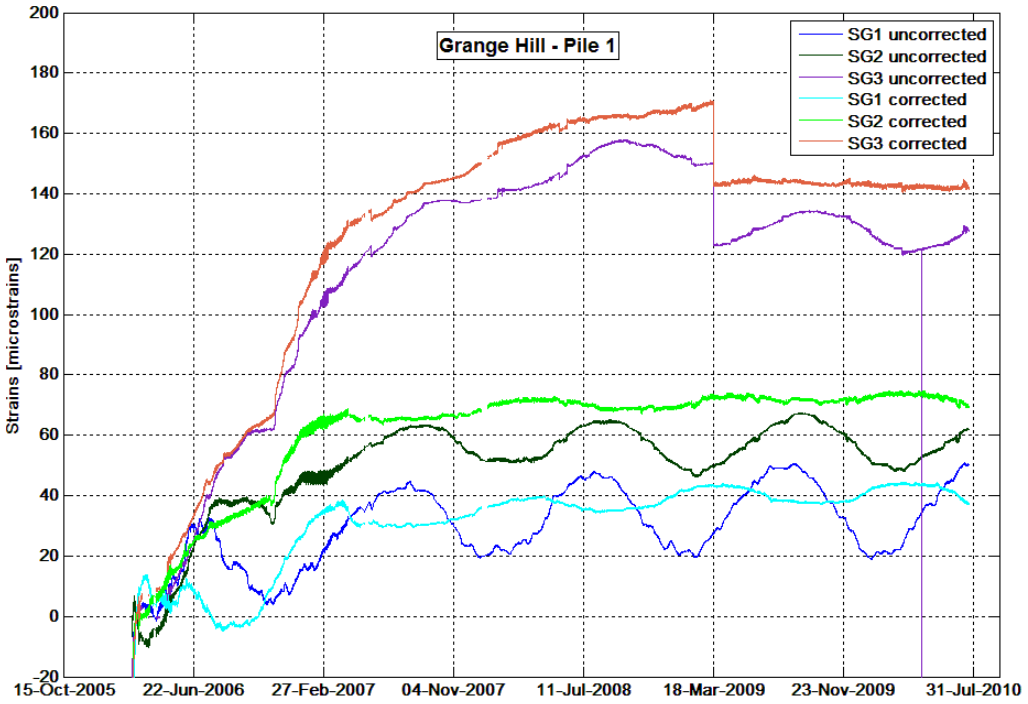

Figure 4.22: *Grange Hill Pile1, comparison of strain profiles for the instruments at the top of the pile*

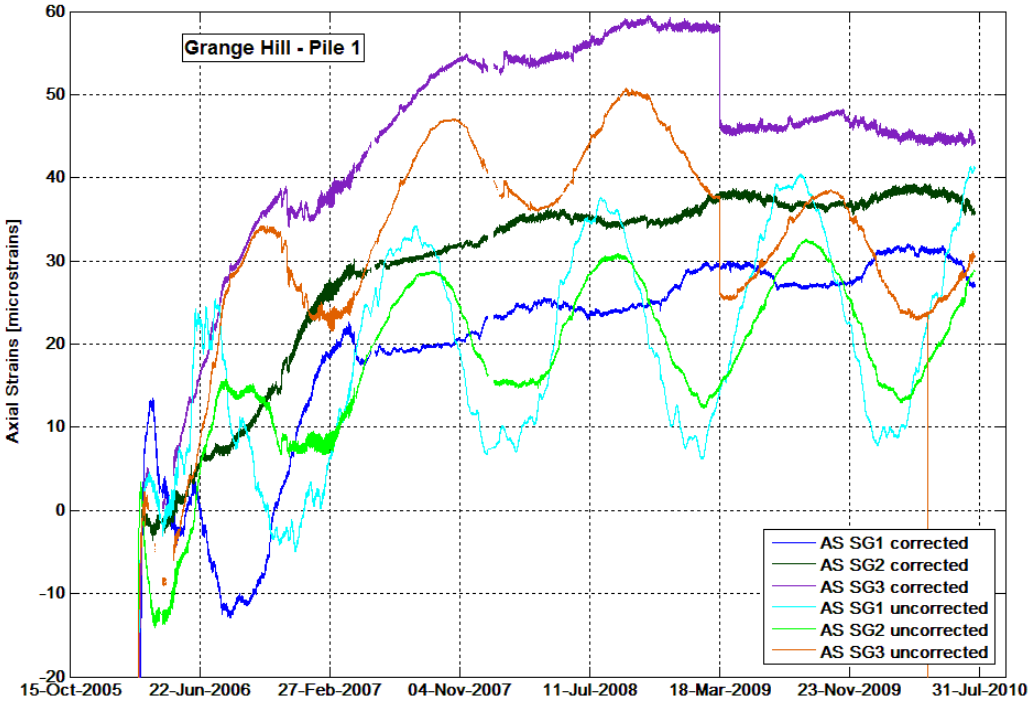

Figure 4.23: *Grange Hill Pile1, comparison of axial strain profiles for the instruments at the top of the pile*

4.4.4.2 Mill Hill

Two instrumented piles were monitored at Mill Hill (par. 3.3) with good records of strains and temperatures. The analysis of the strain/temperature graphs (fig. 4.24 and fig. 4.25) shows that the seasonal loops can be approximated, in most cases, by a nearly vertical line. This means that the strains are only minimally affected by the temperature changes and thus no temperature corrections are needed.

The presence of seasonal loops not connected with temperature changes means that other processes, not directly related to temperature, are seasonally affecting the piles. The strain profiles show peaks in compression in the summer and in tension in the winter, which could be connected to the effects of vegetation as shown by Crilly and Driscoll (2000). This will be discussed in more detail in section 7.2.

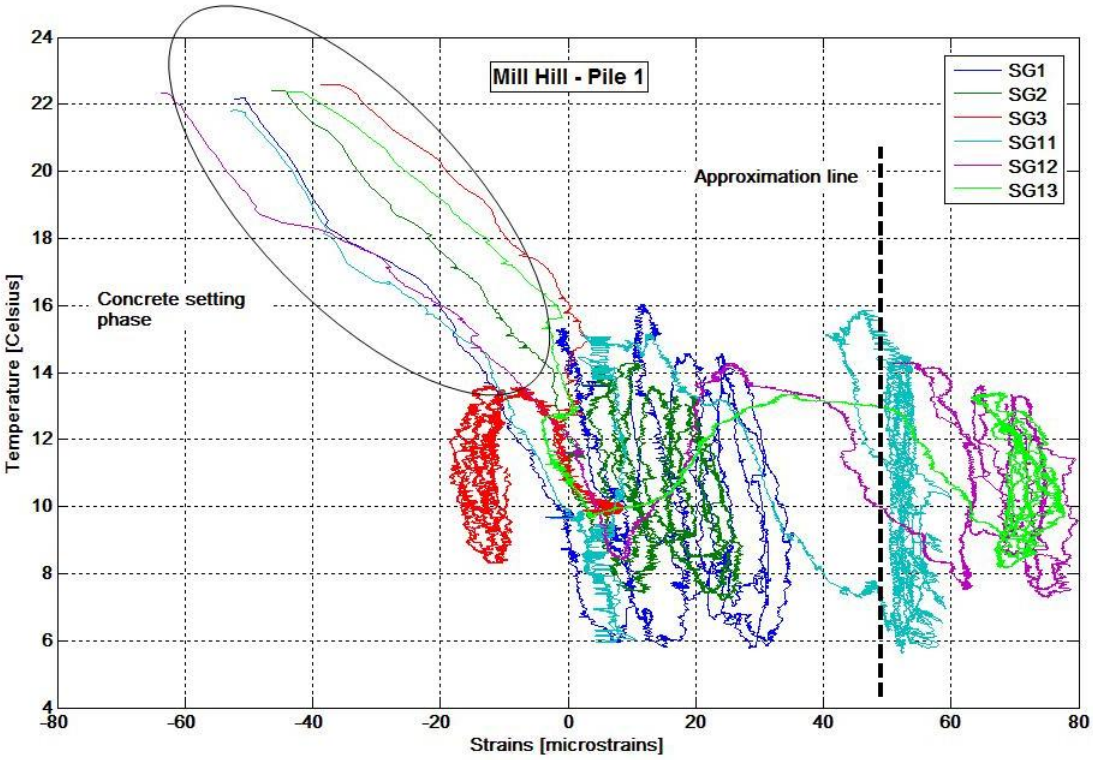

Figure 4.24: *Mill Hill Pile1, strain/temperature graph of the top three instrumented sections.*

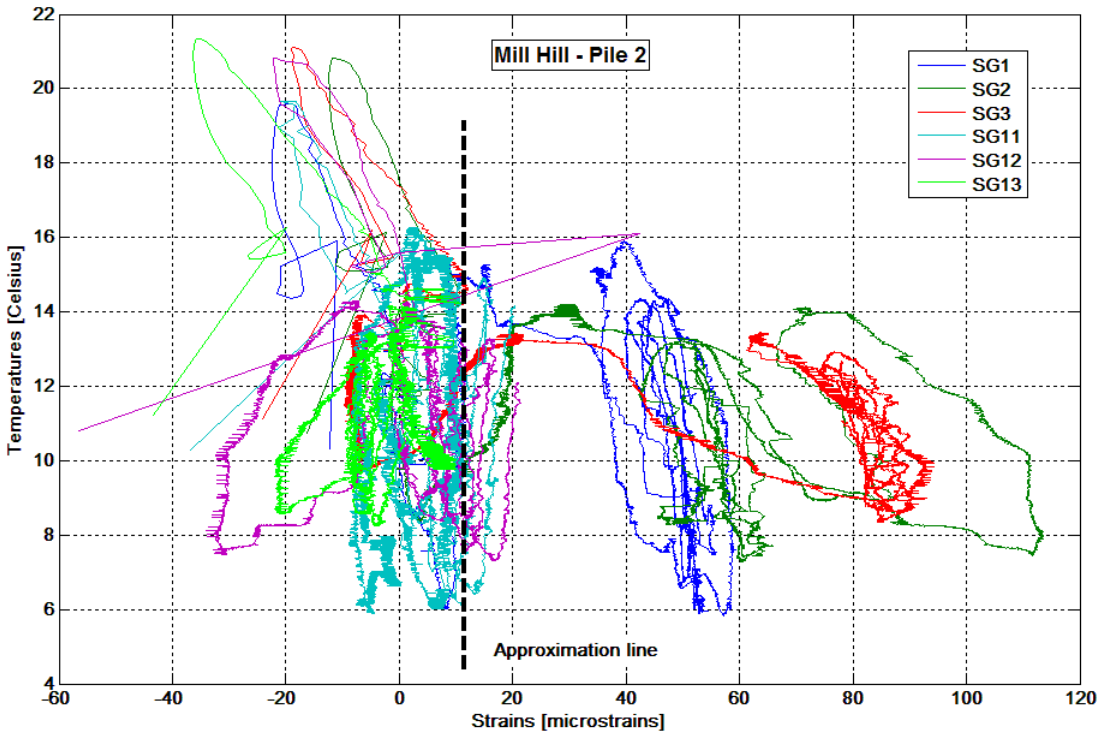

Figure 4.25: *Mill Hill Pile2, strain/temperature graph of the top three instrumented sections.*

4.4.4.3 Leatherhead

Two instrumented piles were monitored at Leatherhead (par. 3.2).

The two strain/temperature graphs (fig. 4.26 and fig. 4.27) show that the instruments are not behaving in the same way as the other piles analysed previously. No loops are present, but all the instruments show a "M" shape graph. This could be mainly related to the strain increase due to the increased load on the pile. If temperature corrections are applied using $\alpha_c = 10 \times 10^{-6}\ ^oC^{-1}$ as suggested by the Eurocode 2 [BS EN 1992 (2004)], the strain profiles show increased peaks and troughs. Visual inspection of a concrete sample from the piles identified the aggregates as chert which means that α_c could be about $12 \times 10^{-6}\ ^oC^{-1}$ (the same value as α_{sg}) and thus no temperature correction is needed. This could explain why part of some strain/temperature graphs are vertical: the temperature variations does not affect the strains, but the increase in load (i.e. an increase in bending strain) develops the "M" shape graph. The seasonal changes in strains are probably connected to other effects not directly related to temperature, thus no temperature corrections are applied.

4.4.5 Temperature correction conclusions

Seasonal changes in strain and axial strain have been observed in seven instrumented piles at three sites. After the realisation that the seasonal variation of strain was in some cases connected to the seasonal variation of temperature, a correction method was

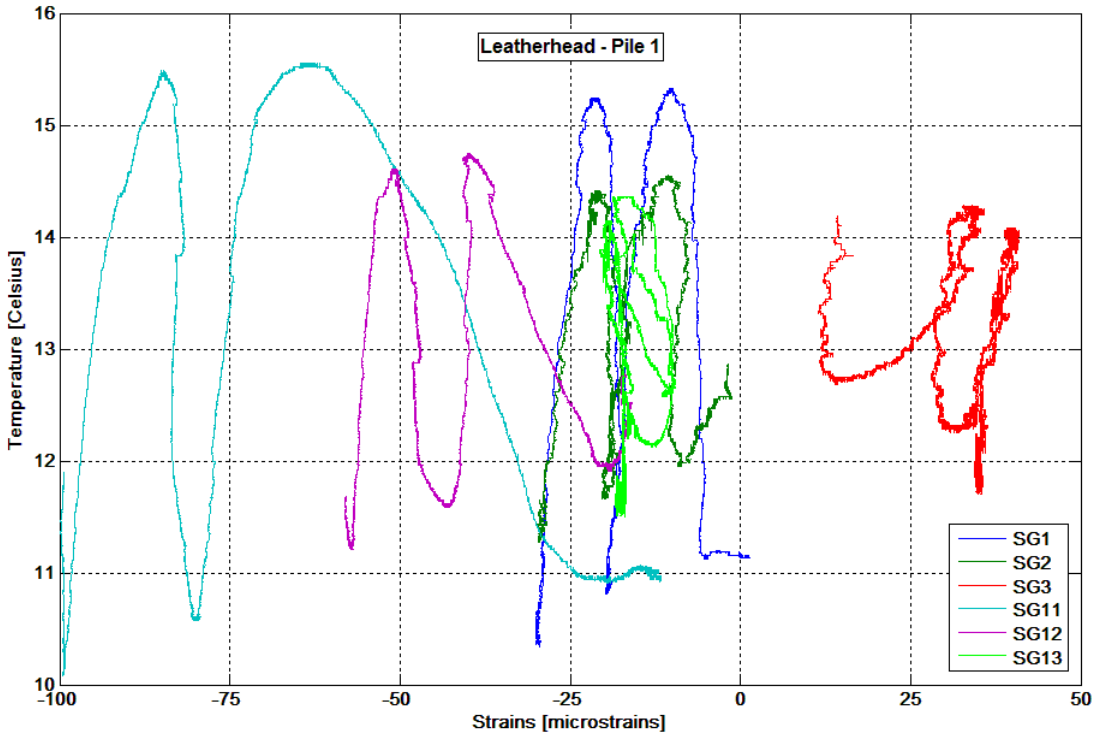

Figure 4.26: *Leatherhead Pile1, strain/temperature graph of the top three instrumented sections.*

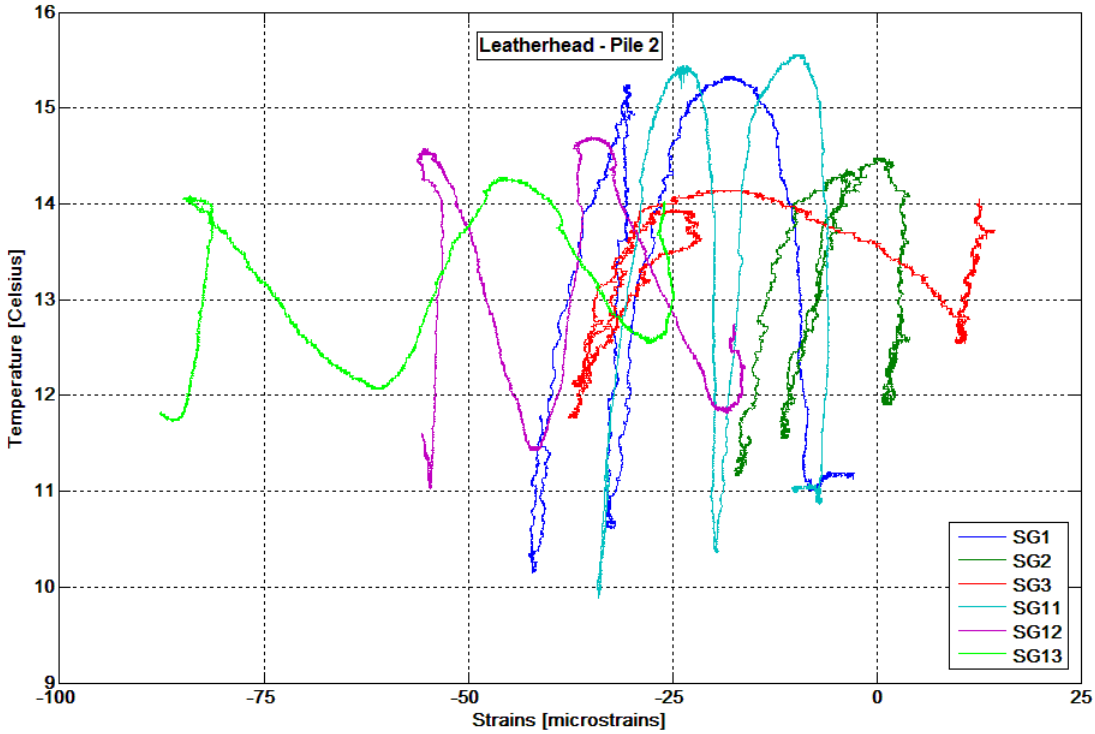

Figure 4.27: *Leatherhead Pile2, strain/temperature graph of the top three instrumented sections.*

developed. This is not a generalised correction method for all the piles, but it can be adapted to the different situations encountered at the different sites.

Strain/temperature graphs are used to identify potential correlations between the two quantities. If the graphs show narrow loops that can be approximated with a line, the slope of this line is used as an "effective" coefficient of differential thermal expansion (between strain gauge and pile) in the temperature correction formula (Equation 4.8). This eliminates all the temperature effects (instrumental, due to pile/soil interactions and due to the restraints) from the readings and consequently the corrected strain graphs shows no temperature related seasonal variations.

In the case of a vertical approximation line, no temperature correction is needed because a change in temperature does not generate a change in strains.

4.5 Broken connections: the case of UP22

This section illustrates the corrections made to data from UP22 (from Ironbridge Phase I) after some breakages occurred to the cables. This is an example of the problems that can occur in the field data analysis and an approach to solve them. The correction method was developed after the collection of more than two years of data, making possible the comparison of the long term behaviour of the different instruments. The method also worked in an iterative way taking into account strains, temperatures, bending moments and displacements, thus using the whole methodology proposed in this thesis. The method is analysed in this chapter because its primary purpose is related to the interpretation of strain gauge data on which the rest of the research is based.

After the installation of the pile (12 January 2007), the data-logger was connected to the strain gauges and the recording started. The cables were then cut during some works around the pile. In this case it was possible to reconnect the cables correctly without the loss of much data. During the building of the road on top of the pile, some of the cables were cut again (5 July 2007). In this case it was not possible to identify the damage and repair it promptly. The cables were reconnected on 13 August 2007, but for some of them it was not possible to match the original positions. The cables were connected again, the data-logger recorded the data, but for these cables it was not possible to know the strain gauges they should be attributed. Strain and temperature profiles were recorded, but for some of them the position in the pile after the breakage was unknown. Strains changed during the one month gap, between breakage and repair, making it difficult to match the profiles before and after the rupture. On the down-slope side most of the position were reasonably certain, while on the up-slope side only the instruments numbered as 9, 10, 12, 14 and 15 (fig. 3.13) were known (since their cables were not cut).

The first step was to match the temperature profiles before and after the breakage. Temperature profiles have specific patterns related to the depth of the instrument. At the top of the pile a strong seasonal variation is recorded, with the peaks nearly corresponding in time with the seasonal hottest periods. Deeper in the ground the

seasonal variations are smoother and the peaks move later in time due to the delay in conduction heat. Below 10m it is very difficult to distinguish the seasonal variations since the temperature is almost constant (fig. 4.28).

After temperature matching, only five instrument positions (5, 7, 8, 11 and 13) in the up-slope side were uncertain since the thermistors were broken. The next step was to try to match the strain profiles (before and after the breakage) where possible. In this case, the main problem is represented by the bending moment calculation. In fact, the calculation needs two strain gauges in a section. The wrong matching of the cables changes the bending moment results. The instrumented section at 20m (instruments 11-26 in fig. 3.13) is important for the profile (fig. A.30) since it correspond to a likely peak in the bending moment (the details of the calculation are in chapter 5). This section has only one certain instrument position in the pair, but the bending moment profile maintains the shape and the peak has only slight variations whichever "free" instrument is coupled with it. The remaining instruments were matched similarly, taking care to maintain consistency in the strain and bending moment profiles before and after the rupture.

Solution of the matching problem gives acceptable results. In that, almost all the instrument depths were at the end of it known. On the other hand, many strain gauges were not giving reliable readings (too much interference, sudden jumps and breakages) after the last cable cutting. This left some gaps in the data needed to calculate the bending moment as some instrumented sections had only one instrument working correctly in the pair.

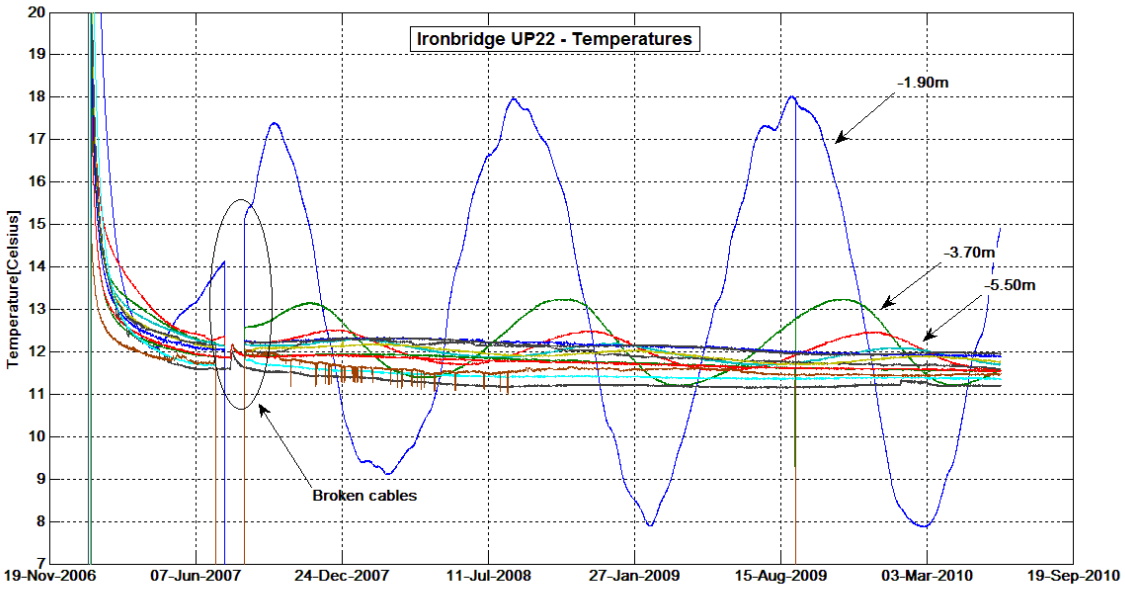

Figure 4.28: *Ironbridge UP22 temperature profiles. The instruments on the top of the pile show large seasonal variations, while the rest have almost constant readings.*

4.6 Detecting concrete cracking with strain gauges

During the analysis of embedded strain gauge readings from the Grange Hill site, some unexpected jumps were found in some strain profiles. These jumps seem to not be related to interference or other instrument problems. They have been considered genuine readings which need a plausible explanation related to the pile behaviour. Figures 4.29 and 4.30 show large jumps (increasing) in the tensile strain and small jumps (decreasing) in the compressive strain. This behaviour can be explained by the opening of a crack (presumably a micro-crack, on the basis of the value of the jumps being few hundred $\mu\varepsilon$) that passes through the strain gauge in tension. Normally it would be expected that the compressive strain increases due to the movement of the neutral axis, but in this particular case, since the position of the strain gauge is far from the edge of the pile section, the strain gauge measures a reduction in strain while at the edge of the section strains increase (fig. 4.31 and fig. 4.32).

In chapter 5, the programs for the calculation of the bending moment are explained. They also calculate the position of the neutral axis (par. 5.1.2). For the two particular cases discussed above, sudden jumps in the position of the neutral axis toward the compressive side of the section are shown (fig. 5.2).

Section 5.2.2.1 analyses and discusses how to calculate the bending moment in the cracked sections and the respective results.

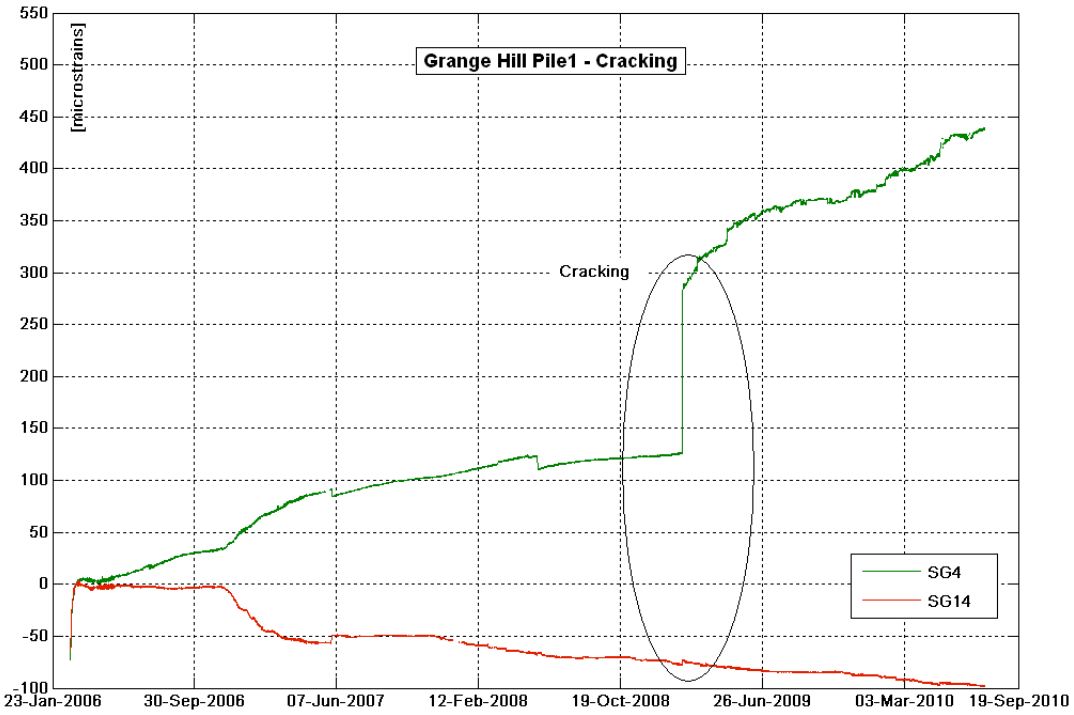

Figure 4.29: *Strains and bending moment profiles for SG 4-14 Pile1*

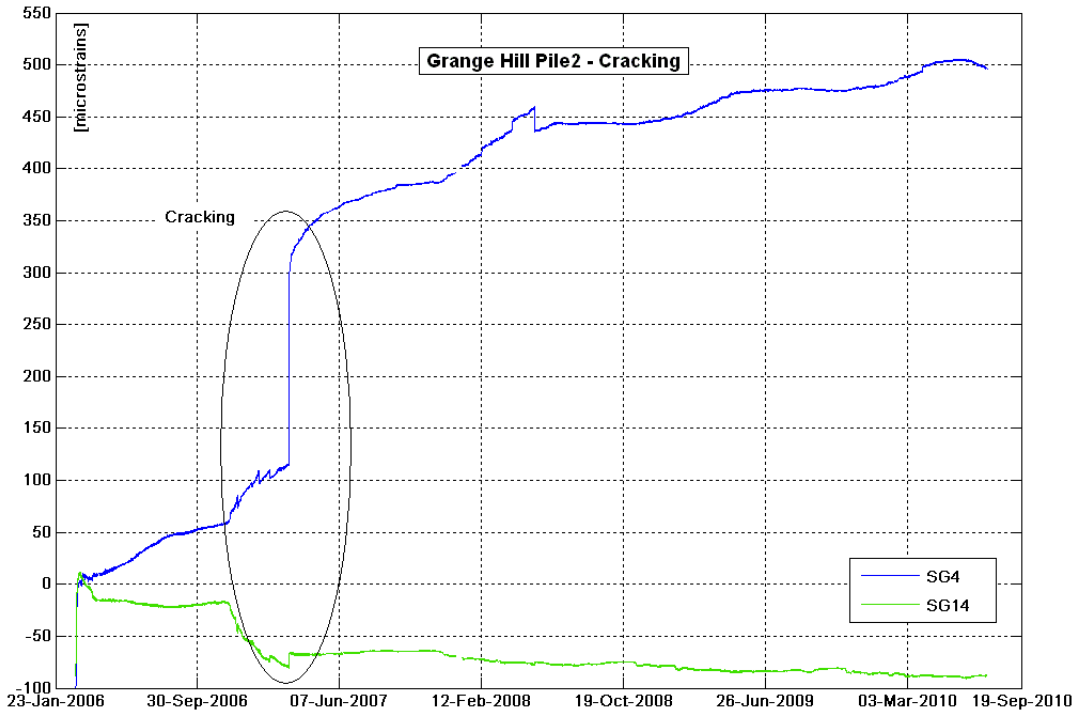

Figure 4.30: *Strains and bending moment profiles for SG 4-14 Pile2*

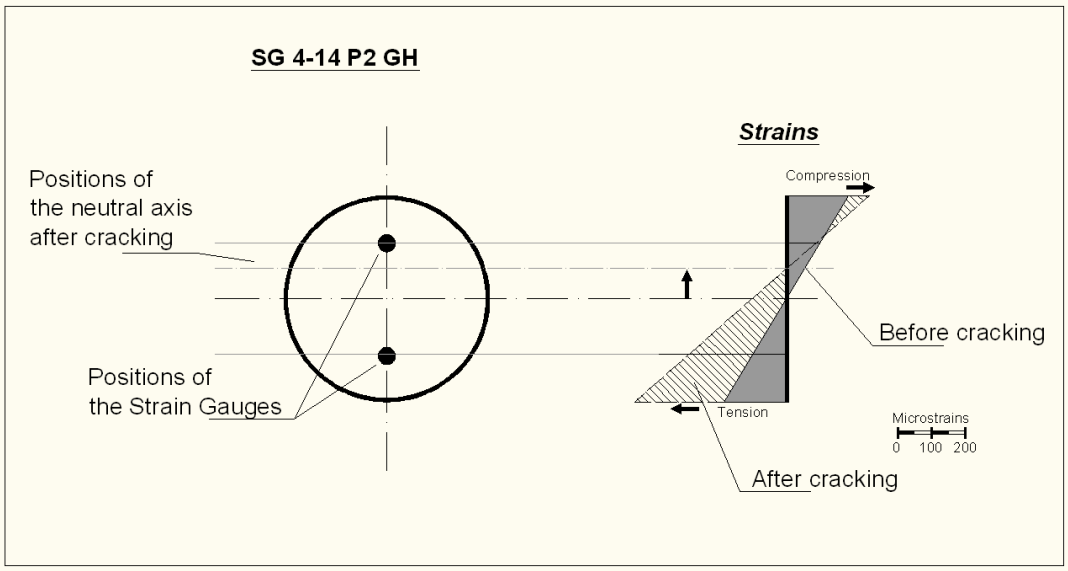

Figure 4.31: *Measured strains in section 4-14P2 before and after cracking*

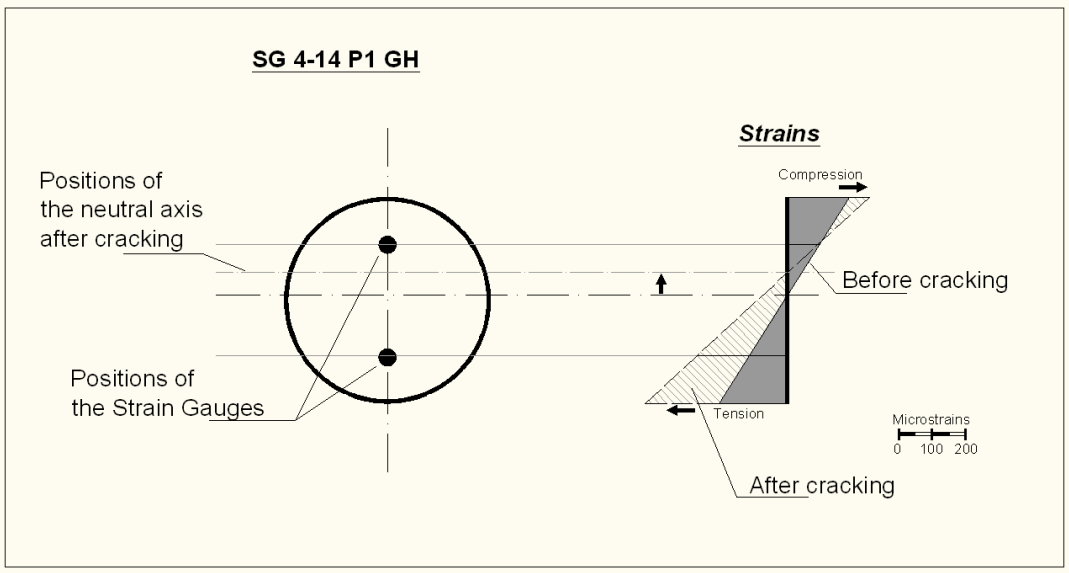

Figure 4.32: *Measured strains in section 4-14P1 before and after cracking*

4.7 Conclusions

This chapter presents the methodology developed and used throughout this research for the analysis of strain gauges data. A comprehensive method was not found in the literature, thus the necessity of studying every aspect of the use of strain gauges in concrete structures and to develop an appropriate approach arose. The methodology developed was then applied to the analysis of each pile.

The important problem of the datum setting is discussed (par. 4.2) and the two approaches used are presented (one takes into account the effects of concrete setting on strain gauges and the other considers the development of bending moment). The method used for understanding the temperature effects and their potential correction is presented along with its application to three case histories (par. 4.4). The method used for the detection of concrete cracking using strain gauges is analysed on two cases recorded during the monitoring (par. 4.6).

Chapter 5

Calculation of bending moment using strain gauge data

This chapter examines the bending behaviour of standard reinforced concrete piles and circular concrete-filled steel tubular piles. The bending moment profile of a pile is important for understanding the structural and geotechnical behaviour of the retaining structure. Back-analysis of the pile behaviour provides insights about the real behaviour of the piles and slope and about the assumptions made during the design stage. The designer can then use it to optimise the design of later new retaining structures.

Structural design methods analyse a pile section knowing (or assuming) the applied loads and then calculating the stresses and strains using the material properties. Factors of safety are always used in this process and the parameters of the materials used are often a standardised approximation of the real values (e.g. the value of the compressive strength of concrete at 28 days). In this research, the loads (and thus the bending moments) applied to the structure are unknown, while the strains are measured. Factors of safety should not be applied, and more realistic material parameters have to be used to determine working loads.

Starting from strain readings, two methods are developed for the calculation of the bending moment which approach cracking in different ways. These are applied to four piles, one from each of the four different sites. The two methods are implemented using Matlab [The Mathworks Inc. (1984-2009)] and coded as two separate programs (later referred to as ACM and MCM). Analysis and discussion of the results shows how, and in which situation the two different methods can be used to determine the development of cracking and the bending moment in the piles.

The use of two strain gauges in an instrumented section implies that it is possible to accurately calculate only the bending moment generated by a load acting parallel to the instrumented diameter (fig. 5.4 and fig. 5.5). The calculation is inaccurate if the maximum bending moment lies on another direction. The pile is then assumed to be in uni-axial loading and it is also assumed that the calculated bending moment is the maximum acting on the pile. The positioning of the strain gauges during the construction of an instrumented pile is essential for an accurate bending moment calculation. Using three or more instruments within a section allows the identification of the exact

direction and value of the maximum bending moment in the pile.

The effects of cracking on the strain readings are also investigated to understand if the measured axial strain is real or "apparent" (i.e. an artifact of the cracking process). The opening of cracks could make the instruments measure a uniform increase in tensile axial strain, related to a possible axial load, even if the pile is in bending only. Axial strains play an important role in the definition of the beginning of the cracking process.

Bending moment convention

Throughout this thesis, bending up-slope is given by positive values of bending moment, while bending down-slope is given by negative values of moment.

5.1 Background and problems

5.1.1 Basic method: application and limitations

Calculation of the bending moment for a pile instrumented with strain gauges can be carried out in different ways. The quickest and easiest approach is to use the standard engineering beam theory formula :

$$M = \frac{E_c I \left(\varepsilon_1 - \varepsilon_2\right)}{y} \tag{5.1}$$

where E_c is the Young modulus of concrete; I is the second moment of area of the transformed section; ε_1 and ε_2 are the strains measured by each pair of strain gauges in a section; and y is the distance between the gauges in each pair. The formula is easy to apply to the strain gauge data, but the identification of the correct value of E_c for the particular concrete used at a given point in time is a problem. A variation in the value of E_c used gives a proportional variation in bending moment. BS EN 1992 (2004) presents a range of values for E_c between 27 and 44 GPa in relation to the variation of f_{ck} (compressive strength of concrete) only; while BS 5400-4 (1990) shows a range for E_c between 25 and 36 GPa. Furthermore, equation 5.1 does not consider the non-linearity (variation with strain) of the Young's modulus of concrete. Another problem relates to the calculation of the second moment of area, since this approach cannot take into account the possible cracking developed of the section (this is usually considered uncracked or fully cracked). The value of I for an uncracked section is correct as long as the neutral axis remains in the centre of the section; when it moves (due to cracking) the calculations become complicated and, in many cases, significant approximations are necessary. Figure 5.1 presents two examples of bending moments calculated with formula 5.1 using different values of E_c and E_g (Young's modulus of grout, for Ironbridge piles only). E_c= 36GPa is used for Leatherhead concrete in this research (a long term value that assumes no developing of creep); E_c= 32GPa is based on the design strength of concrete (also a long term value for no creep); and E_c= 25GPa is the lowest value given by BS 5400-4 (1990), for comparison. The graphs were calculated assuming no

cracking in the concrete and in the grout, thus the neutral axis is lying in the centre of the section. For Ironbridge L2P30 results were also calculated ignoring the grout.

This basic approach is useful for a rapid and approximate estimation of the bending moment when the concrete behaviour can be approximated to linear elastic, the Young's modulus of all the materials is known and cracking effects can be neglected.

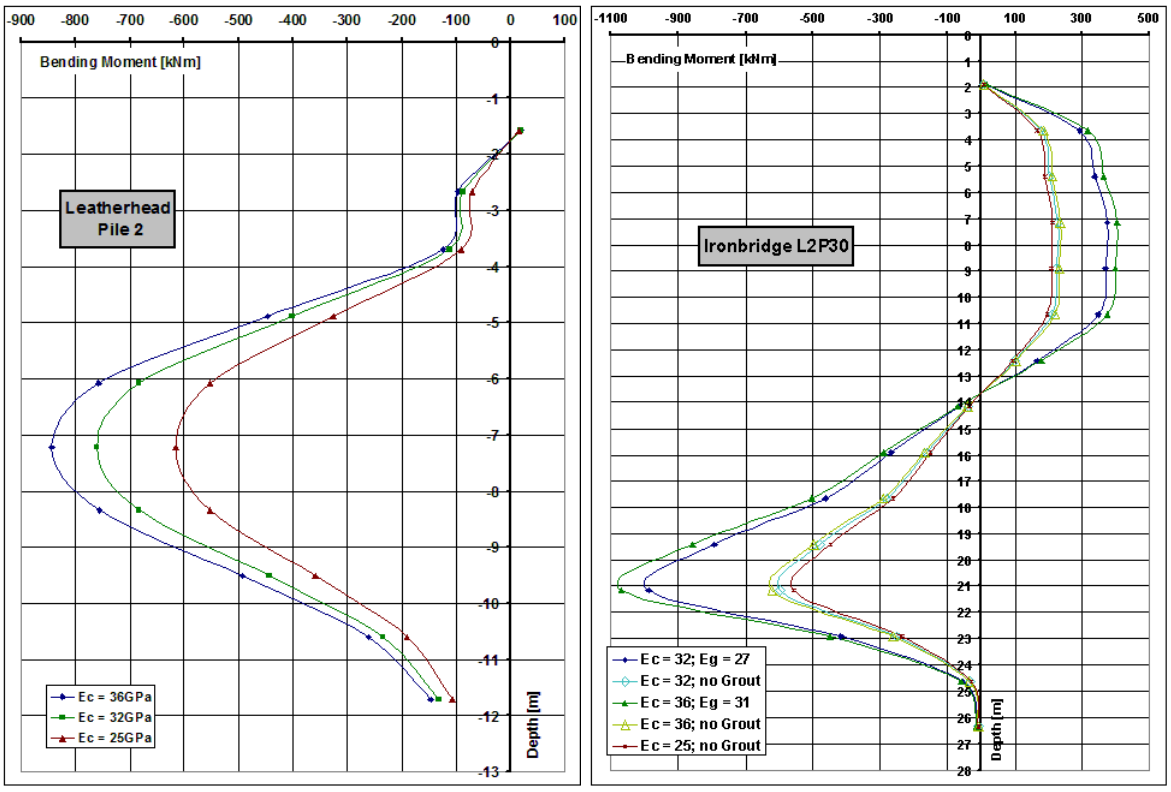

Figure 5.1: *The effect of different values of the Young's modulus of concrete and grout in the calculation of the bending moment using formula 5.1. The piles are considered uncracked, thus the neutral axis always lies in the centre of the section.*

5.1.2 The position of the neutral axis

Assuming that plane sections remain plane, and measuring the strain at two points within the cross section, it is possible to calculate the position of the neutral axis using geometrical relations only. This is a global position, meaning that it is the result of all of the actions working on the pile: bending moment, axial strain and cracking.

The approach developed here performs the calculation for readings from every pair of strain gauges, producing the strain profile of each section. From these, the position of the global neutral axis (denoted X) is calculated. This gives some important information on the loading of the section. If the global neutral axis is outside the section it means that axial forces are overriding; while if it is close to the centre, the section is mainly in bending. Jumps in the X vs. time profile can show the development of cracking at a section, since the neutral axis suddenly moves towards the compressive side when a crack opens (fig. 5.2).

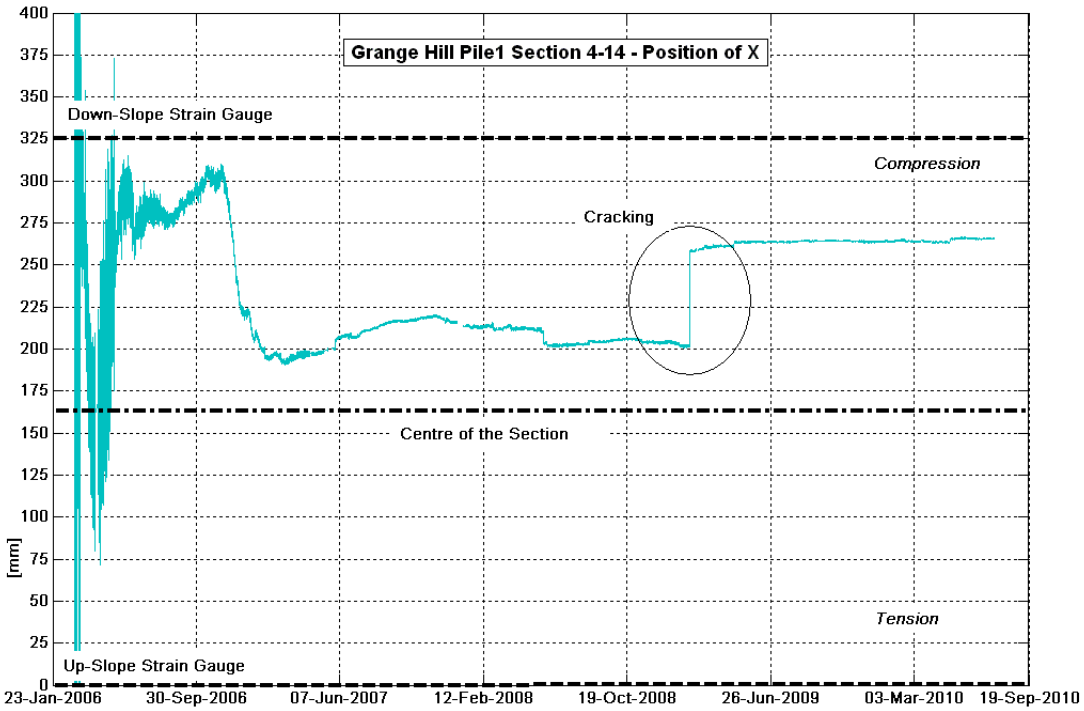

Figure 5.2: *Grange Hill Pile1 section 4-14, time profile of the position of the global neutral axis (X)*

5.1.3 Cracking in reinforced concrete

Cracking affects the calculation of bending moment, as it causes the neutral axis to move. The analysis of the cracking behaviour of the different types of pile sections (standard reinforced concrete and circular concrete-filled steel tubular piles) has been described in section 2.5. The following sections are based on those assumptions and on the stress/strain curves presented in section 2.3.2.

5.1.4 Axial strain effects

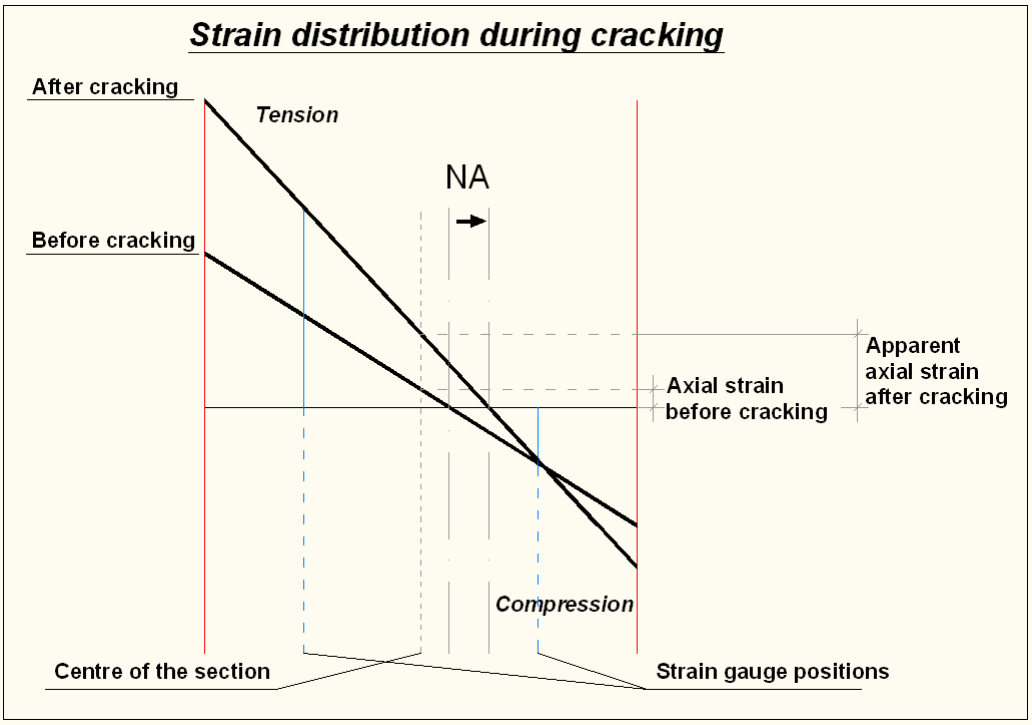

Figure 5.3: *Diagram showing the development of tensile axial strain during cracking of concrete in bending. The strains used in the graph are from Grange Hill Pile1 SG 4-14.*

In the remaining sections of this thesis, the average of the two strain gauge readings in the same instrumented section will be termed "axial strain". It represents a uniform component of axial deformation of the pile section (positive for tension and negative for compression).

Although designed primarily to resist bending, in reality there is always an axial component of the load from the layer of soil (or a capping beam/slab) on the top of the pile or resulting from the settlement, shrinkage or swelling of soil around the pile. The instruments confirm the presence of axial strain in the analysed piles, but it is not possible to clearly define its causes. Furthermore, the measured axial strain could be an artifact of the development of cracking in the instrumented section. When a crack opens, the neutral axis moves toward the compressive side of the section (fig. 5.3) increasing (in tension) the measured axial strain. If this apparent axial strain is used in comparison with the tensile strain limit to check whether the concrete is cracked or not, the described effect generates an error. The cracking limit (i.e. the tensile strain limit at which concrete begin to crack) would be calculated taking into account the cracking effects which are not supposed to have yet developed. This can affect the following bending moment calculation. When the pile is compressed, it is able to carry a greater bending moment without cracking (like a prestressed beam), while if it is in tension the cracking limit decreases.

The key points of the problem can be summarised as follows. By theory, in a

symmetrical section in bending the neutral axis is in the centre. While the measured strains show that the neutral axis is in a different position. This can be caused by an axial load applied to the pile or by concrete cracking. With the actual information about the instrumented piles, it is not possible to identify the exact cause. It is thus assumed to consider the effects of axial strain on the cracking limit calculation only when compressive axial strain affects the whole pile. If the pile is affected by a tensile axial strain, this will not be used in the calculation of the cracking limit.

5.2 Bending moment calculation method

To improve on the calculation of the bending moment using the engineer's beam theory formula (par. 5.1.1) it is necessary to model more accurately the pile section behaviour. More realistic non-linear stress/strain curves may be used rather than a constant E_c, and the development of cracking should be taken into account. A program to do this has been developed using Matlab [The Mathworks Inc. (1984-2009)].

The model approximates the pile section by dividing it in a number of slices (between 48 and 68 depending on the pile section) parallel to the neutral axis for each material forming the pile (figs. 5.5, 5.6 and 5.7). Knowing the strains at two points (from the strain gauge readings) and assuming that plane sections remain plane, it is possible to calculate the strain distribution of the whole section (i.e. the strain at each slice). Using the appropriate stress/strain curves for each material, the stresses at each slice are calculated. The force is calculated by multiplying the slice stress by its area and the moment is obtained by multiplying the force by the distance of the slice from the neutral axis. The bending moment of the whole section is the sum of the single slice moments. This approach also allows the contribution to the bending moment of the different materials forming the pile to be taken into account. In this case the slice moments of a single material are summed for the whole section. Examples are given in section 5.3.2.

In this approach, the most important parameter is the position of the neutral axis. This is directly influenced by the development of cracking in the pile. If no cracking is assumed, then the neutral axis (considering bending strains only) lies in the centre of the section (by symmetry) and the calculation of the bending moment is straightforward. If cracking is occurring, it is necessary first to calculate the position of the neutral axis and then the value of the bending moment. It could be hypothesised that cracking always develops in a concrete beam in bending (once the theoretical tensile strain limit of the concrete is reached) and thus it is more accurate to always assume cracking is taking place. But, since the strains are measured with strain gauges, it could be also possible to assume that the pile is uncracked until the strain gauges show jumps in their readings associated with cracking taking place. Two different approaches are then used:

- An automatic cracking model (ACM), which considers the development of cracking based on the theoretical tensile strain limit of the concrete to determine the position of the neutral axis (par. 5.2.1). This method is used for circular concrete-

filled steel tubular piles (where the strain gauges welded to the steel pipe do not appear to be directly affected by crack propagation), and is one of the approaches used in analysis of the standard reinforced concrete piles.

- A manual correction model (MCM), that ignore the theoretical tensile limit of concrete and assumes that the neutral axis remains in the centre of the section (par. 5.2.2). Only when the strain gauges clearly show cracking (consistent jumps in the strain vs. time profiles), a manual correction of the position of the neutral axis and concrete section in tension is applied. This method is only used in analysis of standard reinforced concrete piles.

The comparison between the results obtained using the two models on the same piles is discussed below in section 5.3.2.

The next sections provide more detail about the two approaches used.

5.2.1 Automatic cracking model (ACM)

The calculation is based on two main assumptions:

- the conservation of plane sections;
- the same strain distribution in the concrete and reinforcement;

These allow the strain distribution in the section (and hence the position of the neutral axis, as explained in par. 5.1.2) to be calculated using the measurements from two strain gauges (fig. 5.4 and fig. 5.5). The position of the neutral axis calculated in this way is the global position, meaning that the section is subjected to both bending and axial strains. The latter affects the strain distribution by moving the position of the neutral axis, but not changing the gradient of strain through the section. The program calculates the slope of the strain distribution (*Grad*, fig. 5.4) using the global position of the neutral axis (X) and the strain measured by the up-slope strain gauge (A):

$$Grad = \frac{A}{X} \tag{5.2}$$

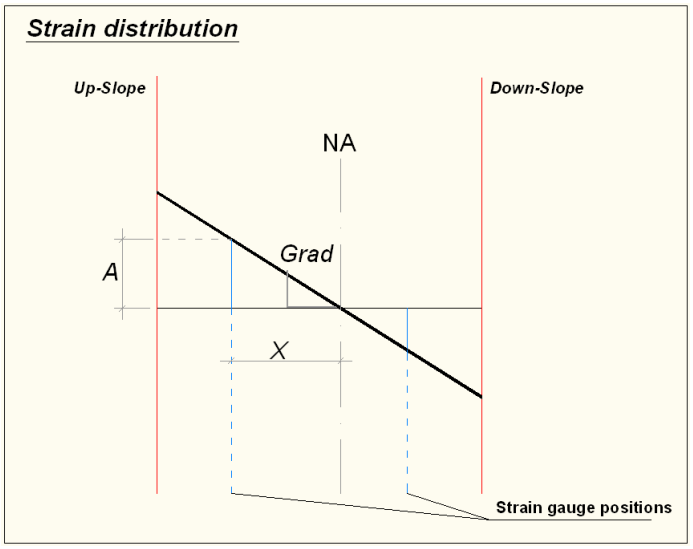

Figure 5.4: *Schematic illustration of the strain distribution of a deformed section used for the calculation of* Grad.

To generalise the problem, and to consider all the possible cases, all the calculations in the program are carried out using absolute values and at the end the result signs are changed using the *HS* matrix (hogging/sagging matrix), which stores the signs for the pile slices.

The section is then divided in a number of slices accordant with the required accuracy (fig. 5.6 and fig. 5.7). The pile section is made of different materials (concrete, steel and sometimes grout) with different proportions along the section. The program, however, considers that every material has the same distribution and it is divided in the same number of slices. The matrix of slice areas contains a value different from zero if the real slice contains the material (active slice) and equal to zero if it does not. This allows different distributions of the different materials to be applied while keeping a single programming code.

For the calculation of the bending moment, the program assigns a position of the neutral axis (at the first step it is in the centre of the section); calculates the strains in each slice using *Grad*; using the stress/strains curves for the particular material (par. 2.3.2) it calculates the stresses; to calculate the force applied in each slice it multiplies the stress by area and then multiplies the force by the distance of the slice from the neutral axis position to calculate the bending moment of each slice. At this point the equilibrium of the slice moments with respect to the assumed neutral axis is checked and if it is not satisfied within an accuracy of 1kNm, the neutral axis position is moved and the cycle is repeated again until the accuracy is reached or cannot be improved by moving the neutral axis a distance equal to $d/1024$ (where d is the pile diameter). When the equilibrium is reached (within 1kNm or $d/1024$), the bending moment of the section is calculated as the sum of all the bending moments of the slices with the correct sign now applied from the *HS* matrix.

Cracking of concrete (in standard reinforced concrete piles) or of the grout ring (in circular concrete-filled steel tubular piles) is considered during the calculation of the

stresses. If the global tensile strain of a slice (considering both bending strains and axial strains) reaches the limit (ε_{t0c} in fig. 2.5), then the slice stress is considered to be zero (the crack is now open). Recognising that a concrete crack cannot recover tensile strength, the area of the slice is set equal to zero for all successive readings, so the generated force (and thus bending moment) is always equal to zero after the opening of a crack. For this reason it is not possible to run only a part of the data (i.e. the last month), because every bending moment calculation is affected by the previous results. Cracking of the concrete core in circular concrete-filled steel tubular piles is not approached in this way. The softening behaviour of the material, after reaching the tensile limit ε_{t0c}, makes the concrete continue to work in tension after the opening of a crack. In this case the program follows the softening line (between ε_{t0c} and ε_{tu} in fig. 2.7) to calculate the stresses and after ε_{tu} is reached the stress of the slice is zero.

The main problem of setting a limit to the tensile strain of concrete related to a code of practice (in this case ε_{t0c} extrapolated from BS EN 1992 (2004)) is that the number and position of the reinforcements is not considered. The limit value is based on the properties of the concrete alone while the effects of the reinforcements are considered for the spacing and depth of cracks only. In practice, piles with few large diameter reinforcement bars will crack more easily than piles with many small diameter reinforcements bars (as introduced in par. 2.5.1). The effect of this is an over-estimation of cracking in the analysis of standard reinforcement concrete piles. The analysis of cracking of the grout ring in circular concrete-filled steel tubular piles does not have this problem since no longitudinal reinforcements are present.

The outputs of the program for each pile section are the contribution to the bending moment associated with each material, as well as the total bending moment.

The program calculates the bending moment at each section of the pile (usually from the top to the bottom) and then it proceeds to the next step in time and does the calculations again.

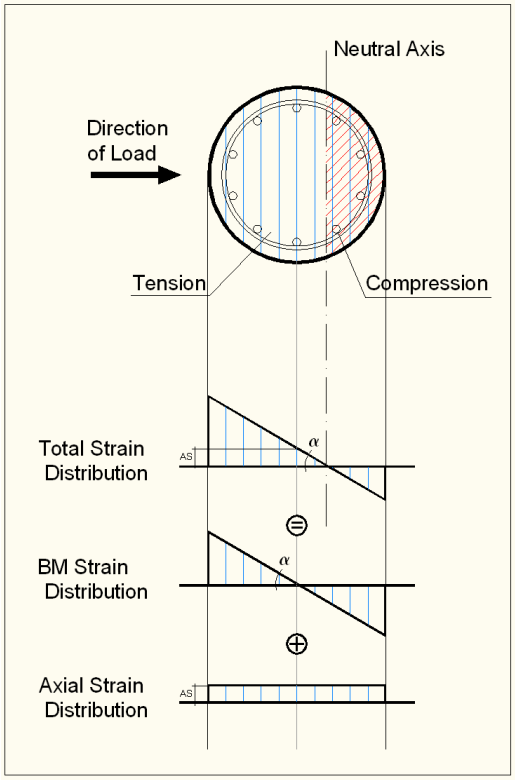

Figure 5.5: *Strain distributions: difference between bending strains and axial strains assuming an uncracked section*

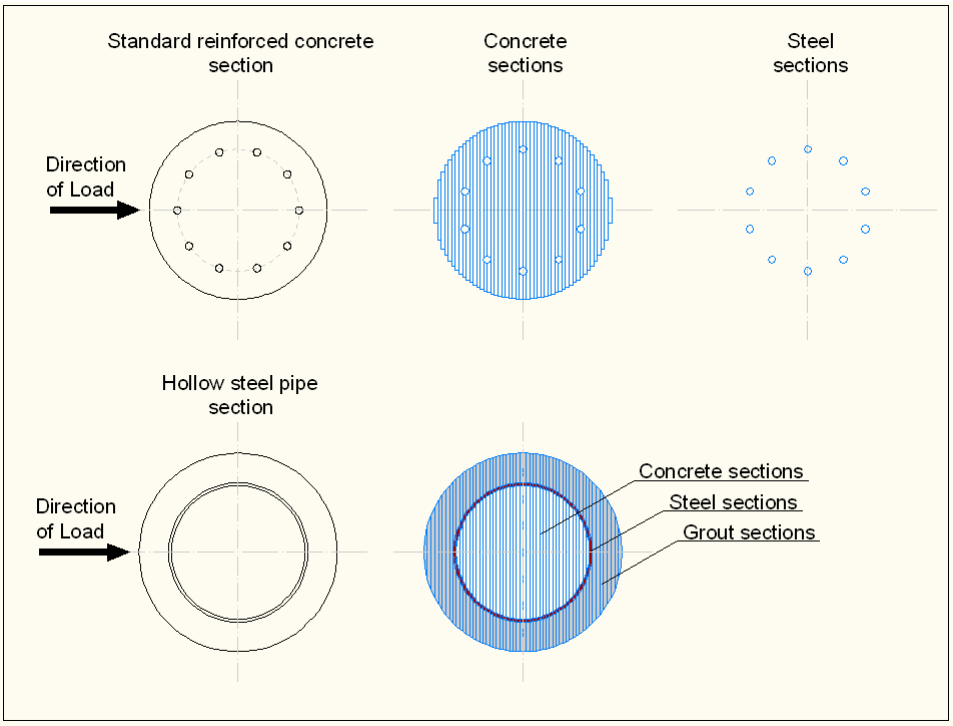

Figure 5.6: *Examples of concrete and steel sections used for the calculation of bending moment*

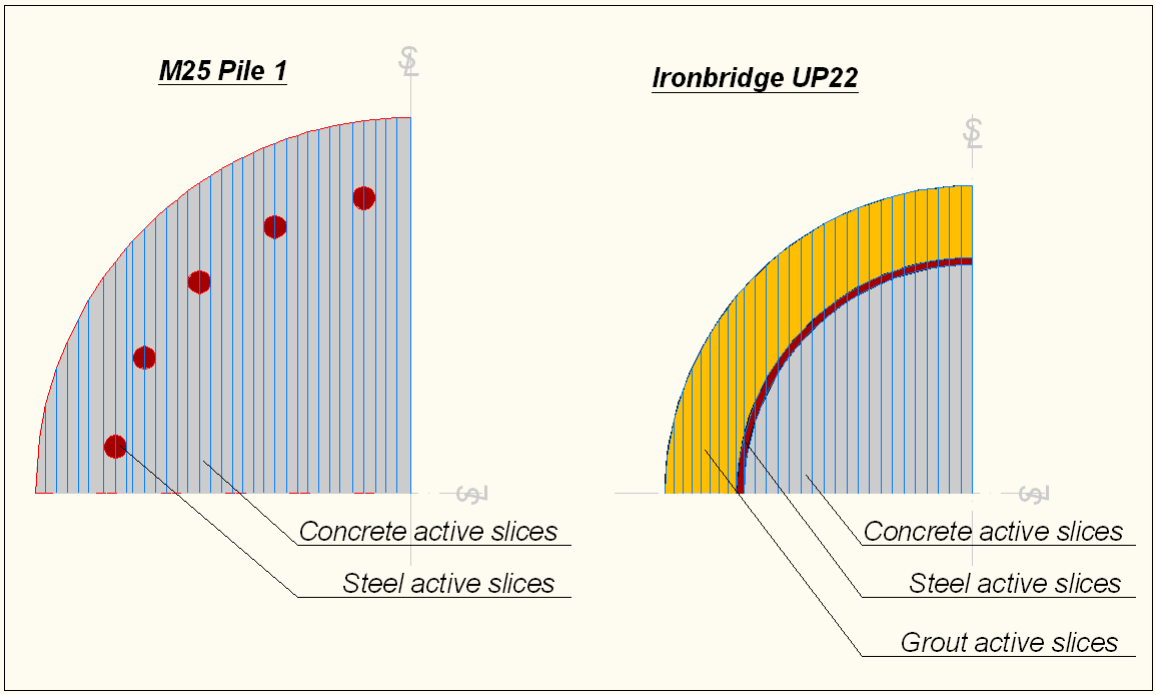

Figure 5.7: *Division of a standard reinforced concrete section and a concrete filled steel tubular pile section into slices for the calculation of the bending moment. Only active slices are considered in the calculation, while the rest of the slices are considered to have area equal to zero, thus they do not resist any moment.*

5.2.2 Manual correction model (MCM)

The program developed to calculate the bending moment without automatically considering the effects of cracking is based on a similar method and assumptions as that considering cracking effects (par. 5.2.1). The Matlab code [The Mathworks Inc. (1984-2009)] has a different structure to that used in the ACM, but the program performs similar calculations. The pile section is divided into slices and the position of the neutral axis is assumed to remain in the centre of the section. Then, the strain distribution is calculated using the gradient of the measured strains (*Grad*) and stresses are obtained from the stress/strain curves (par. 2.3.2.1). At this point the program does not consider any limit for the concrete in tension, and assumes that the tension stress/strains curve is the same as that in compression. When the strain gauges show jumps in the position of the neutral axis, a manual correction of its position and of the number of concrete slices in tension is applied (par. 5.2.2.1). This correction has been applied to only two instrumented sections out of seventy (from seven standard reinforced concrete instrumented piles). This approach is supported by the fact that other instrumented sections in the same piles measure higher tensile strains without signs of cracking and thus a generalised cracking correction (as in the ACM model, par. 5.2.1) may not be the best solution. It is assumed that in the cracked sections the instruments cross the cracks (micro-cracks) while the instruments in the nearby sections are outside the transfer zones, and are thus not obviously affected by cracking (no sudden jumps in the readings). As before, forces are calculated by multiplying the stresses by the area of

the corresponding slices; and bending moments are obtained multiplying these forces by the respective distances between the slices and the neutral axis.

5.2.2.1 Manual correction of cracking effects

This section considers how to correct the bending moment results (for the MCM approach) when the strain gauges show the development of a crack. This applies to a strain gauge bridging a crack or when it is close enough to it to record a jump in the reading connected to the cracking process.

Referring to fig. 5.8(a), the reading when the crack opens is denoted C, while *1* indicates the reading just before C and *2* the reading just after C. The correction for cracking is applied to the change in strain at C, considered as the opening of a crack happening in a short time (less than the interval between each reading, which is an hour).

It is assumed that bending moment and axial strain remain constant between *1* and *2* (a two hour interval) and the superposition of their effects remains possible. Strictly, this is only valid if there is linear elastic behaviour across the whole cross-section. Taking into account the stress/strain curve used for concrete (fig. 2.5) and considering that the measured strains are around $200\mu\varepsilon$, the stress/strain curve can safely be simplified with a line and the assumption can be considered valid.

The mobilised strength of the soil cannot change promptly when the crack opens, thus bending moment and axial strain applied to the pile do not change. As shown before (par. 5.1.4), the instruments show an apparent increase of axial strain as cracking occurs not connected to any real increase of applied load.

The first step is to consider the axial strain as constant between *1* and *2*. The axial strain is calculated in fig. 5.8(b) for *1*, where the solid line shows the total strain distribution. In fig. 5.8(d) the total strain distribution line (solid line) is translated down from the axial strain quantity calculated in *1* to obtain the bending strain distribution (dashed line). This allows the new position of the neutral axis (d_{NABM}) to be found, which will be used in the calculation of the bending moment immediately after cracking has taken place. d_{NABM} is the position of the neutral axis for the bending strains only since the axial strain has been removed during its calculation. It is possible to identify the tensile strain limit at the edge of the section (ε_l), considering that *1* is the strain limit in the strain gauge position just before the crack opens. ε_l is used in *2* to identify the number of slices to be considered cracked (fig. 5.8 (d) and (e)).

The correction is applied at the cracked section only. From *2*, onward in time, the position of the neutral axis is moved from the centre to d_{NABM} for both concrete and reinforcements; and a value of zero stress is assigned to the concrete slices considered cracked. When another cracking event is recorded, the correction process is repeated accordingly.

The mechanical application of the method does leave a residual jump in the bending moment profile due to the approximations made during the calculations (such as the dimension of the slices and the stress/strain curves). A further manual adjustment has

to be made to the number of cracked slices to minimise the jump.

The manual correction should be carried out for each cracking event identified. The corrections applied using this analysis are discussed in par. 5.3.1.

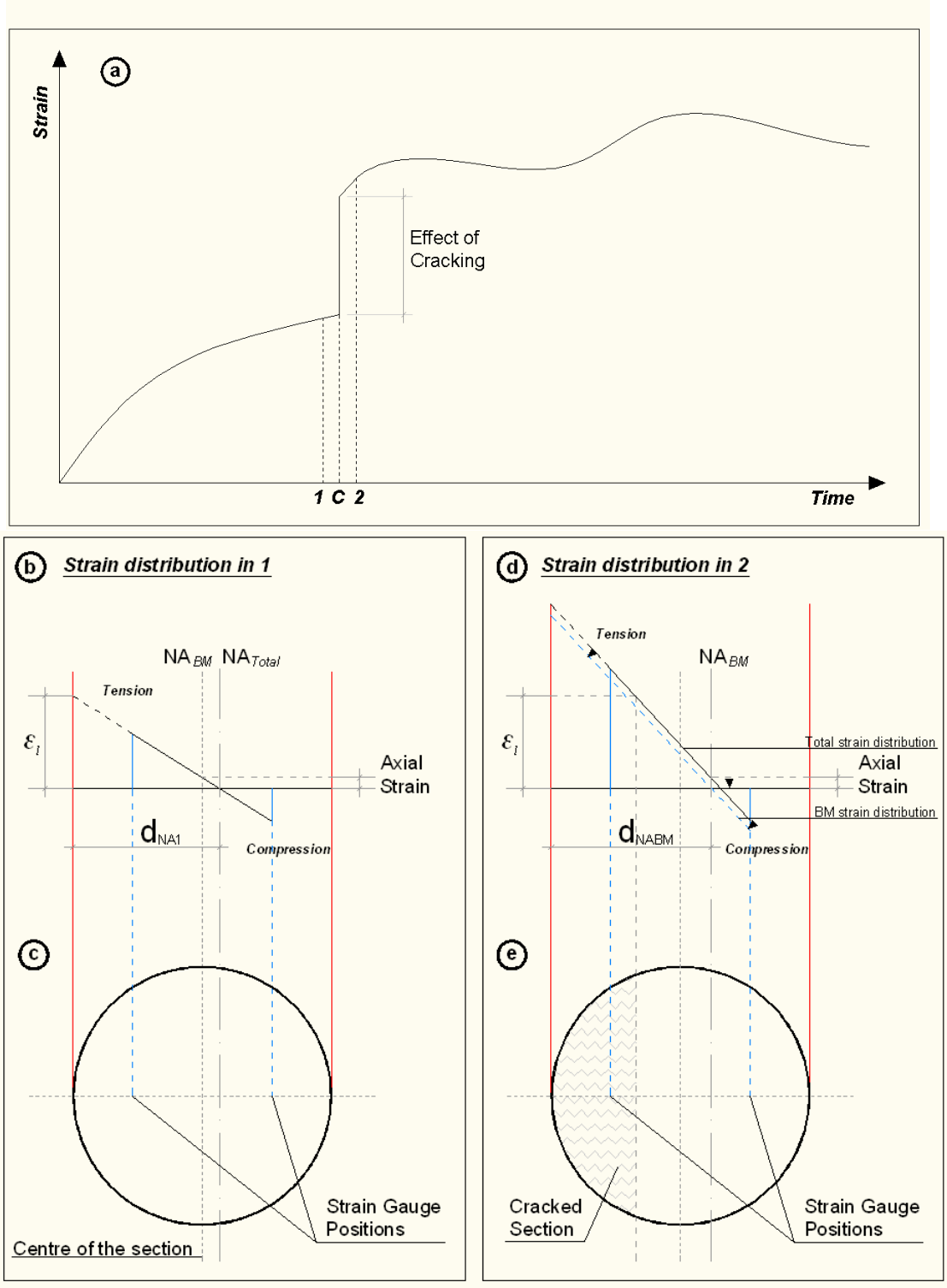

Figure 5.8: *Diagrams for the manual correction of a cracked section. The values of the strains before and after cracking are based on Grange Hill Pile1 data.*

5.3 Application of bending moment calculation methods to case histories

5.3.1 Discussion of the application of the manual correction model (MCM)

The MCM has been applied to each standard reinforced concrete pile, but the specific manual correction of the bending moment (par. 5.2.2.1) has been applied to only two cracking events in two different piles: Grange Hill Pile1 section 4-14 (shown as an example in figs. 5.8, 5.9 and 5.10) and Grange Hill Pile2 section 4-14 (as discussed in par. 4.6). The events occurred in the same section of the two piles but at different times, 5 February 2009 for Pile1 and 11 March 2007 for Pile2. The strain limits (ε_l) are very similar in both cases: 213$\mu\varepsilon$ in Pile1 and 204$\mu\varepsilon$ in Pile2. This could mean that the effective strain limit of concrete for the particular section (considering reinforcement bar and shear link diameters and positions) is about 200$\mu\varepsilon$. The MCM method gives movements of the neutral axis of 71mm for Pile1 and 84mm for Pile2 from the centre. The number of slices cracked (after the necessary minor adjustments to avoid unrealistic jumps in the bending moment graphs as explained at the end of section 5.2.2.1) are 13 in Pile1 (the estimated depth of the crack is 173mm from the tensile boundary of the section) and 15 in Pile2 (the estimated depth of the crack is 202mm from the boundary).

The correction for cracking also decreases the flexural stiffness of the pile. Figure 5.9 shows that the increase in moment from the cracking point to the end of the plot is smaller for the manually corrected bending moment i than for the uncorrected trace, in line with bending theory.

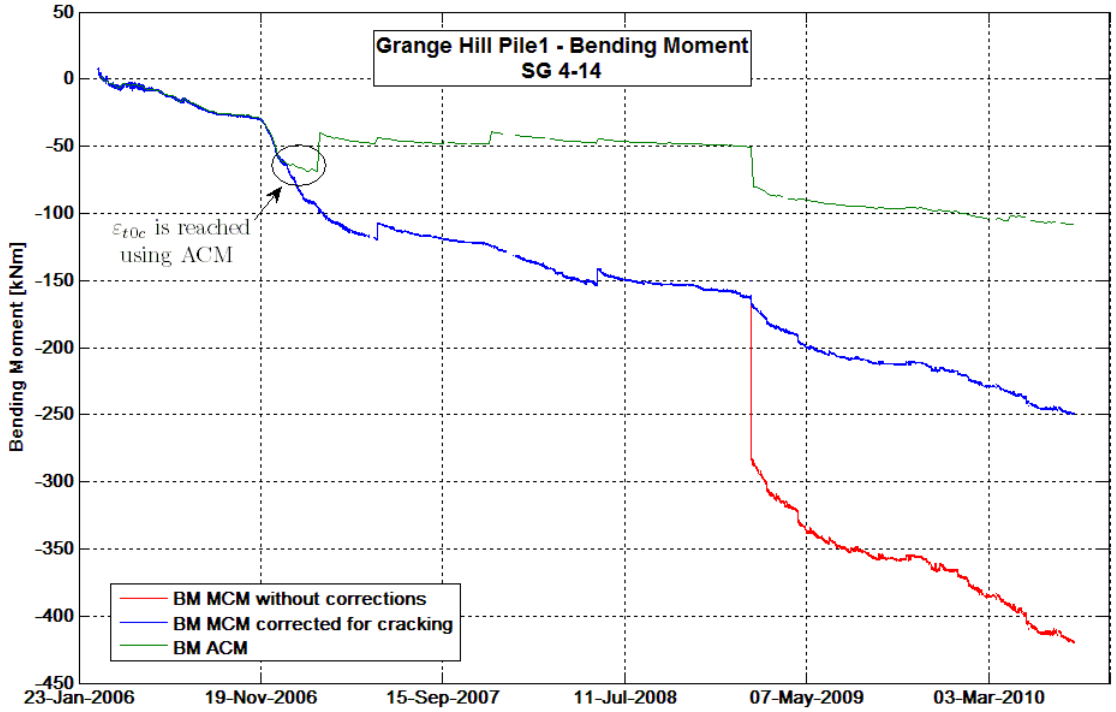

Figure 5.9: *Grange Hill Pile1, comparison between ACM, MCM uncorrected and MCM corrected bending moment profiles for section 4-14 in which cracking was identified (jump in the red and green profiles).*

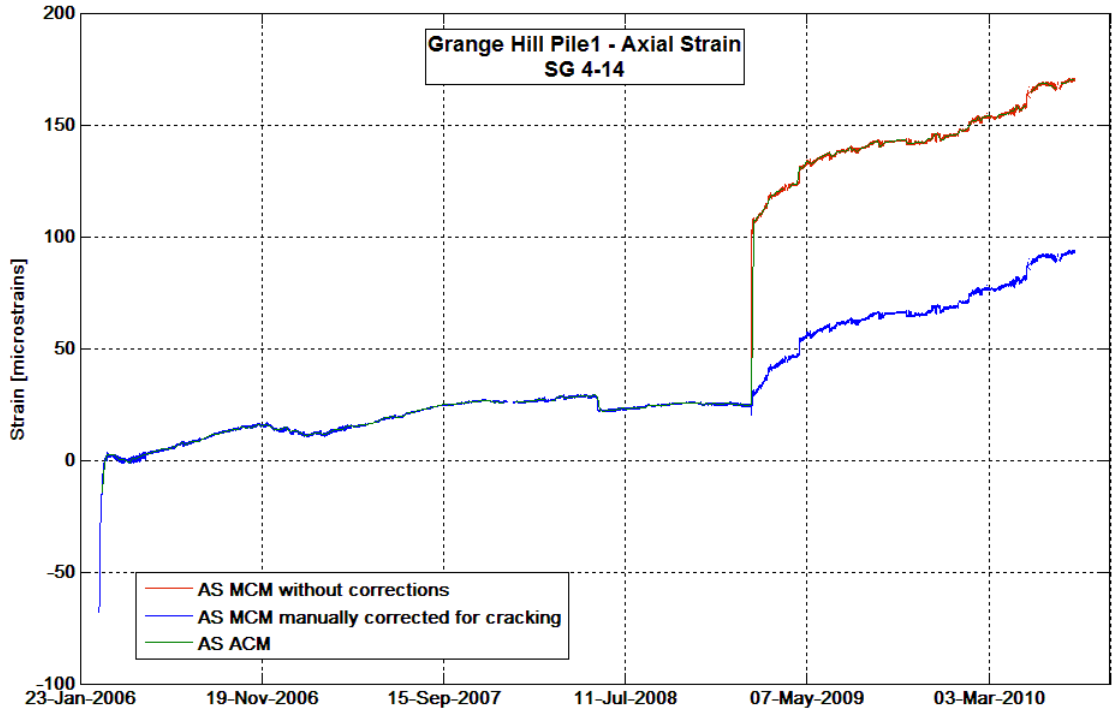

Figure 5.10: *Grange Hill Pile1, comparison between ACM, MCM uncorrected and MCM corrected axial strain profiles for section 4-14 in which cracking was identified (jump in the red and green profiles which are superimposed).*

5.3.2 Application of ACM and MCM

The two different bending moment calculation approaches (ACM and MCM) have been applied to the full set of instrumented piles used in this research. These include seven standard reinforced concrete piles at three different sites (three piles at Grange Hill, two at Mill Hill and two at Leatherhead) and seven circular concrete-filled steel tubular piles at Ironbridge. This section analyses the results of applying the different approaches to the data recorded using different strain gauges types (par. 2.1.1): embedded strain gauges in the standard reinforced concrete piles at Grange Hill and Mill Hill; sister bars in the standard reinforced concrete piles at Leatherhead; and welded strain gauges for the circular concrete-filled steel tubular piles at Ironbridge. The parameters used in each model are given in Table **5.1.**

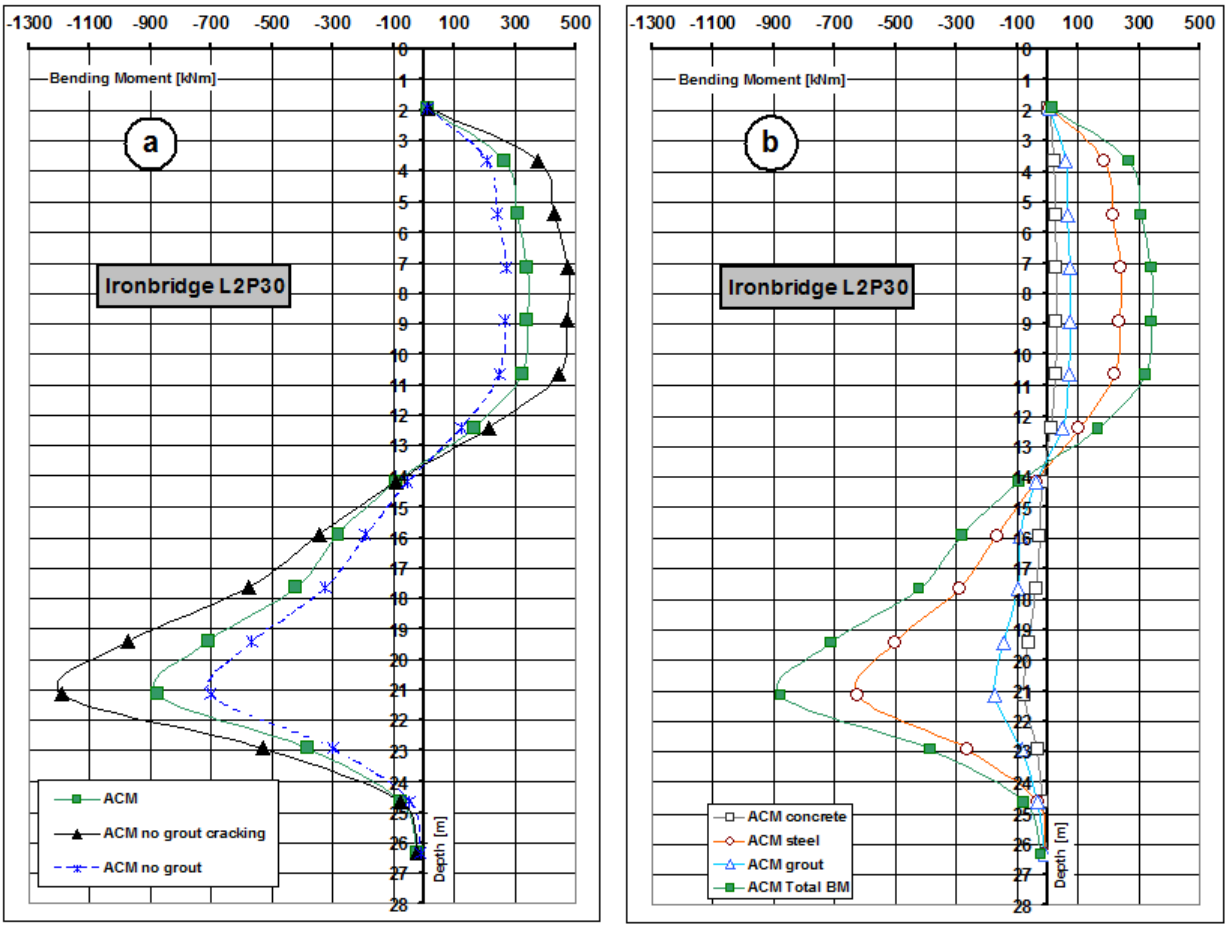

Figure 5.11: *Bending moment profiles with depth for Ironbridge pile L2P30; (a) the profiles showing the differences in bending moment for uncracked grout, partially cracked grout (ACM) and no grout; and (b), bending moment resisted by each material in the pile for the ACM is the total bending moment profile of the pile.*

Since the welded strain gauges are not directly affected by the development of cracking in the concrete (or grout), the circular concrete-filled steel tubular piles have been analysed only with the automatic cracking method (ACM, par. 5.2.1). The standard reinforced concrete piles have been analysed using both methods (ACM, par. 5.2.1 and MCM, par. 5.2.2), to compare the results.

Figure 5.11(a) shows the results of the analysis of Ironbridge pile L2P30 using different assumptions. As expected, the results that consider the development of cracking in the grout are between the no cracked grout profile and the profile ignoring the grout in the calculations. This shows how large the impact of different assumptions about the grout behaviour is on the bending moment calculated.

Figure 5.11(b) shows the bending moments resisted by the different materials of the pile. These graphs have been calculated using ACM, in one case as explained in section 5.2.1, in another case varying the grout properties (*no grout cracking*) and in the other changing the values of the slice areas (*no grout*). The bending moment resisted by the grout is higher than that resisted by the concrete. This happens because even when the grout in tension is cracked, the grout in compression is further than the concrete from the neutral axis and thus its contribution in resisting the bending moment is larger.

The structural effect of grout is usually neglected in the design phase since it is considered a material with poor mechanical properties and because it is considered debonded from the steel reinforcement pipe. In reality the grout can have higher strength than assumed in design, and it is partially connected to the steel tube by the spacers used to keep the steel tube in position during installation (fig. 5.12). The spacers used in the piles at Ironbridge are formed by T12 reinforcement bars welded together and to the steel reinforcement pipe.

Figure 5.12: *Ironbridge instrumented pile. Spacers are welded to the steel reinforcement pipe to keep it in position during installation. They also act as bonding points for the external grout ring.*

As discussed earlier, Grange Hill piles show cracking in one section of each pile (section 4-14, the fourth measurement from the top of the pile in fig. 5.13). In figure 5.13(a) the different bending moment calculation methods are compared. The manual

correction (MCM) is applied following the steps discussed in section 5.2.2.1. The profiles are quite different at the top of the pile where cracking develops, while they are the same in the lower four sections where there is no cracking. Figure 5.13(b) shows the bending moments resisted by the different materials using ACM. Steel resists a larger bending moment than the cracked concrete while the uncracked concrete resists a larger bending moment than the steel since its area and its distance from the neutral axis are greater. The same behaviour is shown by the graphs from the other sites (fig. 5.14 and fig. 5.15). In the Leatherhead pile the difference between the two bending moment profiles (fig. 5.15 (a)) is large, but the strain readings do not show any jumps related to cracking. This may happen due to the different type of instruments used. Sister bars use long reinforced bars (the overall instrument length is usually between 1.00 to 1.40m) to transmit the concrete strain to the vibrating wire instead of the small plates used by embedded strain gauges (overall length between 0.10 and 0.15m). This means that if a crack (more appropriately a micro-crack) opens near to an embedded strain gauge, the instrument can detect it, while if it opens across the length of a sister bar it is not detected due to the redistribution of stresses in the steel bar (which works as a normal reinforcement bar).

In standard reinforced concrete piles, the two bending moment calculation methods (ACM and MCM) give very similar results in the sections where cracking has not yet started, while they show very different results when the bending moment is larger and cracking develops in the models. This is due to some of the assumptions used in ACM when considering cracking. The method identifies when cracking begins using ε_{t0c} (based on $f_{ctk,0,05}$ from BS EN 1992 (2004), par. 5.2.1), which is a statistical strain limit of concrete. This is a limit of the material, but it is not related to the other factors affecting cracking (mainly position and diameter of the reinforcements). Figure 5.9 shows that MCM and ACM give the same bending moment profiles until ε_{t0c} is reached using ACM (other effects of ε_{t0c} are discussed in section 5.3.2.1). Then the two models give a different profiles, but both (ACM and MCM uncorrected) show a jump in the bending moment when the strain gauges measure a cracking event. Another problem is that cracks open in discrete positions (usually randomly) along the pile. Using only a few instrumented sections, it is necessary to approximate the behaviour of the pile between these sections without knowing the real distribution of cracks. The ACM program considers that when the cracking limit is reached, the full depth of pile represented by the instrumented section is cracked. This is not correct when cracking is at the initial stage. Some cracks would be open, but they would also be a distance apart. Between the cracks and outside the respective transfer zones, concrete would still work in tension, thus resisting the applied bending moment. When cracking reaches the stabilised stage, and the transfer zones merge, no concrete in tension is able to resist any bending moment (par. 5.2.1). ACM approximates the cracking as if it is always at the stabilised stage.

Figure 5.16 shows a sensitivity comparison for two sites: Leatherhead Pile2 (MCM and ACM) and Ironbridge L2P30 (ACM with the grout allowed to crack, no cracking and

no grout in the model). The main variable is f_{ck} (characteristic compressive strength of concrete) which makes all the other parameters used in the models change accordingly following BS EN 1992 (2004) Table 3.1. Two sets of parameters were used: those assumed earlier for long term conditions (f_{ck}=55MPa for concrete and f_{ck}=30MPa for grout) and those assumed during the design phase (f_{ck}=30MPa or f_{ck}=35MPa for concrete and f_{ck}=15MPa for grout). In Leatherhead Pile2, the use of the design rather than the long term parameters causes a reduction in the bending moment peak of about 17%; while in Ironbridge L2P30 the difference is about 17% for "no grout cracking condition", 6% for standard ACM conditions and 3% for "no grout". There is a difference of around 85% in the bending moment peak between assuming there is no grout in the model and assuming it is present and uncracked. The sensitivity comparison shows the substantial influence that material parameters and cracking behaviour have on the calculation of bending moment within a pile.

ACM always considers the cracking of concrete when the tensile limit is reached, while MCM always assumes uncracked sections unless there is direct evidence from the strain gauge readings. These are the two extremes for the pile and the "real" bending moment profiles lie in between the two.

Two conclusions can be made:

- ACM is the only method which can be used on all types of pile and all types of strain gauges, since it does not rely on observed cracking. For this, it is extremely important to measure the tensile strength of concrete.
- In circular concrete-filled steel tubular piles, the external grout ring makes significant contribution to the structural behaviour of the pile.

	Concrete					Steel		Grout				
	E_{cm} [GPa]	ε_{c1} [‰]	f_{ck} [MPa]	f_{cm} [MPa]	$f_{ctk0.05}$ [MPa]	E_s [GPa]	f_{yk} [MPa]	E_g [GPa]	ε_{c1g} [‰]	f_{ckg} [MPa]	f_{cmg} [MPa]	$f_{ctk0.05g}$ [MPa]
Grange Hill	35	2.3	50	48	2.5	200	500	-	-	-	-	-
Leatherhead	36	2.4	55	53	2.7	200	500	-	-	-	-	-
Mill Hill	35	2.3	50	48	2.5	200	500	-	-	-	-	-
Ironbridge	36	-	55	53	-	200	500	31	2.1	30	33	1.8

Table 5.1: *Parameters used in the ACM and MCM models for each site.*

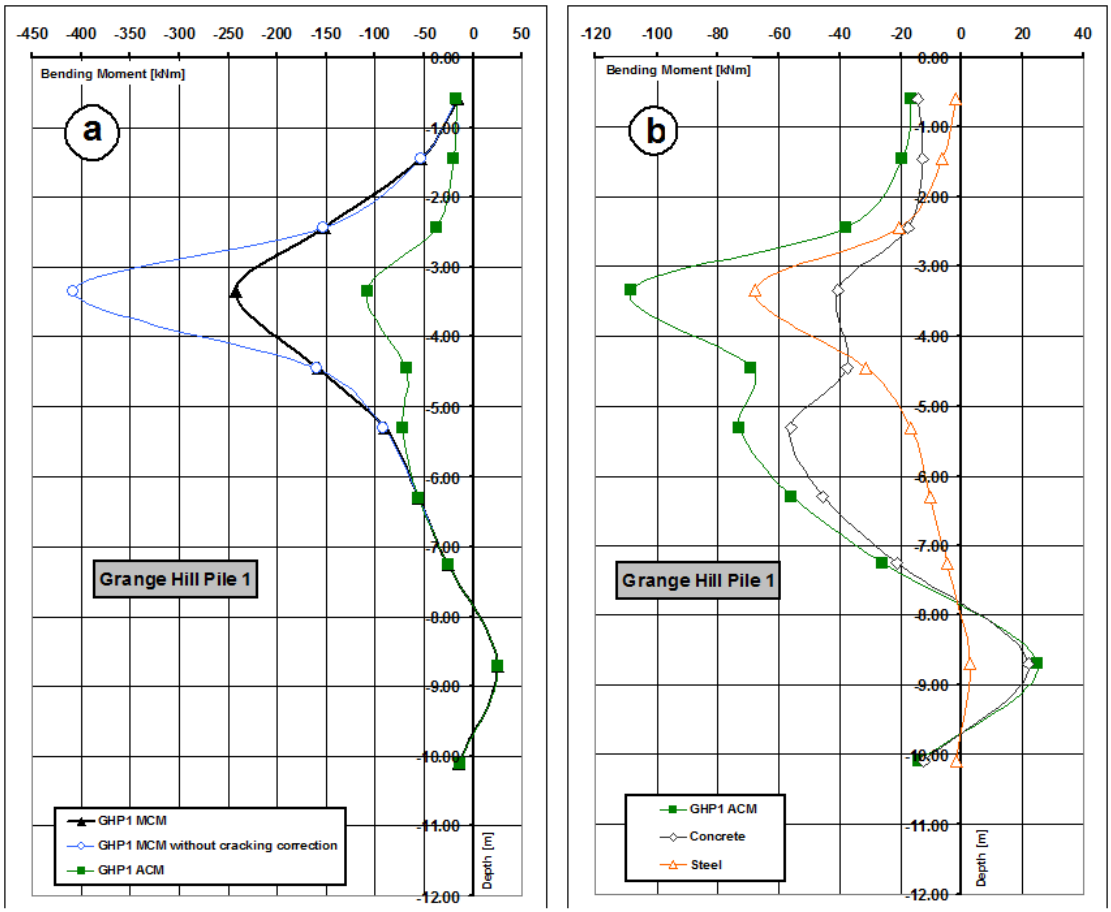

Figure 5.13: *Bending moment profiles with depth for Grange Hill Pile1. (a) comparison between no cracking correction, automatic cracking model (ACM in par. 5.2.1) and manual correction model (MCM in par. 5.2.2). (b) comparison between the bending moments resisted by each material.*

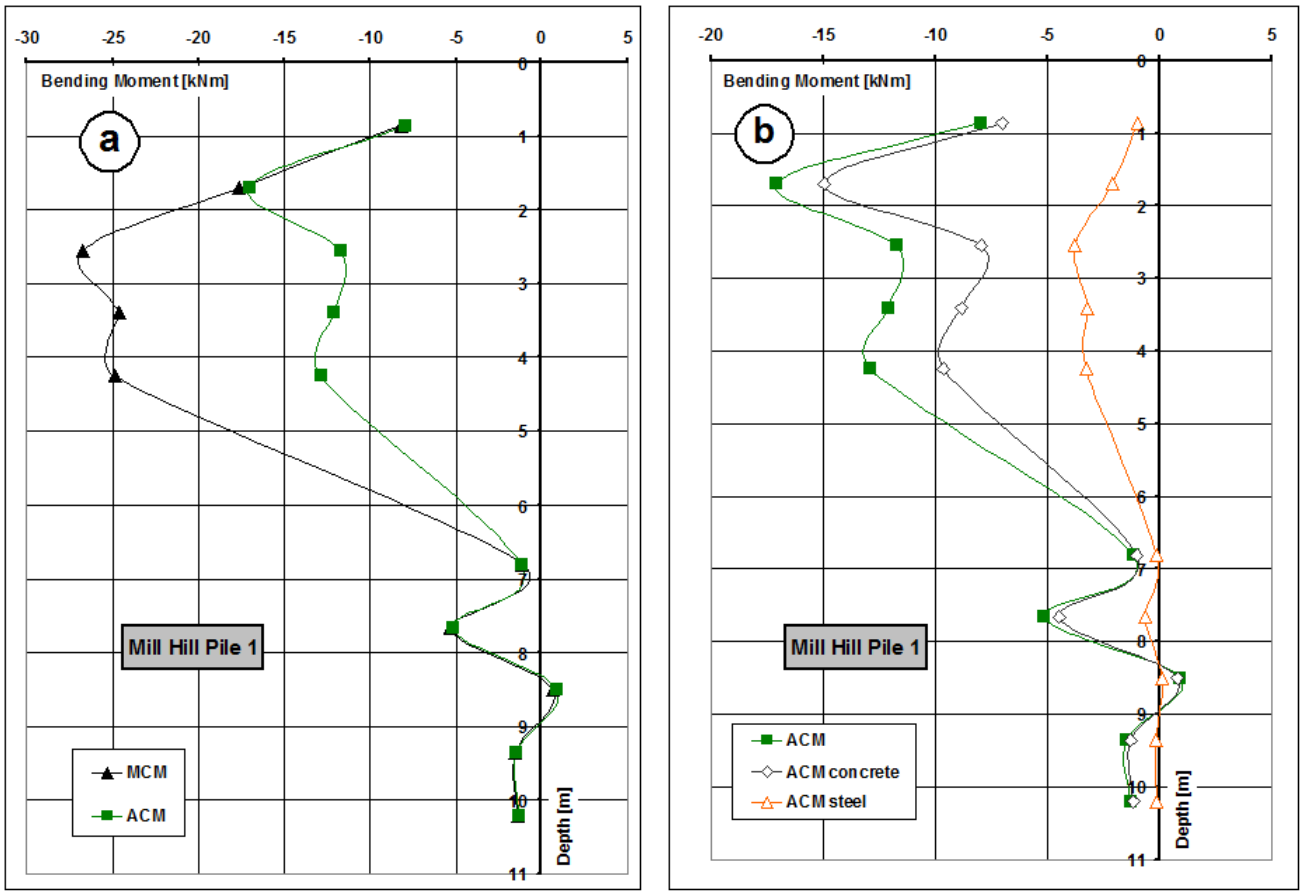

Figure 5.14: *Bending moment profiles with depth for Mill Hill Pile2. (a) comparison between manual correction model (MCM in par. 5.2.2) and automatic cracking model (ACM in par. 5.2.1). The strain gauges are not measuring a cracking event. (b) comparison between the bending moments resisted by each material.*

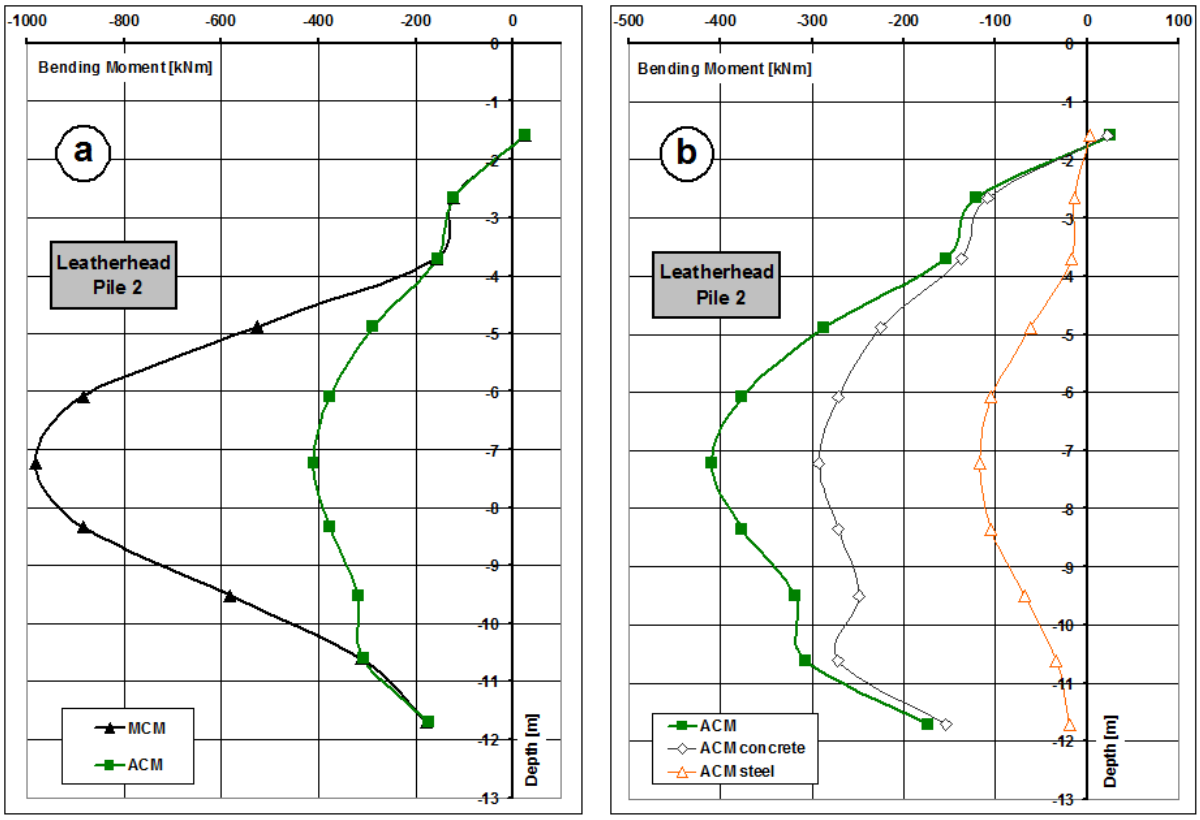

Figure 5.15: *Bending moment profiles with depth for Leatherhead Pile2. (a) comparison between manual correction model (MCM in par. 5.2.2) and automatic cracking model (ACM in par. 5.2.1). The strain gauges are not measuring a cracking event. (b) comparison between the bending moments resisted by each material.*

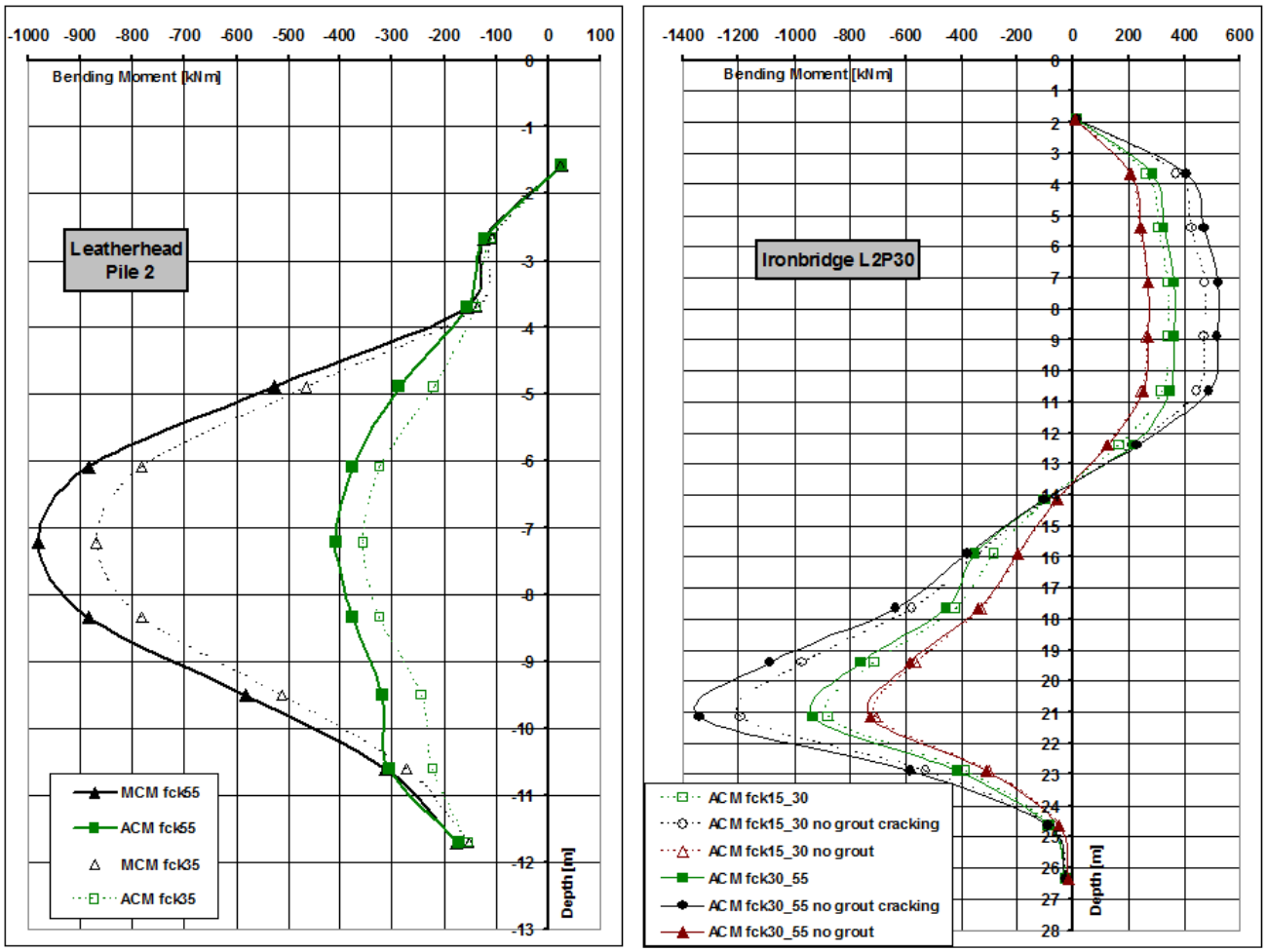

Figure 5.16: *Sensitivity comparison for the bending moment profiles for Leatherhead Pile2 and Ironbridge L2P30. Different values of f_{ck} (characteristic compressive strength of concrete) were used. For Leatherhead Pile2 f_{ck}=55MPa is the measured value, while f_{ck}=35MPa is for design. For Ironbridge L2P30, grout (first value) and concrete (second value) parameters are considered. (15_ 30) are the values from design while (30_ 55) are those assumed for the long term analysis.*

5.3.2.1 The effects of the tensile strain limit of concrete (ε_{t0c}) on ACM

As introduced in section 5.3.2, ACM identifies when cracking begins using ε_{t0c} (based on $f_{ctk,0,05}$ from BS EN 1992 (2004), par. 5.2.1), which is a statistical tensile strain limit of concrete. This implies that the value of ε_{t0c} used in the model is probably different from the real tensile strain limit of the concrete used in the pile. In section 4.6 and 5.2.2.1, the cracking events in the piles at Grange Hill have been introduced and discussed. The use of the tensile strain limit of concrete extrapolated from the analysis of cracking in section 5.2.2.1 gives better results in ACM than using the value based on BS EN 1992 (2004). In the case of Grange Hill Pile1, the approximate value of ε_{t0c} based on $f_{ctk,0,05}$ from BS EN 1992 (2004) is 72$\mu\varepsilon$, while that from the analysis of the cracked section is 200$\mu\varepsilon$ (par. 5.3.1). Figure 5.17 shows the results from ACM using the two different values of ε_{t0c} in comparison with the profile obtained using MCM. As introduced in the discussion of the manual correction applied within MCM (par.

5.2.2.1), the bending moment applied to the pile should remain continuous throughout the cracking event, as long as there are no external actions which make it change. For Grange Hill there are no external actions on the pile likely to cause a sudden jump in the bending moment profile,hence when a crack opens (and there is no compatibility of strains between steel and concrete), the strain readings from the embedded strain gauges show a jump, while the bending moment applied to the pile should not. With no manual correction applied, the ACM results show a jump in the bending moment as cracking takes place. If these jumps are corrected (in this case translating the latter part of the graph to obtain a continuous profile), ACM results using ε_{t0c}= 200$\mu\varepsilon$ are in good agreement with MCM results (fig. 5.18). After the cracking event ACM shows a smaller stiffness (smaller slope of the profile) than MCM.

The ACM bending moment profile calculated using ε_{t0c}= 72$\mu\varepsilon$ needs two different corrections since the opening of the crack in the model does not coincide with the opening of the crack measured by the strain gauges (fig. 5.18).

In conclusion, the corrected profiles in Figure 5.18 show the different results obtained using two different values of ε_{t0c}, and demonstrate the importance of measuring the tensile strain of concrete for a more accurate prediction of the applied bending moment.

In cases in which sister bars are used, where the crack opening is not shown by the instrument, the direct measurement of ε_{t0c} is even more important.

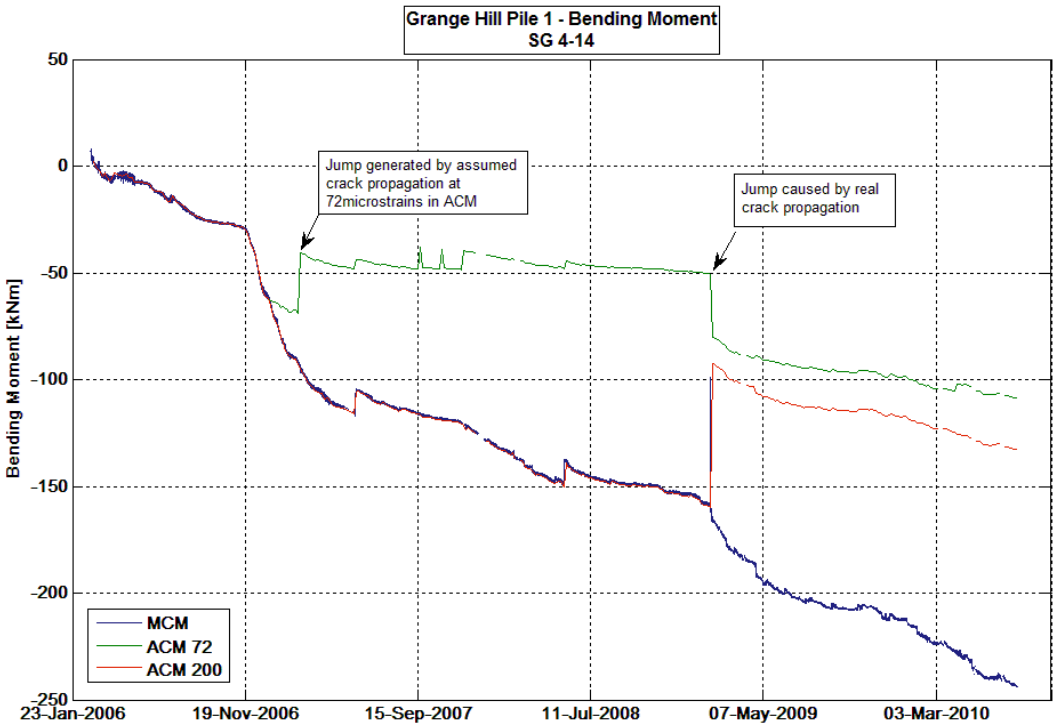

Figure 5.17: *Grange Hill Pile1 SG4-14, comparison between bending moment profiles calculated with MCM, ACM (ε_{t0c}= 72$\mu\varepsilon$) and ACM (ε_{t0c}= 200$\mu\varepsilon$).*

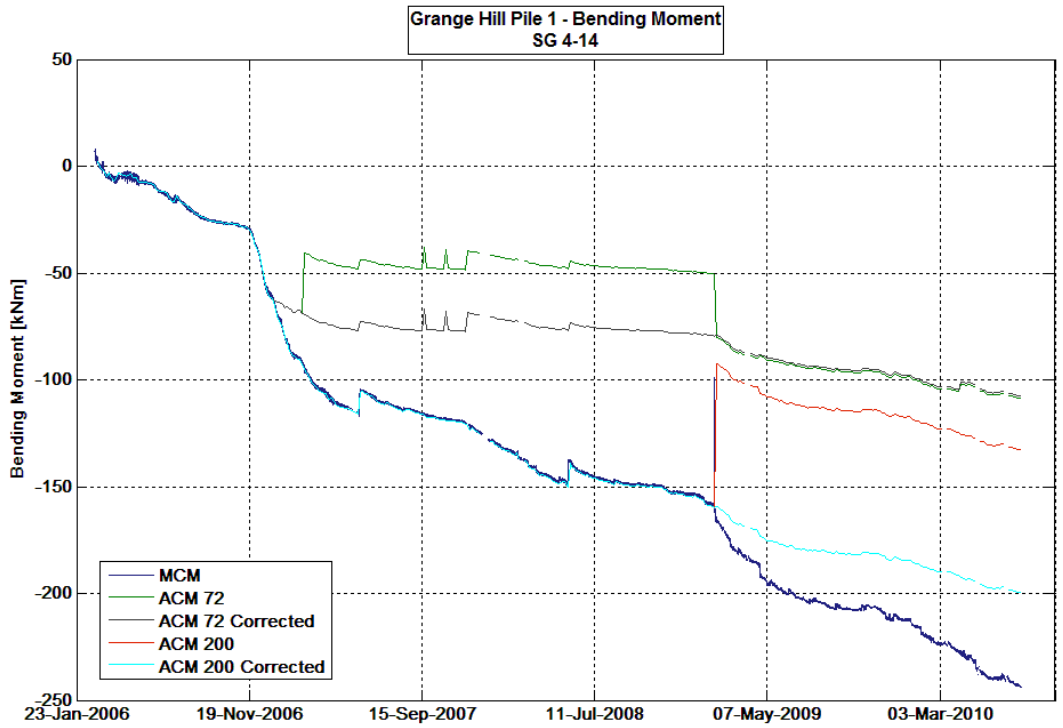

Figure 5.18: *Grange Hill Pile1 SG4-14, comparison between bending moment profiles calculated with MCM, ACM (ε_{t0c}= 72$\mu\varepsilon$), ACM (ε_{t0c}= 72$\mu\varepsilon$) corrected, ACM (ε_{t0c}= 200$\mu\varepsilon$) and ACM (ε_{t0c}= 200$\mu\varepsilon$) corrected.*

5.3.3 Axial strain

In section 5.1.4 the effects of the axial strain calculation have been discussed, identifying the possibility that the measured axial strain could be due to the opening of cracks. This section analyses the effects of the axial strain on the calculation of cracking and vice-versa, using the case history data.

The first example is from Leatherhead Pile2 (fig. 5.19). The axial strain profile shows that the pile is in compression until a depth of about 4m and in tension between 4 and 12m depth. The physical explanation of this could be difficult if the effect of cracking is not taken into account. Considering figure 5.19 (a), the two bending moment models (MCM and ACM) show a large difference in the results between about 4 and 11m depth, where the axial strain is in tension rather than in compression. Cracking could be the reason for the switch to tensile strain. The sister bar strain gauges used in these piles do not show any jumps related to cracking, but this does not mean that cracking is not developing. As discussed earlier, it could be that this particular type of instrument is unable to detect the cracking due to its length.

The Mill Hill axial strain profile (fig. 5.20) shows a similar behaviour with a point at about 7m depth in small compression and the rest of the pile in tension. The bending moment profiles show a very small bending moment at 7m depth.

Grange Hill Pile1 (fig. 5.21) shows tension only axial strains with an obvious peak where a crack is supposed to be opening (around 3.50m depth). This graph supports the hypothesis that when a crack is opening the axial strain profile has an increase in

tensile strain.

Ironbridge Pile L2P30 axial strain profile (fig. 5.22) shows a completely different behaviour. Although the grout ring is calculated to be heavily cracked, the axial strain is all in compression. This may be due to the load of the pile cap and/or the settlement of superficial layers.

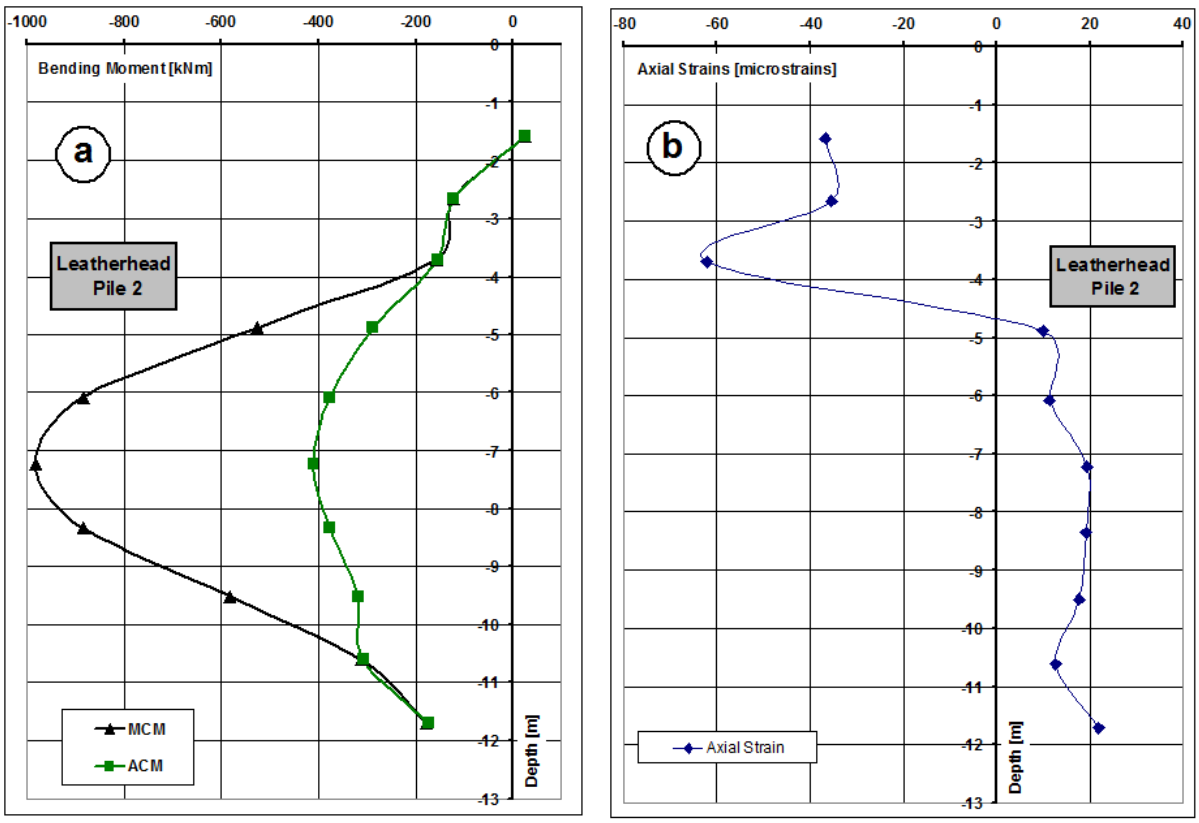

Figure 5.19: *(a) bending moment profiles with depth for Leatherhead Pile2, calculated using MCM and ACM (par. 5.2.1). (b) axial strain profile for Leatherhead Pile2*

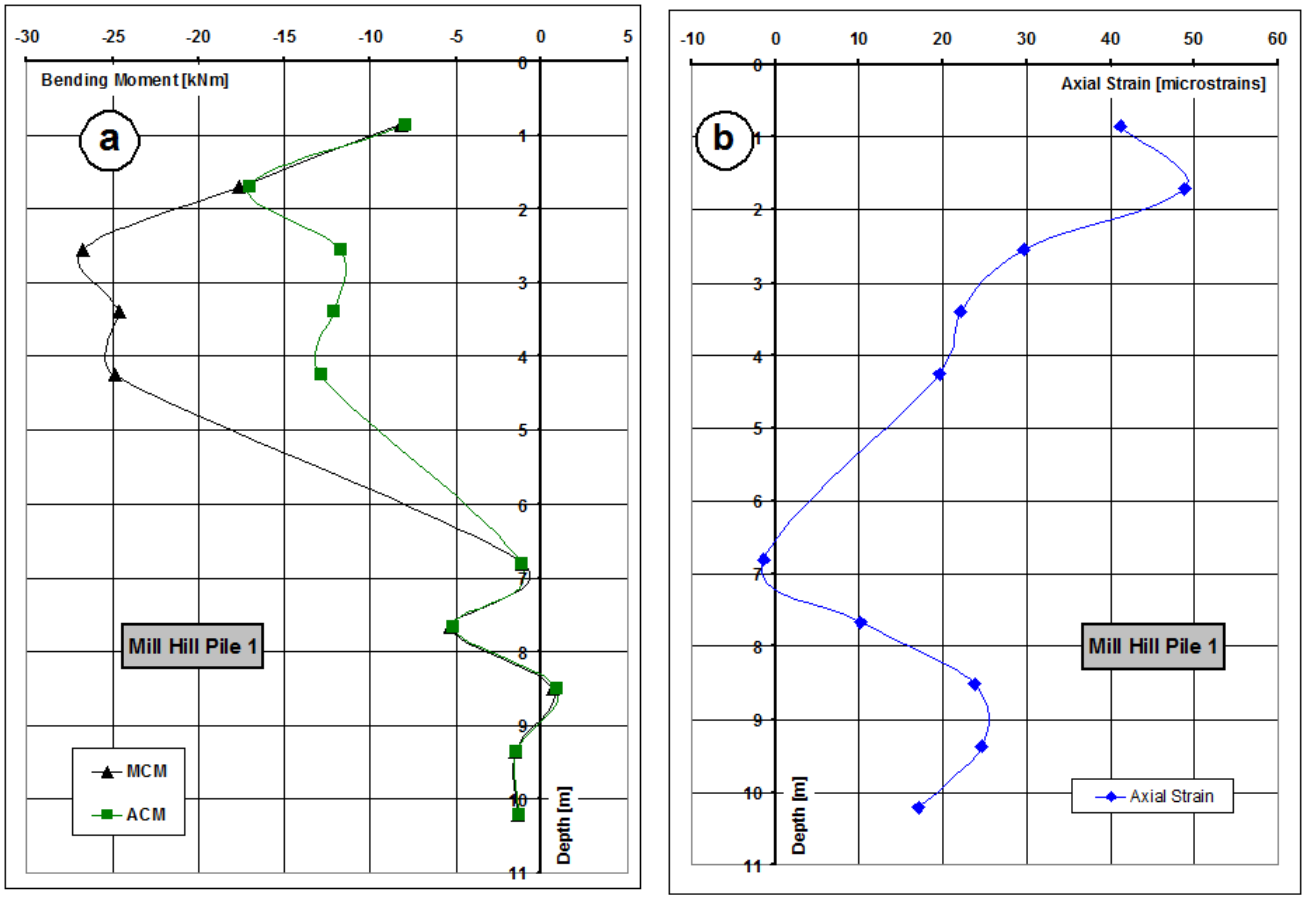

Figure 5.20: *(a) bending moment profiles with depth of Mill Hill Pile1, comparison between MCM and ACM (par. 5.2.1). (b) axial strain profile for Mill Hill Pile1*

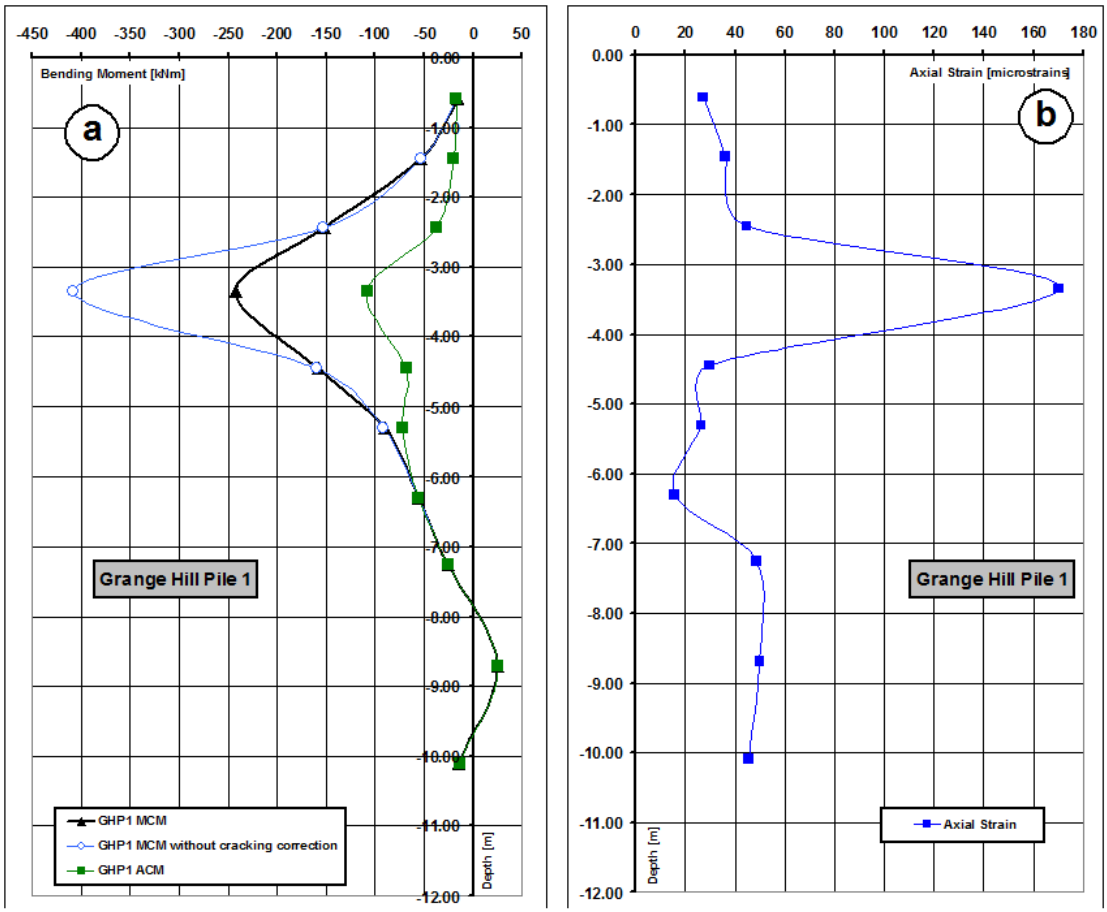

Figure 5.21: *(a) bending moment profiles with depth of Grange Hill Pile1. Comparison between no cracking correction, ACM (par. 5.2.1) and MCM (par. 5.2.2). (b) uncorrected axial strain profile for Grange Hill Pile1 as in figure* ***5.10.***

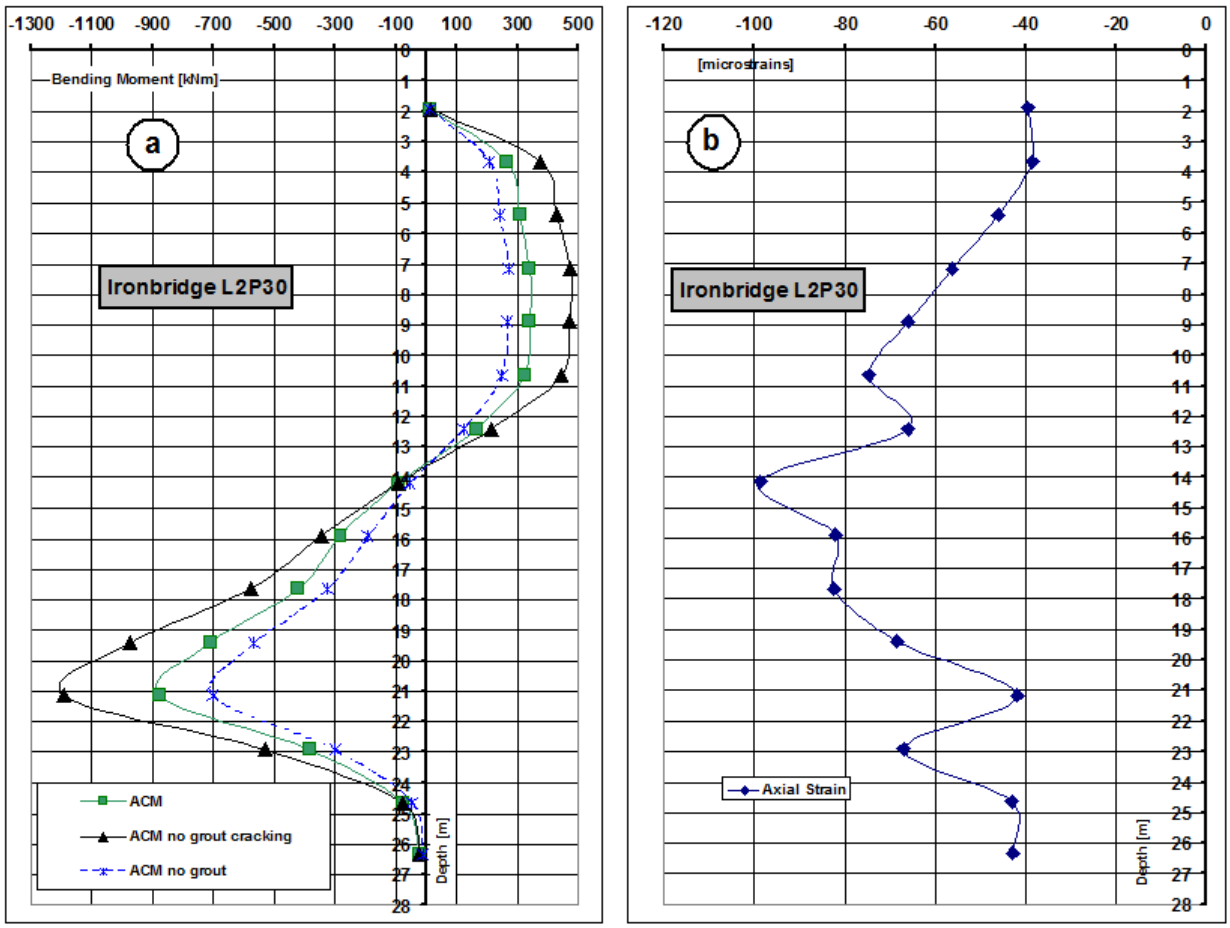

Figure 5.22: *(a) comparison of different bending moment profiles with depth of Ironbridge pile L2P30. (b) axial strain profile for Ironbridge pile L2P30.*

5.4 Bending moment calculation conclusions

This chapter introduces two methods for the calculation of the bending moment in reinforced concrete piles taking into account the non-linearity of the stress/strain relationship and the development of cracking and its consequences. These methods give more accurate results and more information about the section and material behaviour than the engineering bending formula (par. 5.1.1), which was used in the past for the analysis of those type of structure.

In conclusion:

- The automatic cracking model (ACM) analyses the pile as if the cracking is at the stabilised stage. It is thus preferred in the analysis of concrete filled steel tubular piles for which it better describes the behaviour of the grout ring, since it is not reinforced (no transfer zones), and it has very limited tensile strength (from weak material properties). However, the method underestimates the bending moment of a standard reinforced concrete pile since it does not account for tension stiffening (par. 2.5.1) and the effect of the type of reinforcement (number, position and diameter of the bars and shear links). Knowledge of the value of ε_{t0c} (strain limit

of concrete in tension) for specific concretes, rather than the use of a statistical average, is vitally important for an accurate bending moment profile.

- The manual correction model (MCM) initially analyses the pile assuming cracking has not developed. When the strain gauges show clear signs of cracking, a manual correction is applied. The method will overestimate the bending moment in a pile if the strain gauges do not detect a cracking taking place. This method is nonetheless preferred for the analysis of standard reinforced piles when there is the possibility of identifying the cracks (i.e. when embedded strain gauges are used). Instead, the method is not appropriate when sister bars are used, since the crack opening is not shown by the instruments.

- In general, differently reinforced concrete piles instrumented with different types of strain gauge require individual approaches for calculating the cracking effects. For given concrete properties, ACM and MCM give the limits for the bending moment profile, and the real bending moment applied to the pile is likely to lie in between them.

- Comparison of the results from the two different methods gives important information about the development of cracking in the pile. When the two methods give similar results the concrete is uncracked, when they diverge cracking is developing.

- The use of the axial strain in the calculation of the cracking can be misleading. Tensile axial strain can be generated by the opening of cracks and thus may not be related to any applied force (this is termed apparent axial strain). Adding this axial strain to the bending strain to check if the cracking limit is reached gives extending cracks before the real limit is reached (since the axial strain is apparent). For this reason it is better to not use the axial strain during the calculation of the cracking. An exception is represented by Ironbridge Pile L2P30 where the axial strain for the whole pile is in compression. In this case no apparent axial strain is present and it can be used for evaluating cracking.

- The analysis of results obtained using the automatic cracking model (ACM) for the concrete filled steel tubular piles in Ironbridge shows that even if heavily cracked, the grout can resist more bending moment than the concrete core. Neglecting the grout underestimates the bending moment resisted by the pile significantly, by up to 25%.

- Concrete parameters and assumptions on the behaviour of the section (cracked, uncracked or partially cracked) have a substantial influence on the bending moment results. The identification of the correct parameters and the way the section works is essential for accurate results. The same model applied with different assumptions and different material parameters can give results that differ by up to 100% (par. 5.3.2).

Chapter 6

Inclinometer results and curve fitting analysis

The previous chapters explained how to use the data coming from the strain gauges to calculate the bending moment in the piles. This chapter presents the displacements measured by the inclinometers in some of the piles at each instrumented site. Displacements for the remaining piles are shown in Appendix A. A method for the comparison of strain gauge piles and inclinometer readings is developed to check the consistency of the two. This requires the calculation of the bending moment using the displacements measured by the inclinometers. The approach developed by Smethurst (2003) for a similar analysis at another discrete pile site has been used (par. 6.2). A similar problem has been also analysed by Nip and Ng (2005), who developed a method for the calculation of the bending moment from inclinometer readings for a test pile, where the applied load was measured. For discrete piles used to stabilise slopes, the load and its distribution is unknown, thus this method cannot be applied since there are too many unknowns for the system of equations used.

The comparison between strain gauges and inclinometers data involving calculation of bending moment was chosen to follow the previous research done by Smethurst and Powrie (2007). The approach of comparing measured strains with inclinometer data by means of curvature was attempted with unsuccessful results.

Cracking of concrete can change the flexural stiffness of the piles, complicating the comparison between strain gauges and inclinometer results. The relative assumptions made on cracking are discussed in par. 6.2.1.

6.1 Inclinometer results

This section presents the inclinometer results coming from some of the instrumented piles in the four different sites. Positive displacements show a down-slope movement of the pile, while the negative are up-slope. The displacement profiles of the remaining piles are shown in Appendix A.

6.1.1 Grange Hill

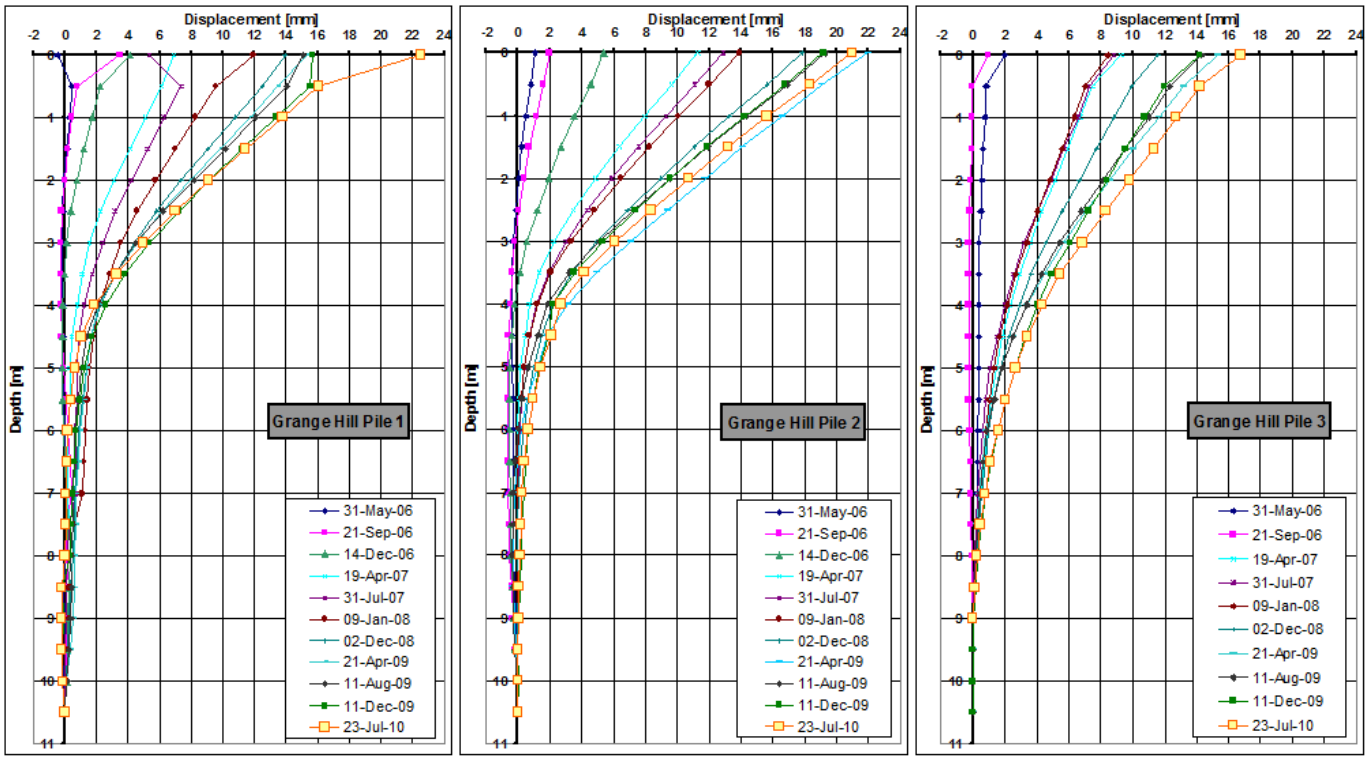

Figure 6.1: *Inclinometer displacement profiles for the instrumented piles at Grange Hill.*

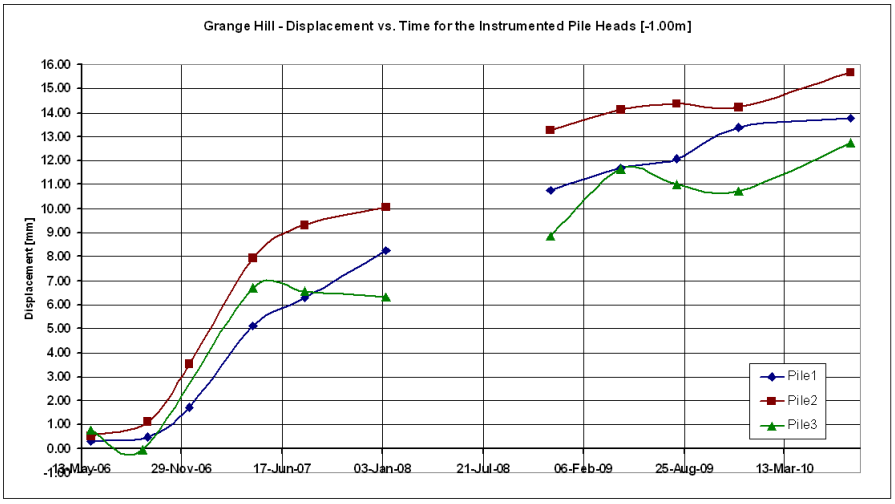

Figure 6.2: *Displacement versus time profiles for the instrumented piles at Grange Hill. The displacements are taken at 1.00m depth from top of the piles.*

The displacement profiles in figure 6.1 show similar behaviours for the three instrumented piles. In Pile1 and Pile2 the significant movement is within the top 5m while in Pile3 significant displacements extend to 7m depth. The displacement versus time profile (fig. 6.2) shows a seasonal variation of the pile head displacements, with the pile head displacement reversing in some of the piles during the summer period. The

pile show increasing displacements with time even if they are subjected to seasonal variations.

6.1.2 Mill Hill

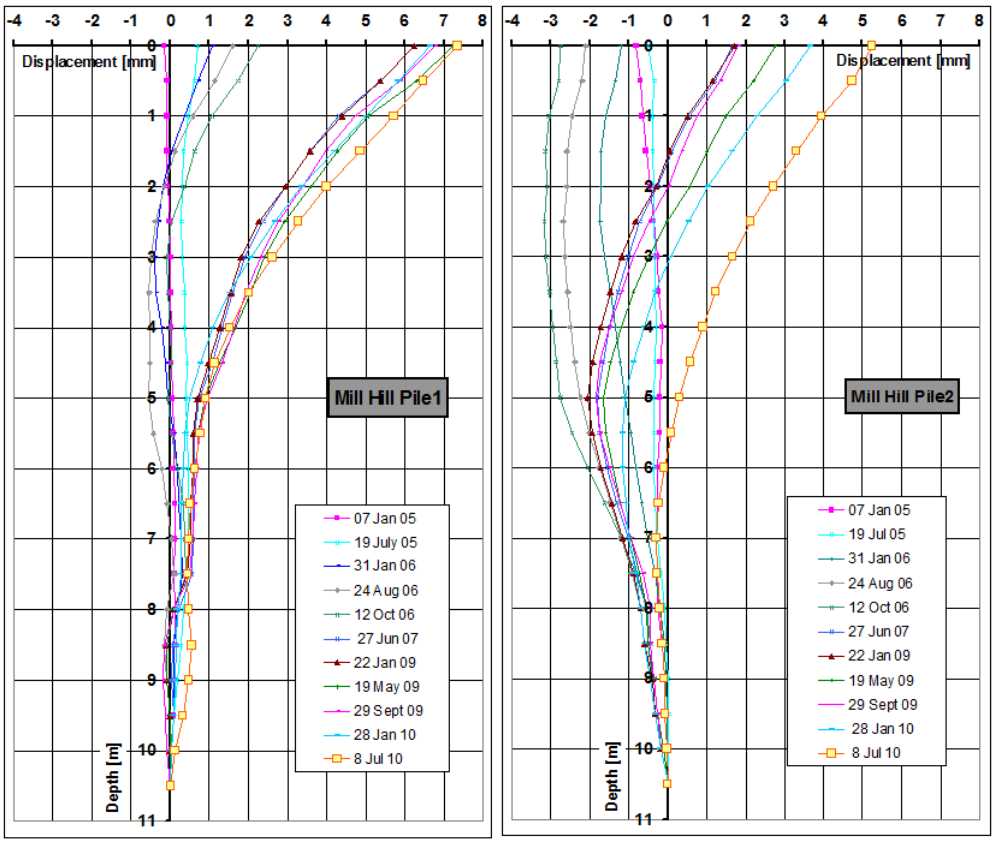

Figure 6.3: *Inclinometer displacement profiles for the instrumented piles at Mill Hill.*

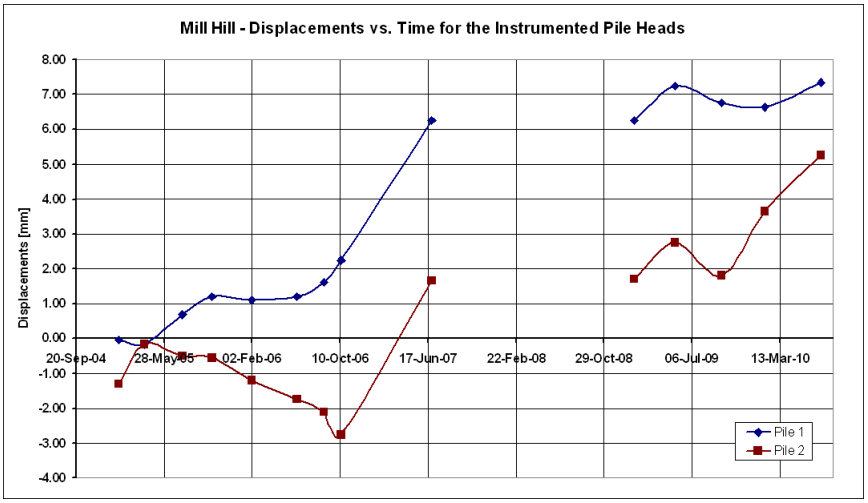

Figure 6.4: *Displacement versus time profiles for the instrumented piles at Mill Hill. The displacements are taken at the top of the piles.*

The displacement profiles for the two instrumented piles are show in figure 6.3. After installation both piles moved up-slope: Pile1 just slightly in the first year, before it then bent down-slope exceeding the initial reading after about two years. Pile2 rotated about 3mm up-slope during the first year after which the pile started to displace back down-slope, although the full displacement profile took more than five years to completely exceed the initial profile. In figure 6.4 the displacements of the pile heads versus time shows seasonal movements in the last two years readings. This behaviour is discussed in section 7.2 with the general behaviour of the slope.

6.1.3 Leatherhead

The two instrumented piles show a very similar displacement behaviour (fig. 6.5) with a constant increase in displacements over time for the full length of the piles. The profiles show that the piles are rotating down-slope. The assumption that the bottom of the pile is fixed (no displacements) makes difficult to locate the position of a potential centre of rotation. Figure 6.6 shows a steady increase in the displacements of the pile heads. The "10 Oct 08" reading for Pile1 (which is the only reading different from the general trend) can be considered as a local temporary movement of the pile.

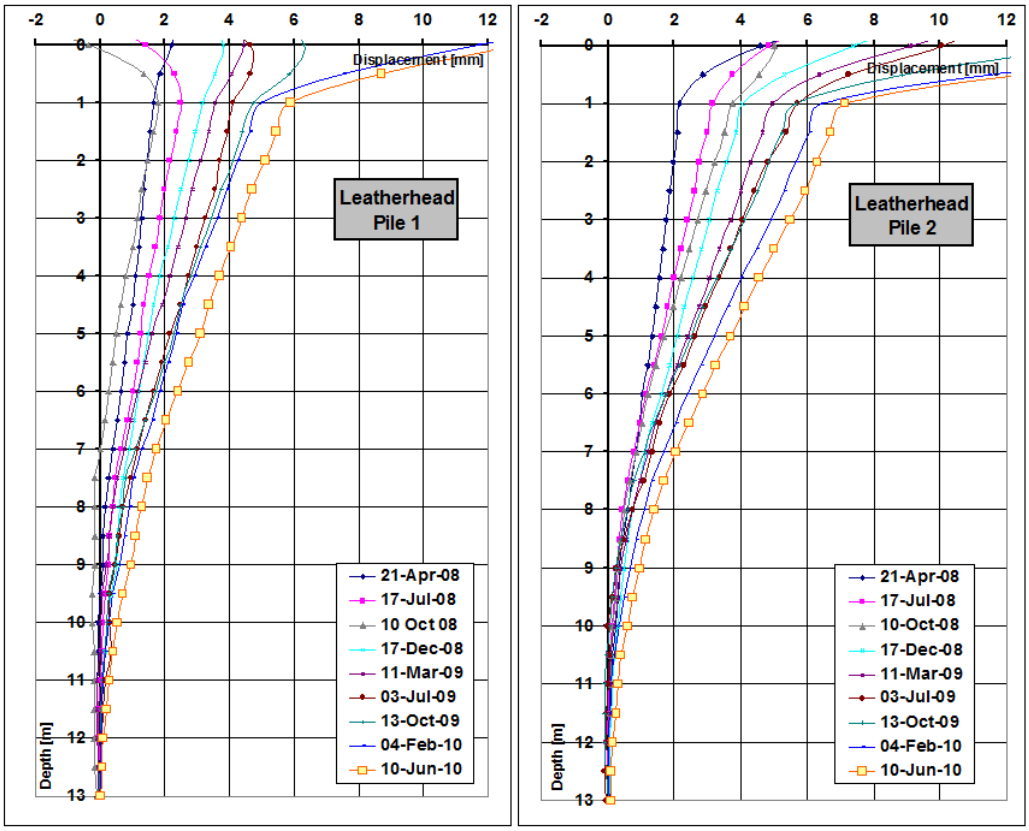

Figure 6.5: *Inclinometer displacement profiles for the instrumented piles at Leatherhead.*

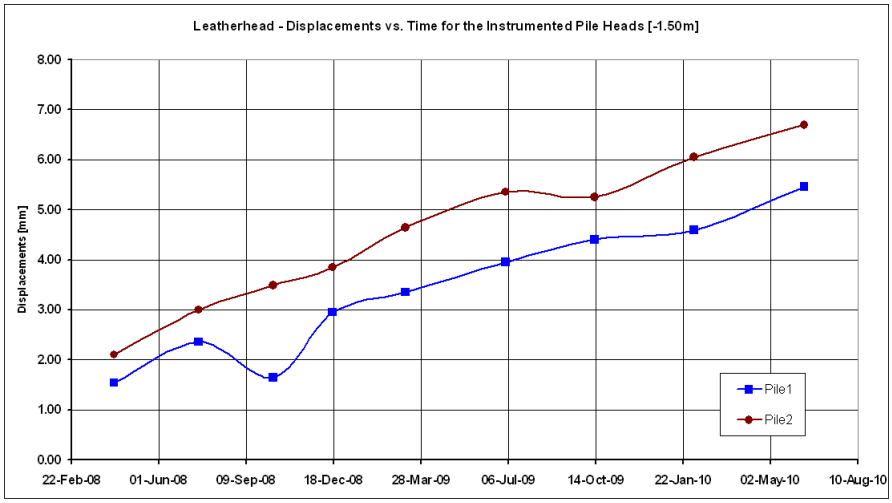

Figure 6.6: *Displacement versus time profiles for the instrumented piles at Leatherhead. The displacements are taken at 1.50m depth from the top of the piles.*

6.1.4 Ironbridge

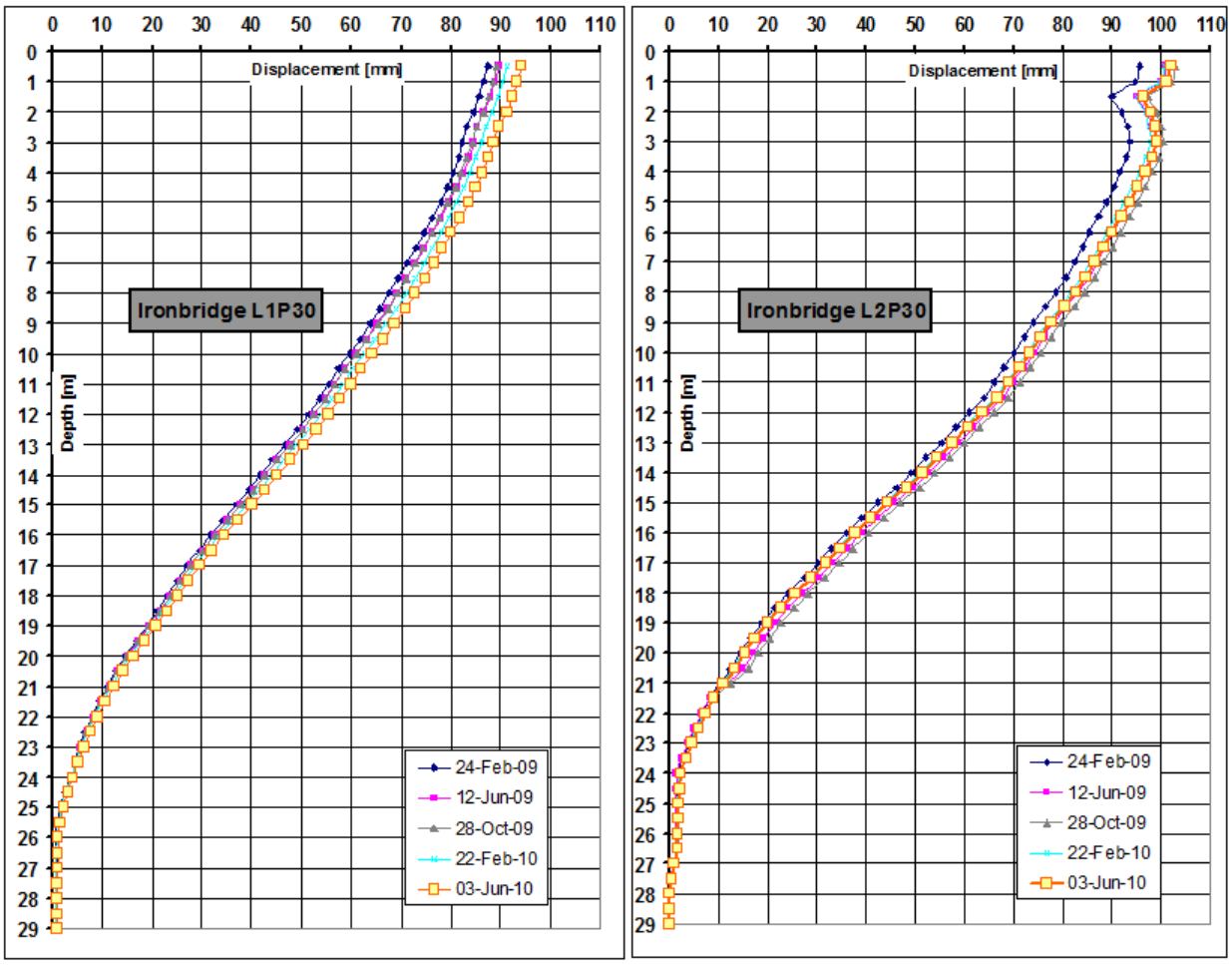

Figure 6.7: *Inclinometer displacement profiles for the instrumented piles at Ironbridge Phase I.*

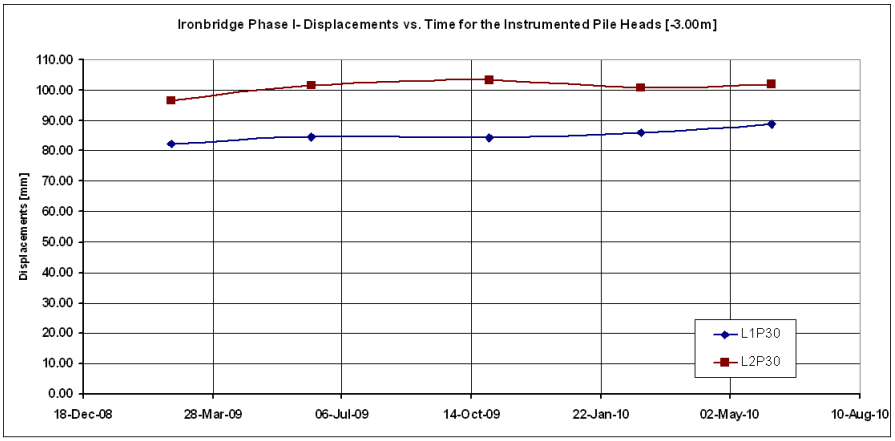

Figure 6.8: *Displacement versus time profiles for the instrumented piles at Ironbridge Phase I. The displacements are taken at 3.00m depth from the top of the piles.*

The displacement profiles (fig. 6.7) show that the two piles have similar bending behaviours. The head displacements are the largest measured in this research, suggesting that the piles are heavily loaded. Figure 6.8 shows that in the last two years, the head displacements (at 3.00m depth from the top of the piles) are almost stable, thus the slope and piles are not moving.

6.2 Curve fitting method

It is possible to calculate the bending moment acting on a a structure, in this case a pile, using inclinometer displacements. Using the engineering beam theory formula (5.1) with the curvature denoted ψ:

$$M = EI\psi \tag{6.1}$$

It is possible to calculate the bending moment from the displacements (described as a curve $w=f(z)$), because:

$$\psi = \frac{\frac{d^2w}{dz^2}}{\left[1 + \left(\frac{dw}{dz}\right)^2\right]^{\frac{3}{2}}} \tag{6.2}$$

where w is displacement and z the curvilinear abscissa along the pile [Ooi and Ramsey (2003)]. Usually $\frac{dw}{dz}$ is very close to 0, and (6.2) becomes:

$$\psi \approx \frac{d^2w}{dz^2} \tag{6.3}$$

It is a common approach when using equation 6.3 to fit a curve or a series of curves (usually called "splines") to the displacements to obtain a known equation of the profile that can then be differentiated. This approach is called "curve fitting". Many methods and many equations can be used to do this; Ooi and Ramsey (2003) studied the problem of choosing the best method. Other authors have developed their own methods [Smethurst (2003), Nip and Ng (2005), de Sousa Coutinho (2006)] which also take into

account other problems such as the variation of the flexural stiffness of concrete in the calculation of bending moment, shear force, and soil pressures.

To apply the curve fitting method, it is usually necessary to develop a spread-sheet or to rely on a dedicated computer program. The fitting curves tends to give an approximate, rather than exact, profile of the curvature. When the equation is differentiated to calculate the bending moment profile (fig. 6.9), numerical errors will increase [Nip and Ng (2005)]. Some authors point out that if further differentiation is carried out from the bending moment equation to evaluate the shear force and the soil pressure, the results may differ from the real performance of the structure [de Sousa Coutinho (2006)]. The same can happen in differentiating the displacement profile to find the bending moment profile.

In general there are two main problems that affect the process:

- the first is connected with the difficulty of approximating a straight line with a curve or a complex profile with a smooth curve. When the approximating curve is integrated or differentiated the result is different from the profile of the real behaviour.

- the second problem is purely mathematical; the integration of a spline gives stable results (if the integration constants are known), while the differentiation can lead to instability (considering it as the set of all numerical problems) or, more usually, to results that differ from the real physical profiles (unreality).

In this research, the curve fitting method suggested by Smethurst (2003) is adopted. This uses a fourth order polynomial function and a variable number of splines to fit the profile of both bending moment and displacements. This model avoids the problems caused by the differentiation (instability and unreality) because it only integrates the splines fitted to the bending moment. Thus to calculate a bending moment profile from the displacements it is necessary to find the best bending moment profile which after integration fits to the inclinometer profile. However, this reduces the precision of the results, but given the high number of other uncertainties (load applied to the pile, soil parameters, concrete parameters, etc...) the method still gives a profile and an acceptable magnitude for bending moment or displacements. The errors connected to the fitting of a series of smooth curves to a measured complex profile remain. Differentiating the spline fitted to the bending moment it is possible to generate shear force and soil pressure profiles.

A rigorous fitting method is not adequate for these purposes. Relying on, for example, the least square fit method does not give acceptable results on the successive steps. It is necessary to smooth the spline. Since the fitted spline is differentiated twice, every small change in its profile will generate large changes in the curve that results from the differentiation. These large changes are usually not reflecting the actual behaviour of the pile (unreality), but they are related to the original spline itself. For having acceptable soil pressure results, it is necessary that the second derivative of the fitted spline is continuous. This problem has a smaller effect on the integrated

results. The fitting spline was smoothed empirically, changing its coefficient case by case to match the results of the second integration with the displacement profile, and to obtain acceptable shear force and soil pressure profiles. These profiles should only be considered as indicative of the general distribution of shear force and soil pressure and not as accurate results. The derivation of the bending moment spline adds errors, but even so, the approximated profiles give useful information about the behaviour of the pile. The base of both the shear force and soil pressure graphs (figs. 6.12, 6.14, 6.16 and 6.19) always show values that are non-zero. In theory, the shear force should be zero at the base of the pile. This is a problem of this curve fitting technique. The top part of the shear force profile is considered reliable.

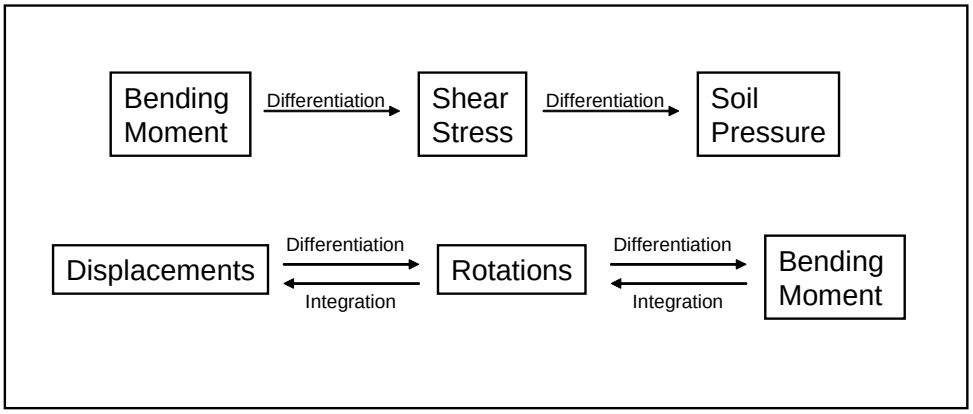

Figure 6.9: *Mathematical operations in the curve fitting model*

6.2.1 Discussion about the stiffness used in the curve fitting method

The curve fitting method used in this research is ultimately based on the engineers beam formula (equation 5.1). One of the problems affecting the use of equation 5.1 is the value of E_cI used in the calculation as introduced in section 5.1.1. The bending moment calculation method (par. 5.2) is used to solve this inconsistency. Equation 5.1 can be rearranged as:

$$E_cI = \frac{My}{(\varepsilon_1 - \varepsilon_2)} \tag{6.4}$$

The value of the bending moment M used in equation 6.4 is that from the application of the bending moment calculation method (par. 5.2). This ensures that that the two methods (that for the calculation of the bending moment from the strain data and that used for the curve fitting) use the same mechanical properties and assumptions about cracking for the concrete.

Equation 6.4 then does not give a unique value of E_cI for the whole pile, but a value for each instrumented section of the pile and each strain reading. The average of the E_cI values for the full pile on the date of the inclinometer reading is used. In the curve fitting if the pile is divided into differently reinforced lengths with different flexural stiffness (e.g. Grange Hill), the average of E_cI in each length of the pile is used.

This approach is used for the piles analysed with MCM (Grange Hill, Mill Hill and Leatherhead) since the neutral axis are usually in the centre of the sections. When ACM (Ironbridge) is used, the flexural stiffness (E_cI) of the pile sections is automatically calculated by the program taking into account the neutral axis movements and the cracking effects. The section is divided in slices and the second moment of area is calculated for each slice of each material (not considering cracked slices). The total second moment of area of the section is then calculated considering the different materials as:

$$I = \sum (I_g \times n_g) + (I_s \times n_s) + I_c \tag{6.5}$$

$$n_g = \frac{E_g}{E_c}; \quad n_s = \frac{E_s}{E_c} \tag{6.6}$$

Where:

I = total second moment of area.

I_g = second moment of area of a grout slice.

I_s = second moment of area of a steel slice.

I_c = second moment of area of a concrete slice.

E_g= Young's modulus of grout.

E_s= Young's modulus of steel.

E_c= Young's modulus of concrete.

6.2.2 Setting of the curve fitting datums

Care has to be taken when comparing the results from different instruments, to ensure that the datum used is the same. If each datum is taken at the same time a comparison is possible, while if they are set at different times, an error will be introduced. For example, this can easily occur with inclinometers and strain gauges when the datalogger starts recording strain just after the pile installation, but the inclinometer datum is taken later (mainly because of site works around the top of the pile). In this case the inclinometer displacements recorded are related to a partial change in the bending moment in the pile, and on adjustment of the strain gauge bending moment is necessary in order to compare both instruments over the same period.

This adjustment was necessary for Leatherhead since the first set of inclinometer readings (forming the inclinometer datum) were carried out nearly three months after the installation of the piles. At this point the strain gauge readings showed that the piles had already developed a significant bending moment and thus some displacements had already taken place. To apply the curve fitting model it was necessary to set a new datum for the bending moments (the same day as the inclinometer datum).

6.3 Comparison between bending moment and displacements results

This section analyses the application of the curve fitting method for the comparison between bending moment and displacement profiles. Four piles from the four instrumented sites are taken as examples.

6.3.1 Grange Hill Pile1

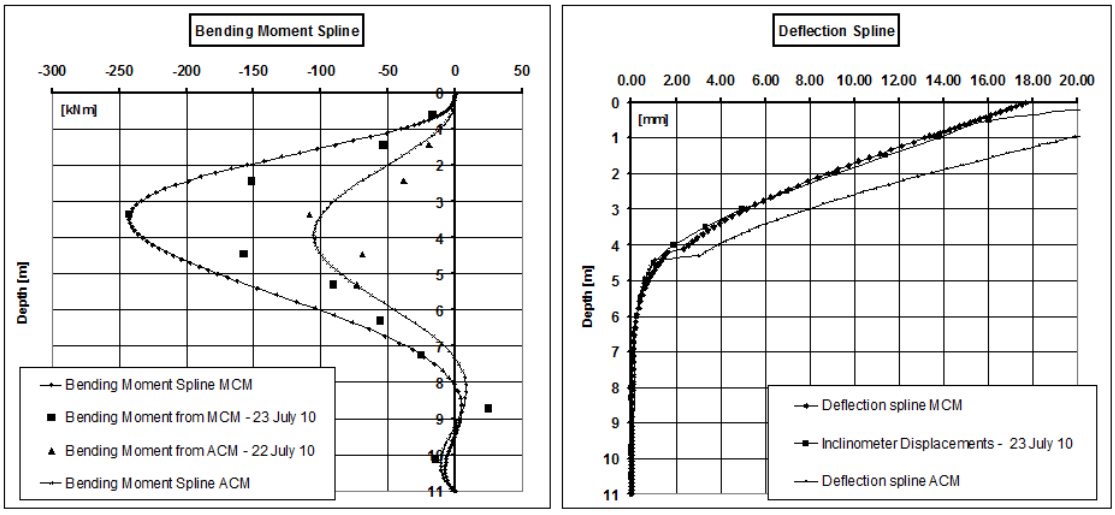

Figure 6.10: *Grange Hill Pile1, bending moment and displacement comparison using the curve fitting method.*

Figure 6.10 shows the comparison using the curve fitting method between the bending moment results (using the MCM and ACM methods) and the inclinometer displacement profile. The splines used for the bending moment approximates the measured points, but when integrated twice they do not quite match the inclinometer displacement profile. A reduction of 10% of the flexural stiffness of the pile in the top 6m with the MCM method allows the displacement spline to fit the measured profile (fig. 6.11). The MCM bending moment profile has been corrected for cracking on section 4-14 (3.45m depth), but more cracks are probably present in the pile, not clearly detected by the other strain gauges. This means that the actual stiffness of the pile is smaller than the one assumed in the calculation using one cracked section only. This is in line with the conclusions of chapter 5 (par. 5.4) which pointed out that the real bending moment profile lies between that calculated with the MCM method and that calculated using ACM (which has a smaller flexural stiffness due to more cracking). Figure 6.10 shows a jump in the displacement profile calculated with ACM. This is due to cracking in the section, the stiffness of the pile decreases, thus the displacement increases.

It is not possible to compare these results with Pile2 since many strain gauges are not reading at present and it is not possible to produce a reasonable bending moment profile.

The displacement splines in figures 6.10 and 6.11 show small jumps where the stiffness of the pile changes due to changes in reinforcement.

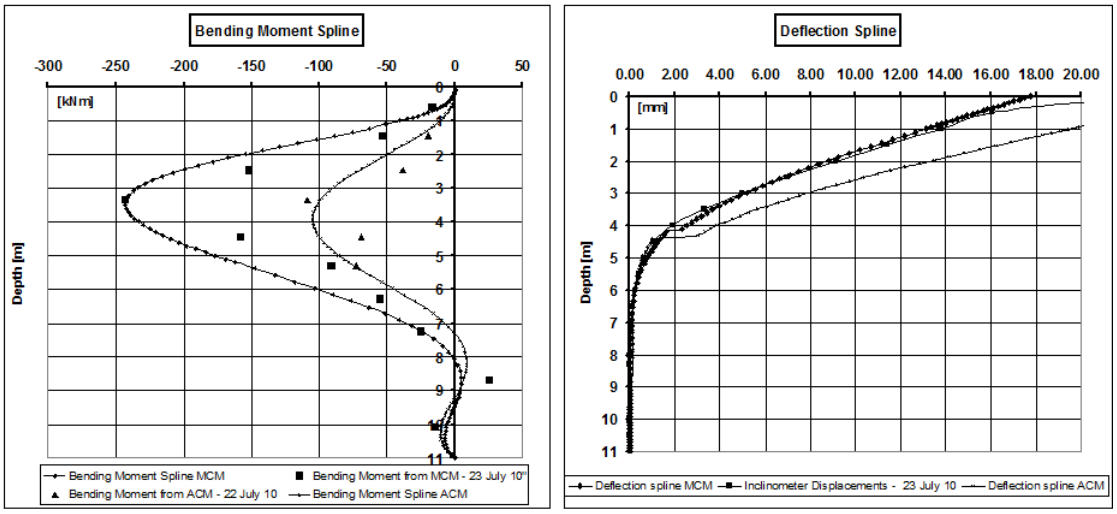

Figure 6.11: *Grange Hill Pile1, bending moment and displacement comparison using the curve fitting method and a 10% reduction of the stiffness of the pile in the MCM.*

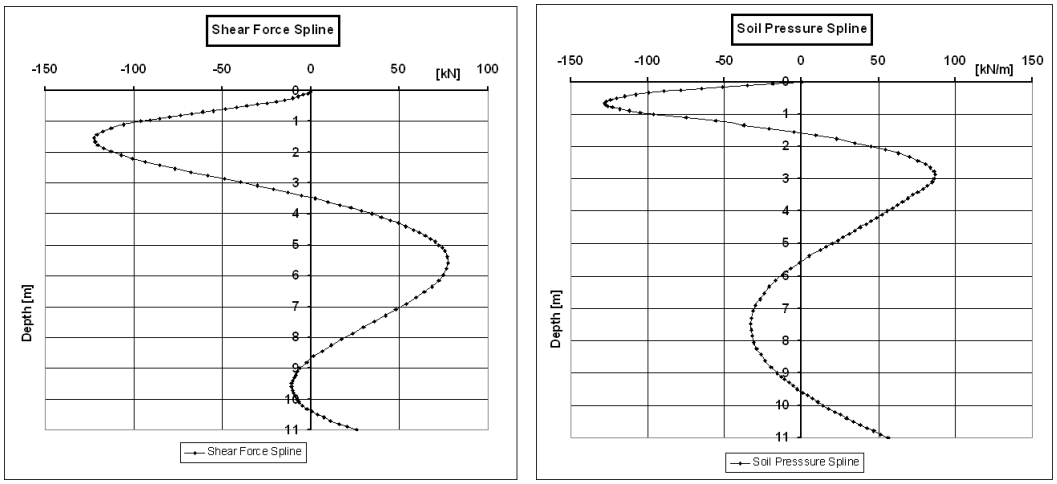

Figure 6.12: *Grange Hill Pile1, shear force and soil pressure profiles calculated using the curve fitting method and a 10% reduction of the stiffness of the pile in the MCM.*

6.3.2 Mill Hill Pile1

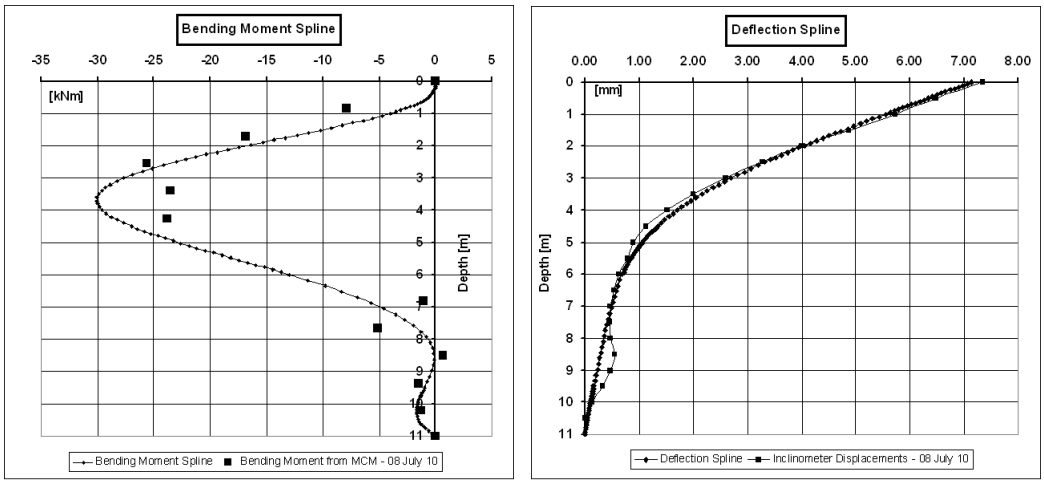

Figure 6.13: *Mill Hill Pile1, bending moment and displacement comparison using the curve fitting method.*

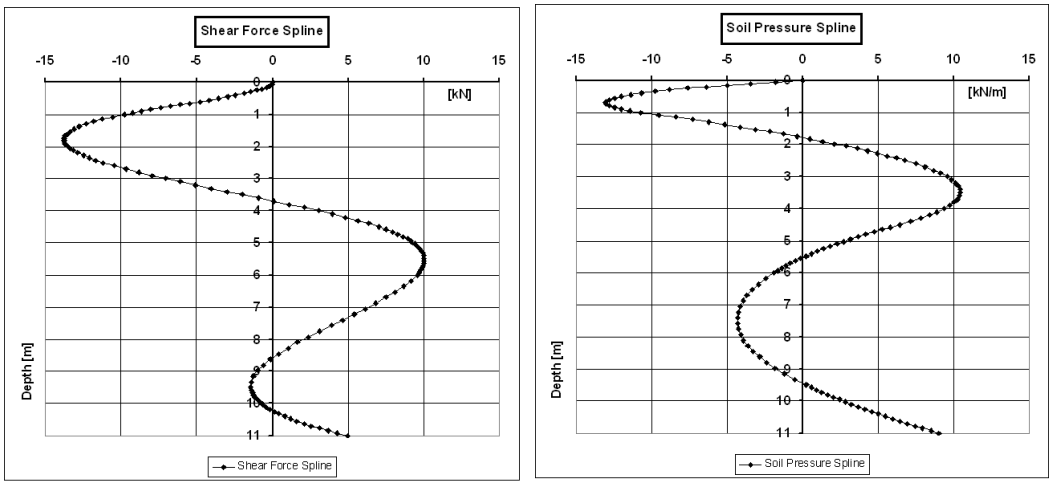

Figure 6.14: *Mill Hill Pile1, shear force and soil pressure profiles calculated using the curve fitting method.*

For Mill Hill, the fitting of the spline to the bending moment profile is not very accurate (fig. 6.13), due to the irregularities in the measured profile, but the spline calculated displacements are a close mach to those measured. The results in the bottom three meters are approximated due to the difficulties of fitting the spline to the measured bending moment profile. The average stiffness of the pile was determined from MCM results, assuming no cracking. The close match between bending moment and displacement suggest that there has been little or no cracking in the pile. The pile has rigidly rotated around its base, as evidenced by the need to impose a rotation on the base of the displacement fit.

6.3.3 Leatherhead Pile2

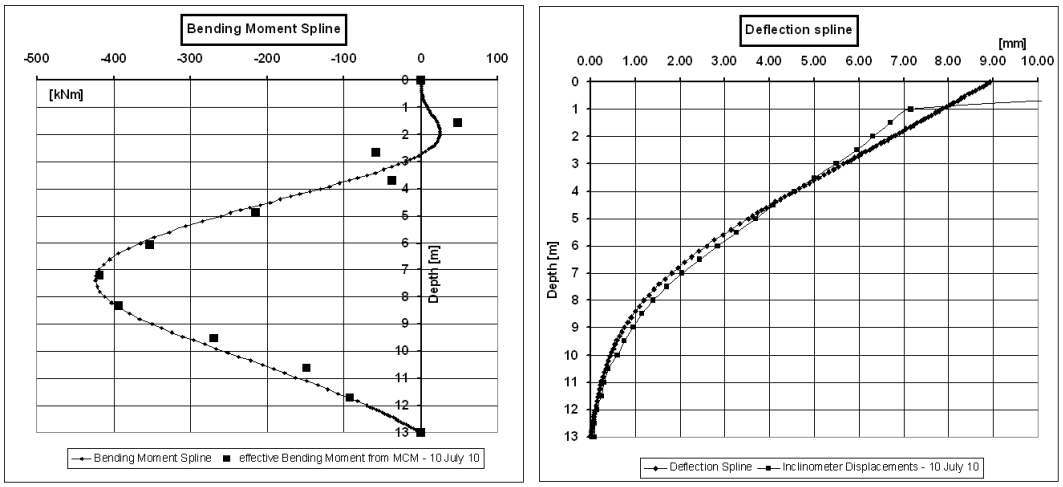

Figure 6.15: *Leatherhead Pile2, bending moment and displacement comparison using the curve fitting method. To allow the comparison, the bending moment profile has been modified to take into account the difference in the original datums for bending moment and displacements.*

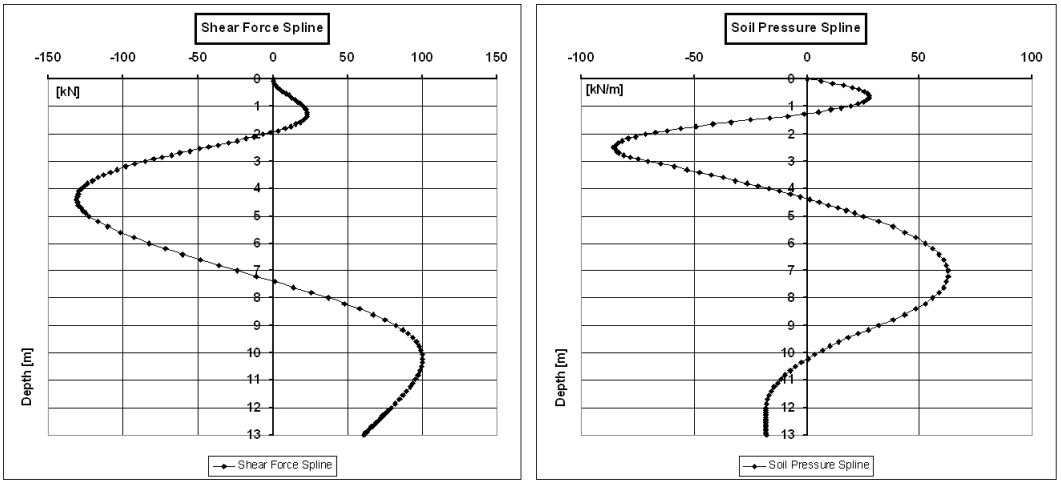

Figure 6.16: *Leatherhead Pile2, shear force and soil pressure profiles calculated using the curve fitting method.*

Figure 6.15 presents the comparison using the curve fitting method between the bending moment results (calculated using the MCM method) and the inclinometer displacement profile. The bending moment profile has been modified to take into account the difference in time of the two original datums (as introduced in par. 6.2.2). It was difficult to fit the general spline to the close changes in curvature of the bending moment profile on the top 3m of the pile. The comparison uses the average stiffness of the pile determined from the MCM results without any modification. This would indicate that cracking is not developing in the pile, in line with the assumption in MCM results.

To perform the fitting of the displacements, it is necessary to rigidly rotate the profile (i.e. the whole pile is rotating rigidly as introduced in section 6.1.3).

6.3.4 Ironbridge L2P30

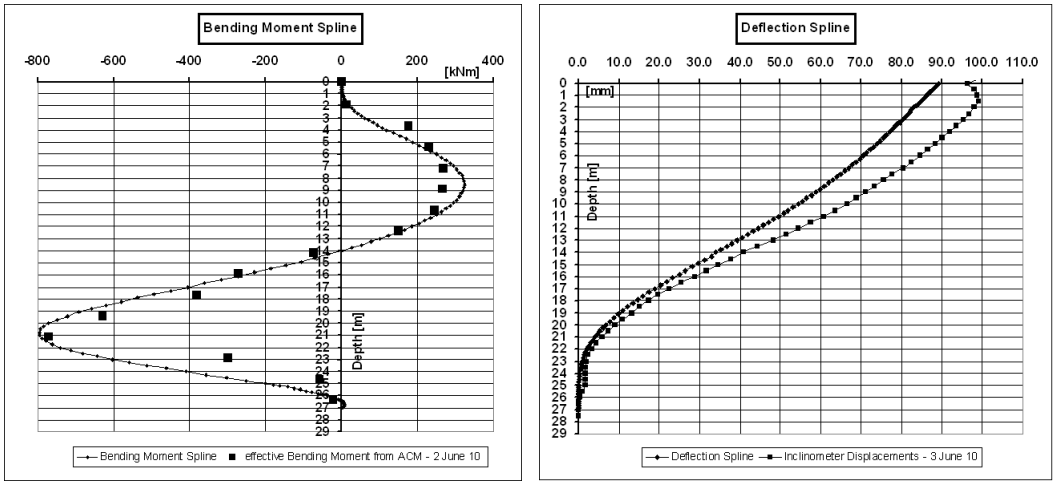

Figure 6.17: *Ironbridge L2P30, bending moment and displacement comparison using the curve fitting method. To allow the comparison, the bending moment profile has been modified to take into account the different datums for bending moment and displacements.*

Figure 6.17 shows the the spline fit to the bending moment profile calculated with ACM and the displacement profile coming from the inclinometer readings. The bending moment profile has been modified to take into account the difference in time of the two initial datums. The calculated deflection spline does not fit with the measured displacements. Reducing the value of the flexural stiffness (E_cI) of 15% leads to a much more accurate curve fit (fig. 6.18). This error in the evaluation of the flexural stiffness is probably due to the approximated material parameters and the calculation assumptions used in the ACM. For example, if the concrete tensile strength used in the model is incorrect, this affects the opening of the cracks, which in turn modifies the second moment of area of the section.

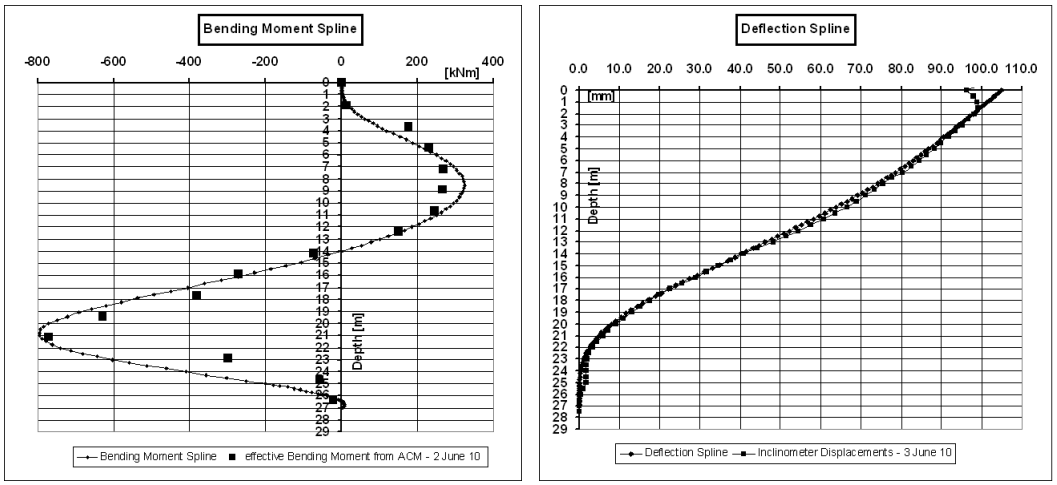

Figure 6.18: *Ironbridge L2P30, bending moment and displacement comparison using the curve fitting method and a 15% reduction of the stiffness of the pile.*

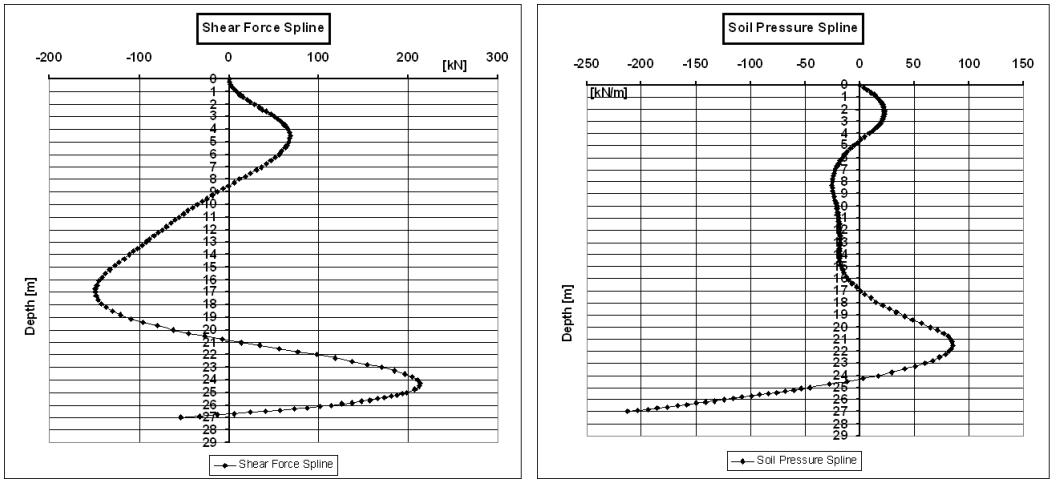

Figure 6.19: *Ironbridge L2P30, shear force and soil pressure profiles calculated using the curve fitting method and a 15% reduction of the stiffness of the pile.*

6.4 Comparison between bending moment and displacements results: conclusions

The readings from the main instrumented piles of the four sites show a generally very good consistency between strain gauge and inclinometer. The variation of flexural stiffness due to cracking can greatly change the results and thus it has to be determined accurately. The flexural stiffness calculated with the MCM and ACM methods had to be reduced by 10% for Grange Hill Pile1 and 15% for Ironbridge L2P30, to achieve a curve fit between bending moments calculated with strain gauges and inclinometers. Thus, it is always necessary to instrument a pile with both strain gauges and inclinometers. The curve fitting allows to check the assumptions about cracking used for the calculation of the bending moment and allows to understand if the real bending moment profile lies close to the results of the MCM or ACM model. This shows that the results of MCM are correct for Leatherhead and Mill Hill, while they are overestimating the bending moment applied to Grange Hill (the stiffness of the pile is smaller than the one estimated, thus the applied bending moment is smaller). For Ironbridge PhaseI piles, ACM results are overestimating the applied bending moment. The overestimating results are due to the approximated concrete parameters and cracking assumptions used in the models.

Chapter 7

Geotechnical interpretation

This chapter analyses the slope and pile behaviour for the instrumented sites using the information collected with the instrumentation and the analysis procedures introduced in the previous chapters. Each instrumented site is analysed independently to describe the particular pile bending behaviours, the processes acting on the piles, and the behaviour of the slope.

The bending moment, displacement, shear force and soil pressure profiles (the latter two from the curve fitting analysis) are compared with the theoretical analysis carried out by Poulos (1999). The author analysed the pile/soil behaviour of discrete piles in three idealised cases that are termed flow mode, intermediate mode and short pile mode (fig. 7.1). The "flow mode" develops when the slip surface is shallow and the unstable soil becomes plastic and flows around the top of the pile [Poulos (1999)]. The "intermediate mode" occurs when the soil strength in both the unstable and stable soil is fully mobilised; the slip plane passes through the central part of the pile and the pile head movement exceeds the unstable soil movements [Poulos (1999)]. The "short pile mode" implies that the slip plane is deep and the length of the pile in the stable soil is relatively short; the unstable soil carries the pile and drags it through the stable soil layer fully mobilising the soil strength of the stable layer [Poulos (1999)]. These modes are based on the limit equilibrium mechanisms given by Viggiani (1981), with the difference that the latter considers the pile/soil behaviour at the ultimate state, while Poulos (1999) considers also the behaviour in service. Poulos (1999) elastic analysis can also calculate the displaced shape of the pile and the bending moment and shear force profiles, which are not determined by the Viggiani (1981) limit equilibrium solutions.

One of the differences between some of the instrumented piles and the theoretical analysis is the existence of a clear slip plane. Piles were installed in two of the sites (Grange Hill and Mill Hill) to increase the factor of safety of the slope and limit soil movements to prevent the development of a clear slip plane. The pile design assumed a slip plane determined from slope stability analysis, while soil movements have occurred at the sites, clear slip surface has not developed, and the installation of the piles may mean that it forms differently to that assumed in design. At the other two sites (Leatherhead and Ironbridge), a clear slip plane was developed before the installation of the piles, as assumed in the theoretical analysis.

Poulos (1999) also considers the slip surface depth (z_s) required to alter the behaviour of the pile. Using the ratio z_s/L (where L is the length of the pile) the author identifies the behaviour of the piles as: $z_s/L \backsimeq 0.2$ flow mode; $z_s/L \backsimeq 0.6$ intermediate mode; $z_s/L \backsimeq 0.9$ short pile mode.

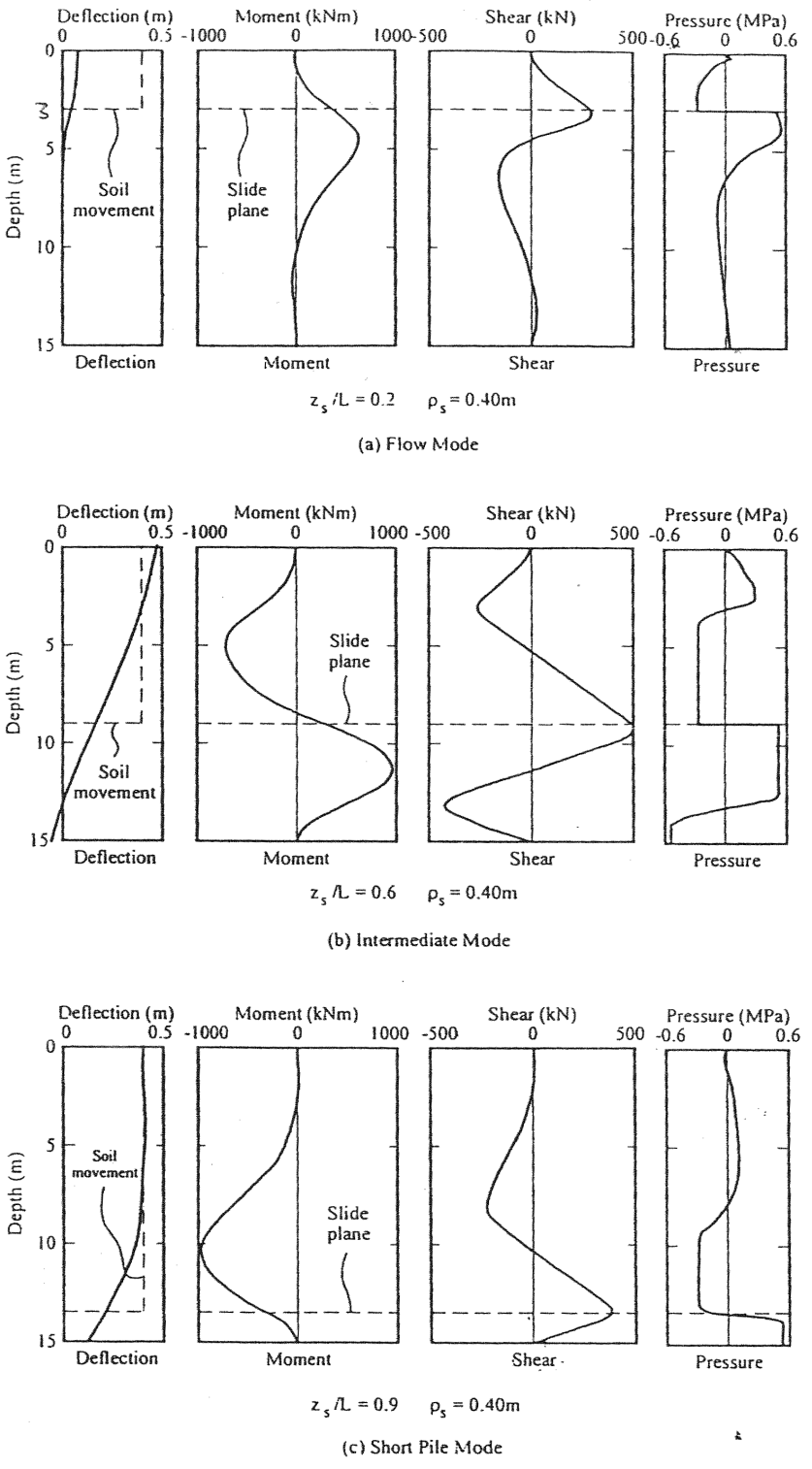

Figure 7.1: *Pile behaviour modes for different depths of soil increment from Poulos (1999). The conventions for bending moment and shear force are opposite to those used in this research.*

7.1 Grange Hill

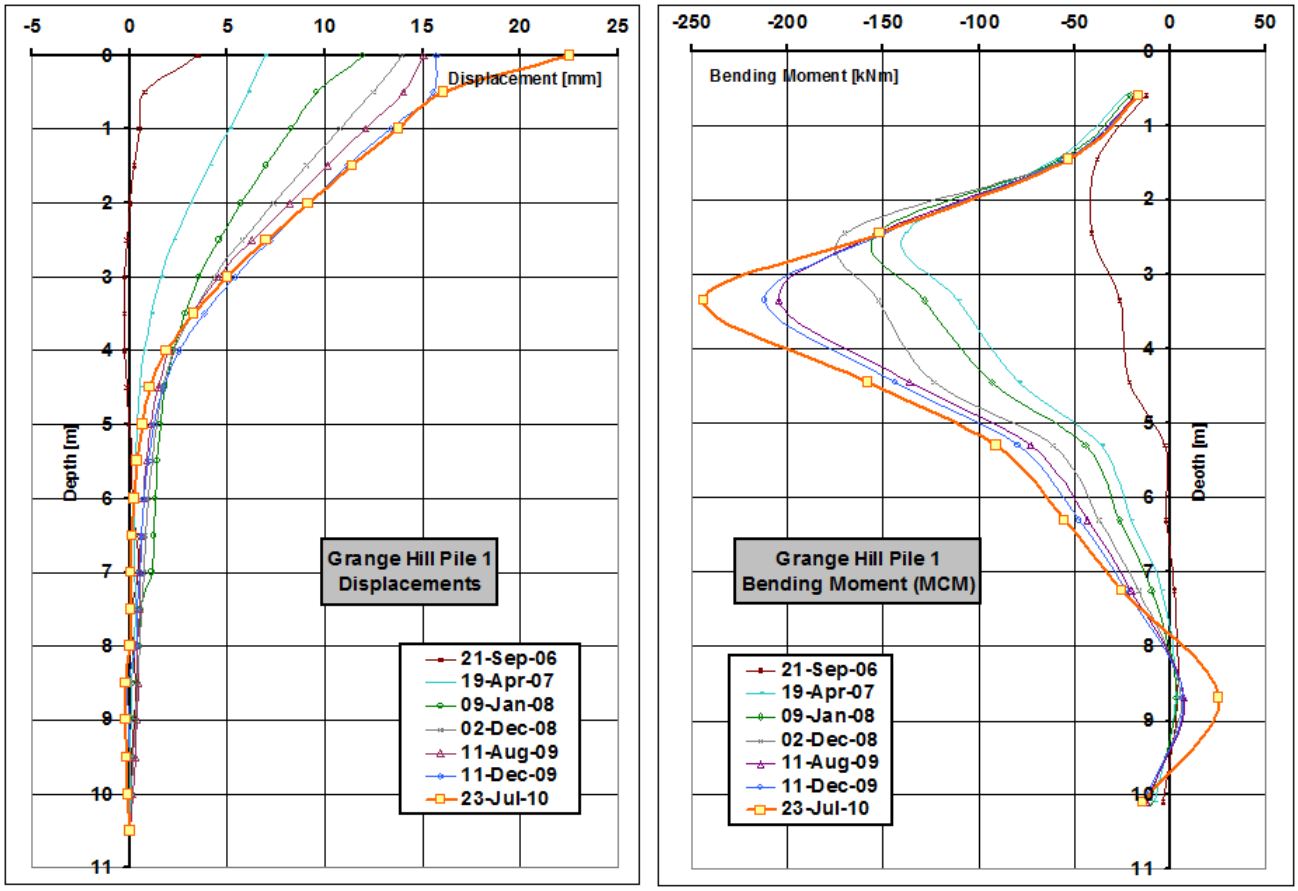

Figure 7.2: *Grange Hill Pile1, displacements and bending moments (calculated with MCM) for the whole monitoring period*

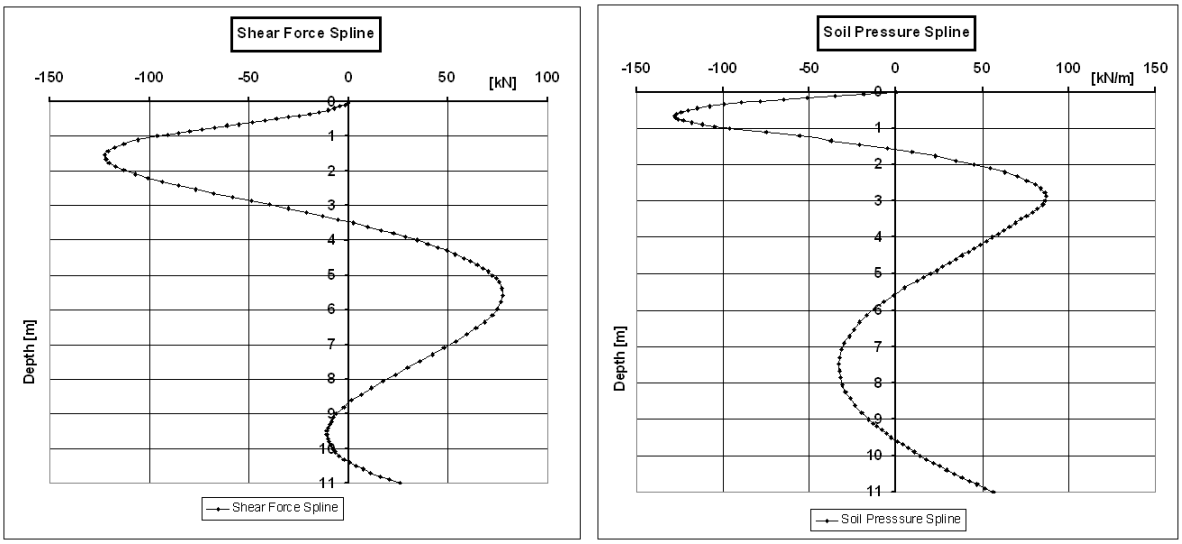

Figure 7.3: *Grange Hill Pile1, shear force and soil pressure profiles calculated using the curve fitting method for the 23 July 2010 results and a 10% reduction of the stiffness of the pile.*

The particular concrete mix and steel reinforcements (par. 3.1.1) are the most influential factors affecting the readings from the Grange Hill piles. The concrete mix is responsible for the "temperature effects" discussed and corrected in section 4.4.4.1, while both concrete mix and reinforcement bars are related to the development of cracks in the piles (par. 5.3.1).

Pile1 is used as the main pile in the analysis since many strain gauges in Pile2 are not reading at present. Figure 7.2 shows the development of the displacements and bending moments in the pile over time. Inclinometer and strain gauge results are consistent and show that the pile is loaded by the movement of the top soil layers. The strain gauges at 3.35m depth detected the development of cracks (in February 2009 for Pile1 and in March 2007 for Pile2). This is also reflected by the shape of the bending moment profiles which change after cracking.

Displacement, bending moment, shear force and soil pressure profiles (fig. 7.3) are a close match with the Poulos (1999) profiles for the flow mode (fig. 7.1). Theoretically a slip surface should be around 2m depth, where the shear force has a peak and the soil pressure changes sign. In this case $z_s/L = 0.18$, very close to the theoretical value of 0.20 suggested for development of the flow mode.

As introduced in section 3.1, the Grange Hill piles were installed as preventative remedial works since the factor of safety of the slope was lower than expected. No slip planes were detected before the pile installation. Stability analysis of the slope found the slip plane with the lowest factor of safety to be positioned around 6m depth on the pile line [Brown and Root Consulting report for Infraco BCV Limited (2002)], and this was used in the design of the piles. This is also the basis of the different reinforcements along the pile; the bending moment peak was expected in the central part of the pile, so less reinforcements were put in the top and the bottom sections. In reality no slip planes developed after the installation of the piles, which are instead loaded by superficial movements where the reinforcements are smaller, increasing the cracking of concrete. Durrani (2006) shows a similar behaviour in his numerical analysis of slope stability with and without discrete piles. If pile installations occurs before the slip plane is developed, piles can radically change the behaviour of the slope, preventing the formation of deep seated slip surfaces and only allowing the possibility of superficial movements of the top layers. In this case, the design of the piles has to be based on an accurate slope stability analysis considering both the unreinforced slope and the slope stabilised with the piles. In any case, it is better to use uniform reinforcements along the full length of the pile to account for behaviours different to that assumed in design.

The movement of soil between the piles was analysed using the inclinometers installed in the slope and in the other piles (fig. 7.4). Three inclinometers (B5, B6 and C2) were installed mid-way between adjacent piles for this purpose. B5 and B6 are 16m long, compared to 11m long inclinometers in the piles. The displacement datum for all tubes was fixed to zero at the base of the piles (11m depth). The same was done for Pile3 and C2, but the datum depth was 9m in this case. Figure 7.5 shows the comparison between the displacements of the piles and the soil in between them.

Pile1, Pile2 and B5 show similar displacements for the piles and the soil, with no clear movement of soil between the piles. Pile2, BP4 and B6 show different pile and soil displacements with a substantial movement of the soil in between the piles. Pile3 and C2 displacements show the largest soil movement, with the surface displacement of C2 twice the displacement measured on Pile3.

These results show that Grange Hill piles are behaving like the theoretical "flow mode" predicted by Poulos (1999). The displacements and the behaviour of the soil along the pile row is not uniform.

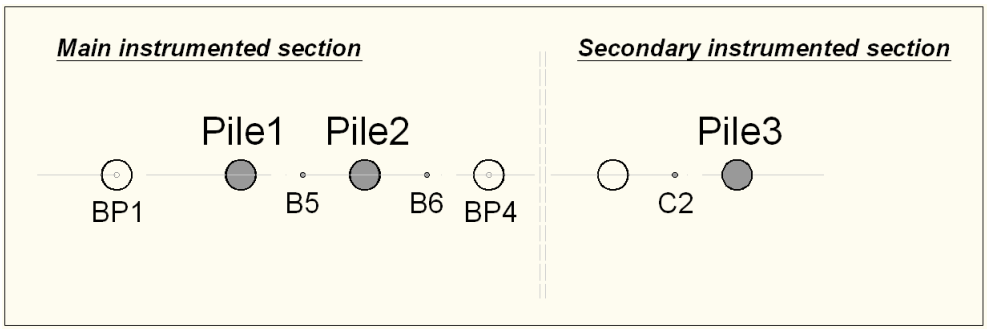

Figure 7.4: *Grange Hill, plan of the inclinometers*

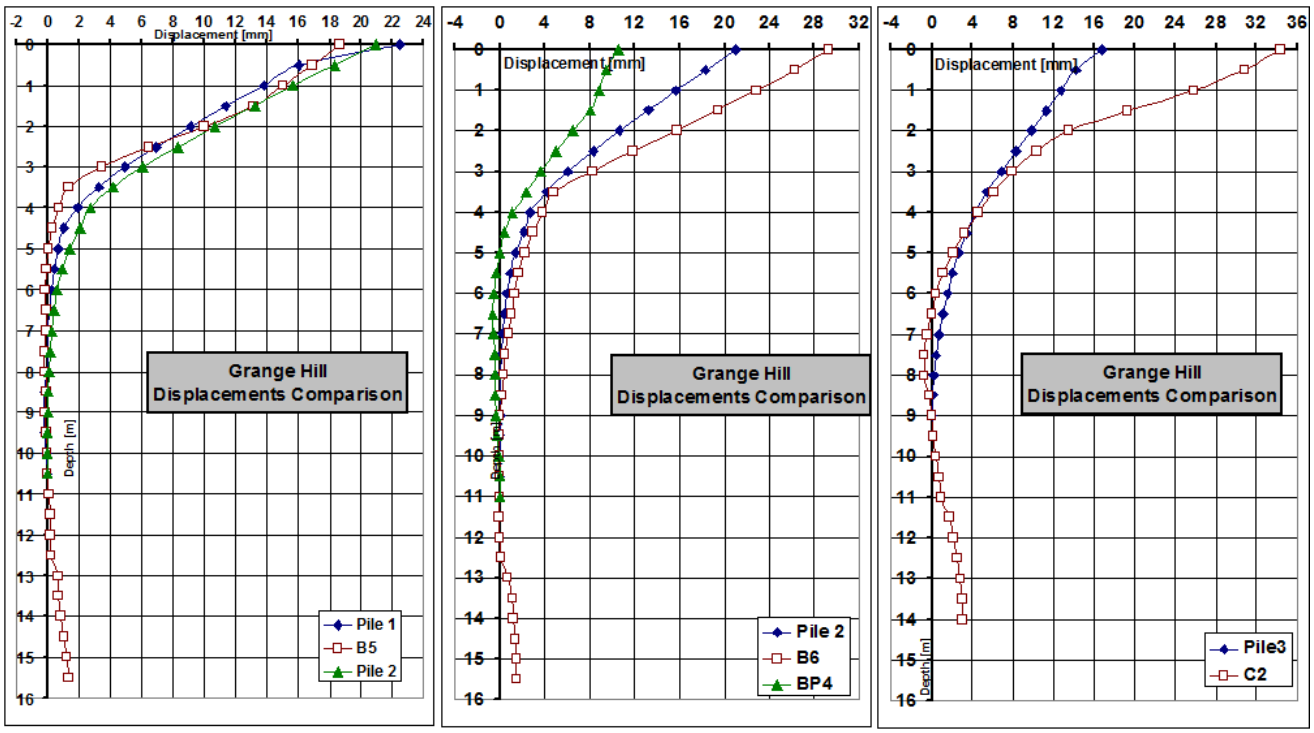

Figure 7.5: *Grange Hill, comparison between pile displacements and soil displacements in between the piles.*

7.2 Mill Hill

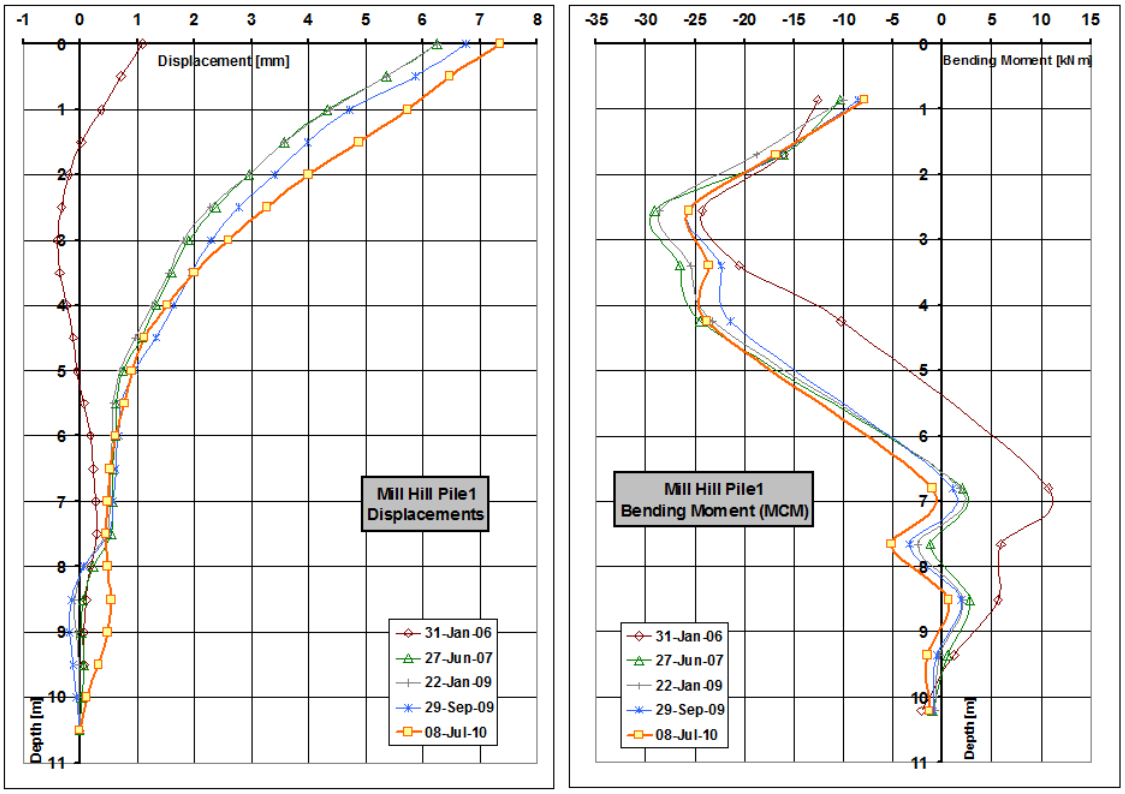

Figure 7.6: *Mill Hill Pile1, displacements and bending moments (calculated with MCM) for the full monitoring period*

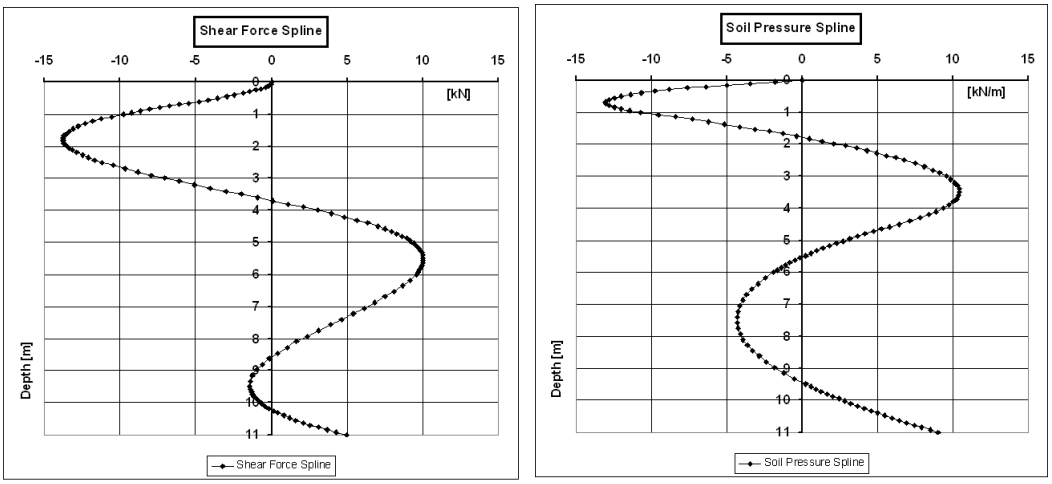

Figure 7.7: *Mill Hill Pile1, shear force and soil pressure profiles calculated using the curve fitting method for the 8 July 2010.*

The analysis of Mill Hill bending moment and displacement profiles (Pile1 is taken as example in figure 7.6) shows that the piles are lightly loaded and subjected to smaller displacements in comparison with Grange Hill. Figure 7.6 also shows that the displacements are increasing with time while the bending moment peaks oscillate between 24 and 30 kNm instead of increasing. This can be explained with a rigid rotation of the

whole pile/soil system, supported by the fact that the displacement profiles also show some movements at the base of the pile. Figure 7.8 and 7.9 show seasonal changes in the top instrumented sections of the pile. These can be related to the effects of the vegetation, the precipitation or both; the annual pattern is repeated for nearly four years. The hypothesis is that the pile is cyclically loaded and unloaded (seasonal changes in strains and bending moment) while the piles rotates. Figure 6.4 shows that the pile head displacements have seasonal variations. It is possible to analyse these behaviours because the piles are lightly loaded, so instead of the load effects, the movements of the soil due to the vegetation or the precipitations are recorded by the instrumented piles. Considering the piles to be uncracked (par. 6.3.2), the axial strain profiles can be considered reliable. The profiles from the top sections (fig. 7.10) show peaks in tension at the end of winter and troughs (less axial tensile strain) at the end of summer. Considering that the piles are lightly loaded, that the slope is covered by thick vegetation and that the temperature is not affecting the instrumentation (par. 4.4.4.2), this behaviour can be related to that described by Crilly and Driscoll (2000). During the winter the clay soil swells since the precipitation is greater than the evapotranspiration, while during the summer it shrinks because the precipitation is smaller than the evapotranspiration. Piezometer data could be used to support this explanation. The pore water pressure profile would show peaks when the clay swells and troughs when it shrinks (negative pressure due to soil suction). This research focused on the behaviour of the piles only, thus the piezometer data have not been analysed.

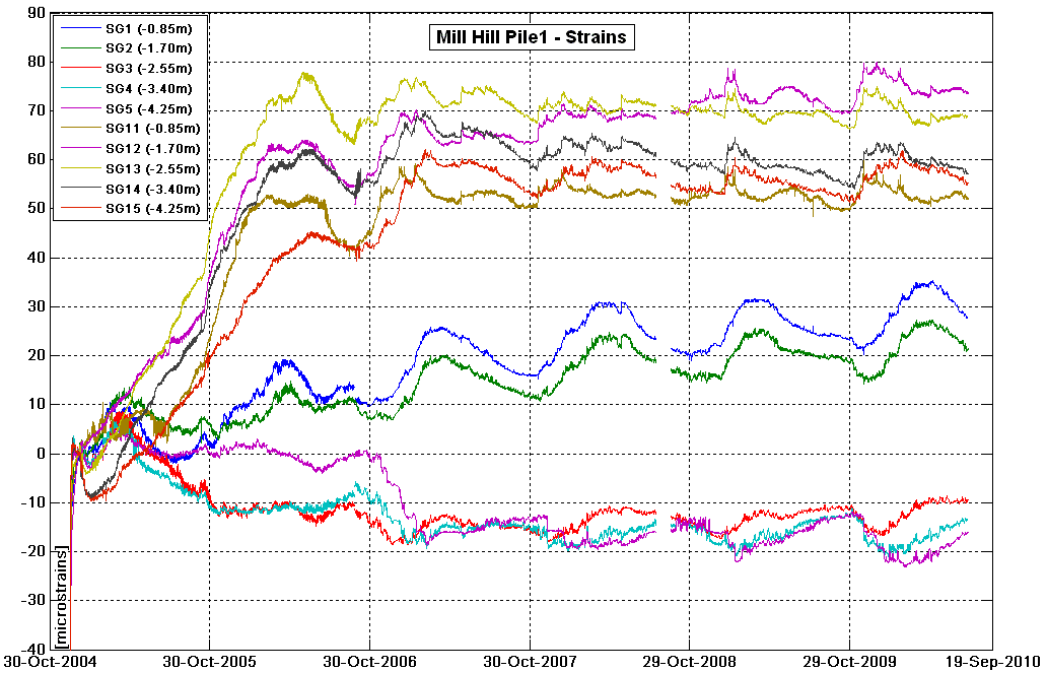

Figure 7.8: *Mill Hill Pile1, measured strains for the instruments in the top half of the pile.*

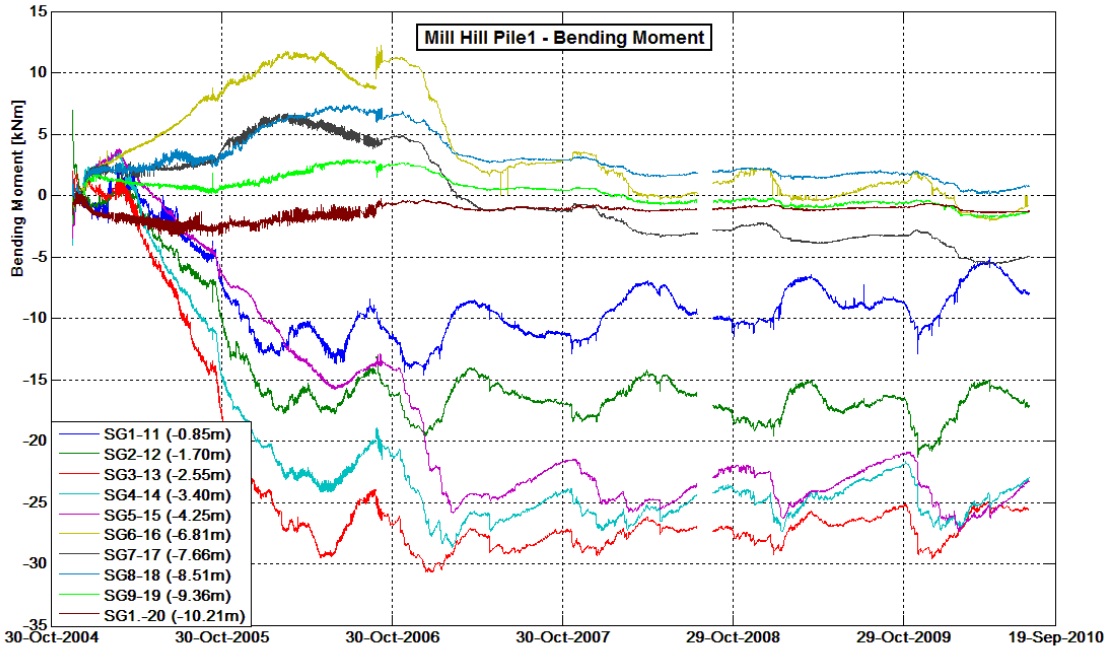

Figure 7.9: *Mill Hill Pile1, bending moment (MCM) versus time.*

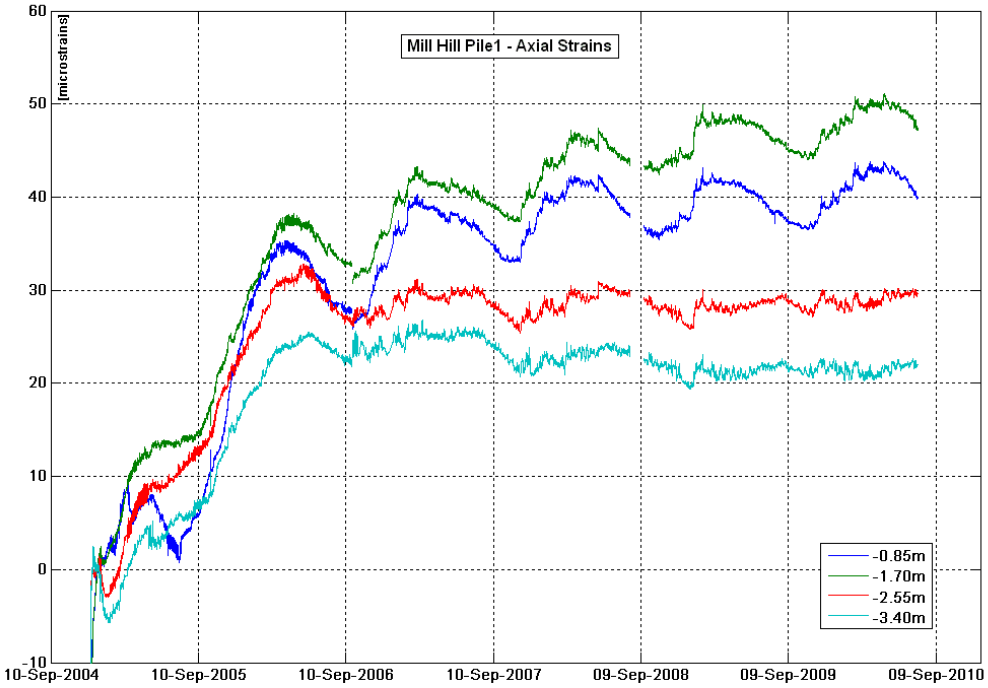

Figure 7.10: *Axial strain for the top four sections of Mill Hill Pile1. The profiles show seasonal variations related to the effects of vegetation and precipitation.*

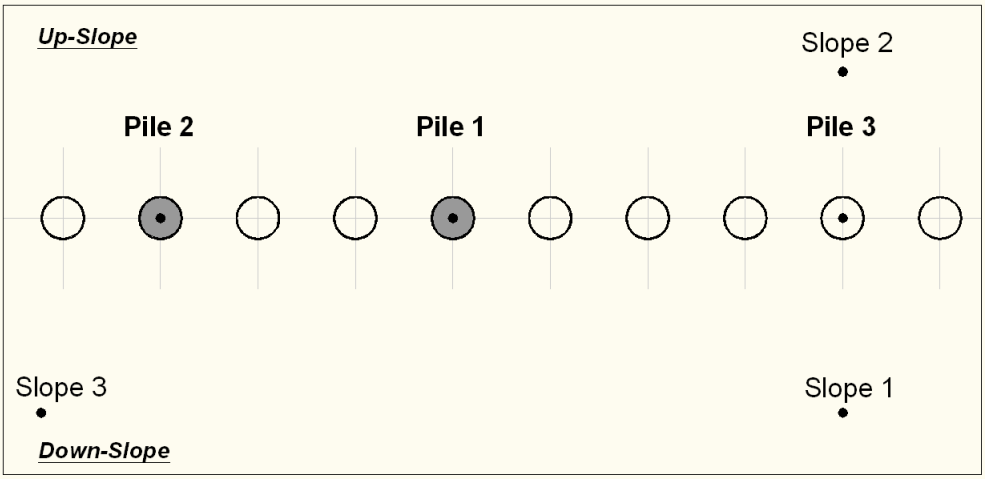

Figure 7.11: *Mill Hill, plan of the inclinometers.*

The profiles for the pile (fig. 7.6 and 7.7) identify the behaviour as a flow mode (fig. 7.1). The hypothetical slip surface based on Poulos (1999) assumptions (i.e. the slip plane is approximately at the same depth of the shear force peak) can be assumed around 2.00m depth (no slip plane develops in reality), giving $z_s/L = 0.18$. No inclinometers were installed between the piles as the distances between them are very small (0.7m or 1.5 diameters between the centres, thus 0.25m between the edges of the piles). Instead, three inclinometers (Slope1, Slope2 and Pile3) were installed in line to check the relative movements between the slope and the piles (fig. 7.11). The measured displacements are shown in Figure 7.12, where the base of Pile3 is taken as the zero displacement datum for both pile and soil movements (as for Grange Hill piles in par. 7.1). Both Slope1 (down-slope of the pile row) and Slope2 (up-slope) measured larger displacements than Pile3. Slope2 measured a soil movement towards the pile between 2 and 10m depth as if the up-slope soil is pushing against Pile3. Slope1 measured an up-slope movement over depths corresponding to the bottom part of the pile, and a down-slope movement above this.

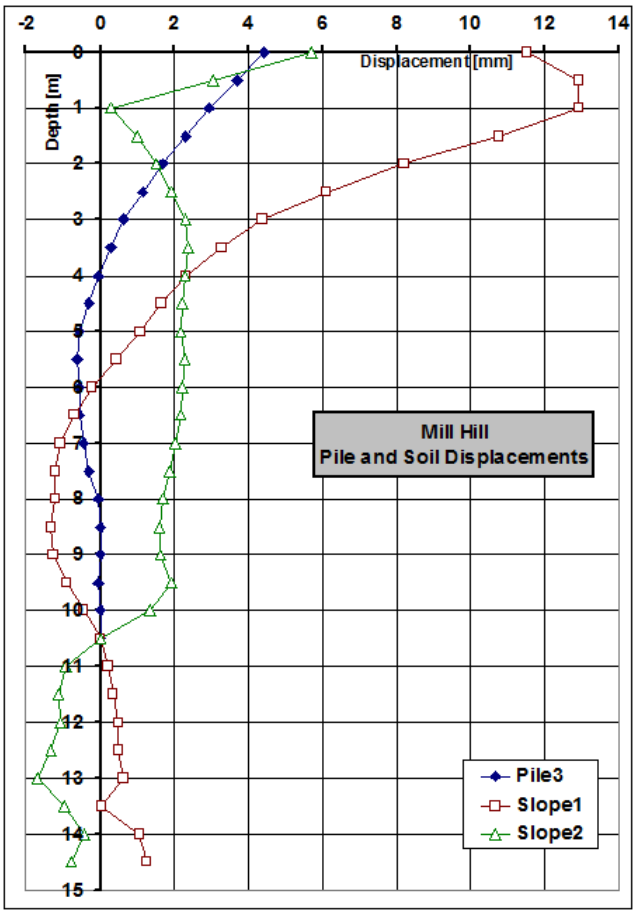

Figure 7.12: *Mill Hill, displacements measured in Pile3, Slope1 and Slope2 on the 8 July 2010.*

7.3 Leatherhead

Pile 2 is considered to give typical results for Leatherhead. The results coming from Pile1 are shown in Appendix A.2.1. Figure 7.13 shows the recorded displacements and the bending moments calculated with MCM for the whole monitoring period. Both graphs show an increase in displacements and bending moments with time, demonstrating that the slope is still moving. The displacements are no larger than 8mm, but there is some displacement along the full pile, suggesting a rigid rotation. The shape of the displacement profile shows that the pile is not fixed within the deepest soil layer, as in the case of the Grange Hill piles (fig. 7.2). The bending moment profiles, calculated using MCM, show that the peak is approaching 1000kNm, with no signs of cracking in the concrete. This is supported by the curve fitting analysis which does not require any stiffness adjustment for the curve fit to match the displacement profile (par. 6.3.3). Also, the strain gauges (sister bars in this case) do not show any jumps in reading related to cracking, but their strain transmission method (long reinforcement bars) may help to prevent this (as discussed in section 2.5.1.1).

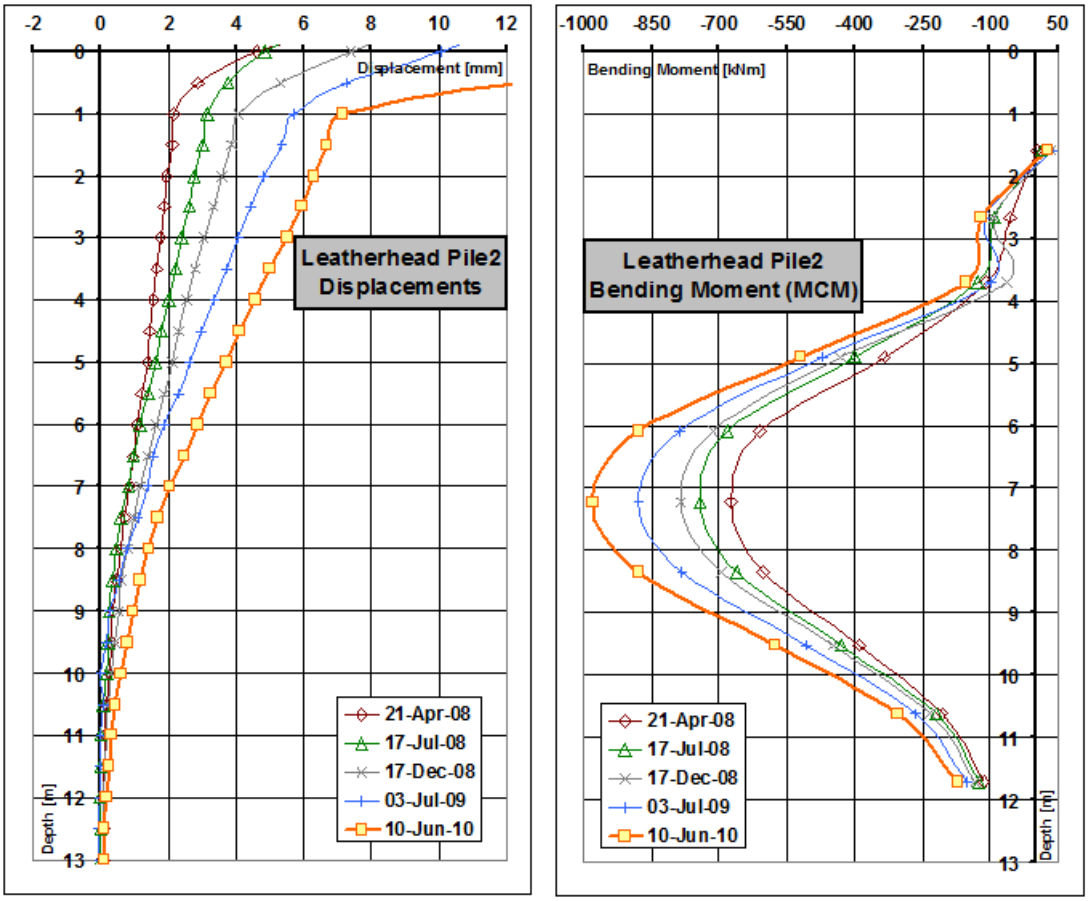

Figure 7.13: *Leatherhead Pile2, displacements and bending moments (calculated with MCM) along the full monitoring period*

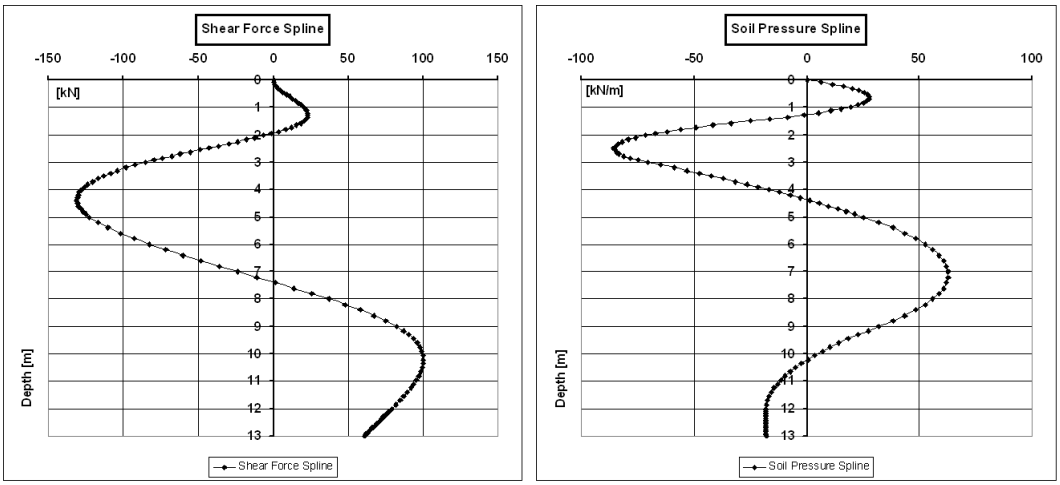

Figure 7.14: *Leatherhead Pile2, shear force and soil pressure profiles calculated using the curve fitting method for the 10 June 2010.*

The pile behaviour can be considered to be in between the flow mode and the intermediate mode. As in the flow mode, the pile shows only one bending moment peak, but the inclinometer profile does not show good fixity at the bottom. The position of the slip plane can be assumed around 5m depth (where the shear force spline shows

a peak). This gives a z_s/L ratio of 0.38 which is in between 0.2 (flow mode) and 0.6 (intermediate mode). The shapes of the shear force and soil pressure profiles (fig. 7.14) are slightly closer to those of the intermediate mode than the flow mode. The pile is too short to clearly work in flow mode and too long and stiff to clearly work in the intermediate mode.

No inclinometers were installed in the soil, thus it is not possible to compare the behaviour of the piles with the behaviour of the slope. Instead, six piles (fig. 7.15) were monitored with inclinometers, showing very similar displacements along the pile row (fig. 7.16).

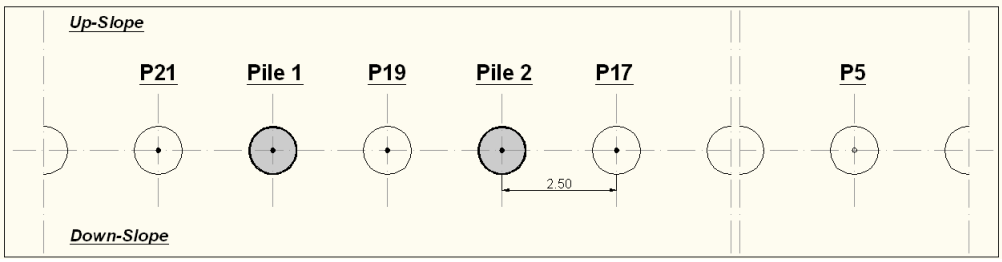

Figure 7.15: *Leatherhead, plan of the piles instrumented with inclinometers*

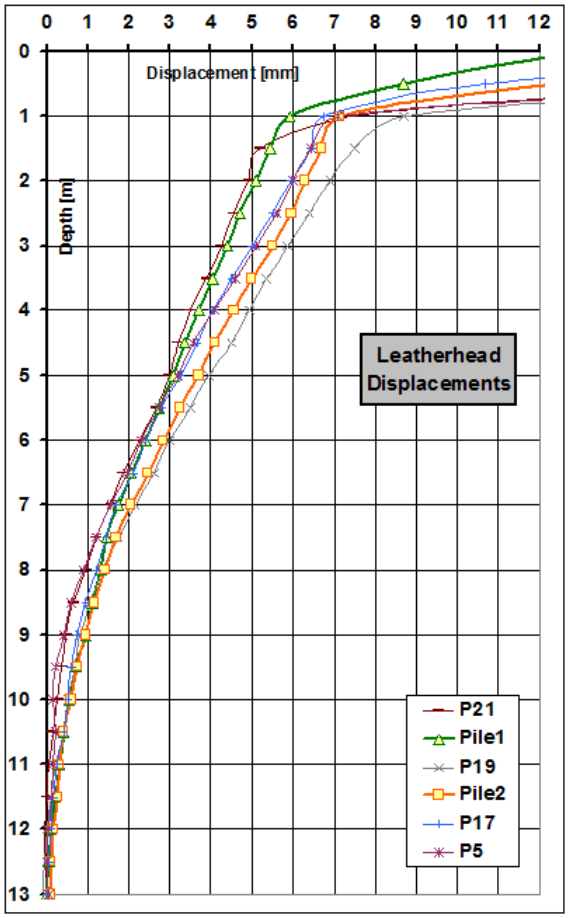

Figure 7.16: *Leatherhead, displacements profiles for all the instrumented piles, 10 June 2010.*

7.4 Ironbridge

7.4.1 Phase I

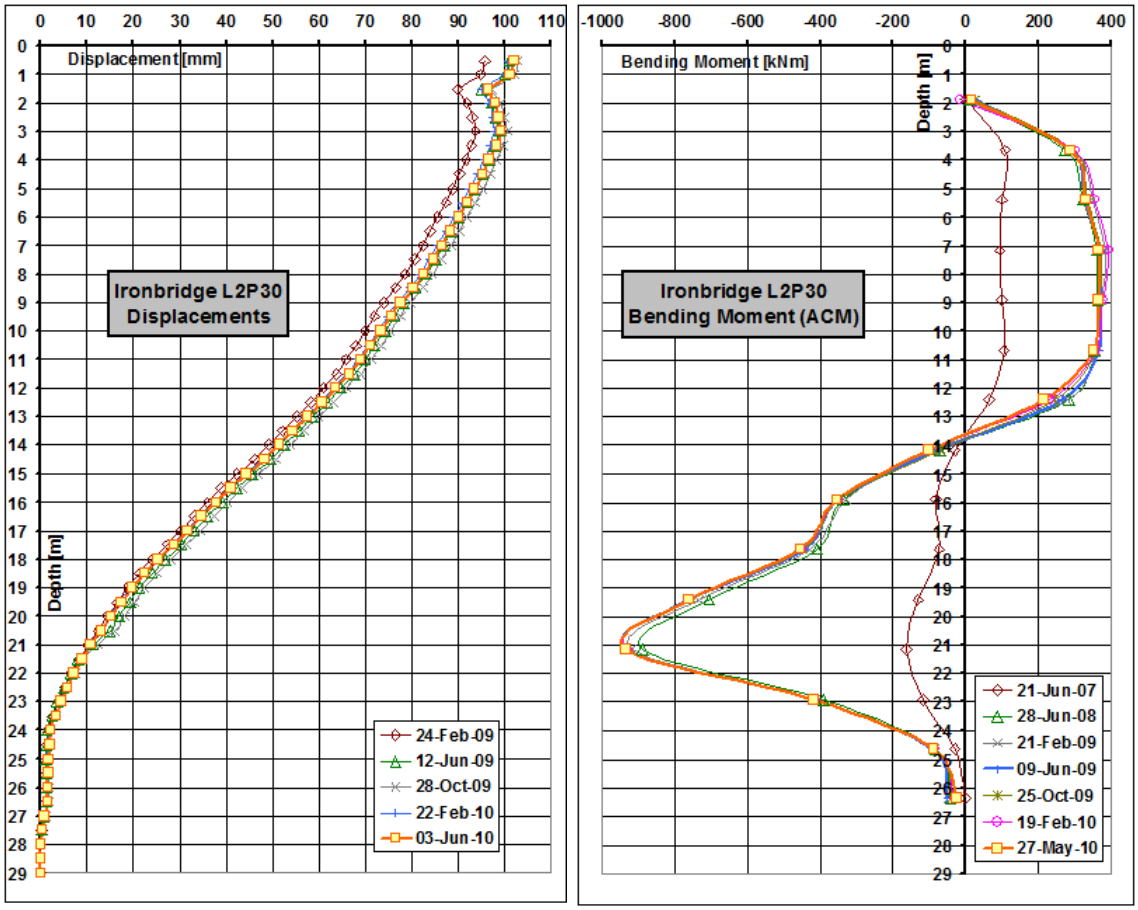

Figure 7.17: *Ironbridge L2P30, displacements and bending moments (calculated with ACM) for the full monitoring period*

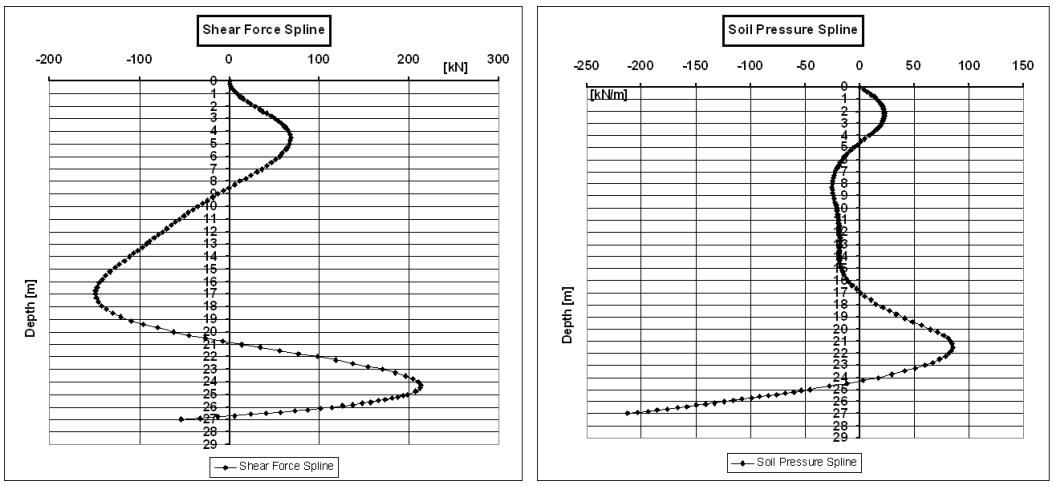

Figure 7.18: *Ironbridge L2P30, shear force and soil pressure profiles calculated using the curve fitting method and a 15% reduction of the stiffness of the pile.*

L2P30 is assumed to give typical results for Phase I piles. Figure 7.17 shows the displacements and bending moment profiles.

The bending moment results were analysed in section 5.3.2 showing that the grout is heavily cracked in tension, but it is still working in compression. This is also supported by the curve fitting comparison (par. 6.3.4). Inclinometer and strain gauge results are close, if the stiffness of the pile from the ACM is reduced by 15% in the curve fit. This error may come from the assumptions made to determine the concrete parameters and stress/strain curves.

The change in curvature detected by the inclinometer in the top 2m of the pile could be connected with the fracture of the concrete in the connection between the pile and the pile-cap. The connection can be considered as a hinge which does not transmit moment. This is confirmed by the bending moment profile which is close to zero around 2m depth. Both profiles (fig.7.17) also confirm that the pile base is fixed within the bedrock, as below 25m depth, displacements and bending moments are very close to zero.

Not much variation is shown throughout the last two years by both displacement and bending moment profiles (fig.7.17). It was not possible to collect inclinometer readings before February 2009, but the bending moment versus time profiles (fig. 7.19) show that the pile was mostly loaded before October 2007, and the readings remain almost constant after April 2009. It is assumed that the development of displacements follows the pattern of development in the bending moment since the bottom of the pile is fixed in the bedrock (any bodily rotation of the pile would produce an increment of the displacements but not of the bending moment).

In conclusion, it can be considered that the pile was loaded between May and October 2007, when the cracking in the grout and the fracture in the pile-cap connection developed. After October 2007 the increase in load and displacements slowly diminished and at the moment the slope can be considered stabilised since the pile displacements and bending moments are almost constant.

L2P30 is clearly working in the intermediate mode with the characteristic two bending moment peaks (one positive and one negative) and with the respective different curvatures in the displacement profile (fig. 7.17). The slip surface can be assumed to be around 17m depth where the shear force spline shows a peak (fig. 7.18). This gives $z_s/L = 0.64$, very close to 0.6 assumed by the theory. Shear force and soil pressure profiles are in line with the theoretical behaviour (fig. 7.1). As the soil pressure spline has to be made up of a series of smooth curves, the profile does not show any abrupt transition in the profile between positive and negative as may be expected on a real pile adjacent to the sliding surface.

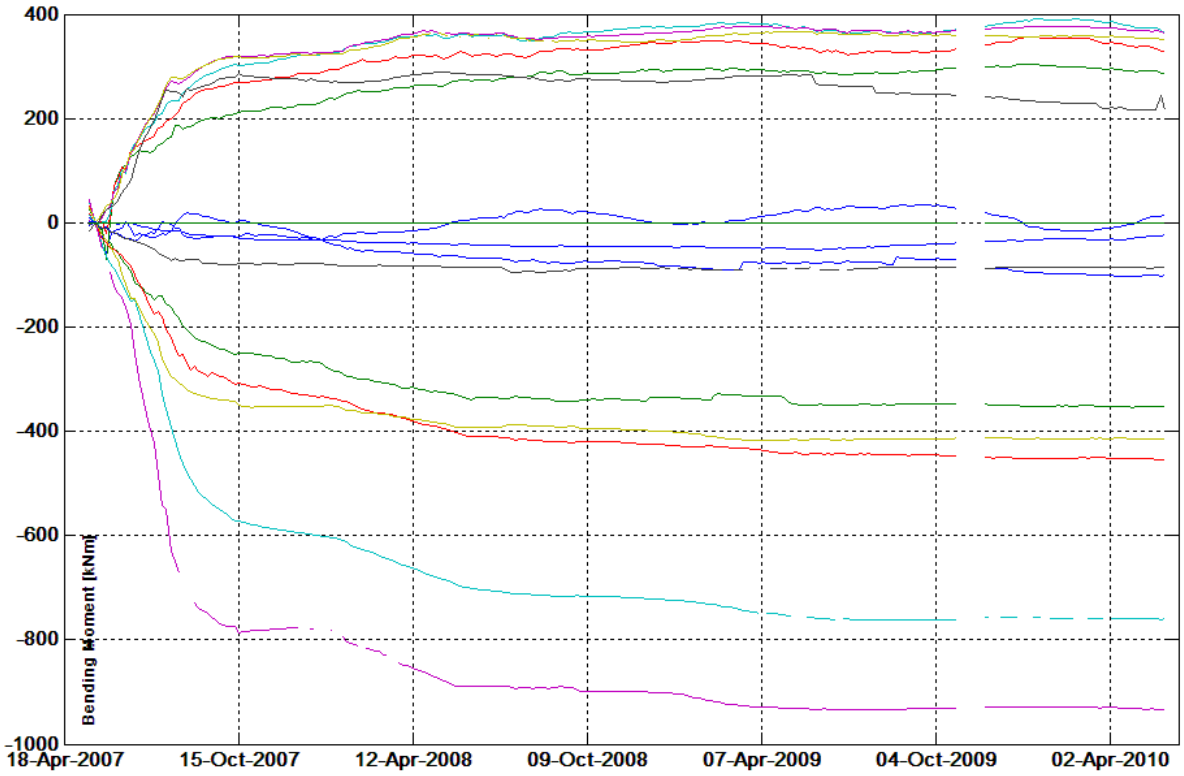

Figure 7.19: *Ironbridge L2P30, bending moment (ACM) versus time to show the general loading behaviour of the pile: most of the loading happened before October 2007; the load was almost constant during the last year monitoring.*

7.4.2 Phase II

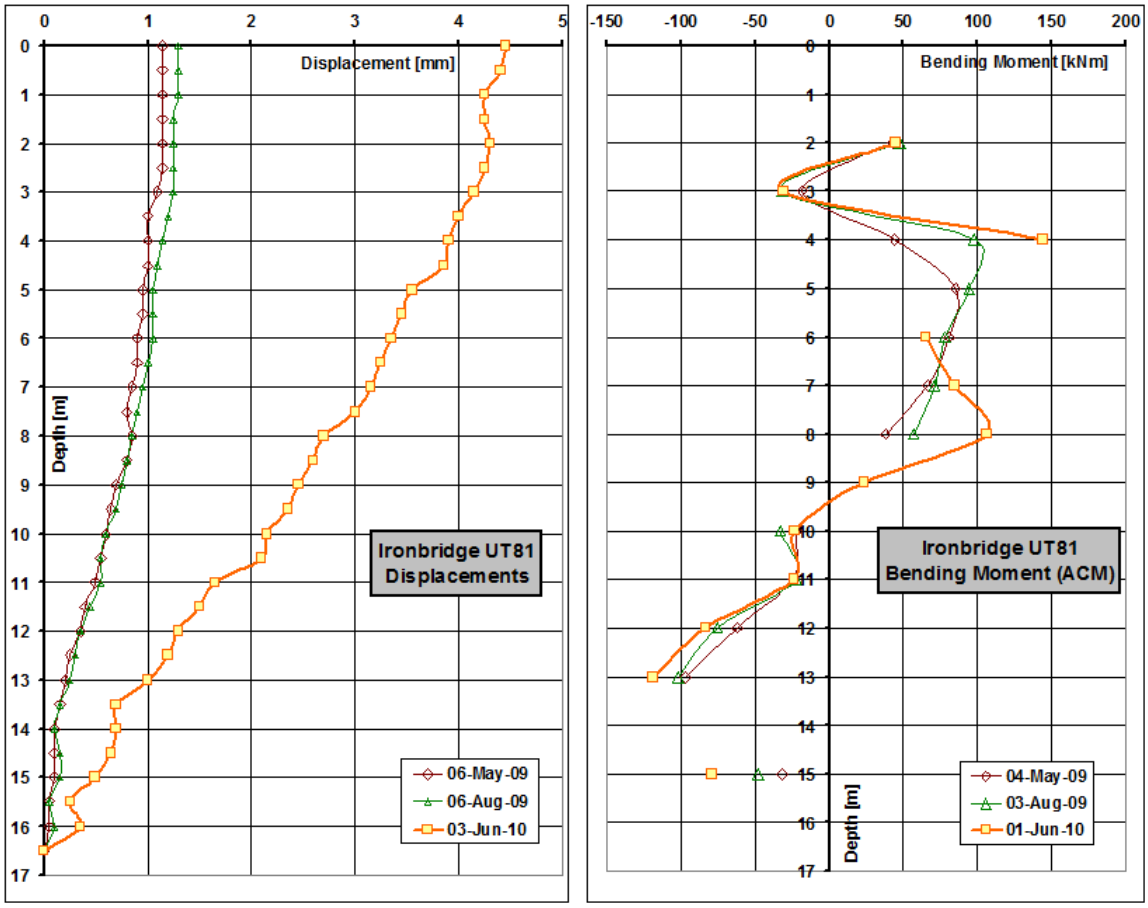

Figure 7.20: *Ironbridge UT81, displacements and bending moments (calculated with ACM) for the full monitoring period*

UT81 is analysed for Phase II. Figure 7.20 shows the displacement and bending moment profiles. Unfortunately some strain gauges are not reading at the moment and the bending moment profile shows some gaps. This pile is investigated to understand if it is rotating with the soil mass while it is also bending. The displacement profiles show that the pile mainly moves between August 2009 and June 2010. The total displacement is still small, but the shape of the profile shows that the pile is not well fixed within any stable layer. The bending moment profile is changing with time in the top half of the pile while in the bottom half it maintains the same shape and slowly increases in magnitude. The magnitudes of the bending moment peaks and total displacements are small compared to the values measured in Phase I. The analysis of the bending moment versus time profiles (fig. 7.23) shows that the bending moment is increasing in few sections only, while it remains nearly constant in the others.

The curve fitting analysis results are quite complicated. The shape of the bending moment profile is difficult to interpolate with a spline, figure 7.21 and 7.22 shows the results. The pile can be assumed to behave in the intermediate mode whilst also rotating. It is not possible to know the position of the centre of the rotation, the assumption that the base of the pile is fixed is just a convention, and in reality the point of rotation

may be above the base. It could be more accurate to do a precision survey of the position of the head of the pile and to refer the displacement to that. From the shear force profile, it can be assumed that the slip surface lies approximately around 11m depth, giving a $z_s/L = 0.65$ (close to the theoretical 0.6).

In conclusion, it can be assumed that the pile is loaded by the slope and is behaving in the intermediate mode, while it is also rotating. The maximum bending moment and the head displacement of the pile are still small in comparison with Phase I results. A longer monitoring period is necessary to fully understand if the piles have fully stabilised this section of the slope.

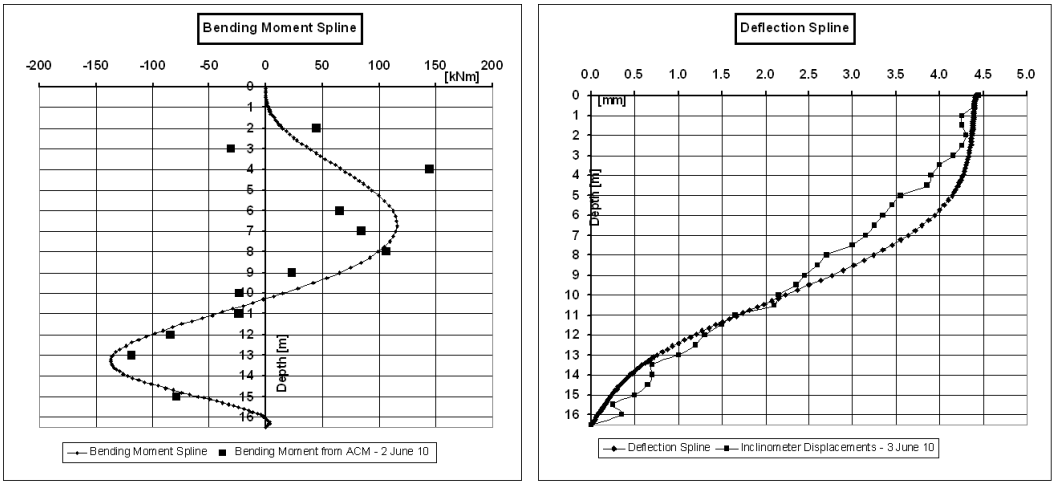

Figure 7.21: *Ironbridge UT81, bending moment and displacement comparison using the curve fitting method.*

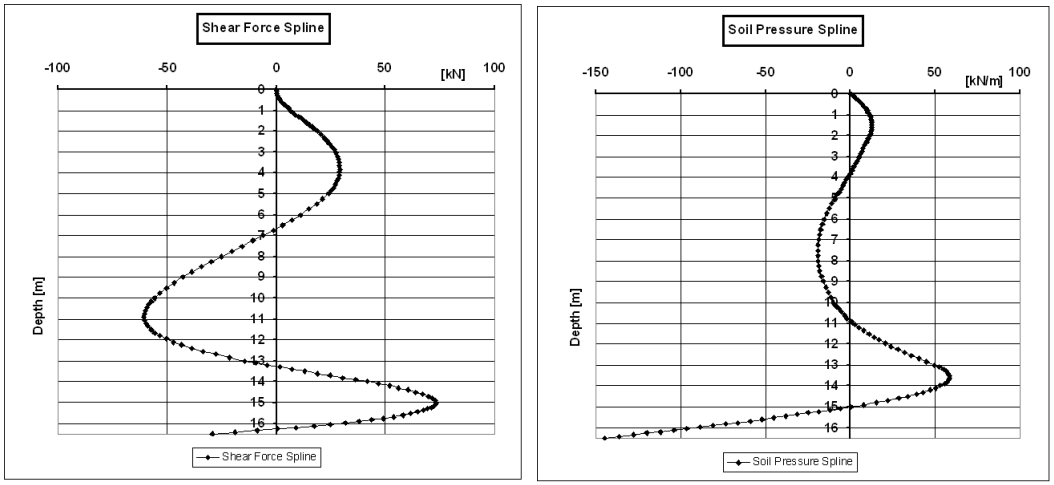

Figure 7.22: *Ironbridge UT81, shear force and soil pressure profiles calculated using the curve fitting method.*

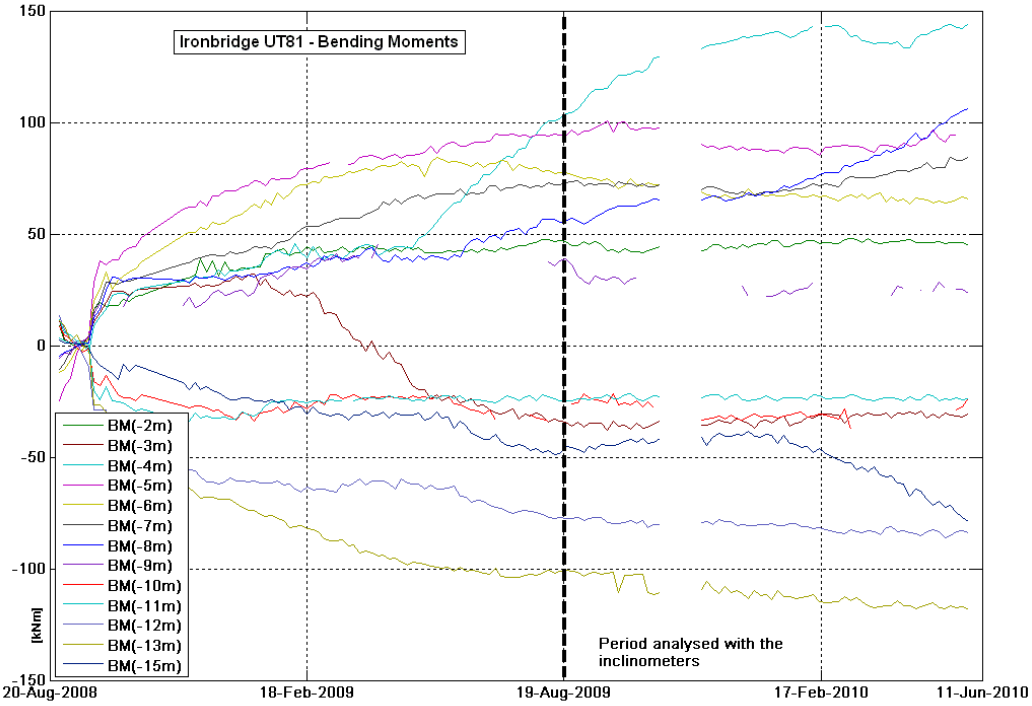

Figure 7.23: *Ironbridge UT81, bending moment (ACM) versus time to show the general behaviour of the pile. Most of the loading happened shortly after installation, while in the period analysed with the inclinometer only few instrumented sections show bending moment changes.*

7.4.3 Lloyd's Head

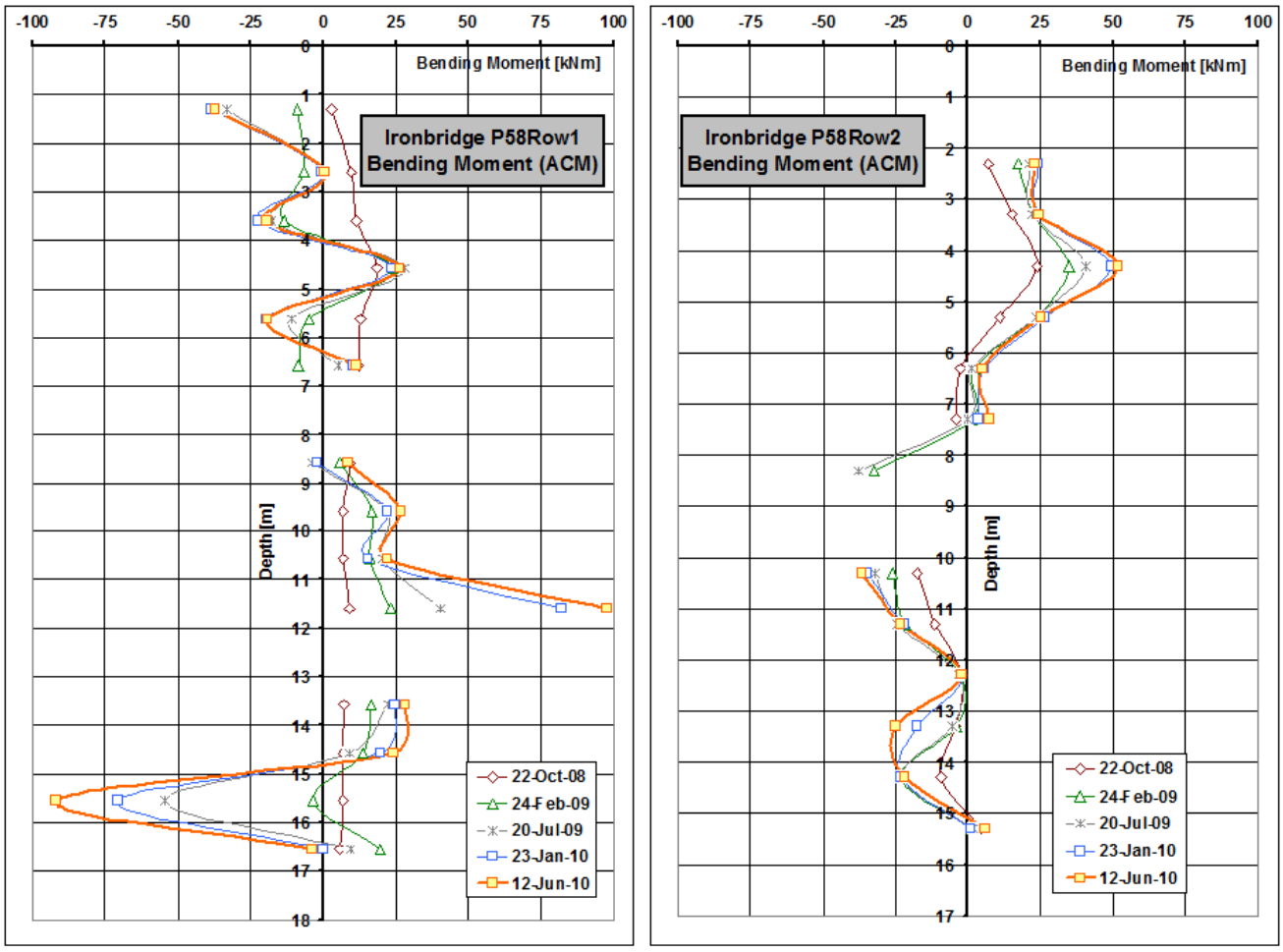

Figure 7.24: *Ironbridge Lloyd's Head, bending moment profiles (calculated with ACM) for P58Row1 and P58Row2.*

Figure 7.24 shows the bending moment profiles for the Lloyd's Head piles. As mentioned before (par. 3.4.5), no inclinometers were installed in the piles. Thus, the information about the pile behaviour is from the strain gauges only. This also means that it is not possible to know if stiffness adjustment are necessary, if the piles are fixed in the bedrock or if they are rotating. The bending moment profiles of the two piles show small bending moments, compared to Phase I piles. It is not possible to accurately localise the slip planes without the shear force profile, but the bending moment change in sign can be used as rough approximation. P58Row2 (up-slope row) behaves similarly to the intermediate mode, and the sign of the bending moment changes around 8m depth. P58Row1 (down-slope row) has a confused behaviour in the top 8m and shows a kind of intermediate behaviour in the bottom 9m. The change in sign of the bending moment happens around 15m depth. P58Row2 (up-slope row) does not show much difference between the different measured profiles, while P58Row1 (down-slope row) shows a bending moment increase with time in the bottom 9m. It is also necessary a longer monitoring period for these piles to fully understand their behaviour.

7.5 Comparison between bending moment calculation methods

For a complete interpretation of the pile behaviour, the bending moment results obtained in this research using ACM and MCM (and considering all the assumptions on the material properties) are compared with the results coming from a simplified approach that uses the engineering formula (formula 5.1) and the concrete parameters related to the site specifications. This gives, for all the analysed sites, the same value of $f_{ck,cube}$=35 N/mm^2 which using BS EN 1992 (2004) generates an E_c=32GPa. The impact of different parameters on the use of the engineering formula has been discussed in section 5.1.1. The strain gauge data used in the comparison are the same, and have been corrected using the methodology discussed in Chapter 4 before applying the different models.

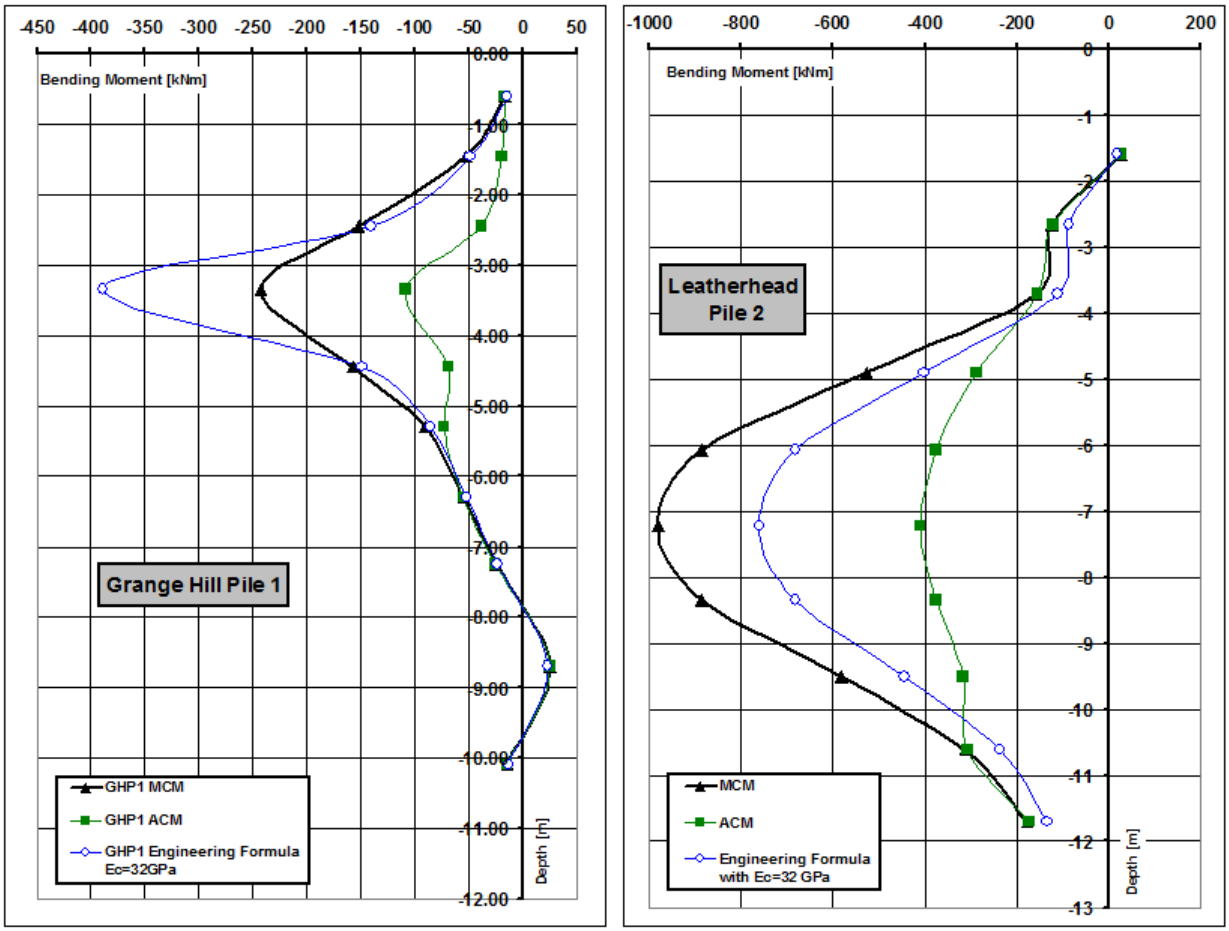

Figure 7.25: *Comparison between the bending moment profiles coming from different models for Grange Hill Pile 1 and Leatherhead Pile 2.*

Grange Hill

Figure 7.25 shows the results using the three different methods. The engineering formula profile shows a peak in the cracked section (at 3.35m depth) which largely overestimates the bending moment applied to the pile. The engineering formula does

not allow to analyse and correct the cracking effects giving a wrong bending moment peak which can lead the designer to increase the pile reinforcements.

Leatherhead

Figure 7.25 shows that the engineering formula results lie between ACM and MCM profiles. Due to the use of sister bars, no additional information about the developing of cracking is present, making the analysis of the results difficult. In this case, a measured value of ε_{t0c} would allow ACM to give more accurate results (as introduced in section 5.3.2.1).

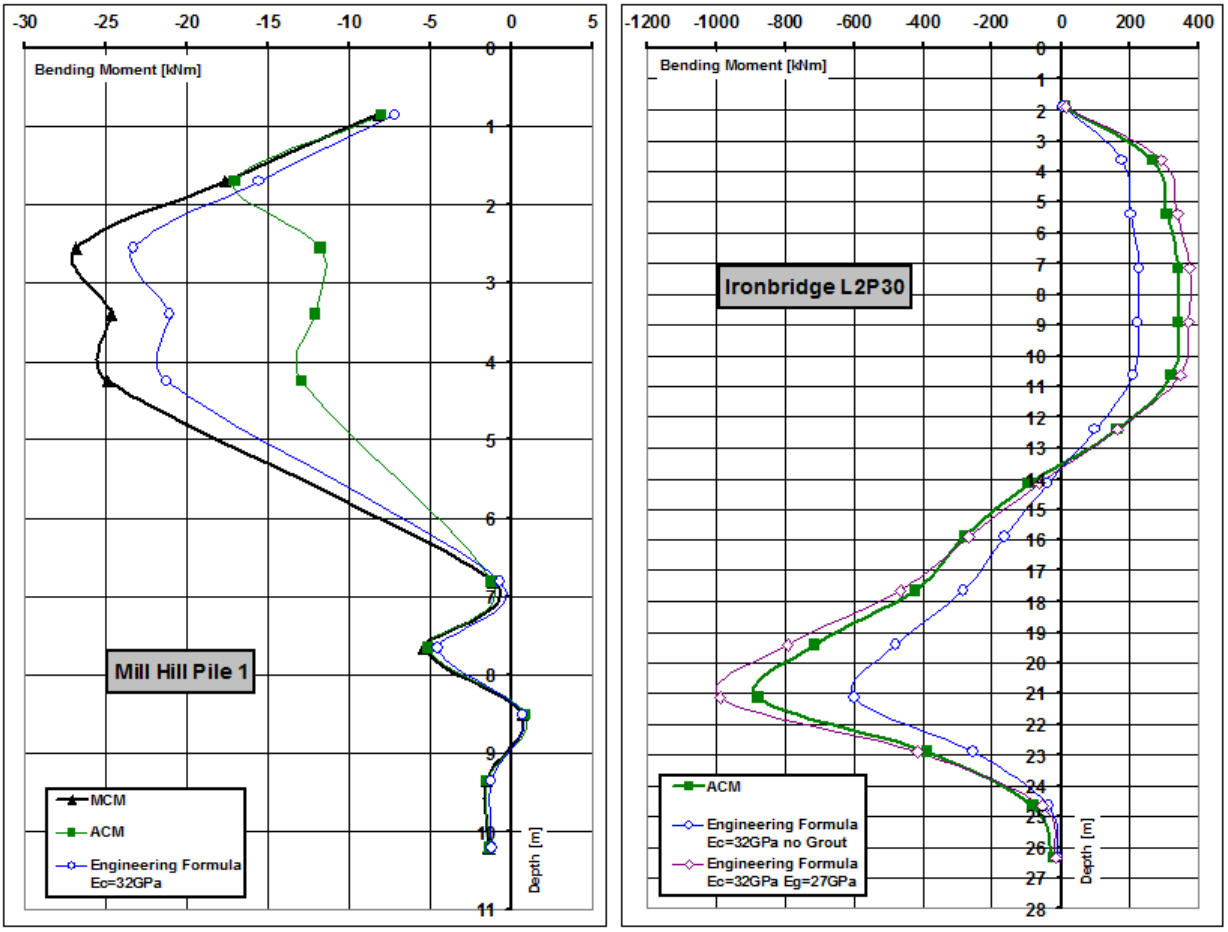

Figure 7.26: *Comparison between the bending moment profiles coming from different models for Mill Hill Pile 1 and Ironbridge L2P30.*

Mill Hill

Mill Hill bending moment results are shown in figure 7.26. The engineering formula profile lies between ACM and MCM profiles. In this case, since cracking is not expected due to the small strains measured, the difference between the engineering formula and MCM profiles are due to the choice of the E_c value used.

Ironbridge

Figure 7.26 shows the results for L2P30. In this case, the engineering formula has been applied in one case considering the effects of the grout and in the other case

neglecting them. The latter largely underestimate the bending moment applied to the pile in comparison with ACM results. Instead, the engineering formula results considering the grout over-predict the applied bending moment since the developing of cracking is not considered. In this case ACM considers a more correct behaviour for the concrete filled steel tubular pile that takes into account the effects of the grout. Using the engineering formula could, in one case, lead to underestimate the bending moment, leading the designer to decrease the pile capacity; and in the other case to overestimate bending moment with consequent increase in the pile reinforcements and dimensions.

In conclusion, the use of a simple method that considers the engineering formula and the concrete parameters related to the site specifications can lead to the wrong bending moment results. Only in one case, when the pile is lightly loaded (Mill Hill), the simple method and MCM give similar results. In the other cases, since the simplified method does not consider cracking and long term values of the parameters, the generated profiles can either overestimate or underestimate the applied bending moment. A profile that overestimates the bending moment can lead the designer to increase the dimensions or the number of piles in future similar structures; while an underestimated profile can lead to diminishing them. In particular, the simplified method does not analyse the developing of cracking, failing to give more information about the durability of the piles. In fact, if ACM or MCM show that several sections are cracked, corrosion of the reinforcement could be taking place diminishing the expected serviceability of the structure.

The piles from the four analysed sites do not show strains larger than $500\mu\varepsilon$, which means that the concrete stress/strain behaviour can still be approximated as linear. If structures with larger strains are analysed, the results from ACM and MCM (which use the non-linear stress-strain curves for concrete) would better estimates the applied bending moment than the use of a method based on the engineering formula (which assumes a linear stress/strain relation for concrete).

7.6 Conclusions about the geotechnical interpretation of instrumented sites

This chapter shows that the behaviour of the analysed piles can be described with the two of the three theoretical modes developed by Poulos (1999). Grange Hill and Mill Hill piles behave in the *"flow mode"*, most of Ironbridge piles follow the *"intermediate mode"*, while Leatherhead piles have a behaviour halfway between the two modes.

The monitoring shows that the instrumented sites have been stabilised and very small movements are taking place at the present. In particular, Ironbridge PhaseI shows that the pile heads moved about 100mm in the first year and then no further important movements developed in the last two years. The other instrumented piles show displacements smaller than 5mm after the first year of monitoring. This shows that the slopes have been stabilised.

The Grange Hill results show that the installation of the piles modified the behaviour of the slope and instead of the expected deep seated slip surface, superficial movements developed (par. 7.1).

The Mill Hill piles are lightly loaded and this allows monitoring of the effects of climate and vegetation on the stabilised slope. The slope swells (putting the piles in tension) during the winter, and shrinks (compressing the piles) during the summer (par. 7.2).

The analysis of inclinometer profiles also shows a small bodily rotation of some of the piles (Mill Hill, Leatherhead and Ironbridge UT81). The movements are still very small, but this changes the behaviour of the pile from the common design assumption that the piles are fixed at the base.

The use of a more simplified method for the calculation of the bending moment (as analysed in section 7.5), could have lead to incompatibility during the comparison between bending moment and displacement profiles. This means that a wrong evaluation of the stiffness of the pile and the bending moment profile would have made difficult to apply the curve fitting method explained in Chapter 6. ACM and MCM approaches used in this research instead, give results that need minimal corrections (15%) during the curve fitting comparison, giving more reliability on the results, since both instruments (strain gauges and inclinometers) agree on the generated profiles. This in turn makes possible to estimate the profiles of shear force and soil pressure, and the comparison with the theoretical models developed by Poulos (1999).

The simplified method can still be used when the measured strains allow to simplify the concrete behaviour as linear (par. 2.3.2.1) and no cracking has been measured. MCM and ACM can instead be used in a wider range of situations since the non-linear behaviour of concrete and the effects of cracking are taken into account.

Chapter 8

Conclusions

8.1 Conclusions

This section summarises the results achieved in this research. Due to the complexity of the research and the many factors affecting the data analysis and the calculation models used, the conclusions are multiple. Detailed discussion of the concluding results for each topic are at the end of each chapter or specific section.

- Creep and shrinkage can be neglected in the structural analysis of piles (or other underground structures) in saturated soil (par. 2.4).
- A method for the interpretation of strain gauge data considering different types of interference and the effects of the datum position has been developed (par. 4.1, 4.2 and 4.3).
- A method for the analysis of the effects of temperature on strain gauge readings and the potential corrections has been developed and tested on the instrumented piles from three sites (par. 4.4). Strain/temperature graphs are used to identify where the corrections have to be applied and the effective coefficient of thermal expansion to be used.
- The behaviour of strain gauges during cracking has been analysed. The results are different depending on the type of instrument used: embedded strain gauges can detect cracking (if the crack is close to the instrument) while sister bars and welded strain gauges did not show any presence of cracking when it was expected (par. 2.5.1.1 and 4.6). Strain gauges are not the best instruments for measuring or detecting cracking since they are influenced differently depending on the relative position between the cracks and the instrument.
- The bending moment calculation is affected by many factors: cracking, concrete parameters, stress/strain relations and the calculation method adopted. Two methods for the calculation have been developed and used on different type of piles. One method automatically considers the opening of the cracks (ACM) and is best suited for concrete-filled steel tubular piles. The other method does

not consider the opening of cracks until the strain gauges detect cracking taking place, then the results are corrected accordingly (MCM); this method may be better suited to standard reinforced concrete piles instrumented with embedded strain gauges (sister bar strain gauges do not show the opening of cracks). The results from these methods are supported by the inclinometer results. If all the factors affecting the bending moment calculation are not carefully considered, the results calculated using different assumptions and parameters can have differences up to 100% (par. 5.4).

- The results of the bending moment calculation on the Ironbridge piles show that in concrete-filled steel tubular piles, the grout ring has a structural effect (it increases the flexural stiffness) even when the part in tension is cracked. Neglecting the structural effect of the grout ring underestimates significantly (by up to 25%) the bending moment results (par. 5.4).

- The curve fitting method for the comparison of strain gauge and inclinometer results developed by Smethurst (2003) has been improved and applied to each instrumented pile. This method is used to check the consistency of results from the two instruments and to give insights on the bending moment results, showing if the method used (MCM or ACM) correctly estimates the profiles. The method confirms the consistency of results between the two instruments when the piles are not cracked (using MCM). A discrepancy on the stiffness of the piles of 10% for standard reinforced piles (MCM) and of 15% for concrete-filled steel tubular piles (ACM) is shown when cracks developed. This error is coming from the inaccuracies in the determination of the concrete parameters and from approximation and assumptions used in the cracking models (par. 6.4).

- The results from strain gauges, inclinometers and curve fitting method show that the piles behaviour follows the models described by Poulos (1999). Grange Hill and Mill Hill piles behave in the *"flow mode"*, most of the Ironbridge piles follow the *"intermediate mode"*, while Leatherhead piles have a behaviour halfway between the two modes (par. 7.6).

- Discrete piles used to stabilise a slope, where the slip surface is not developed, modify the behaviour of the slope. During the design process, it may be more accurate to dimension the piles considering the behaviour of the stabilised slope instead of the behaviour of the slope without piles. It is also safer to use uniform steel reinforcement along the piles (par. 7.6).

- The effects of climate and vegetation on the slope and on lightly loaded piles has been detected. The slope swells (putting the piles in tension) during the winter, and shrinks (compressing the piles) during the summer (par. 7.6). In the analysed case (Mill Hill) this seasonal effect has a minor influence on the general behaviour of the piles.

- The monitoring shows that the instrumented sites have been stabilised and generally very small movements have occurred. In particular, Ironbridge PhaseI pile heads moved about 100mm in the first year and then no further important movements have developed in the last two years. The other instrumented piles show displacements smaller than 5mm after one year of monitoring. This shows that the slope have been stabilised.

- Each site, and sometimes each pile, has specific problems and needs specific approaches and solutions. The analysis method cannot be standardised, but it has to be flexible to take into account every factor that can affect the readings and the following analysis results.

8.2 Further work

This research on the long term analysis of reinforced concrete piles can be further enhanced. The obvious first step is the continuation of the monitoring and data analysis of the actual instrumented sites. This can give further insights on the long term behaviour of stabilised slopes and discrete piles.

The assumptions and approximations used in this research to model the behaviour of the piles are many, and each of them can be improved with further work:

- The behaviour of reinforced concrete in the ground is still approximated. A better understanding of the concrete properties and processes (mostly shrinkage and creep) could be achieved with the study of concrete samples cast in different soils under different moisture conditions. A methodology for the determination of more realistic stress-strain curves will improve the results of the bending moment calculation.

- Concrete cracking and its development have a fundamental effect on the bending moment calculation. A more detailed study about concrete cracking and the development of more appropriate instruments to detect the cracks in underground structures will expand the understanding of pile subject to concrete cracking.

- The measurement of the soil pressures against the pile and the relative soil and pile displacement profile can further increase the understanding of mechanisms of pile stabilisation. The curve fitting method can be used to compare the soil pressure profile with bending moment and displacement profiles. The method could be enhanced to use integration only, avoiding the numerical problems of the differentiation process.

- When all the issues affecting the monitoring and the structures are understood, the strain gauges analysis, bending moment calculation and curve fitting method could be combined in a unique generalised procedure and translated in a more user-friendly program.

- The methodology developed in this thesis may also be used on other geotechnical instrumented structures (e.g. retaining walls, diaphragm walls, etc...) to monitor and analyse their behaviour. This could also improve the understanding of the development of creep and shrinkage in concrete structures where a part is in contact with the ground and the other is in open air.

References

ACI Committee 209 (1992). Prediction of creep, shrinkage and temperature effects in concrete structures, *ACI Manual of Concrete Practice 1994* .

Acker, P. and Ulm, F. (2001). Creep and shrinkage of concrete: physical origins and practical measurements, *Nuclear Engineering and Design* **203**: 143–158.

Barr, B., Hoseinian, S. B. and Beygi, M. A. (2003). Shrinkage of concrete stored in natural environments, *Cement and Concrete Composites* **25**: 19–29.

Batten, M., Powrie, W., Yu, H. T. and Leiper, Q. (1999). Use of vibrating wire strain gauges to measure loads in tubular steel props supporting deep retaining walls, *Proceeding Institution of Civil Engineers, Geotechnical Engineering* **137**: 3–13.

Bazant, Z. P. (2001). Prediction of concrete creep and shrinkage: past, present and future, *Nuclear Engineering and Design* **203**: 27–38.

Bazant, Z. P., Cusatis, G. and Cedolin, L. (2004). Temperature effect on concrete creep modeled by microprestress-solidification theory, *Journal of Engineering Mechanics* **130-6**: 691–699.

Bazant, Z. P., Hauggaard, B., Baweja, S. and Ulm, F. J. (1997). Microprestress-solidification theory for concrete creep. i: aging and drying effects, *Journal of Engineering Mechanics* **123 No. 11**: 1188–1194.

Bianchini, A. C., Kesler, C. E. and Lott, J. L. (1968). *Cracking of reinforced concrete under external load*, ACI Publication.

Borosnyoi, G. and Balazs, G. (2005). Models for flexural cracking in concrete: the state of the art, *Structural Concrete* **6 No 2**: 53–62.

Broms, B. B. (1964). Lateral resistance of piles in cohesive soils, *Journal of Soil Mechanics and Foundations Division* **90**: 27–63.

Brown and Root Consulting report for Infraco BCV Limited (2002). The main assessment report, investigation the stability and reporting on the condition of the earthwork: Earth structure investigations and assessment, chigwell to grange hill, site c03 (c/056/cor 0920m - 1155 m), assessment report., *Technical report.*

BS 5400-4 (1990). Steel, concrete and composite bridges, *BS 5400-4* .

BS 8007 (1987). Design of concrete structures for retaining aqueous liquids, *BS 8007* .

BS EN 12390-2 (2000). Testing hardened concrete, *BS EN 12390-2* .

BS EN 12390-3 (2002). Testing hardened concrete, *BS EN 12390-3* .

BS EN 1992 (2004). Eurocode 2: design of concrete structure, *BS EN 1992-1-1* .

Crilly, M. S. and Driscoll, R. M. C. (2000). The behaviour of lightly loaded piles in swelling ground and implications for their design, *Proceeding Institution of Civil Engineers, Geotechnical Engineering* **143**: 3–16.

de Sanctis, S. (2006). *Indagine sperimentale su travi in c.a. inflesse rinforzate con frp*, Master's thesis, Universita' degli Studi di Bologna, Facolta' di Ingegneria, D.I.S.T.A.R.T.

de Sousa Coutinho, A. G. F. (2006). Data reduction of horizontally load full-scale tests on bored concrete piles and pile groups, *Journal of Geotechnical and Geoenvironmental Engineering ASCE* **132**: 752–769.

Dunnicliff, J. (1993). *Geotechnical instrumentation for monitoring field performance*, Wiley.

Durrani, I. (2006). *Numerical modelling of discrete pile rows to stabilise slopes*, PhD thesis, University of Nottingham.

Fellenius, B. H., Kim, S. R. and Chung, S. G. (2009). Long-term monitoring of strain in instrumented piles, *Journal of Geotechnical and Geoenvironmental Engineering* **135**: 1583–1595.

Gardner, N. and Zhao, J. (1993). Creep and shrinkage revisited, *ACI Materials Journal* **90**: 236–246.

Gawin, D., Pesavento, F. and Schrefler, B. A. (2006). Hygro-thermo-chemo-mechanical modelling of concrete at early ages and beyond. Part II: shrinkage and creep of concrete, *International Journal for Numerical Methods in Engineering* **67**: 332–363.

Goel, R., Kumar, R. and Paul, D. K. (2007). Comparative study of various creep and shrinkage prediction models for concrete, *Journal of Materials in Civil Engineering* **19-3**: 249–260.

Hassoun, M. N. and Al-Manaseer, A. (2005). *Structural Concrete*, Wiley.

Knowles, R. and Park, R. (1969). Strength of concrete-filled steel tubular columns, *Journal of Structural Division, ASCE* **95**: 2565–87.

Lee, K., Lee, H., Lee, S. and Kim, G. (2006). Autogenous shrinkage of concrete containing ground granulated blast-furnace slag, *Cement and concrete research* **36**: 1279–1285.

Liang, Q. Q. (2011a). High strength circular concrete-filled steel tubular slender beam-columns, part i: Numerical analysis, *Journal of Constructional Steel Research* **67**: 164–171.

Liang, Q. Q. (2011b). High strength circular concrete-filled steel tubular slender beam-columns, part ii: Fundamental behaviour, *Journal of Constructional Steel Research* **67**: 172–180.

Liang, Q. Q. and Fragomeni, S. (2009). Nonlinear analysis of circular concrete-filled steel tubular short columns under axial loading, *Journal of Constructional Steel Research* **65**: 2186–2196.

Liang, Q. Q. and Fragomeni, S. (2010). Nonlinear analysis of circular concrete-filled steel tubular short columns under eccentric load, *Journal of Constructional Steel Research* **66**: 159–169.

M25 Sphere, for the Highways Agency (2007). Remedial works proposal, earthwork no: 10191 (site 6): M25, j9 j10, mp65 5a 20m and mp65 6a 35m., *Technical report*.

Mott MacDonald report for Tube Lines (2004). Detailed design report. finchley central to mill hill east, n054/em2, em3, em5, em6, em7. embankment stabilisation works. reference 213608, *Technical report*.

Muir Wood, A. (2004). *The early effects of shrinkage and temperature change on a reinforced concrete pile*, Master's thesis, University of Southampton, School of Civil Engineering and Environment.

Neville, A. M. (1970). *Creep of concrete: plain, reinforced, and prestressed*, North Holland Publishing company.

Neville, A. M. (1995). *Properties of Concrete (4th edition)*, Longman Group Limited, Essex.

Ng, C. W. W., Lings, M. L. and Nash, D. F. T. (1992). Back-analysiing the bending moment in a concrete diaphragm wall, *The Structural Engineer* **70**: 421–426.

Nield, S., Williams, M. and MacFadden, P. (2003). Measurement of low-amplitude hysteresis behavoiur of concrete by high-precision vibrating wire strain gauges, *Key Engineering Material* **245-246**: 315–322.

Nip, D. C. N. and Ng, C. W. W. (2005). Back-analysis of laterally loaded bored piles, *Geotechnical Engineering* **158**: 63–73.

Norwest Holst Soil Engineering Limited report for Infraco BCV Limited (2002). The main site investigation findings, borehole logs, limited (actually very limited) lab testing, and survey drawings is in: Report on a ground investigation at earth structure project, central line package c, asset c056/cts2, site c03, chainage c/056/cor 0920m-1155m chigwell to grange hill, *Technical report*.

O'Brien, A. S. (2007). Rehabilitation of urban railway embankments - investigation, analysis, stabilisation, *Proc. of the 14th International Conference SMGE* . Madrid.

Ooi, P. and Ramsey, T. (2003). Curvature and bending moments from inclinometer data, *International journal of geomechanics ASCE* **3**: 64–74.

Patsch, A., Gerbaudo, C. and Prato, C. (2002). Analysis and testing of piles for ship impact defenses, *Journal of Bridge Engineering* **7**(4): 236–244.

Pickett, G. (1942). The effect of change in moisture content on creep of concrete under a sustained load, *ACI Journal* **38**: 333–355.

Poulos, H. G. (1999). *Slope Stability Engineering*, Balkema, Rotterdam.

Roesler, J. and Barenberg, E. (2000). Effect of static and fatigue cracking on concrete strain measurements, *Transportation Research Record* **1684**: 51–60.

Smethurst, J. A. (2003). *The use of discrete piles for infrastructure slope stabilisation*, PhD thesis, University of Southampton, School of Civil Engineering and Environment.

Smethurst, J. A. and Powrie, W. (2007). monitoring and analysis of the bending behaviour of discrete piles used to stabilise a railway embankment, *Geotechnique* **57**: 663–677.

Tatro, S. (2006). *Significance of tests and properties of concrete and concrete-making materials*, ASTM Intrnational Standards Worlwide STP 169D.

The Mathworks Inc. (1984-2009). Matlab(r2009b).

Viggiani, C. (1981). Ultimate lateral load on piles used to stabilise landslides, *Proc. 10th Int. Conf. Soil Mechs. Foundn. Engs. Stockolm.* **3**: 555–560.

Watstain, D. and Bresler, B. (1974). *Reinforced Concrete Engineering*, Wiley Interscience, chapter 4, pp. 151–193.

Zhao, Q. et al. (2006). Influence of fly ash proportion on creep characteristics of high-performance concrete and its mechanism, *Journal of the Chinese Ceramic Society* **34**: 446–451. Abstract in English article in Chinese.

Appendix A

Appendix

This appendix presents strains vs. time, bending moment vs. time, bending moment vs. depth, and displacements vs. depth profiles for each instrumented pile. The data have been processed following the methods and assumptions described in chapter 4 and chapter 5. The pile names and instrument positions are based on the site descriptions presented in chapter 3. The profiles show the general behaviour of the piles. It is difficult to fully label the plots of strains and bending moments with time since many lines are overlapped. However, the plots do give an idea of the overall changes in strain and bending moment with time, and the attached CD contains the electronic data which can be used for a more specific data analysis.

A.1 Grange Hill

A.1.1 Pile1

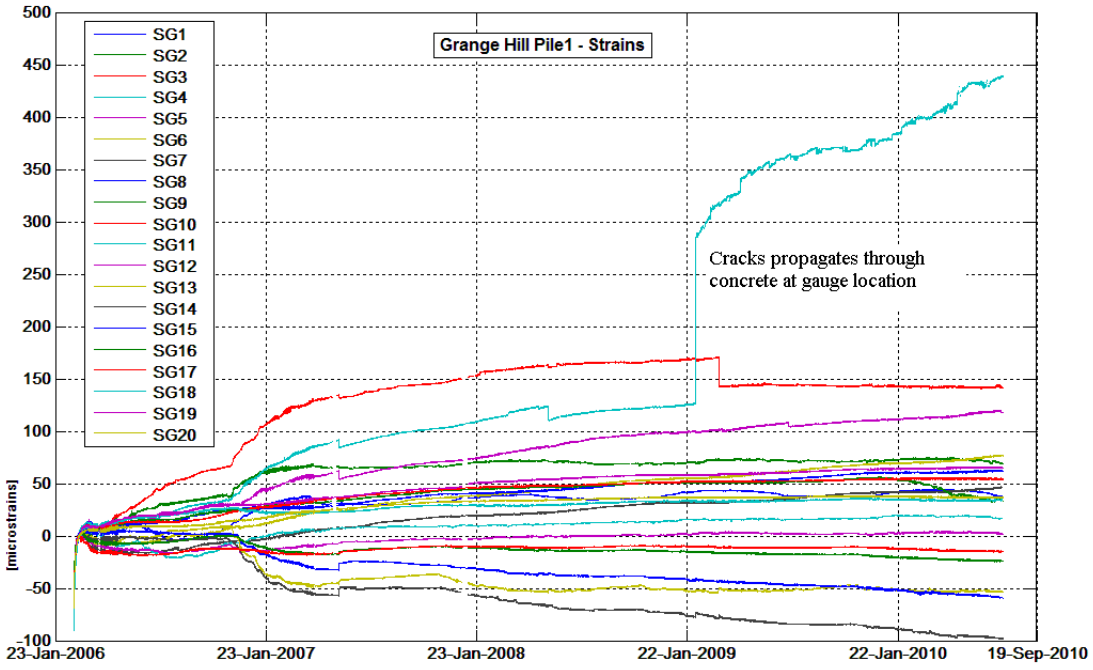

Figure A.1: *Grange Hill Pile1, strain profiles for all the instruments in the pile.*

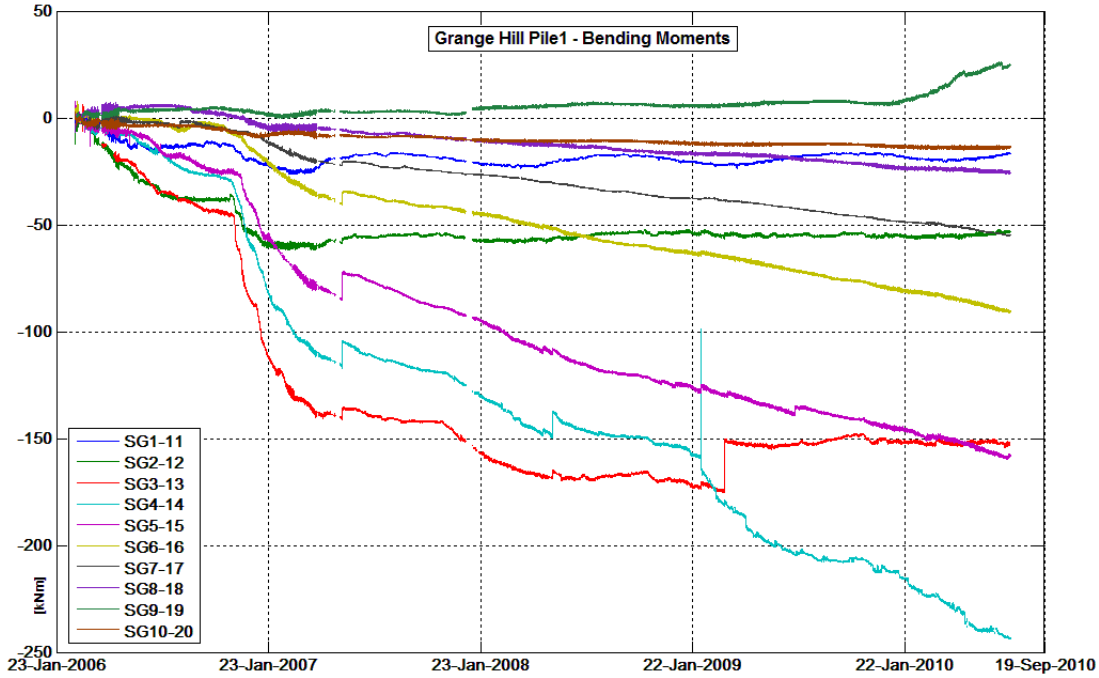

Figure A.2: *Grange Hill Pile1, bending moment profiles for all the instrumented sections in the pile.*

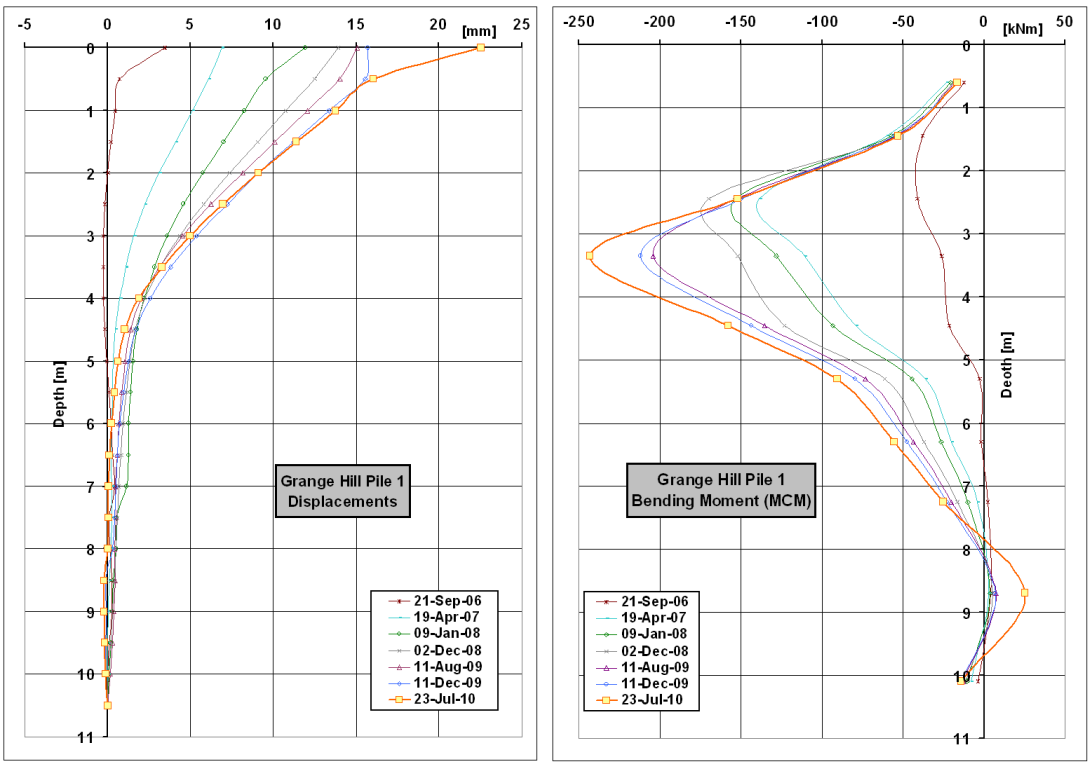

Figure A.3: *Grange Hill Pile1, displacements and bending moments (calculated with MCM) for the whole monitoring period*

A.1.2 Pile2

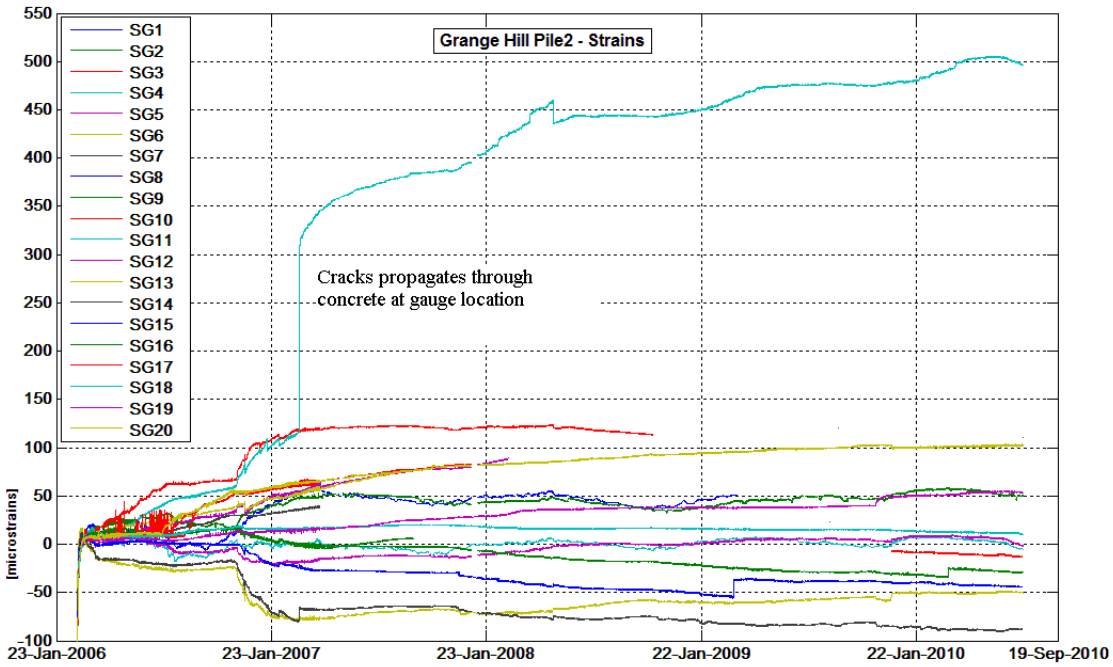

Figure A.4: *Grange Hill Pile2, strain profiles for all the instruments in the pile.*

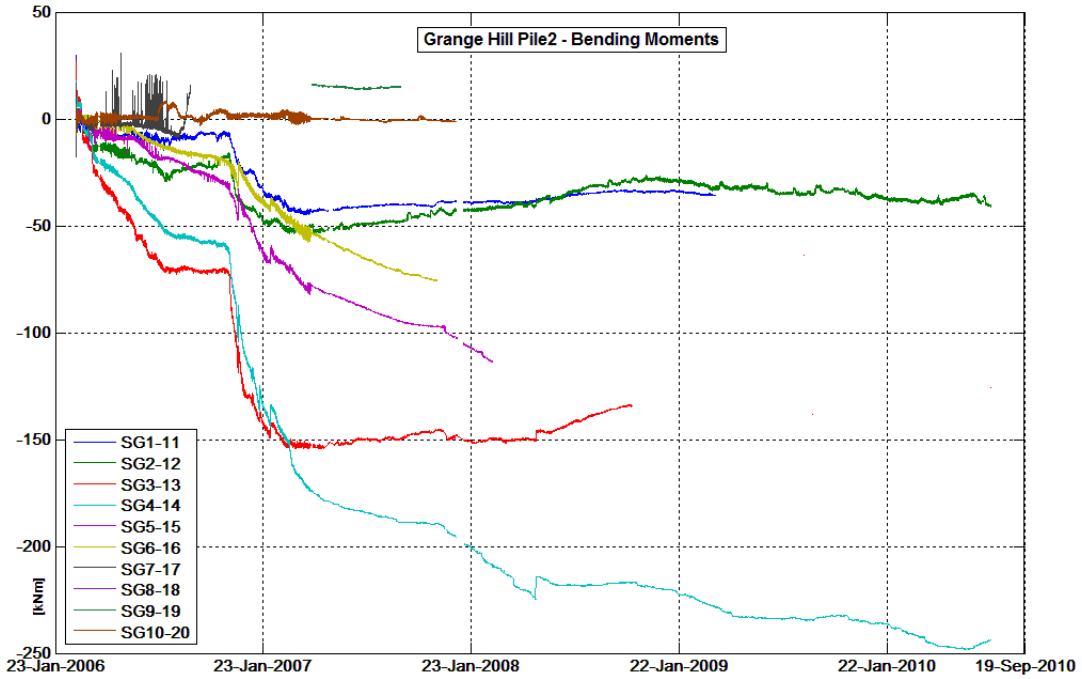

Figure A.5: *Grange Hill Pile2, bending moment profiles for all the instrumented sections in the pile.*

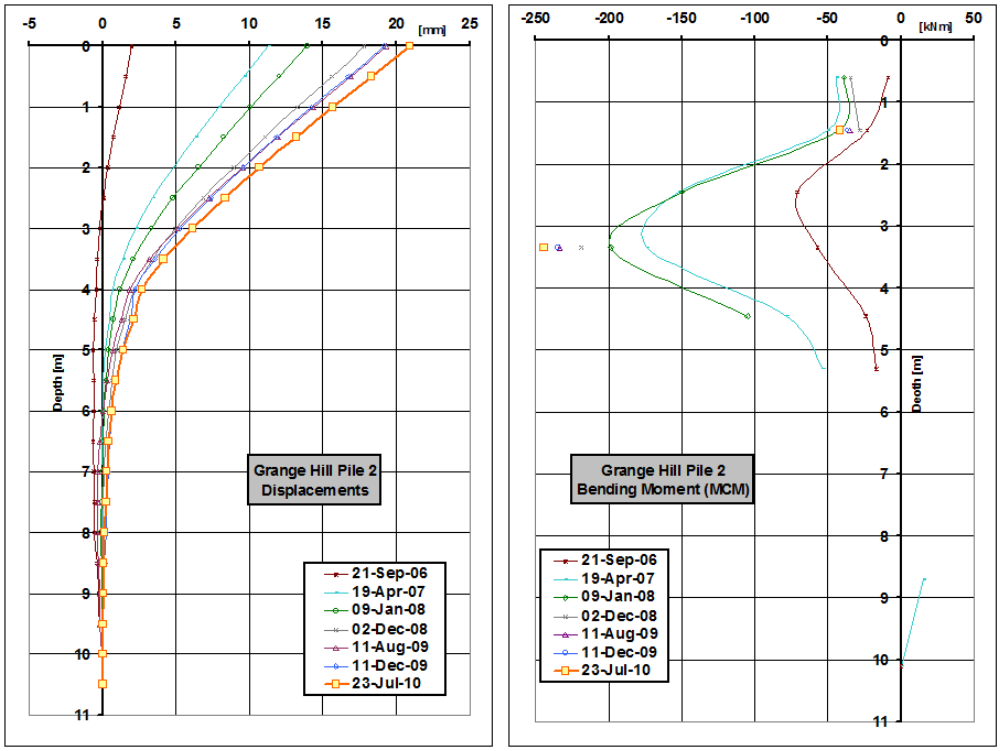

Figure A.6: *Grange Hill Pile2, displacements and bending moments (calculated with MCM) for the whole monitoring period*

A.1.3 Pile3

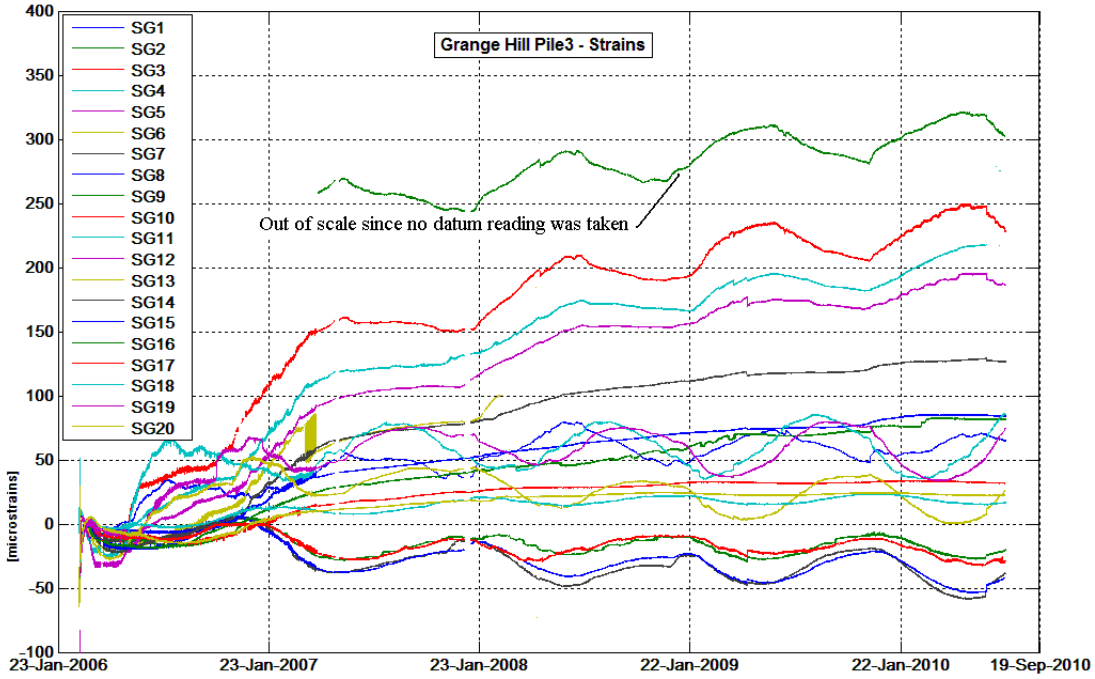

Figure A.7: *Grange Hill Pile3, strain profiles for all the instruments in the pile.*

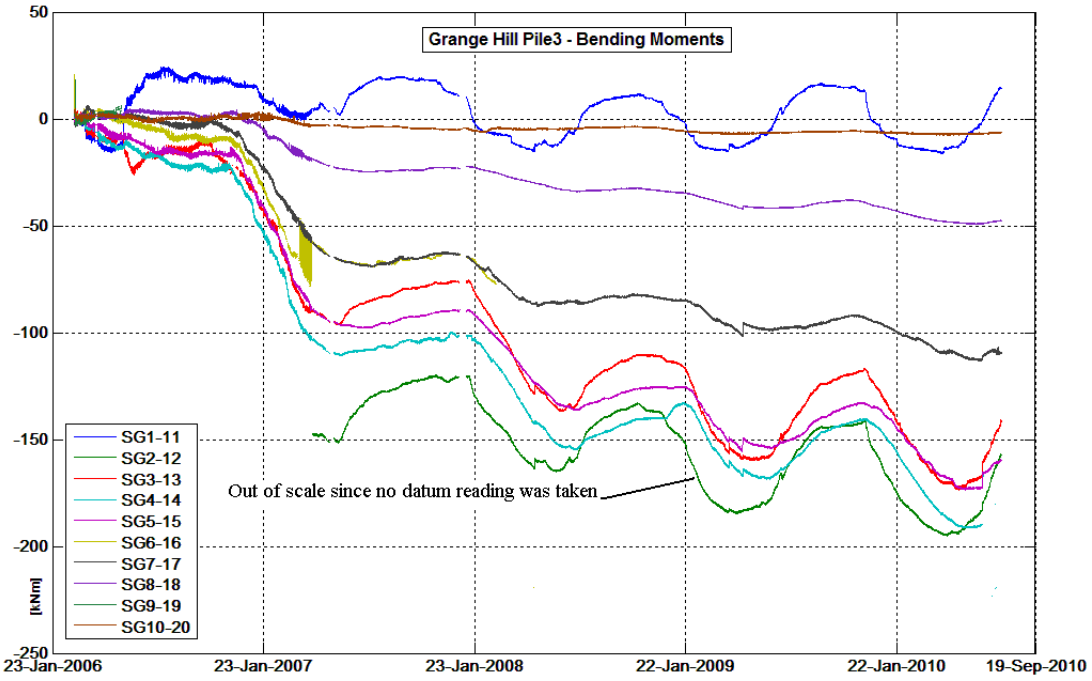

Figure A.8: *Grange Hill Pile3, bending moment profiles for all the instrumented sections in the pile.*

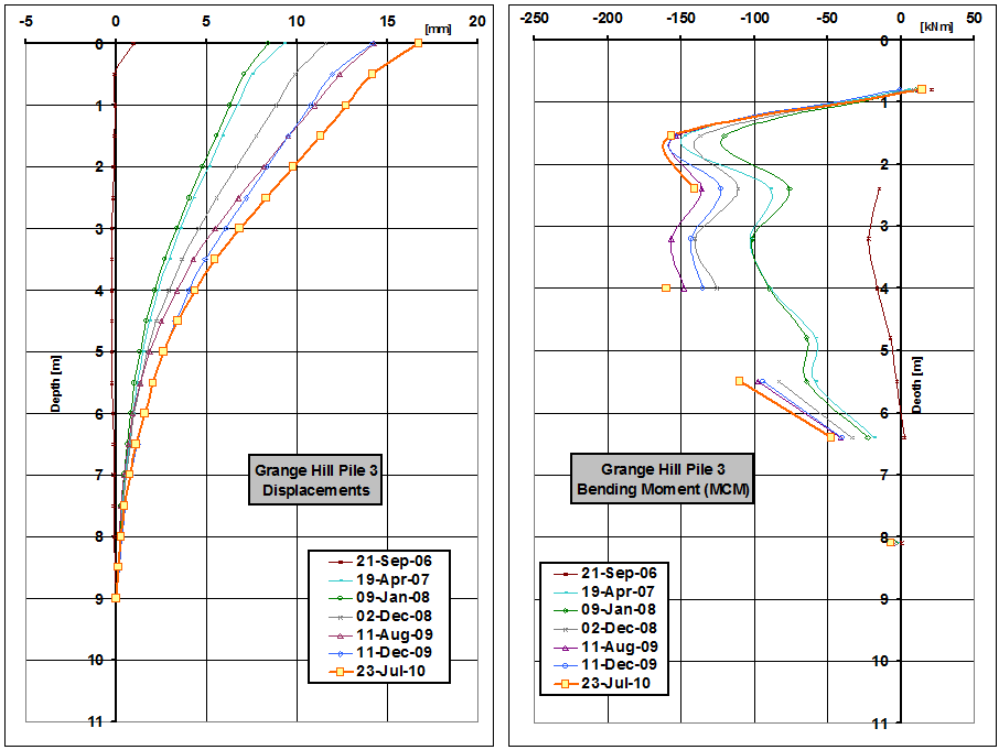

Figure A.9: *Grange Hill Pile3, displacements and bending moments (calculated with MCM) for the whole monitoring period*

A.2 Leatherhead

A.2.1 Pile1

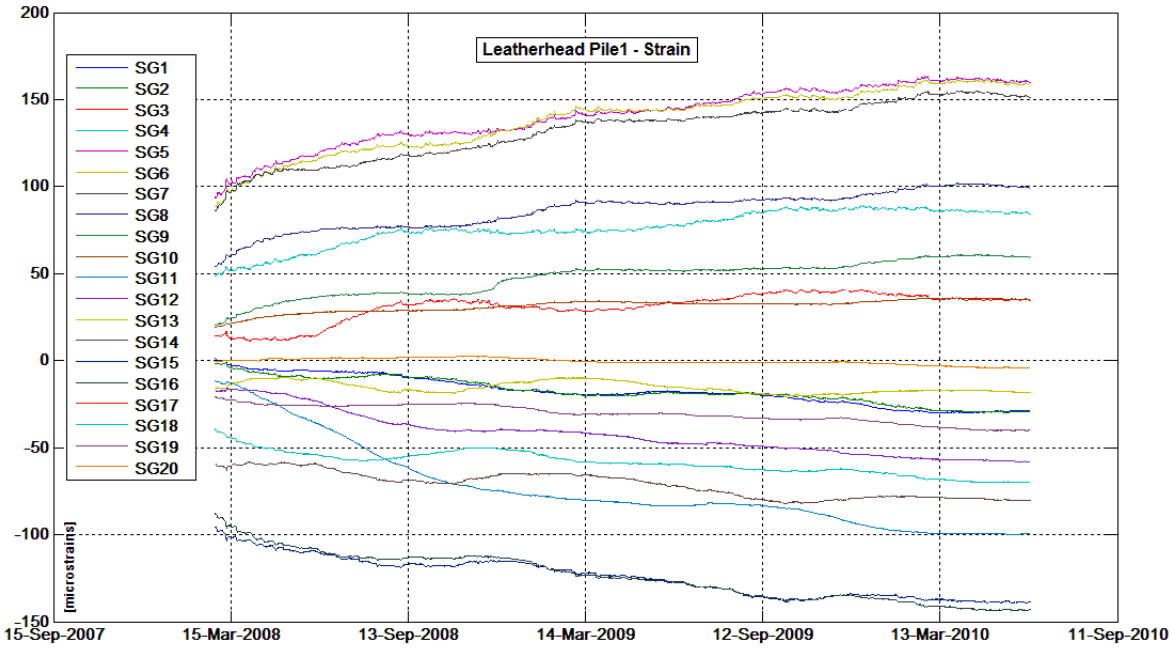

Figure A.10: *Leatherhead Pile1, strain profiles for all the instruments in the pile.*

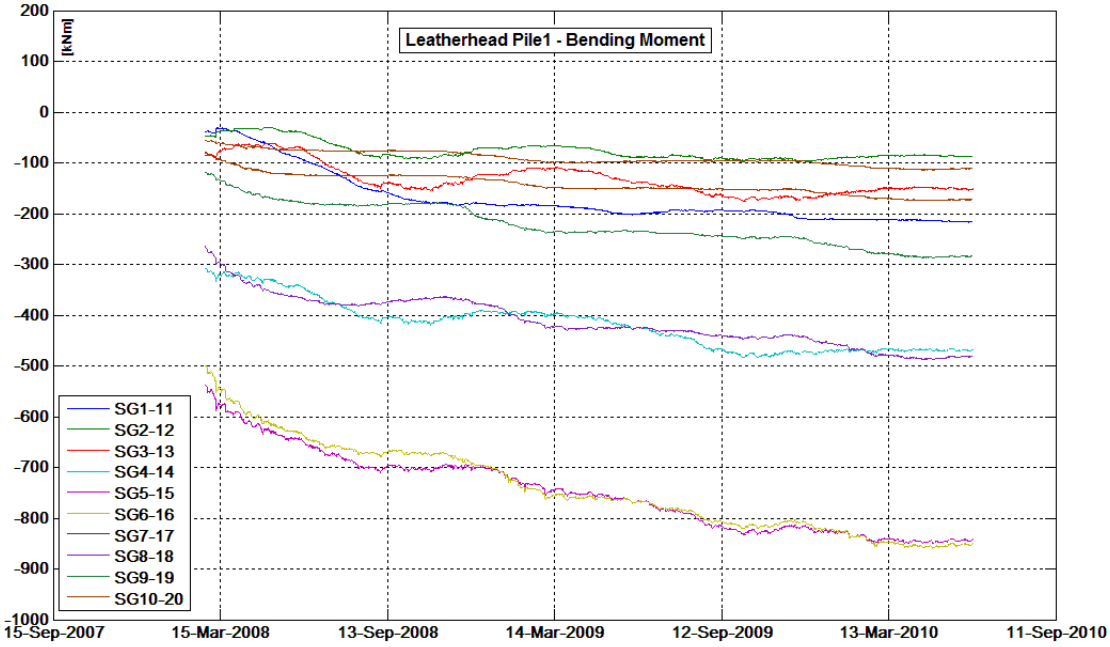

Figure A.11: *Leatherhead Pile1, bending moment profiles for all the instrumented sections in the pile.*

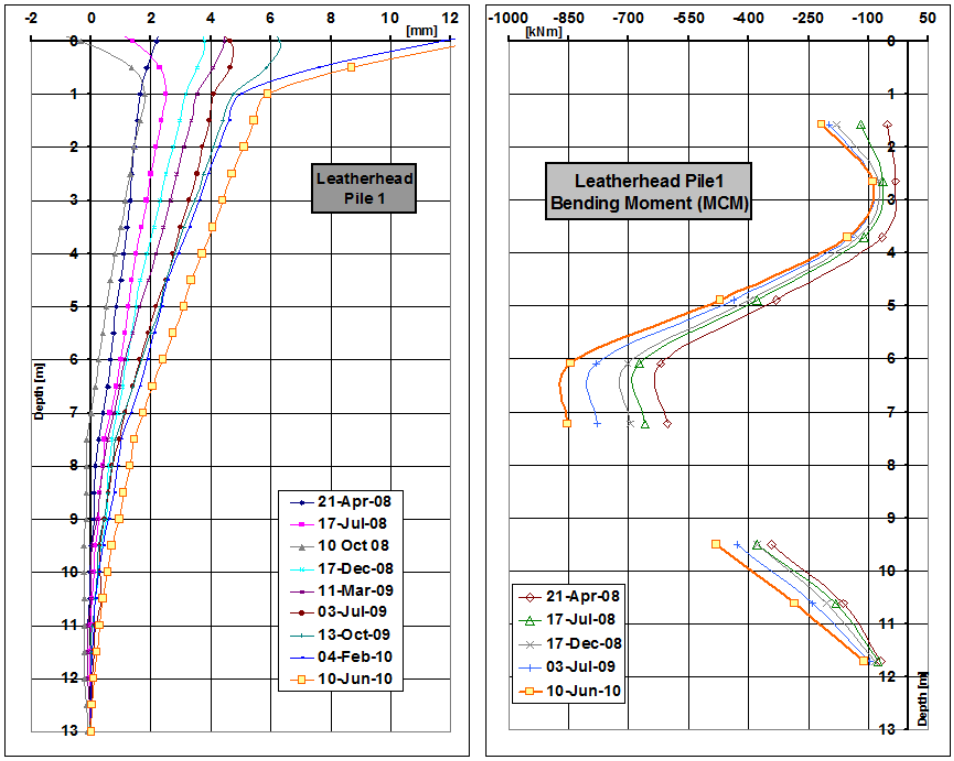

Figure A.12: *Leatherhead Pile1, displacements and bending moments (calculated with MCM) along the full monitoring period*

A.2.2 Pile2

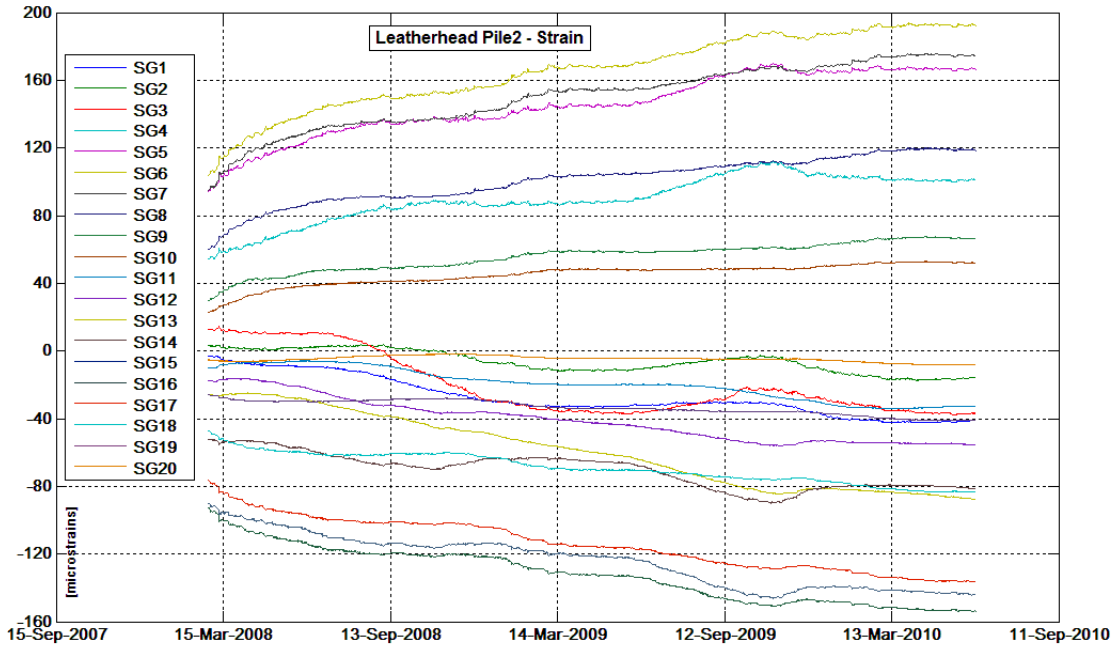

Figure A.13: *Leatherhead Pile2, strain profiles for all the instruments in the pile.*

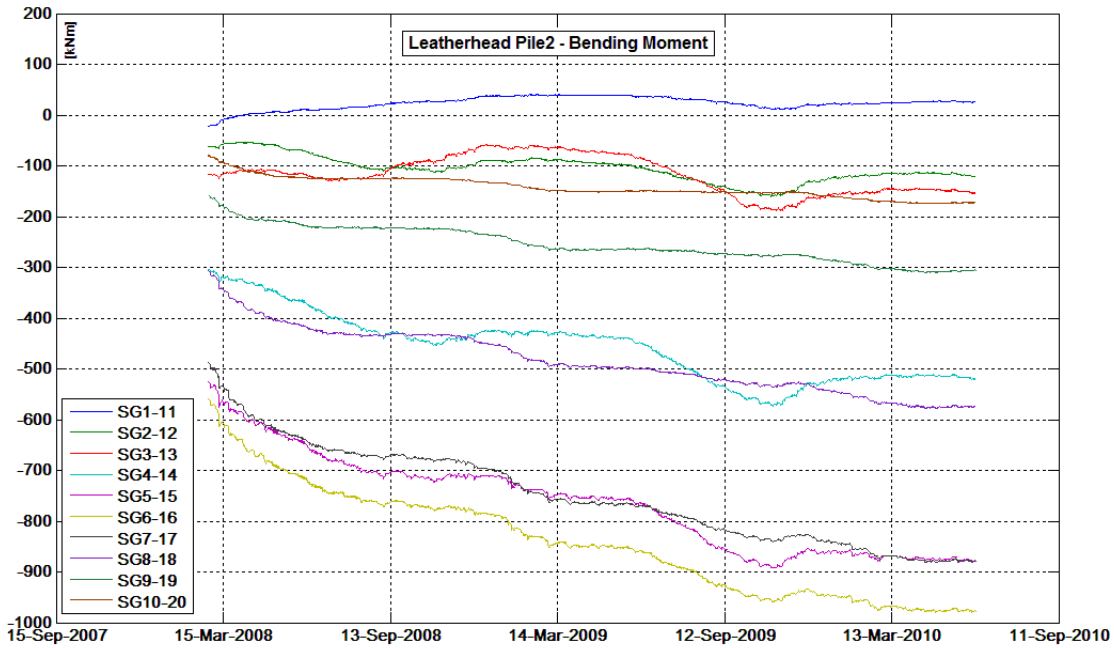

Figure A.14: *Leatherhead Pile2, bending moment profiles for all the instrumented sections in the pile.*

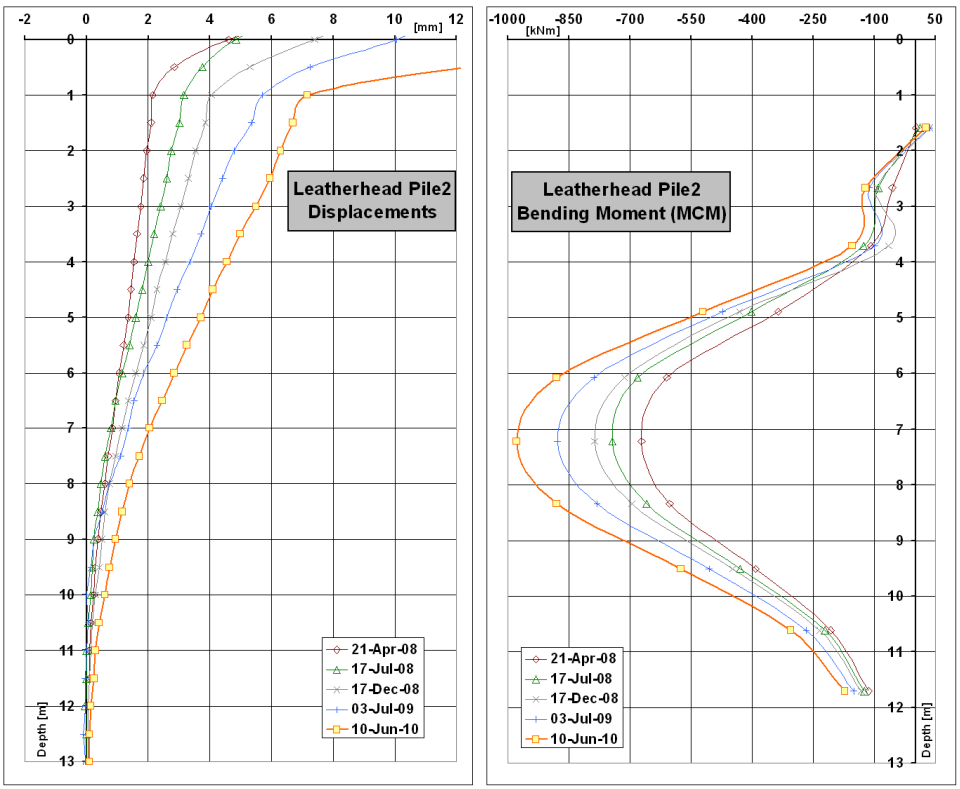

Figure A.15: *Leatherhead Pile2, displacements and bending moments (calculated with MCM) along the full monitoring period*

A.3 Mill Hill

A.3.1 Pile1

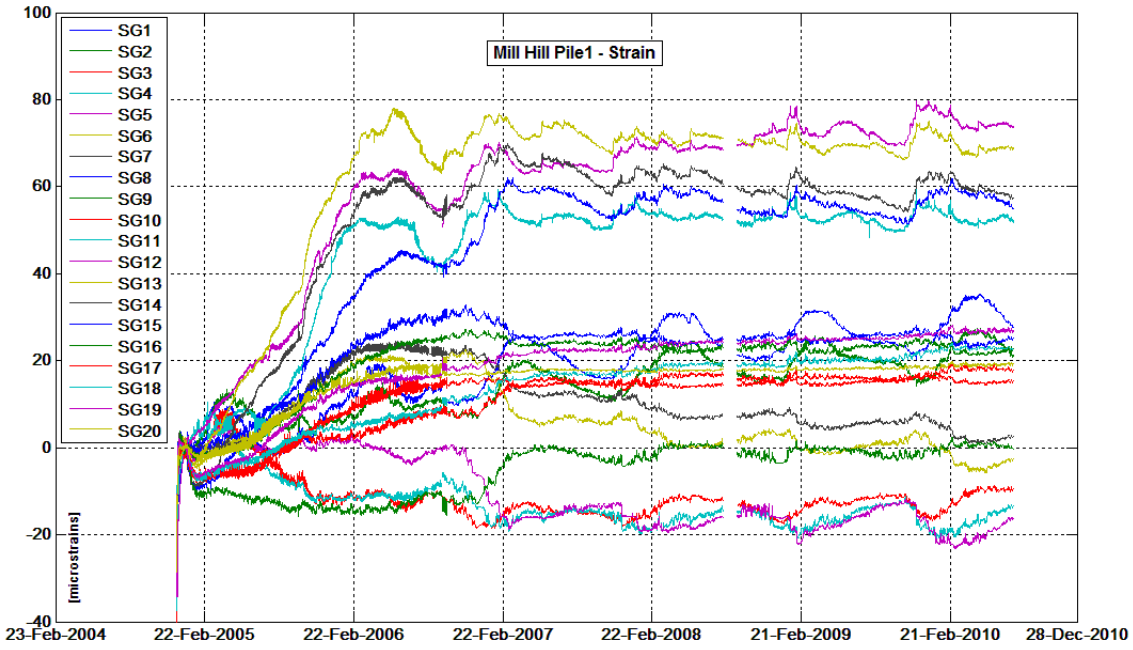

Figure A.16: *Mill Hill Pile1, strain profiles for all the instruments in the pile.*

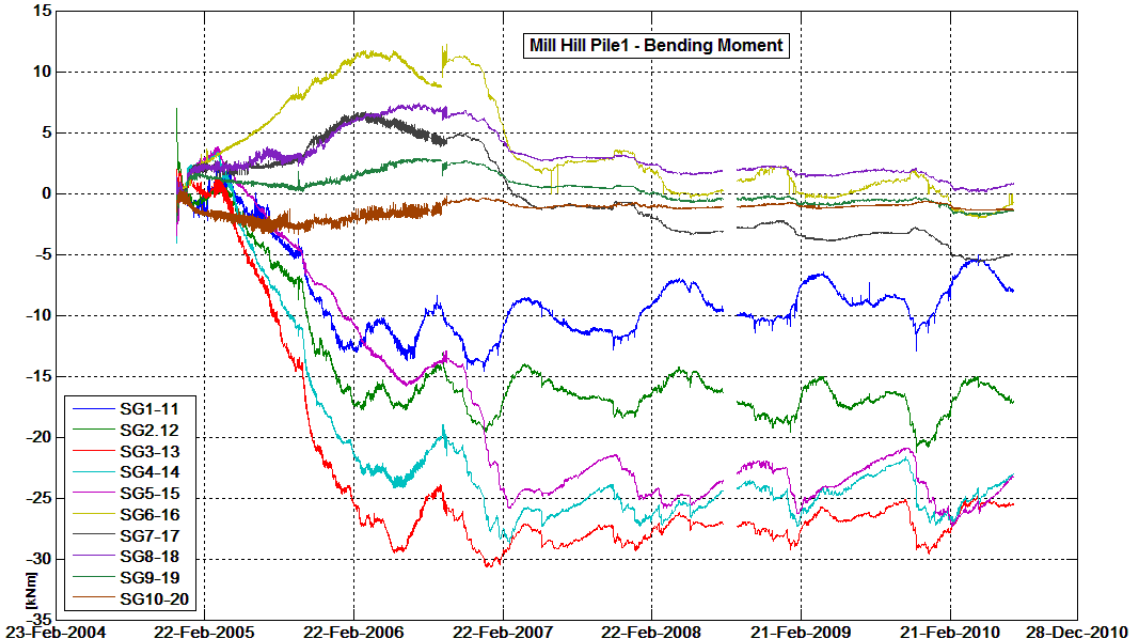

Figure A.17: *Mill Hill Pile1, bending moment profiles for all the instrumented sections in the pile.*

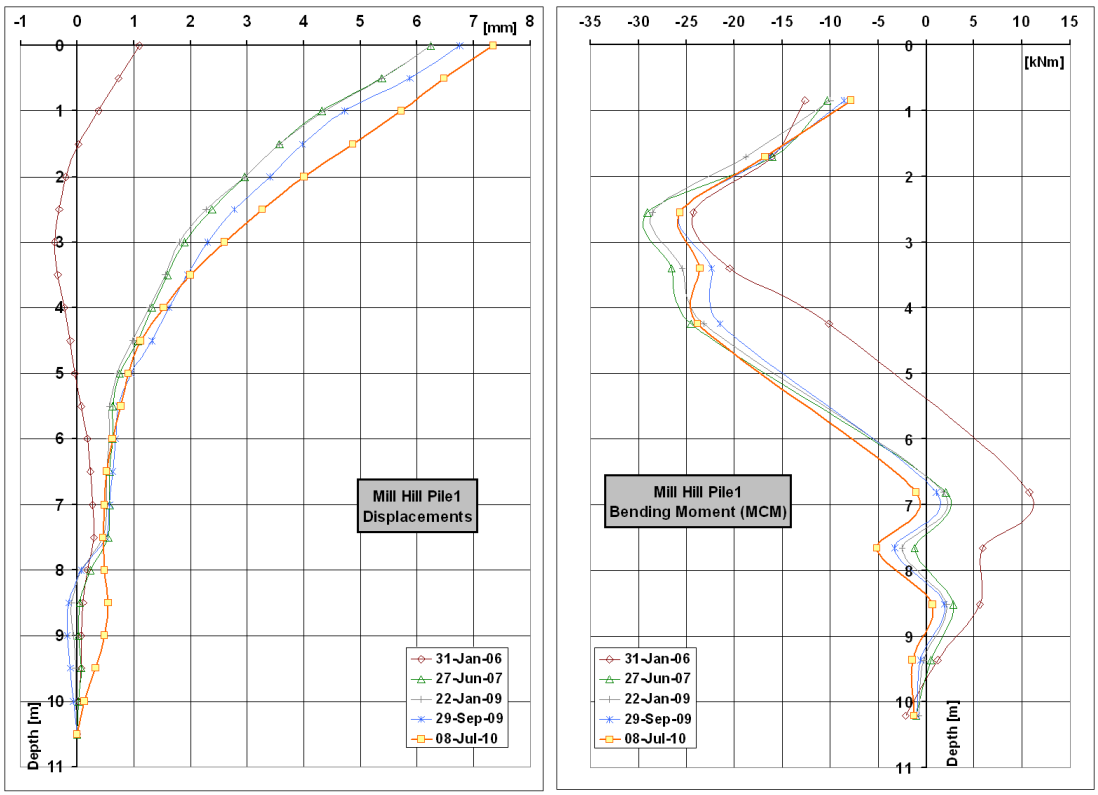

Figure A.18: *Mill Hill Pile1, displacements and bending moments (calculated with MCM) for the full monitoring period*

A.3.2 Pile2

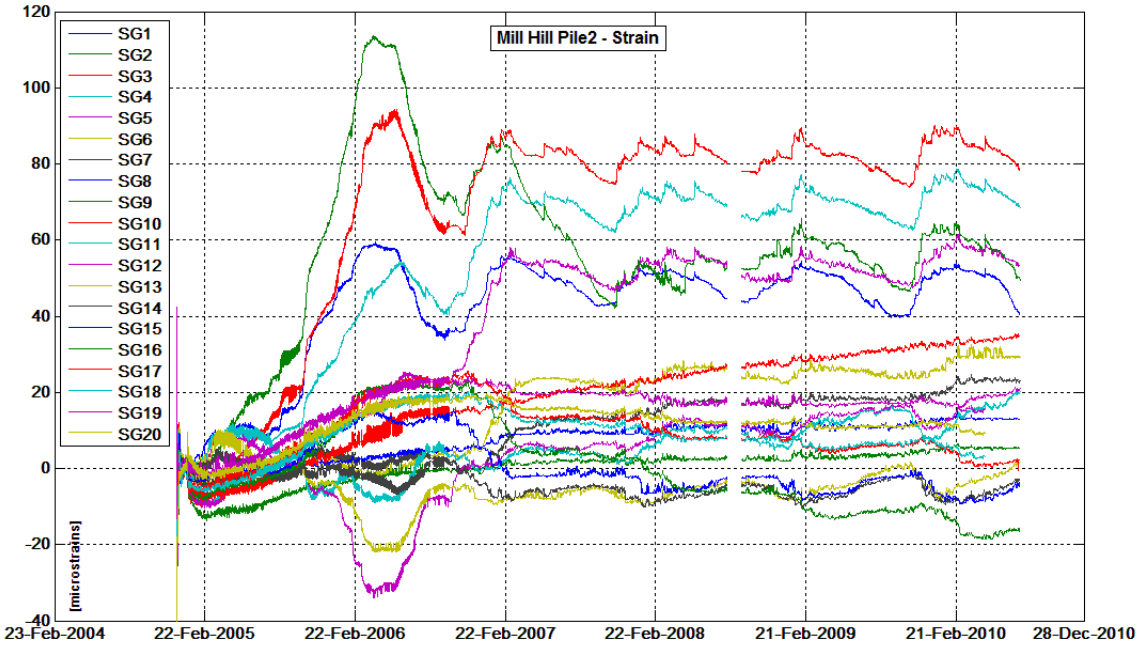

Figure A.19: *Mill Hill Pile2, strain profiles for all the instruments in the pile.*

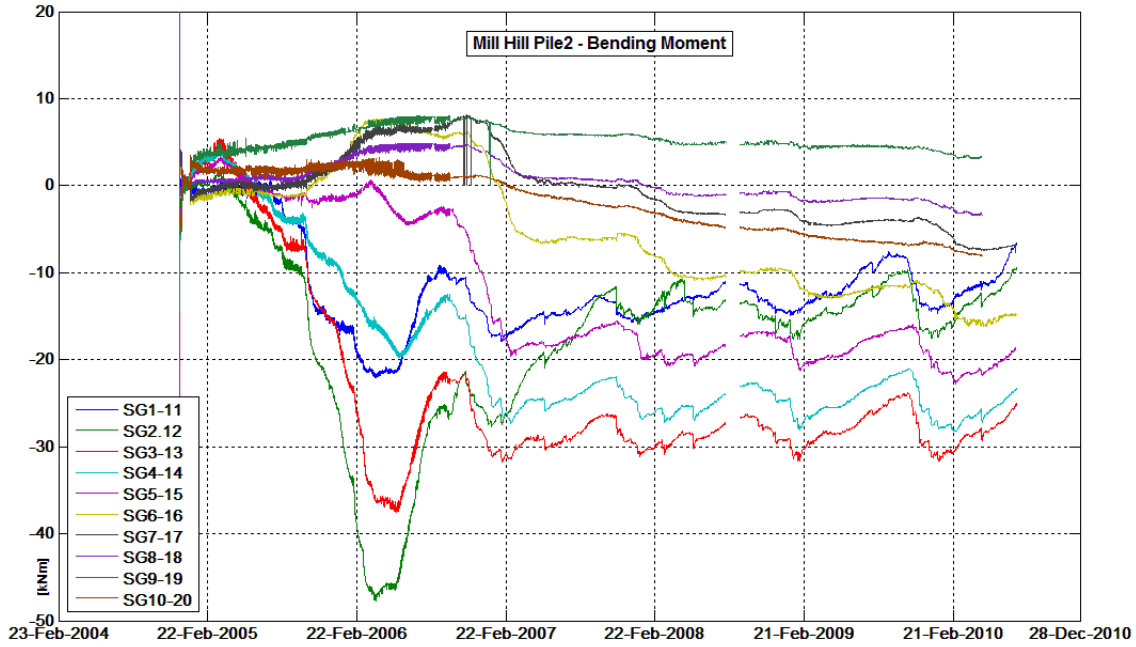

Figure A.20: *Mill Hill Pile2, bending moment profiles for all the instrumented sections in the pile.*

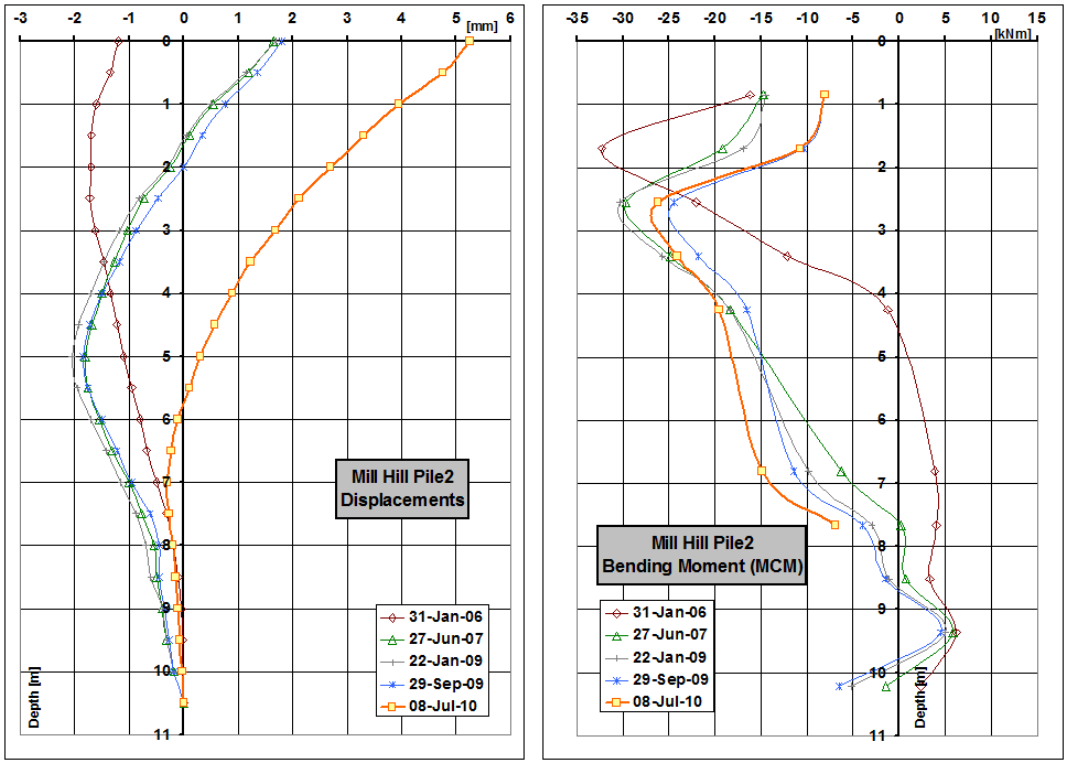

Figure A.21: *Mill Hill Pile2, displacements and bending moments (calculated with MCM) for the full monitoring period*

A.4 Ironbridge

A.4.1 Phase I

A.4.1.1 L1P30

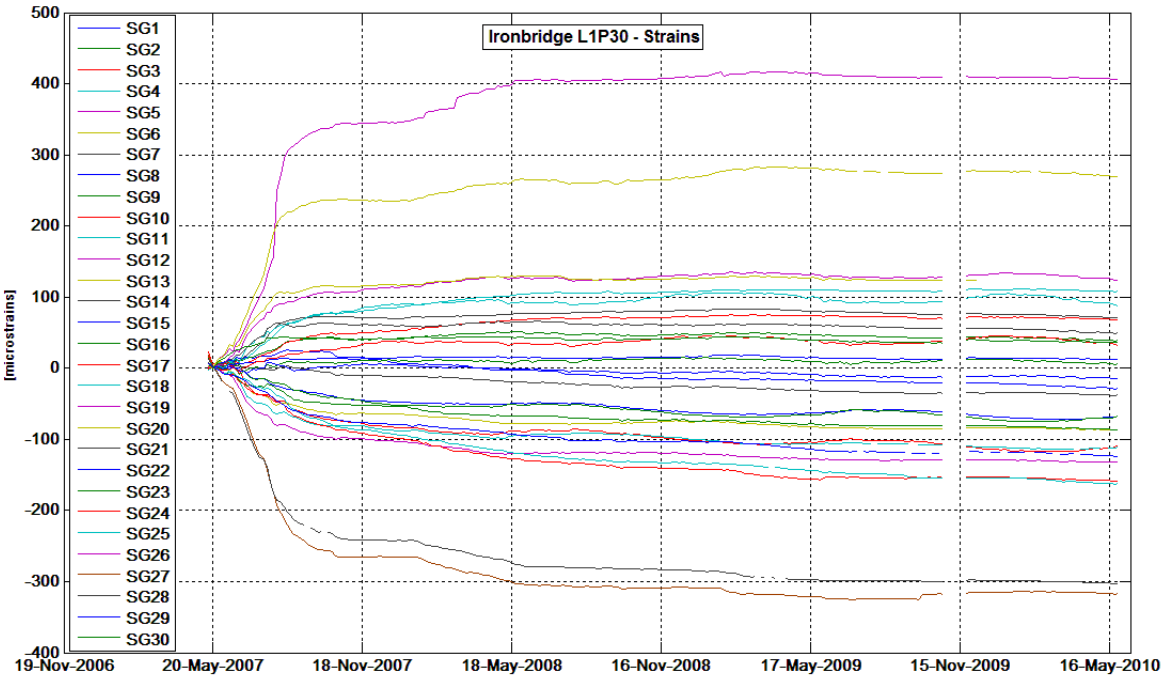

Figure A.22: *Ironbridge L1P30, strain profiles for all the instruments in the pile.*

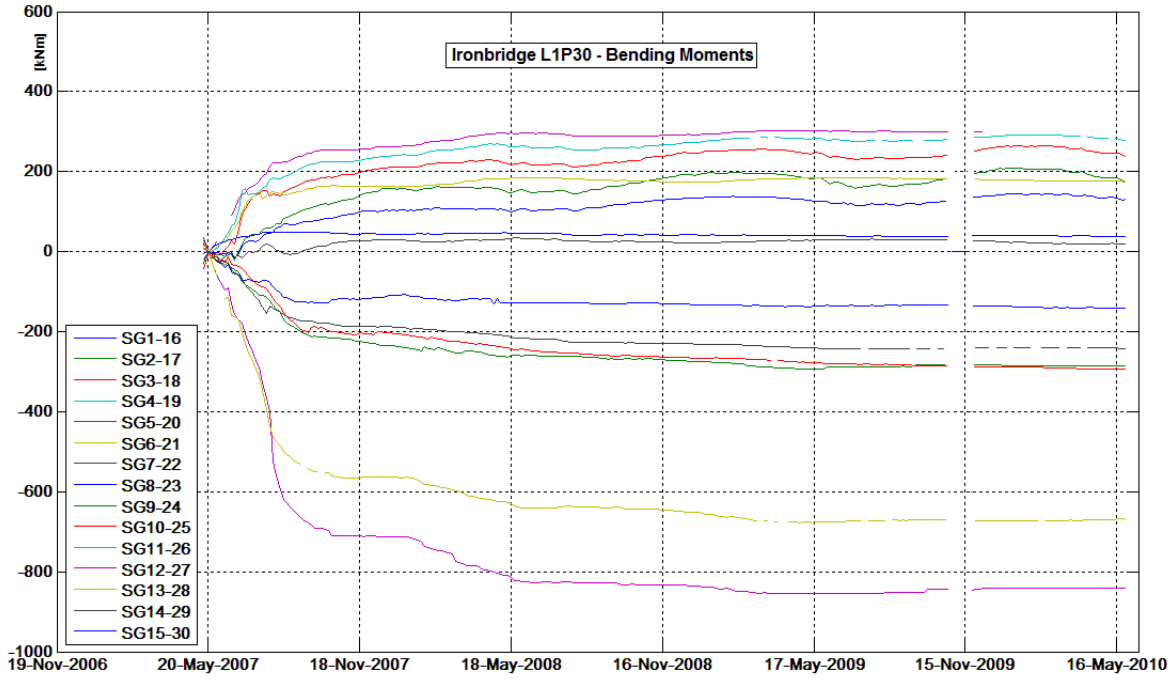

Figure A.23: *Ironbridge L1P30, bending moment profiles for all the instrumented sections in the pile.*

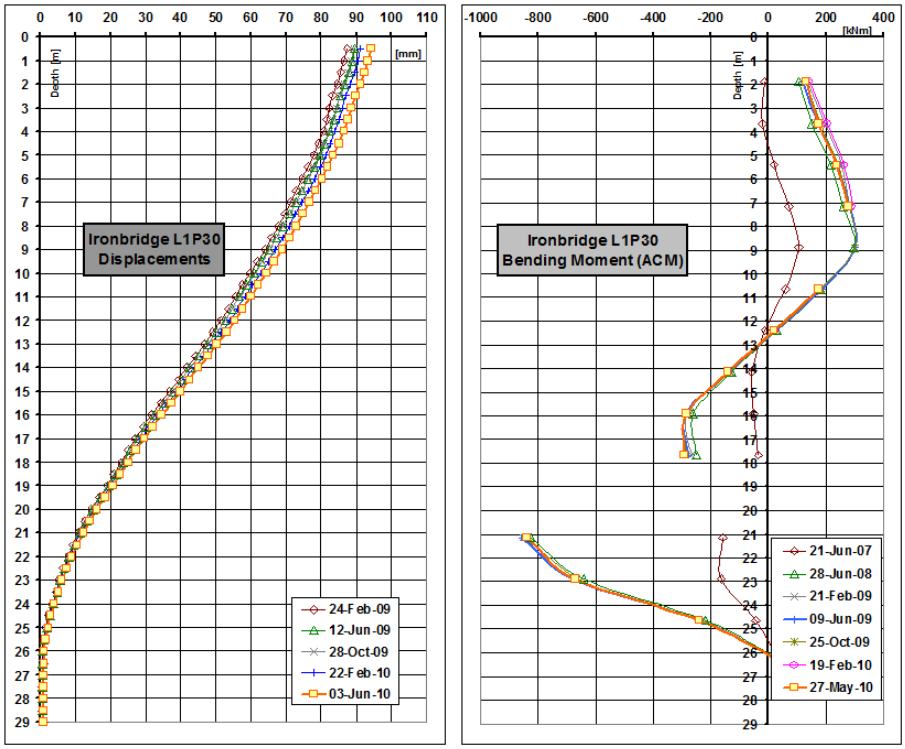

Figure A.24: *Ironbridge L1P30, displacements and bending moments (calculated with ACM) for the full monitoring period*

A.4.1.2 L2P30

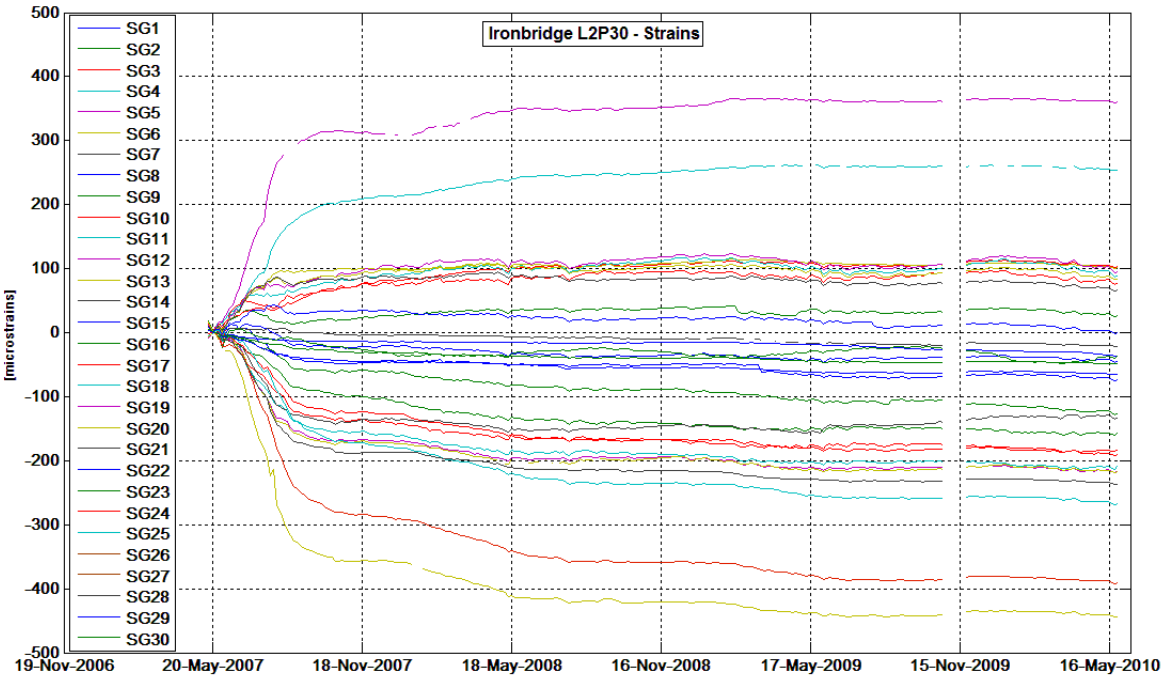

Figure A.25: *Ironbridge L2P30, strain profiles for all the instruments in the pile.*

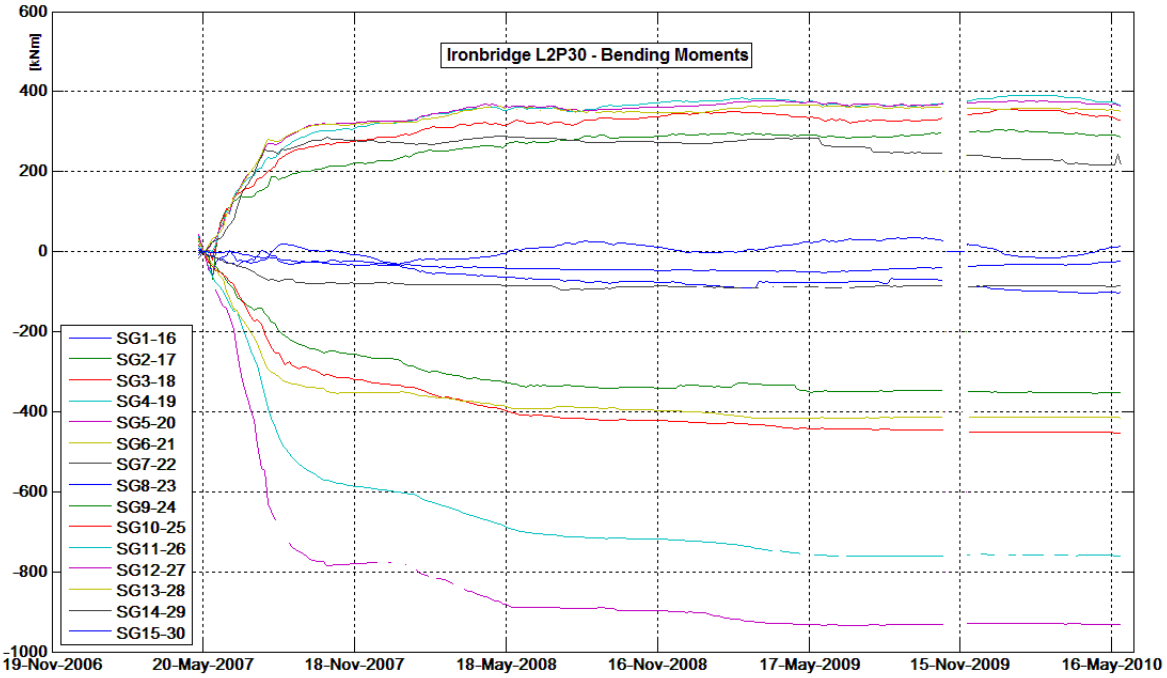

Figure A.26: *Ironbridge L2P30, bending moment profiles for all the instrumented sections in the pile.*

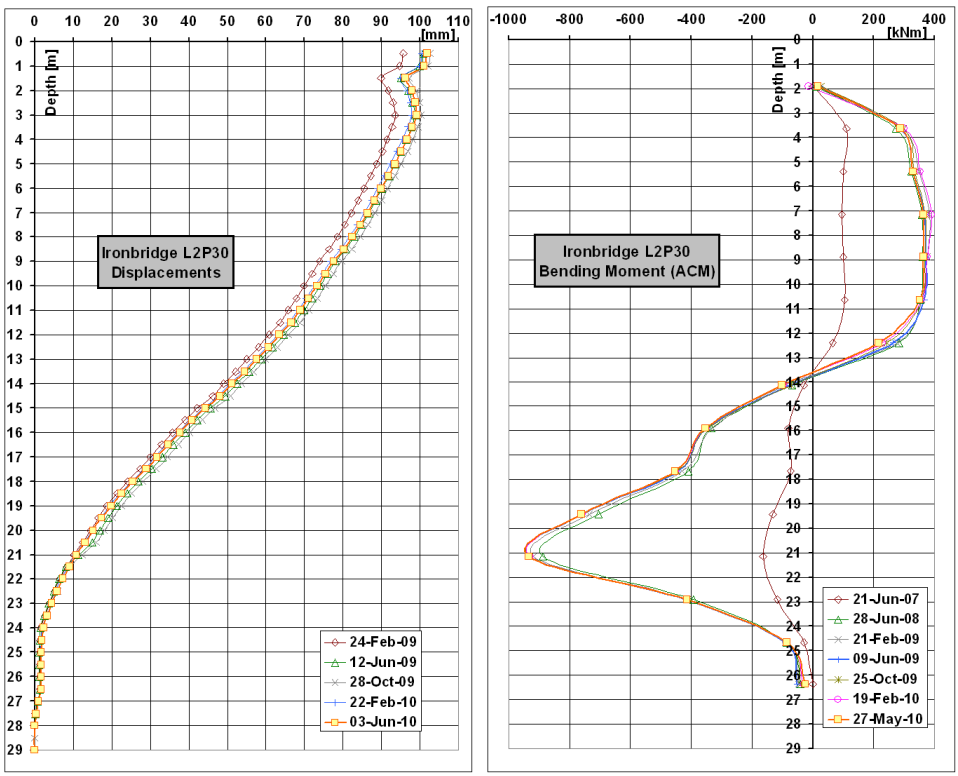

Figure A.27: *Ironbridge L2P30, displacements and bending moments (calculated with ACM) for the full monitoring period*

A.4.1.3 UP22

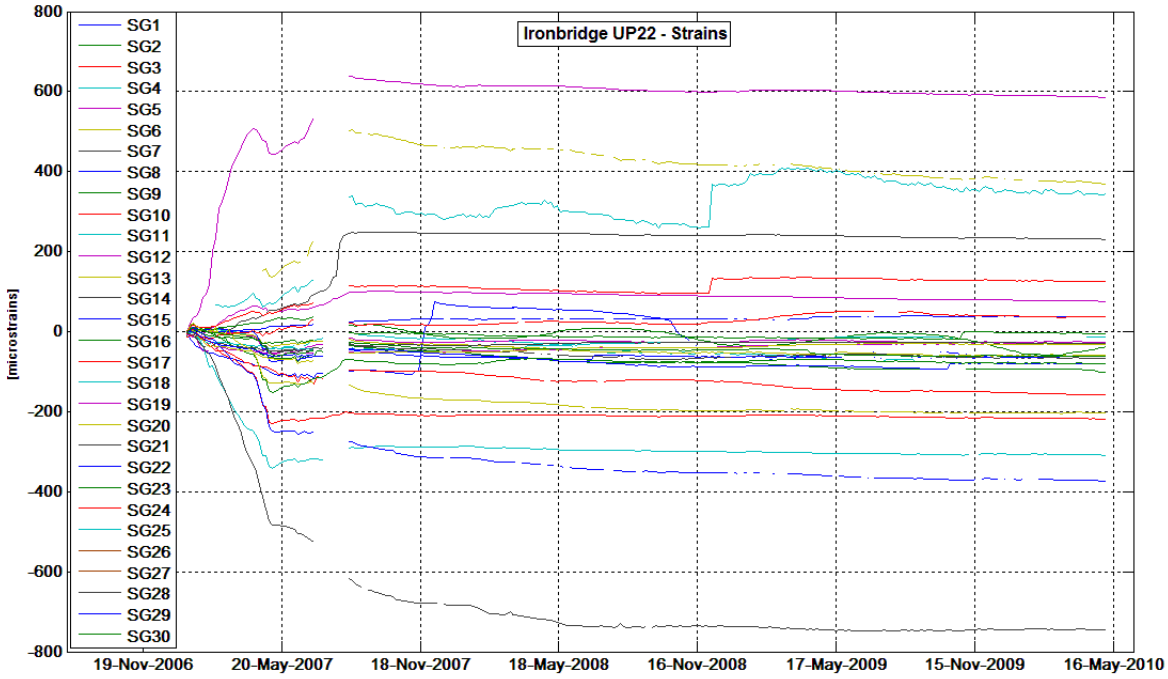

Figure A.28: *Ironbridge UP22, strain profiles for all the instruments in the pile.*

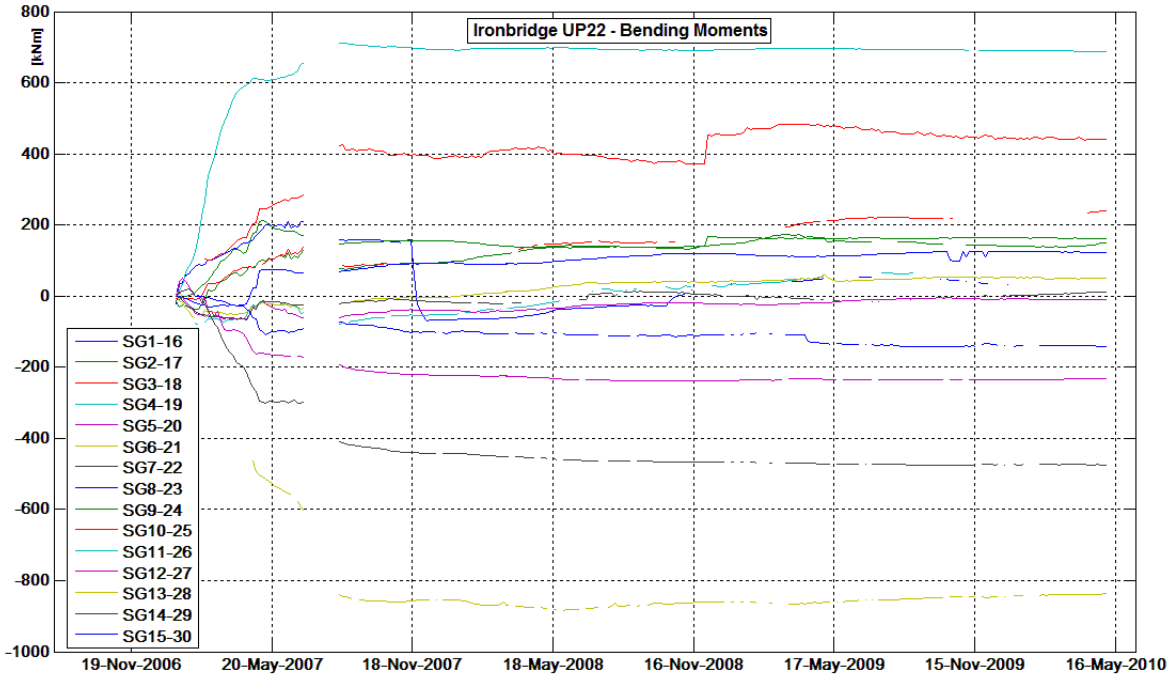

Figure A.29: *Ironbridge UP22, bending moment profiles for all the instrumented sections in the pile.*

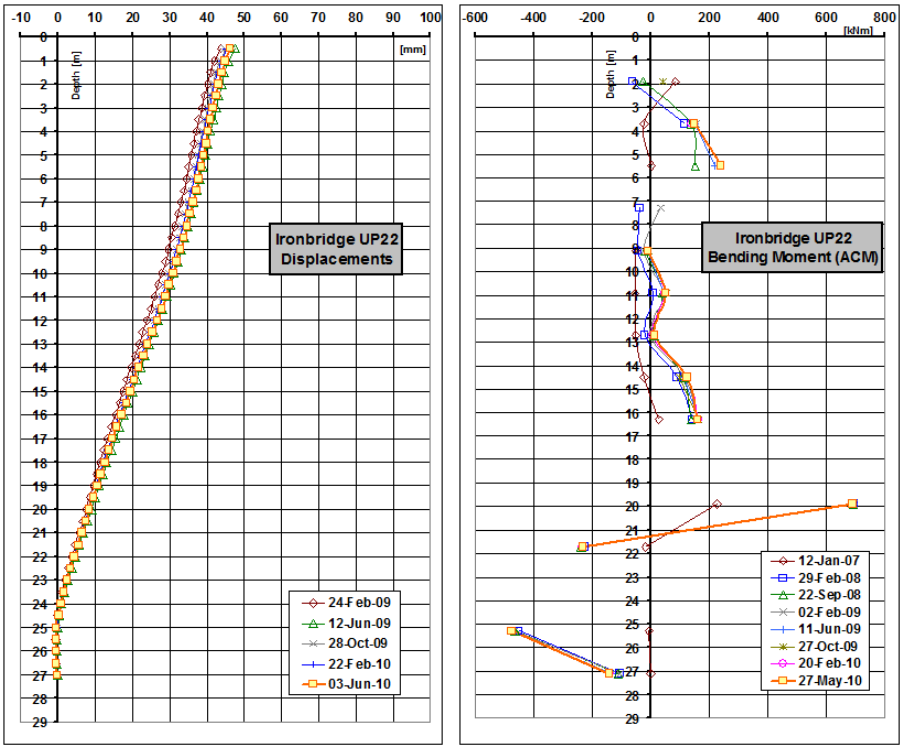

Figure A.30: *Ironbridge UP22, displacements and bending moments (calculated with ACM) for the full monitoring period*

A.4.2 Phase II

A.4.2.1 UT81

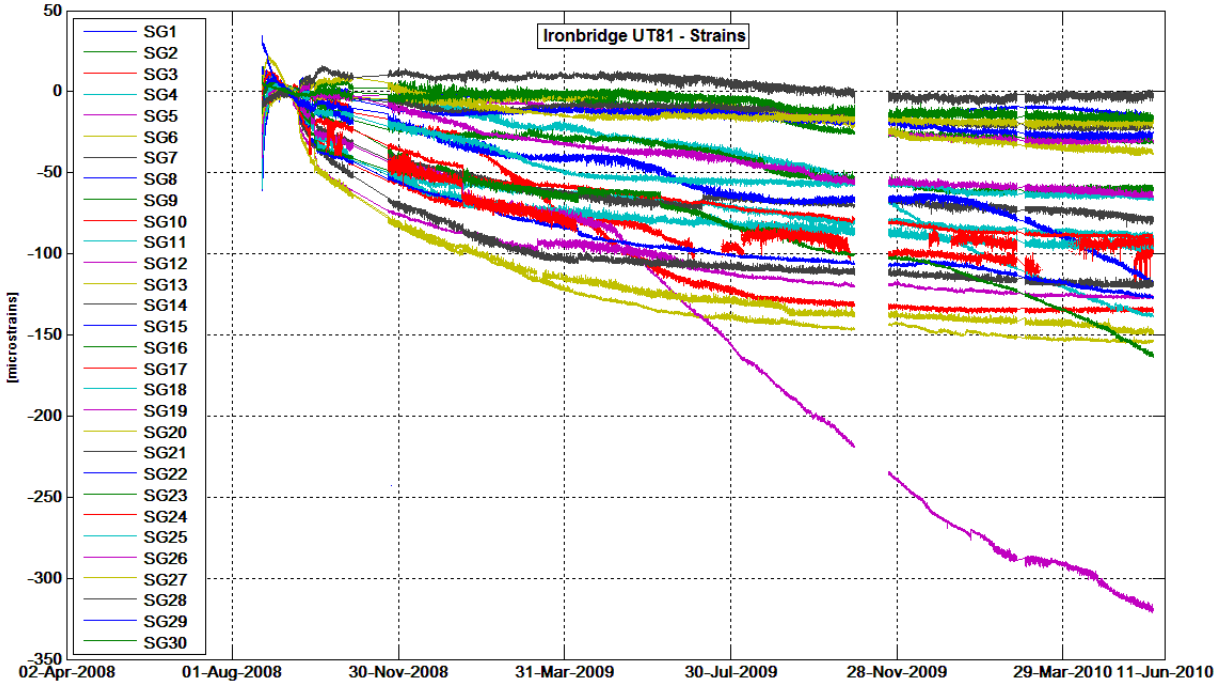

Figure A.31: *Ironbridge UT81, strain profiles for all the instruments in the pile.*

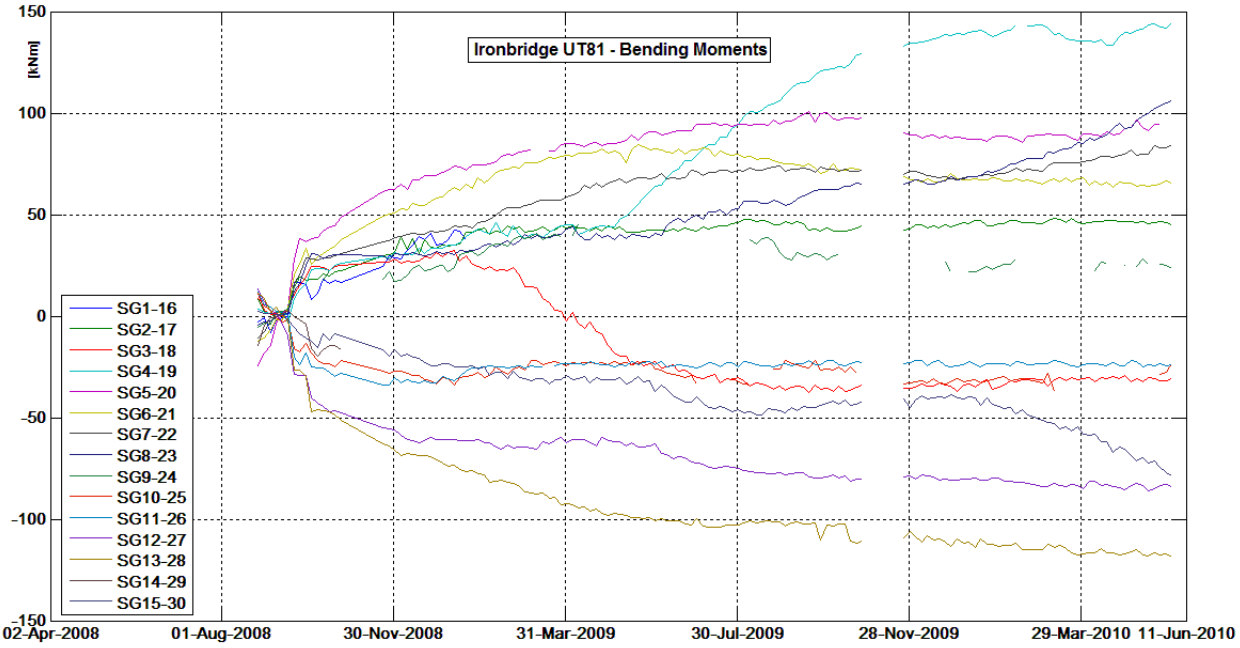

Figure A.32: *Ironbridge UT81, bending moment profiles for all the instrumented sections in the pile.*

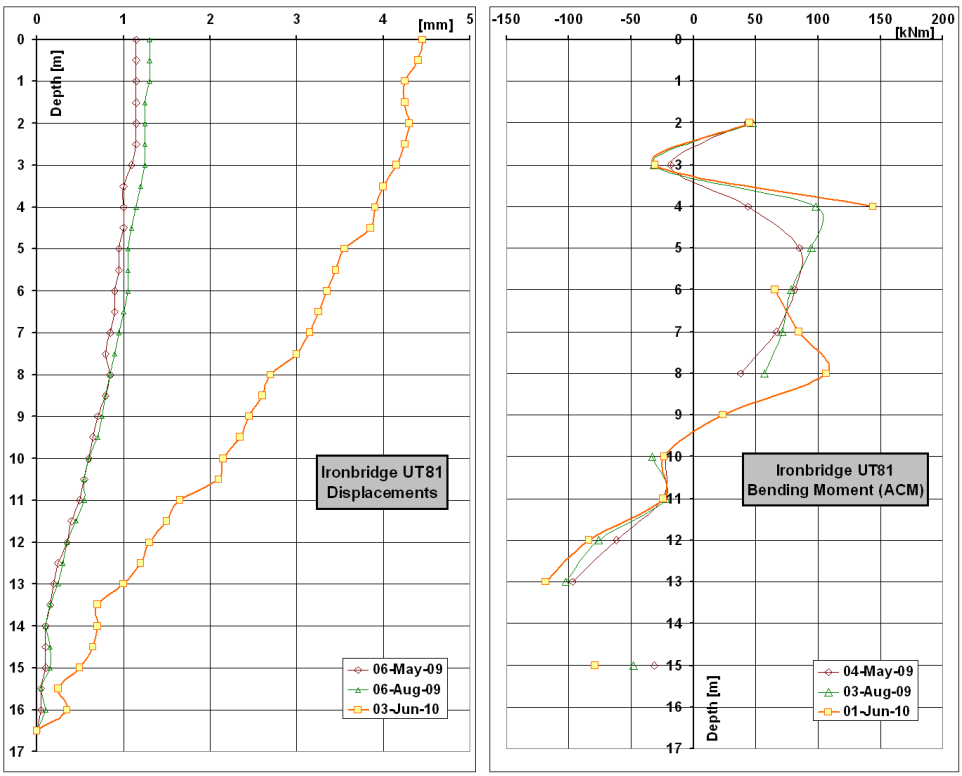

Figure A.33: *Ironbridge UT81, displacements and bending moments (calculated with ACM) for the full monitoring period*

A.4.2.2 LT56

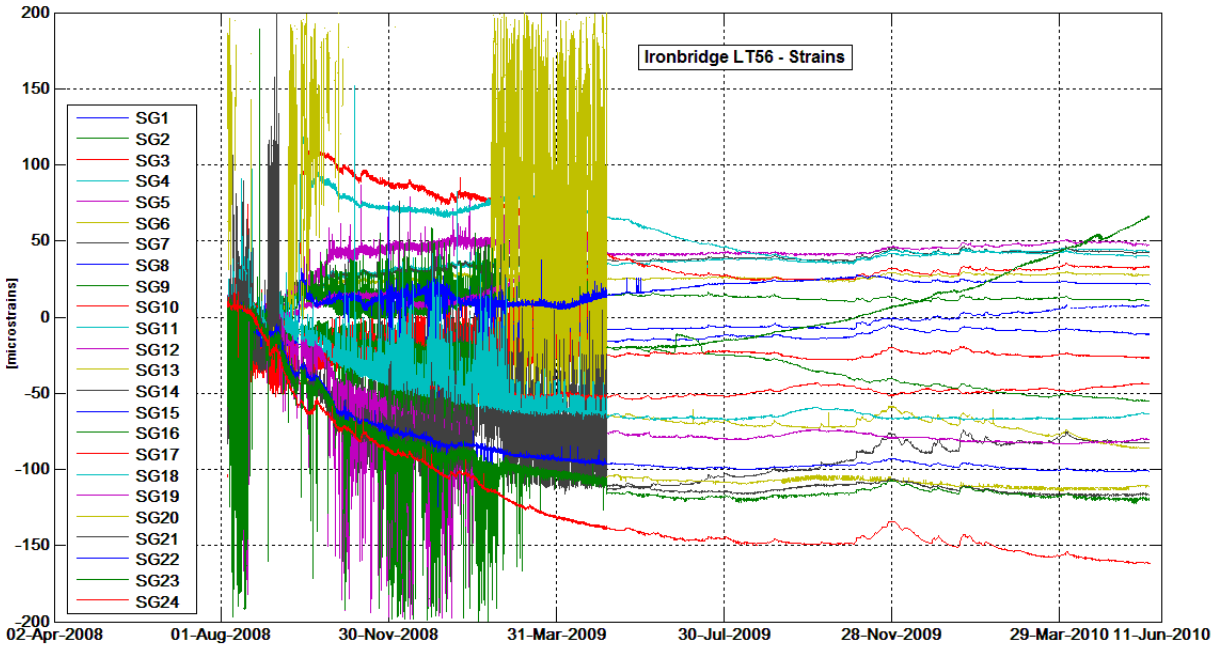

Figure A.34: *Ironbridge LT56, strain profiles for all the instruments in the pile. Interference is due to some early problems in the data-logger connections.*

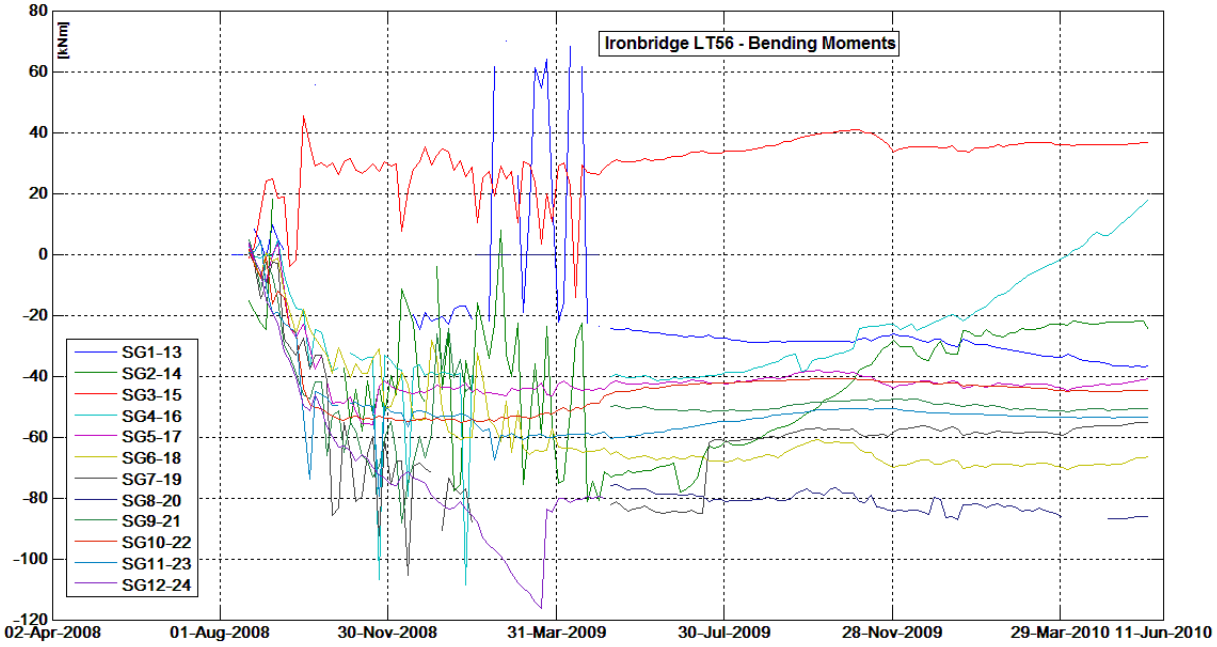

Figure A.35: *Ironbridge LT56, bending moment profiles for all the instrumented sections in the pile. Interference is due to some early problems in the data-logger connections.*

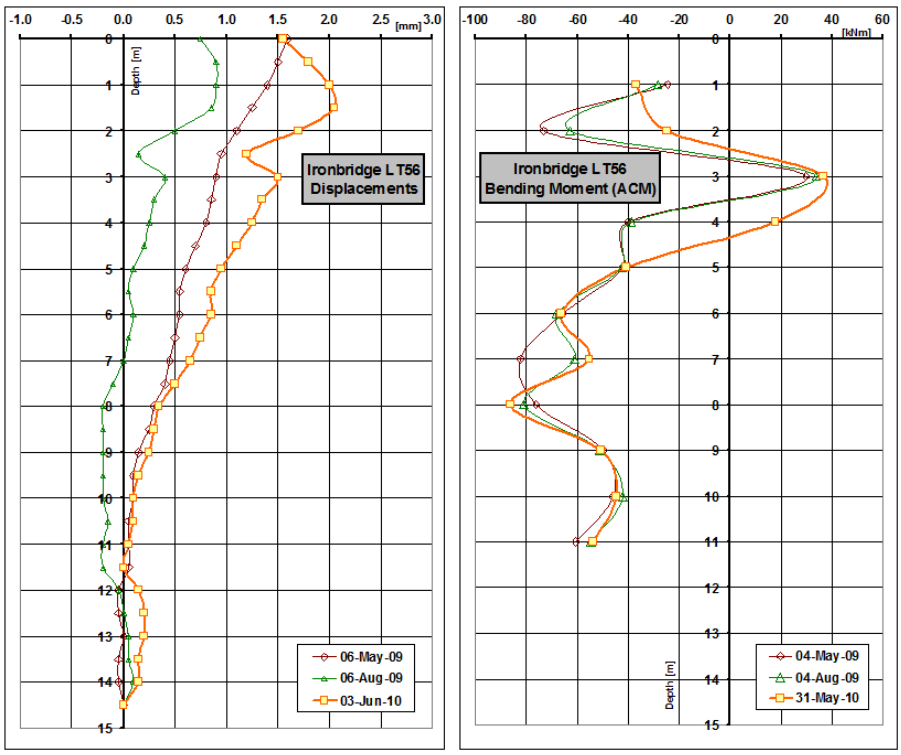

Figure A.36: *IronbridgeLT56, displacements and bending moments (calculated with ACM) for the full monitoring period*

A.4.3 Lloyd's Head

A.4.3.1 P58Row1

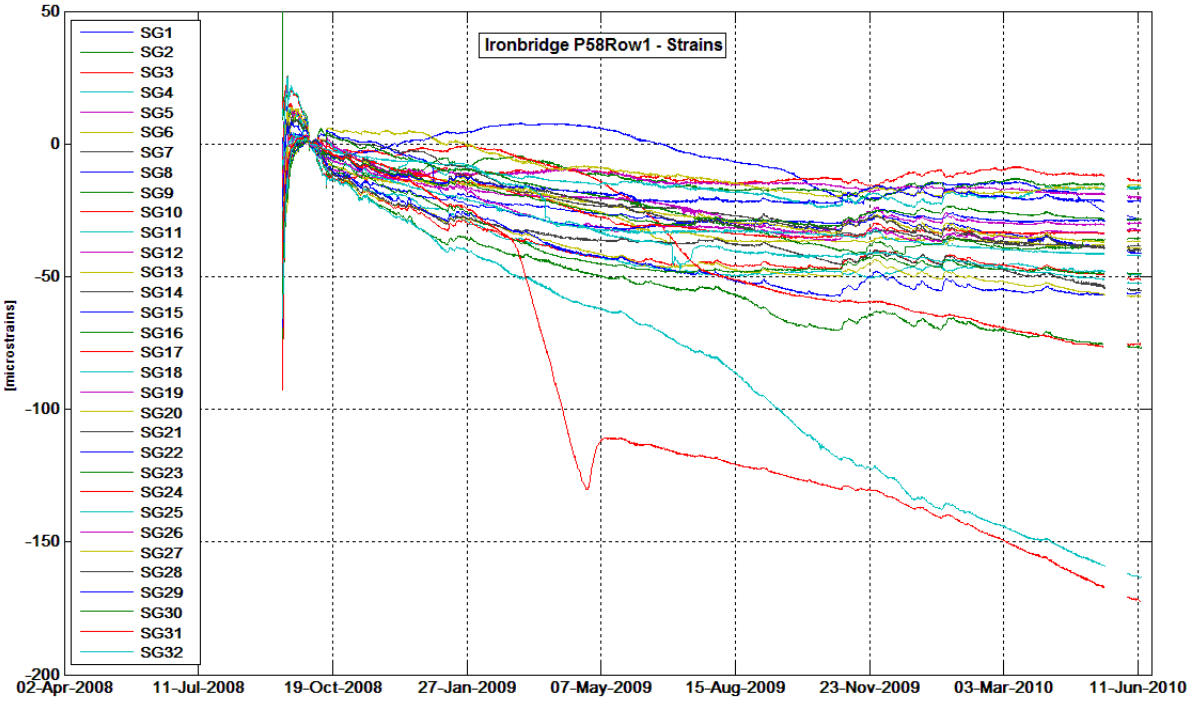

Figure A.37: *Ironbridge P58Row1, strain profiles for all the instruments in the pile.*

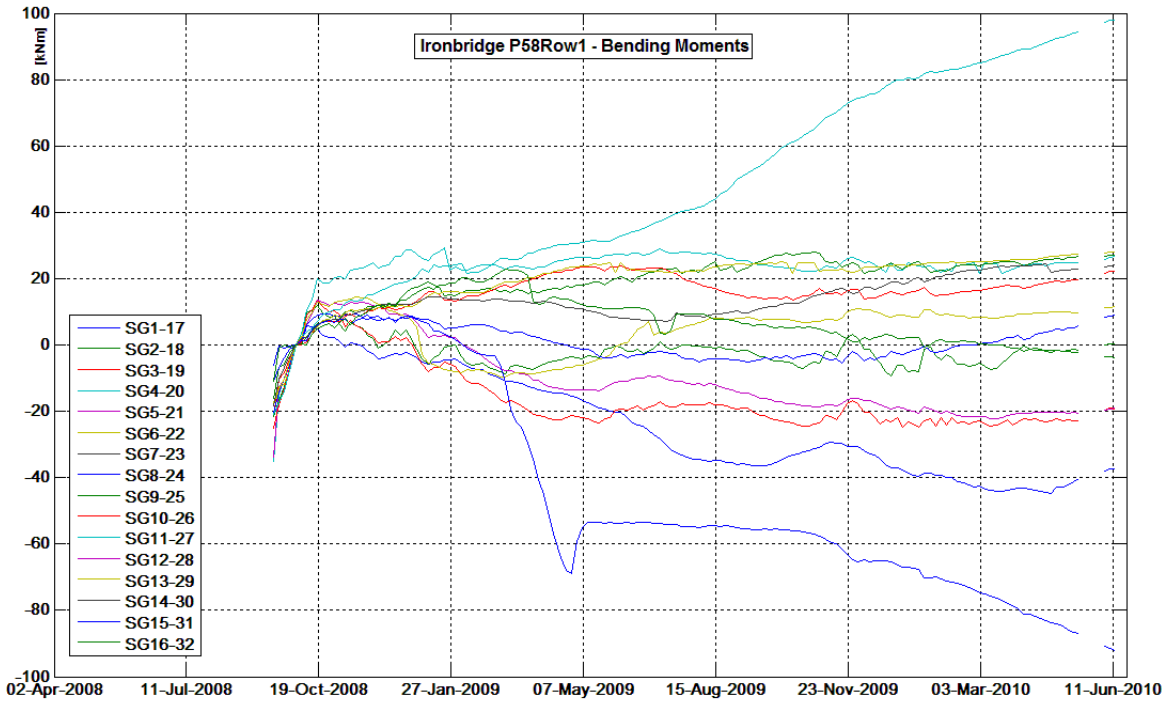

Figure A.38: *Ironbridge P58Row1, bending moment profiles for all the instrumented sections in the pile.*

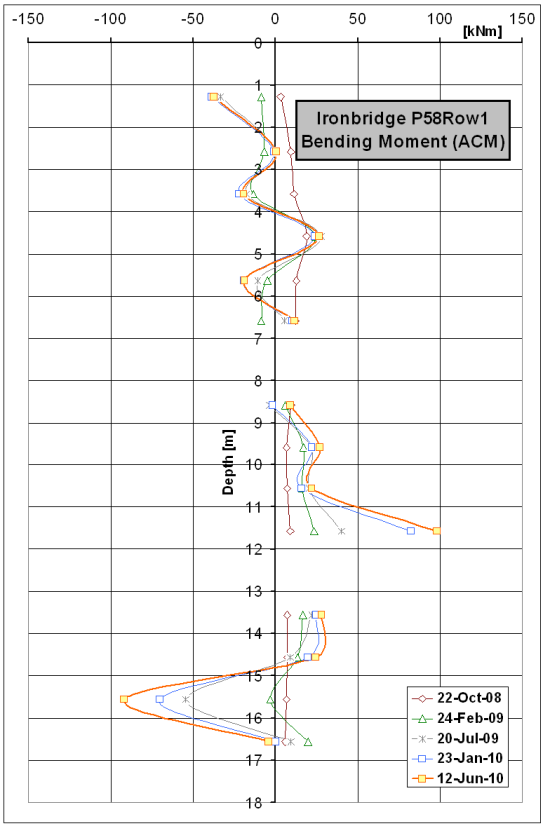

Figure A.39: *Ironbridge P58Row1, bending moment profiles (calculated with ACM) for the full monitoring period.*

A.4.3.2 P58Row2

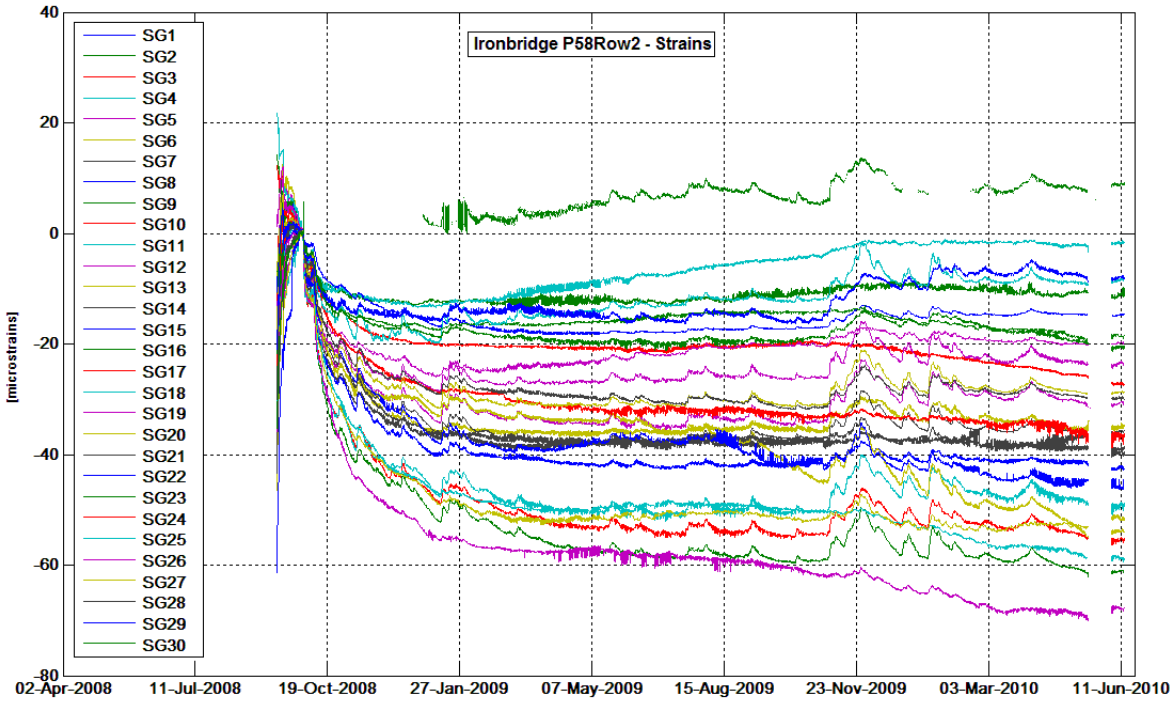

Figure A.40: *Ironbridge P58Row2, strain profiles for all the instruments in the pile.*

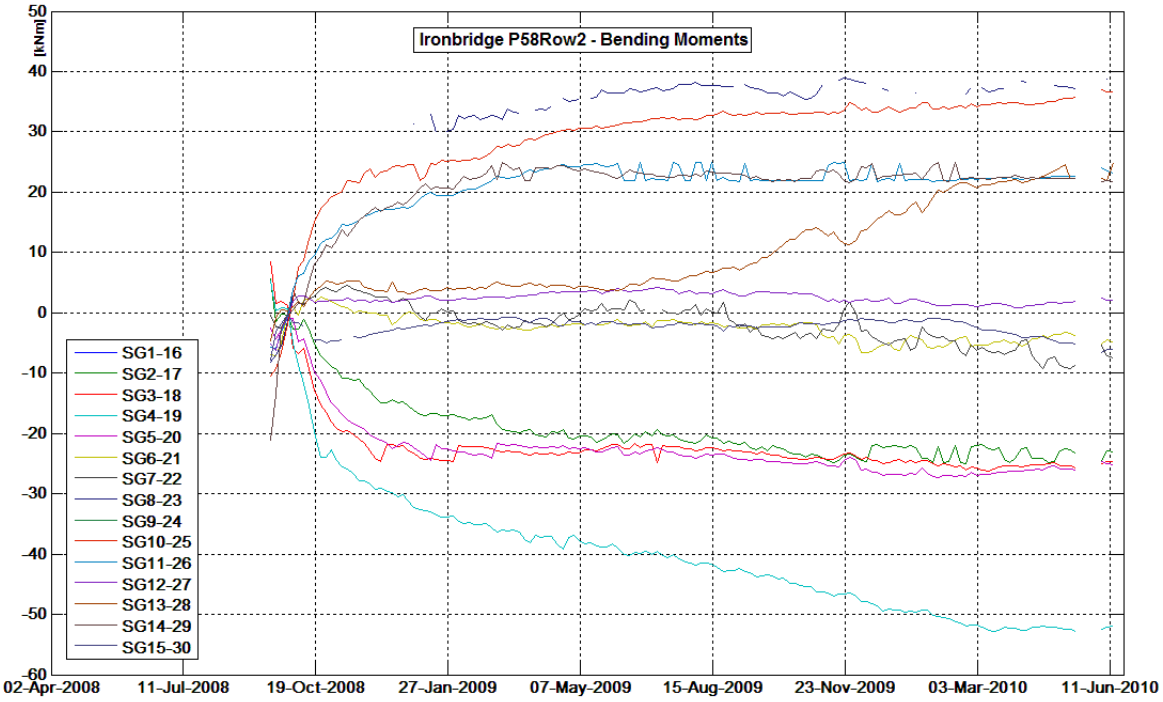

Figure A.41: *Ironbridge P58Row2, bending moment profiles for all the instrumented sections in the pile.*

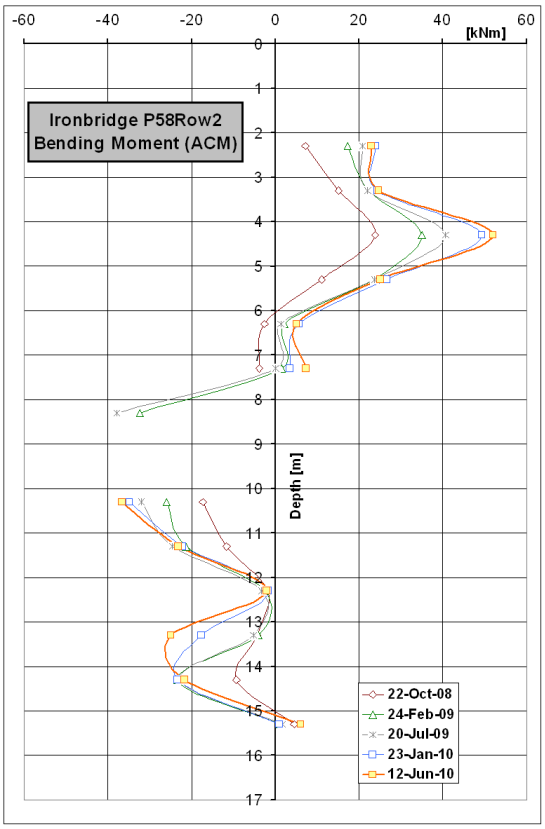

Figure A.42: *Ironbridge P58Row2, bending moment profiles (calculated with ACM) for the full monitoring period.*